Copyright Warning & Restrictions

The copyright law of the United States (Title 17, United States Code) governs the making of photocopies or other reproductions of copyrighted material.

Under certain conditions specified in the law, libraries and archives are authorized to furnish a photocopy or other reproduction. One of these specified conditions is that the photocopy or reproduction is not to be "used for any purpose other than private study, scholarship, or research." If a, user makes a request for, or later uses, a photocopy or reproduction for purposes in excess of "fair use" that user may be liable for copyright infringement,

This institution reserves the right to refuse to accept a copying order if, in its judgment, fulfillment of the order would involve violation of copyright law.

Please Note: The author retains the copyright while the New Jersey Institute of Technology reserves the right to distribute this thesis or dissertation

Printing note: If you do not wish to print this page, then select "Pages from: first page # to: last page #" on the print dialog screen

ABSTRACT

CONSTRUCTION AND ASSESSMENT OF A COMPUTER GRAPHICS-BASED MODEL FOR WHEELCHAIR PROPULSION

by
Brooke Marie Odle

Upper limb overuse injuries are common in manual wheelchair using persons with spinal cord injury (SCI), especially those with tetraplegia. Biomechanical analyses involving kinetics, kinematics, and muscle mechanics provide an opportunity to identify modifiable risk factors associated with wheelchair propulsion and upper limb overuse injuries that may be used toward developing prevention and treatment interventions. However, these analyses are limited because they cannot estimate muscle forces *in vivo*. Patient-specific computer graphics-based models have enhanced biomechanical analyses by determining *in vivo* estimates of shoulder muscle and joint contact forces. Current models do not include deep shoulder muscles. Also, patient-specific models have not been generated for persons with tetraplegia, so the shoulder muscle contribution to propulsion in this population remains unknown. The goals of this project were to: (i) construct a dynamic, patient-specific model of the upper limb and trunk and (ii) use the model to determine the individual contributions of the shoulder complex muscles to wheelchair propulsion.

OpenSim software was used to construct the model. The model has deep shoulder muscles not included in previous models: upper and middle trapezius, rhomboids major and serratus anterior. As a proof of concept, kinematic and kinetic data collected from a study participant with tetraplegia were incorporated with the model to generate dynamic simulations of wheelchair propulsion. These simulations included: inverse kinematics, inverse dynamics, and static optimization. Muscle contribution to propulsion was

achieved by static optimization simulations. Muscles were further distinguished by their contribution to both the push and recovery phases of wheelchair propulsion. Results of the static optimization simulations determined that the serratus anterior was the greatest contributor to the push phase and the middle deltoid was the greatest contributor to the recovery phase.

Cross correlation analyses revealed that 80% of the investigated muscles had moderate to strong relationships with the experimental electromyogram (EMG). Results from mean absolute error calculations revealed that, overall, the muscle activations determined by the model were within reasonable ranges of the experimental EMG. This was the first wheelchair propulsion study to compare estimated muscle forces with experimental fine-wire EMG collected from the participant investigated.

CONSTRUCTION AND ASSESSMENT OF A COMPUTER GRAPHICS-BASED MODEL FOR WHEELCHAIR PROPULSION

by
Brooke Marie Odle

A Dissertation
Submitted to the Faculty of
New Jersey Institute of Technology
and Rutgers University Biomedical and Health Sciences, Newark, NJ
in Partial Fulfillment of the Requirements for the Degree of
Doctor of Philosophy in Biomedical Engineering

Joint Program in Biomedical Engineering

January 2014

APPROVAL PAGE

CONSTRUCTION AND ASSESSMENT OF A COMPUTER GRAPHICS-BASED MODEL FOR WHEELCHAIR PROPULSION

Brooke Marie Odle

Dr. Trevor Dyson-Hudson, Dissertation Advisor Date
Associate Professor of Physical Medicine and Rehabilitation, Rutgers University

---

Dr. Gail Forrest, Committee Member Date
Associate Professor of Physical Medicine and Rehabilitation, Rutgers University

---

Dr. Richard Foulds, Committee Member Date
Associate Professor of Biomedical Engineering, NJIT

Dr. Alicia Koontz, Committee Member Date
Associate Professor of Rehabilitation Science and Technology, University of Pittsburgh

---

Dr. Sheldon Lin, Committee Member Date
Associate Professor of Orthopedics, Rutgers University-NJMS

Dr. Bryan Pfister, Committee Member Date
Associate Professor of Orthopedics, NJIT

Dr. Jeffrey Reinbolt, Committee Member Date
Assistant Professor of Mechanical, Aerospace, and Biomedical Engineering, University of Tennessee

BIOGRAPHICAL SKETCH

Author: Brooke Marie Odle

Degree: Doctor of Philosophy

Date: January 2014

Undergraduate and Graduate Education:

- Doctor of Philosophy in Biomedical Engineering,
  New Jersey Institute of Technology, Newark, NJ, 2014

- Master of Science in Biomedical Engineering,
  New Jersey Institute of Technology, Newark, NJ, 2009

- Bachelor of Science in Bioengineering,
  University of Pittsburgh, Pittsburgh, PA, 2006

Major: Biomedical Engineering

Presentations:

Odle, B. M. (2012). Integrating Wheelchair Propulsion Research in a Lesson on Slope. *National Science Foundation GK12 Annual Meeting*, Washington, DC, March 16-18.

Odle, B. M., Forrest, G. F., Reinbolt, J., & Dyson-Hudson, T. A. (2011). Development of an OpenSim Shoulder Model for Manual Wheelchair Users with Tetraplegia. *Proceedings of the ASME 2011 International Mechanical Engineering Congress & Exposition,* Denver, CO, November 11-17.

Odle, B. M., Forrest, G. F., Reinbolt, J., & Dyson-Hudson, T. A. (2011). OpenSim Shoulder Model for Manual Wheelchair Users with Tetraplegia. *Hyper Summer School*, Salamanca, Spain, September 18-23.

Odle, B. M., Dyson-Hudson, T. A., & Forrest, G. F. (2011). Progress Towards the Development of a Computational Model of the Shoulder in Wheelchair Users with Tetraplegia. *Motor Control Summer School- VII*, Ligonier, PA, June 9-13.

Odle, B. M., Forrest, G. F., & Dyson-Hudson, T. A. (2011). Towards the Development of a Computational Model of the Shoulder in Wheelchair Users with Tetraplegia. *Alliance for Graduate Education and the Professoriate Science Fair (City University of New York Alliance): Inspiring the Next Generation of Scientists*, New York, NY, March 11.

Odle, B. M., Irving, A., & Foulds, R. A. (2009). Evaluating Interventions with an Adaptive Video Game Platform for Children with Cerebral Palsy. *Rehabilitation Engineering and Assistive Technology Society of North America Annual Conference*, New Orleans, LA, June 23-27.

Odle, B. M., Irving, A., & Foulds, R. A. (2009). Usability of an Adaptable Video Game Platform for Children with Cerebral Palsy. *Proceedings of the 35th Annual Northeast Bioengineering Conference at Harvard-MIT Division of Health Sciences and Technology*, Cambridge, MA, 73, April 3-5.

Odle, B. M., Swift, K. M., Irving, A., & Foulds, R. A. (2008). Usability of Training Students to Create Adaptive Video Games for Children with Orthopedic Disabilities. *Proceedings of the 34th Annual Northeast Bioengineering Conference at Brown University*, Providence, RI, pp 180-181, April 4-6.

Irving, A. & Odle, B. M. (2008). Development of an Adaptable Video Game Platform as a Novel Educational Experience for Children in the Field of Assistive Technology. *Proceedings of the 34th Annual Northeast Bioengineering Conference at Brown University*, Providence, RI, pp 115-116, April 4-6.

Koontz, A. M., Yarnall, M., Price, R., Odle, B., Sisto, S. A., & Boninger, M. L. (2007). Lateral Transfer Movement Strategies among Persons with Paraplegia. *Rehabilitation Engineering and Assistive Technology Society of North America*, Phoenix, AZ, June 15-19.

Odle, B., Yarnall, M., & Koontz, A. M. (2007). Upper Limb Joint Kinematics During a Wheelchair Transfer of Persons with Paraplegia. *Society of Hispanic Professional Engineers National Technical and Career Conference*, Denver, CO, January 10-13.

Dedicated to my mother, Harriett Diaz:
Mom, this journey has been just as much yours as it has been mine.

"I look up to the mountains- does my help come from there?
My help comes from the LORD, who made heaven and earth!
He will not let you stumble; the one who watches over you will not slumber.
Indeed, he who watches over Israel never slumbers or sleeps.
The LORD himself watches over you! The LORD stands beside you as your protective shade.
The sun will not harm you by day, nor the moon at night.
The LORD keeps you from all harm and watches over your life.
The LORD keeps watch over you as you come and go, both now and forever."

Psalm 121 NLT

ACKNOWLEDGMENT

First and foremost, I would like to thank my Dissertation Advisor, Dr. Trevor Dyson-Hudson, for his insight, support, and mentoring. Thank you, Dr. Gail Forrest, my Dissertation Co-advisor, for your support and mentoring. Dr. Jeff Reinbolt, thank you for all of your technical assistance and guidance with OpenSim. I would also like to thank Dr. Richard Foulds, Dr. Alicia Koontz, Dr. Sheldon Lin, and Dr. Bryan Pfister for their guidance. I would also like to thank my Academic Advisor, Dr. Sergei Adamovich.

I would like to thank the National Science Foundation Alliance for Graduate Education and the Professoriate, the Alfred P. Sloan Foundation, the Roothbert Fund, and the Alpha Kappa Alpha Educational Advancement Foundation for their generous funding to complete my dissertation research. The study was also funded by the New Jersey Commission on Spinal Cord Injury Research.

I would like to thank Misagh Mansouri and Kristin Morgan, of the Reinbolt Research Group, for their technical assistance with OpenSim and encouragement. I would also like to thank the Kessler Foundation. Special thanks to Jerome Allen, Dr. William Bauman, Chris Cirnigliaro, Venkata Gade, Andrew Kwarciak, Dr. Megan Mitchell, Daniel Pierce, Dr. Rakesh Pilkar, Arvind Ramanujam, Dr. Kevin Terry, and Mathew Yarossi for their technical assistance in the lab. Thank you, Jennifer Colombo, Natalia Ikheloa, and Milda Woods for your assistance.

Lastly, I want to thank my loving family and friends for their support. Special thanks to my mother Harriett, grandmother Mary, Dr. Karen Hare, Dr. Darnell Simon, Zara Williams, Clarisa Gonzalez-Lenahan and the Christ Church congregation for being my prayer warriors. Special thanks to Children's Ministry and Quest/YAM at Christ Church for their prayers and encouragement. Khady, Suwah, Laura, Kim and Ian- thanks for your friendship and words of encouragement! Thank you, Alaine Allen, for reminding me of my purpose!

TABLE OF CONTENTS

TABLE OF CONTENTS
(Continued)

Chapter **Page**

TABLE OF CONTENTS
(Continued)

TABLE OF CONTENTS
(Continued)

Chapter **Page**

LIST OF TABLES

LIST OF FIGURES

List of Figures

(Continued)

NOMENCLATURE

3D	Three-Dimensional
ANOVA	Analysis of Variance
CDRFPRC	Christopher and Dana Reeve Foundation Paralysis Resource Center
DOF	Degrees of Freedom
DXA	Dual Energy X-ray Absorptiometry
EMG	Electromyography
GUI	Graphical User Interface
ID	Inverse Dynamics
IK	Inverse Kinematics
ISNCSCI	International Standards for Neurological Classification of Spinal Cord Injury
Kessler	Kessler Foundation Research Center
MAE	Mean Absolute Error
MVC	Maximum Voluntary Contraction
NSCISC	National Spinal Cord Injury Statistical Center
RMS	Root Mean Square
ROI	Region of Interest
SCI	Spinal Cord Injury
Stanford VA Model	Upper Extremity Model (Holzbaur et al., 2005)

CHAPTER 1

INTRODUCTION

1.1 Objectives

The objectives of this dissertation are twofold: (i) construct a freely accessible, computer graphics-based, patient-specific, musculoskeletal model capable of generating dynamic simulations of wheelchair propulsion; and (ii) as proof of concept, investigate the individual contribution of the shoulder complex muscles to wheelchair propulsion using kinematic, kinetic, and fine-wire electromyography (EMG) data from an individual with spinal cord injury (SCI).

This novel model may serve as a valuable clinical tool and advance the identification of risk factors associated with manual wheelchair use and shoulder pain and injury. The construction and evaluation of such a model necessitates a better understanding of spinal cord injury, wheelchair propulsion biomechanics, and computer graphics-based modeling.

1.2 Spinal Cord Injury

There are approximating 273,000 persons with a SCI in the United States, with 12,000 new traumatic injuries each year (NSCISC, 2013). Results from a recent population-based survey suggest these numbers may be even higher, with 1.275 million people reporting paralysis as a result of spinal cord injury or disease (CDRFPRC, 2009).

Spinal cord injury occurs when there is damage to the neural elements within the spinal canal and can be caused by traumatic (e.g., motor vehicle crashes, falls, acts of violence, sports) or non-traumatic (e.g., cancer, vascular injury, transverse myelitis,

spinal stenosis) injuries. Damage to the neural elements in the cervical spine results in partial or complete loss of motor and/or sensory function in the upper limbs, as well as typically the trunk and the lower limbs—a condition termed *tetraplegia* (also known as *quadriplegia*). Damage to neural elements in the thoracic, lumbar, or sacral spine spare upper limb function, but depending on the level of the injury the trunk and lower limbs may be involved—this condition is termed *paraplegia* (ISNCSCI, 2012).

Spinal cord injury primarily affects younger individuals, with nearly half of all injuries occurring between the ages of 16 and 30 (NSCISC, 2013). Due to advances in medical care and rehabilitation, the estimated life expectancy of individuals with SCI is now closer to that of the general population (NSCISC, 2013). Although the survival rates have increased, individuals with SCI are at an increased risk for secondary medical complications associated with aging (Geisler et al., 1983; Gellman et al., 1988; Pentland & Twomey, 1991; Sie et al., 1992). One of these secondary medical complications is shoulder pain.

1.3 Shoulder Pain in Spinal Cord Injury

Disorders of the shoulder are among the most frequent causes of musculoskeletal pain and disability in individuals with SCI (Consortium of Spinal Cord Medicine, 2005; Dyson-Hudson & Kirshblum, 2004; Sie et al., 1992). Shoulder pain may be more common in individuals with tetraplegia. Sie et al. (1992) observed that 46% of subjects with tetraplegia compared to 36% of those with paraplegia reported shoulder pain. Curtis et al. (1999b) reported that 78% of those with tetraplegia compared to 59% of those with paraplegia reported shoulder pain since becoming wheelchair users, with 59% and 42% reporting current shoulder pain.

Due to lower limb paralysis and impaired function, many individuals with SCI rely on their upper limbs for mobility and other activities of daily living. They use manual wheelchairs to participate in their community and for mobility. The repeated performance of weight-bearing upper limb activities (e.g., wheelchair propulsion, transfer, weight shifts) places a great deal of stress on the bones, joints, soft tissues of the shoulder complex, placing these structures at significant risk for overuse and injury (Dyson-Hudson and Kirshblum, 2004). Chronic overuse associated with these repetitive forces occurring at the shoulder complex during wheelchair propulsion is a likely contributor to overuse injuries in individuals with SCI (Bayley et al., 1987; Consortium of Spinal Cord Medicine, 2005; Nichols et al., 1979; Pentland & Twomey, 1994). Nichols et al. (1979) were the first to report an association between chronic SCI and shoulder pain, coining the term "wheelchair users shoulder."

The shoulder is a joint of mobility, not stability, and exhibits the greatest amount of motion found in any joint in the human body (Wilk, 1997). The shoulder joint is actually a complex of four separate joints/articulations: the glenohumeral joint, the acromioclavicular joint, the sternoclavicular joint, and the scapulothoracic joint. The glenohumeral joint exhibits significant physiologic motion. However, only a few millimeters of humeral head actually come into contact with the glenoid fossa at any given time; therefore, stabilization of the humeral head within the glenoid is accomplished through the combined efforts of the ligamentous structures and the surrounding shoulder musculature. The stabilizers of the shoulder may be divided into passive stabilizers (bony architecture, ligamentous structures) and active stabilizers (the neuromuscular system). The primary active stabilizers of the glenohumeral joint consist

of the rotator cuff muscles (supraspinatus, infraspinatus, subscapularis, and teres minor), the deltoid, and the long head of the biceps muscle, with the teres major, the latissimus dorsi, and the pectoralis major muscles functioning as secondary stabilizers (Figure 1.1). These muscles act together to provide movement of the arm (Table 1.1), while at the same time stabilizing the shoulder joint during these dynamic activities (Wilk, 1997).

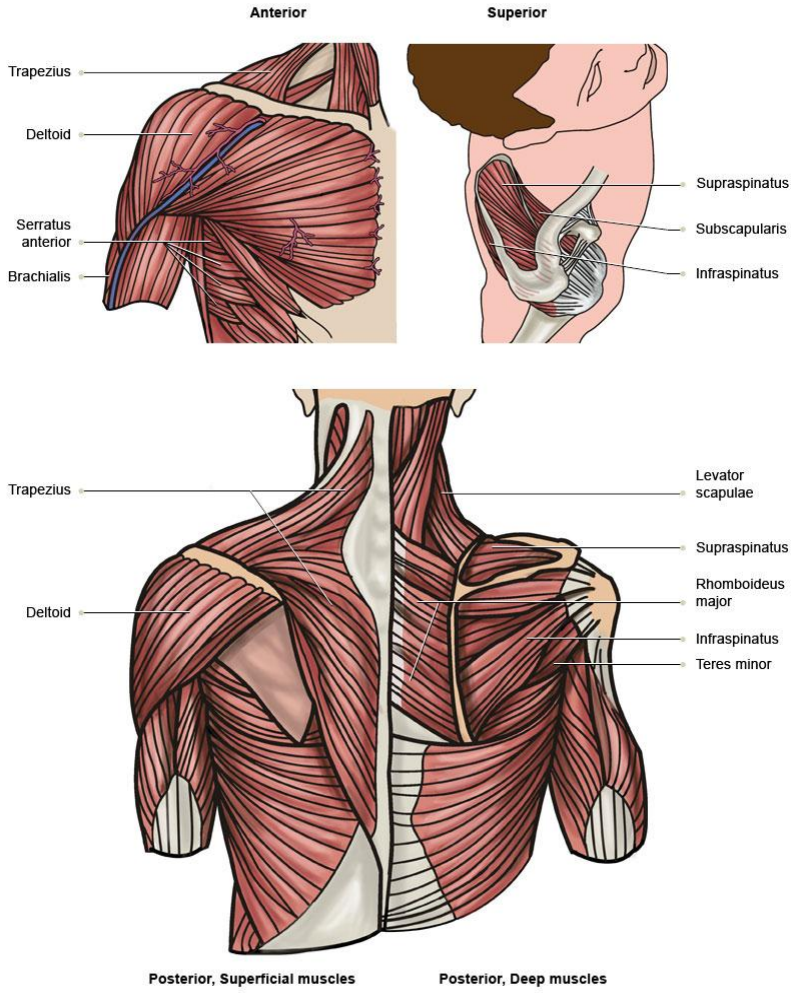

Figure 1.1 Primary and secondary active stabilizers of the glenohumeral joint. The muscles of the shoulder complex are presented in anterior, superior, and posterior views.

Source: http://author.webset-lms.com/repository/4984/a642f33a-4010-4458-9486-0e1ec12ddb16.jpg accessed Feburary 9, 2013.

Table 1.1 Muscles of the Shoulder, their Spinal Cord Level(s) and Action(s)

Muscle	Spinal Level(s)	Action(s)
Scapulohumeral Muscles		
Deltoid: Anterior Deltoid	C5, 6	shoulder flexion
Deltoid: Middle Deltoid	C5, 6	shoulder flexion, abduction
Deltoid: Posterior Deltoid	C5, 6	shoulder abduction, extension
Rotator Cuff: Supraspinatus	C5, 6	shoulder abduction
Rotator Cuff: Infraspinatus	C5, 6	shoulder external rotation
Rotator Cuff: Teres minor	C5, 6	shoulder external rotation
Rotator Cuff: Subscapularis	C5, 6	shoulder internal rotation
Teres major	C5, 6	shoulder adduction, internal rotation, extension
Axioscapular Muscles		
Serratus anterior	C5, 6, 7	scapular protraction, upward rotation
Trapezius	Cranial Nerve XI	scapular elevation, retraction, rotation
Rhomboids	C5	scapular retraction
Levator scapula	C5	scapular elevation
Axiohumeral Muscles		
Clavicular portion of Pectoralis major	C5, 6	shoulder flexion, adduction, internal rotation
Sternal portion of Pectoralis major	C7, 8, T1	shoulder adduction, internal rotation
Pectoralis minor	C8, T1	scapular protraction
Latissimus dorsi	C6, 7, 8	shoulder adduction, extension, internal rotation
Upper Arm Muscles		
Biceps brachii	C5, 6	elbow flexion, shoulder flexion
Triceps brachii	C6, 7, 8	elbow extension, shoulder adduction

Source: Adapted with permission from Dyson-Hudson and Kirshblum, Shoulder pain in chronic spinal cord injury, part I: Epidemiology, etiology, and pathomechanics, *Journal of Spinal Cord Medicine* 2004; 27:4-17. ©The Academy of Spinal Cord Injury Professionals, Inc.

Due to impairment of the cervical myotomes, shoulder muscle imbalances and/or weakness may be more pronounced in individuals with tetraplegia (Curtis et al., 1999a; Powers et al., 1994). Partial innervation and impaired balance of shoulder, scapular, and thoracohumeral muscles may place individuals with tetraplegia at higher risk for developing shoulder pain, especially during weight-bearing upper limb activities like wheelchair propulsion, transfers, and pressure reliefs (Curtis et al., 1999a; Curtis et al., 1999b; Kulig et al., 2001; Mulroy et al., 1996; Powers et al., 1994; Reyes et al., 1995).

Due to impaired abdominal-thoracic musculature, individuals with lower cervical-level (C5 – C8) injuries often assume a "C"-shaped kyphotic trunk position for stability (Hobson & Tooms, 1992; Minkel, 2000). This position, which results in excessive scapular protraction, can lead to further overstretching and weakening of the scapular retractors (middle trapezius and rhomboids) (Curtis et al., 1999a; Burnham et al., 1995).

It has been established that shoulder pain in manual wheelchair users with SCI is a clinical problem, especially in individuals with tetraplegia. In an effort to understand the relationship between manual wheelchair propulsion and shoulder pain and injury in SCI, this clinical problem sparked research interest in the optimization of wheelchair set-up, wheelchair propulsion style, and wheelchair propulsion mechanics. Current clinical practice guidelines on preserving upper limb function in persons with SCI stress the importance of minimizing frequency and force during manual wheelchair propulsion and also recommend that manual wheelchair users avoid potentially injurious or extreme positions at the shoulder, including extreme internal rotation and abduction (Consortium for Spinal Cord Medicine, 2005). A prerequisite to the scientific approach toward optimization of wheelchair propulsion involves a biomechanical analysis of wheelchair propulsion (Cerquiglini et al., 1981).

1.4 Wheelchair Propulsion Biomechanics

In an effort to gain a better understanding of the relationship between manual wheelchair propulsion and shoulder pain and injury in SCI, researchers and clinicians conducted biomechanical analyses of wheelchair propulsion. Research experiments were conducted in laboratory settings due to the specialized equipment needed for the studies. Although these laboratory settings facilitated data collection for the researchers, they were artificial

representations of the environments manual wheelchair users encounter in real life. Therefore, researchers made great strides to ensure that their experimental setup reproduced conditions of wheelchair propulsion as closely as possible to real life.

Wheelchair propulsion is typically described as two phases of hand and arm movement: the propulsive phase and the recovery phase. During the propulsive (push) phase, the individual's hands are in contact with the pushrim of the wheelchair and there is special application of force to that rim in order to increase or maintain velocity of the wheelchair. The recovery phase occurs after the propulsive phase and it is during this phase that the arms are brought back to a position where a new propulsive phase can begin (Sanderson & Sommer, 1985). These definitions allowed researchers to compare findings during the push phase with those of the recovery phase. The results of these biomechanical analyses concluded with the identification of modifiable risk factors, which would hopefully aid in the development of prevention and treatment interventions.

In order to understand motion of the shoulder during wheelchair propulsion, researchers investigated kinematics. Cerquiglini et al. (1981) found that a single plane analysis of wheelchair propulsion was insufficient. They conducted a three-dimensional (3D) kinematics analysis of the upper limb during wheelchair propulsion and determined that the shoulder joint exhibits the largest displacement. In order to further understand the significant arcs of motion that occur in all three planes of motion, other researchers investigated 3D shoulder kinematics during wheelchair propulsion. Reflective markers were placed on the anatomical landmarks of the trunk and upper limb and the location of these markers in 3D space were tracked throughout propulsion. Researchers used coordinate systems to determine the joint angles for the shoulder, elbow, wrist, and trunk.

However, a standard sequence for coordinate systems did not exist, so individual researchers chose their own sequence (Xu et al., 2012). For example, Cerquiglini et al. (1981) based their calculations on methods used in gait studies presented by Cappozzo et al. (1975; 1978). Newsam et al. (1999) used a data analysis technique based on a 3D global coordinate system where the glenohumeral joint was the center of an imaginary globe. Veeger et al. (1997) and Cooper et al. (1999) described shoulder kinematics with three Euler angle rotations of the humerus relative to the reference frame of the thorax. This selection of different coordinate systems resulted in difficulties in making comparisons across studies (Collinger et al., 2008; Wu et al., 2005). To promote better communication between clinicians and researchers, the Standardization and Terminology Committee of the International Society of Biomechanics (ISB) proposed a joint coordinate system for the shoulder, elbow, wrist, and hand (Wu et al., 2005).

In order to understand the forces and moments generated at the shoulder during wheelchair propulsion, researchers investigated 3D shoulder kinetics. Kulig et al. (1998) used an instrumented wheel, reflective markers, a standard wheelchair, and a wheelchair ergometer to study free, fast, and inclined wheelchair propulsion. They found increased shoulder joint loads during fast and inclined propulsion. They suggested that these increased loads may lead to compression of subacromial structures against the overlying acromion. Expanding upon their work, Koontz et al. (2002) investigated shoulder kinematics and kinetics during slow and fast speeds of wheelchair propulsion. Their experimental setup entailed instrumented pushrims, reflective markers and each study participant's wheelchair on a dynamometer. The authors reported that the net joint forces and moments were higher when the shoulder was near its end range of motion on the

pushrim. They also reported that the shoulder was placed in a more compromised position during the fast propulsion speed.

Although these studies greatly contributed to the wheelchair propulsion biomechanics community, researchers also encountered difficulties with comparing shoulder kinetics results across studies due to differences in experimental setup and testing conditions (Cooper et al., 1999; Finley et al., 2004; Koontz et al., 2002; Kulig et al., 1998; Mulroy et al., 2005). Moreover, there was no standard coordinate system for reporting shoulder joint kinetics, so researchers used different coordinate systems (Cooper et al., 1999; Finley et al., 2004; Koontz et al., 2002). The ISB coordinate system was only for kinematic studies (Collinger et al., 2008; Wu et al., 2005). Recently, Morrow et al. (2009) and Desroches et al. (2010) explored expressions for upper limb joint kinetics during wheelchair propulsion.

Using the standardized ISB joint coordinate system and recognizing the inconsistencies in experimental setup and design across previous studies, Collinger et al. (2008) conducted a multisite study of persons with paraplegia to investigate shoulder biomechanics during the push phase of propulsion. They analyzed shoulder kinematics and kinetics at two different speeds during wheelchair propulsion. Even though they reported shoulder kinematics in terms of the ISB standards, they recognized that there were no standards for reporting shoulder joint loading. Therefore, they used the same local coordinate systems for both kinematic and kinetic analyses. Due to the design of the multisite study (three biomechanics laboratories at research institutions: 61 study participants), they were also able to investigate the effect of pain and participant demographics on propulsion. Their findings suggested that body weight was the primary

factor that affected shoulder forces. They also observed peak shoulder joint loading when the arm is extended and internally rotated, suggesting that this positon may be injurious to the shoulder (Collinger et al., 2008).

While some researchers were investigating shoulder kinematics and kinetics, others were investigating EMG to understand upper limb muscle recruitment patterns during wheelchair propulsion. Early studies by Cerquiglini et al. (1981) and Harburn and Spaulding (1986) used surface EMG to investigate muscle activity during wheelchair propulsion. However, the surface EMG technique was limited to recording the activity of the superficial shoulder muscles (Figure 1.1) because electrodes were placed on the surface of the skin. Another disadvantage of this technique is that the quality of the signal is impaired due to electrode positioning, movement artifact, and adipose tissue. Mulroy et al. (1996; 2004) improved upon these previous studies by performing fine-wire EMG. The fine-wire EMG technique can be used to record the activity of deep muscles (Figure 1.1) because small needles are inserted directly into the muscle belly. Mulroy et al. (1996) found that the pectoralis major, supraspinatus, middle and posterior deltoids, subscapularis, and middle trapezius were most vulnerable to fatigue in individuals with paraplegia and recommended endurance training. To further expand upon their work, Mulroy et al. (2004) investigated shoulder complex muscle activity in manual wheelchair users with paraplegia and tetraplegia. The authors indicated that the middle trapezius and serratus anterior are active during wheelchair propulsion. Their studies suggest that the pectoralis major, supraspinatus, middle and posterior deltoids, subscapularis, middle trapezius, and serratus anterior have important roles in wheelchair propulsion.

Although the integration of kinematics and kinetics provided a better understanding of the relationship between wheelchair propulsion and shoulder pain in SCI, researchers understood the importance of the findings from EMG studies and recognized the need to investigate kinematics, kinetics, and EMG simultaneously. A comprehensive analysis of kinematics, kinetics, and EMG in wheelchair propulsion studies would provide a complete understanding of the relationship between wheelchair propulsion and shoulder pain in SCI. Cerquiglini et al. (1981) were the first to combine kinematics, kinetics, and EMG (in addition to electrocardiographic tracings, blood pressure estimations, oxygen consumption and pulmonary ventilation) to provide a method for describing upper limb biomechanics during wheelchair propulsion. However, they used an instrumented wheelchair that was propelled by a cranking arm, as opposed to the more conventional pushrim. Indeed, the pushrim style wheelchair is the most commonly used wheelchair in individuals with mobility impairment such as SCI, and therefore, warranted investigation (Sanderson & Sommers, 1985). Expanding upon this work, Dubowsky and colleagues (2009) were able to integrate kinematics, kinetics, and EMG with an individual's own conventional pushrim style wheelchair to investigate the demands on the shoulder during wheelchair propulsion. The purpose of their study was to simultaneously compare pushrim forces, upper limb kinematics, and shoulder EMG during wheelchair propulsion in wheelchair users with paraplegia to able-bodied controls. They hypothesized that the results of an integrated approach would be sensitive enough to distinguish the two study groups based on kinematics, kinetics, and EMG profiles. By simultaneously collecting, quantifying and comparing kinematics, kinetics, and EMG, the authors were able to make comprehensive interpretations about shoulder motion during

propulsion with respect to maximum voluntary contraction (MVC), they found that individuals with paraplegia used a greater percentage of their posterior deltoids, biceps, and triceps. The individuals with paraplegia also reached a peak anterior deltoid firing almost 10° earlier on the pushrim, while reaching peak posterior deltoid firing almost 10° later on the pushrim. The authors also noted that the able-bodied controls had no triceps activity in the early stages of propulsion while the individuals with paraplegia demonstrated triceps activity throughout propulsion. The EMG data were further analyzed by the computation of "muscle energy"- the percentage of EMG throughout propulsion. The authors also determined that greater muscle energy resulted in a greater resultant joint force in the shoulder and elbow. They suggested that this greater muscle energy may result in shoulder pathology. They also concluded that greater muscle energy may result in fatigue and contribute to shoulder pain and pathology over time.

The experimental data from Dubowsky et al. (2009) also had another purpose. Data from this study were used as inputs to a patient-specific computer graphics-based model that was capable of calculating *in vivo* shoulder joint contact forces (Dubowsky et al., 2008; Sullivan et al., 2007). A limitation to the previously described biomechanical techniques was that they did not allow for the determination of *in vivo* shoulder joint contact forces or shoulder muscle forces. Dubowsky and colleagues ultimately intended to compare the differences in computed joint forces (Dubowsky et al., 2008) with the differences they found in their experimental study (Dubowsky et al., 2009). Their rationale for determining *in vivo* muscle forces was that the muscle forces influenced the shoulder joint forces, which may result in shoulder pain and pathology (Dubowsky et al., 2009). Therefore, this allows for investigations of understanding the shoulder muscle

forces generated during propulsion and how to adjust those forces to minimize the shoulder joint contact forces, and potentially prescribe interventions to address shoulder pain in manual wheelchair users with SCI.

1.5 Computer Graphics-based Musculoskeletal Models

The work of Dubowsky et al. (2009) highlighted a limitation of the experimental wheelchair propulsion biomechanics studies-- the inability to determine *in vivo* joint contact forces in the absence of invasive means. Also, there is no way to directly measure muscle forces *in vivo* (Correa et al., 2011; Dubowsky et al., 2008; Erdemir et al., 2007; Nikooyan et al., 2010). Dubowsky et al. (2009) realized the significance of determining *in vivo* muscle forces: the differences in muscle forces are responsible for increasing shoulder joint forces, which may result in shoulder pain or pathology. Computer graphics-based models are able to estimate muscle and joint contact forces with inverse dynamics-based optimization, dynamic optimization, and EMG-driven modeling (Correa et al., 2011; Erdemir et al., 2003; Lloyd & Besier, 2003; Pandy & Andriacchi 2010; Zajac, 1993). Another limitation of experimental biomechanics analyses is the inability to establish cause and effect relationships in complex dynamic systems (Delp et al., 2007; Seth et al., 2011). Thus, determining the functions of muscles from experiments is not straightforward (Delp et al., 2007). Computer graphics-based models can also be used for "what if?" studies, like changing the excitation pattern of a muscle and observing the resulting motion (Delp et al., 2007; Reinbolt et al., 2011).

Muscle-actuated dynamic simulations are becoming a viable approach for determining how the elements of the musculoskeletal system interact to produce movement (Seth et al., 2011), especially for investigations of the upper limb. Given the

complexity of the shoulder and its multiple degrees of freedom, the shoulder is a challenging joint to model. There are few existing shoulder models that have been developed with the complexity to simulate realistic movement of the shoulder. These include the Swedish shoulder model (Hogfors et al., 1991; Karlsson & Peterson, 1992), the Newcastle Model (Charlton & Johnson, 2006), the shoulder part of the AnyBody modeling system (Damsgaard et al., 2006), the Delft Shoulder and Elbow Model (van der Helm, 1994), and the SIMM Upper Extremity Model (Holzbaur et al., 2005).

As indicated by the work of Dubowsky et al. (2009), computer graphics-based modeling of the shoulder is the next step in identifying modifiable risk factors from wheelchair propulsion biomechanics data. Of the models previously listed, the Delft Shoulder and Elbow Model (van Drongelen et al., 2005a; 2005b; 2011; Veeger et al., 2002), the shoulder part of the AnyBody model (Dubowsky et al., 2008; Sullivan et al., 2007), and the SIMM Upper Extremity Model (Morrow et al., 2010; Rankin et al., 2010; 2011) were investigated for wheelchair propulsion applications. Early shoulder models such as the Dutch Shoulder and Elbow Model (van der Helm, 1994; van Drongelen et al., 2005a; 2005b; 2011; Veeger et al., 2002) were used to investigate shoulder load and muscle forces generated by manual wheelchair users with SCI and able-bodied controls. However, the model could not be individualized to the individuals with SCI investigated, as they were not "patient-specific models" (i.e., models that are tailored to the individual).

Patient-specific models may be used as clinical tools, enhancing the recommendations made by wheelchair propulsion biomechanics studies. Treatments for individuals with mobility impairments are standard, with a "one size fits all approach".

However, for manual wheelchair users with SCI, that approach is inadequate (Fregly et al., 2012). Patient-specific models are personalized, so they may be used to assess the effectiveness of a treatment, identify individuals that can be treated with particular interventions, and predict which treatment should be performed on a patient and how it should be performed (Fregly et al., 2012).

Dubowsky et al. (2008; Sullivan et al., 2005; 2007) were the first to develop a patient-specific model for manual wheelchair propulsion. The three dimensional model was developed using AnyBody (AnyBody Technology A/S, Aalborg, Denmark) software, which allowed for patient-specificity by altering the properties of the rigid-bone geometries and the muscle geometries. The model was used to investigate the minimization of forces at the shoulder. The significance of using a computational model to minimize shoulder joint contact forces was to address the kinetic studies that reported high joint loading at the shoulder. Moreover, by having a systematic integration of biomechanical data available, Dubowsky et al. (2009) were able to conclude that the muscle activity differences between the participant groups studied may be due to the kinematic and kinetic differences between the two groups. Inputting these data in their model would allow them to understand how differences in kinematics and kinetics influenced *in vivo* muscle activity. An inverse dynamics-based approach was utilized to estimate shoulder joint contact forces during wheelchair propulsion. AnyBody's min/max objective function was used with the inverse dynamics-based optimization. The model was validated with kinematic, kinetic, and surface EMG data from two participants with paraplegia one able-bodied control (Dubowsky et al., 2008). Participants were asked to propel at a self-selected speed and data was collected for ten consecutive push strokes.

Dubowsky et al. (2008) used a mean absolute error (MAE) analysis to compare computed muscle forces with experimental EMG. The (bilateral) muscles included in the analysis were: anterior deltoid, middle deltoid, posterior deltoid, pectoralis major, trapezius, biceps, and triceps. The mean MAE for each participant demonstrated a good correlation (0.137 – 0.193). The mean MAE across all investigated muscles and participants also demonstrated a good correlation (0.165). The mean MAE for all three participants for each muscle demonstrated a good correlation, with the exception of the triceps (0.389 and 0.369 for left and right triceps, respectively). Since the mean MAE across participants and muscles demonstrated a good correlation, the authors determined that their model could be used to analyze shoulder joint forces during propulsion (Dubowsky et al., 2008). They also suggested that the model may serve as a prescriptive tool in determining axle placement for newly injured patients or may be used in an intervention to address shoulder pain relief. However, the model was constructed with AnyBody software, which is not free. AnyBody also has limited tools for extracting meaningful information from simulations, as it does not allow for muscle activation dynamics or forward dynamics. Lastly, full access to source code was not provided, making it difficult for other biomechanics researchers to extend their capabilities (Delp et al., 2007).

Morrow et al. (2010) expanded upon this work by using the three dimensional SIMM Upper Extremity Model (Stanford VA Model) to investigate shoulder joint contact forces during different wheelchair activities (e.g., level propulsion, ramp propulsion, and weight relief lifts). The significance of this model is that it was freely available, unlike the AnyBody model described above. The purpose of using a model for such an analysis was to determine the shoulder joint contact forces during various wheelchair activities

and potentially address the relative risk of each activity to the shoulder impingement. The model was validated with kinematic, kinetic, and surface EMG data collected from twelve manual wheelchair users. Morrow used SIMM software (Software for Interactive Musculoskeletal Modeling, Musculographics, Inc., Santa Rosa, CA) to include patient-specificity based on reflective marker locations and patient body mass. The static optimization approach (inverse dynamics-based approach) was used to determine joint contact forces during the wheelchair activities. The object functions evaluated with the static optimization included a linear minimization of muscle activation (Kaufman et al., 1991), minimax stress formulation minimizing the maximum muscle stress (An et al., 1984), and non linear minimization of the sum of muscle stress cubed (Lin et al., 2004). Shoulder muscle forces were also validated with a MAE analysis. The shoulder muscles included in the analysis included the right anterior deltoid, middle deltoid, posterior deltoid, pectoralis major, latissimus dorsi, biceps, and triceps. The MAE values across all subjects and muscles demonstrated a good correlation for each objective function evaluated: 0.11 (linear), 0.11 (minimax stress), and 0.10 (nonlinear). The computed peak shoulder force during level propulsion was similar to the computed peak shoulder force of Lin et al.'s (2004) model. Their study revealed that the peak forces generated were greatest during ramp propulsion and weight relief lifting and the least during level propulsion. Therefore, they suggested that ramp propulsion and weight relief lifting may have a greater potential to cause shoulder injury. Even though their study computed lower shoulder joint contact forces during level propulsion, Morrow et al. (2010) noted this observation in relation to the impingement risk of level propulsion is inconclusive due to the frequency with which propulsion is performed. Nonetheless, their work was

important because they demonstrated that a patient-specific model could be used to determine shoulder joint contact forces during wheelchair activities and may be able to address the potential impingement risk associated with each activity.

Rankin et al. (2010; 2011) were the first to use the Stanford VA Model to generate forward dynamic simulations of wheelchair propulsion. Building upon the work of Morrow et al. (2020), Rankin et al. (2010; 2011) incorporated trunk lean in the model and constrained hand translation to follow the circular path of the pushrim. They used the model to investigate the influence of push force effectiveness on upper limb demand during wheelchair propulsion (Rankin et al., 2010). The significance of the simulation study was to investigate the relationship between fraction of effective force and upper limb demand. The clinical significance of this is the incidence of shoulder pain and injury, which may be a result of the high loading at the shoulder and low mechanical efficiency (i.e., ratio of external work to metabolic cost) of wheelchair propulsion (Finley et al., 2004; Mercer et al., 2006).

Boninger et al. (1997) found that manual wheelchair users generate non-tangential handrim forces that do not contribute to the forward acceleration of the wheelchair, which resulted in an inefficient use of generated muscle force. To quantify force effectiveness during a push, previous studies (Boninger et al., 1999; Dallmeijer et al., 1998; Lin et al., 2009) used the ratio of tangential to total handrim force (fraction of effective force) and found mean values between 0.26 and 0.81 (a value of 1.0 represents an entirely tangential force). Therefore, the redirection of the handrim force in a more tangential direction might improve mechanical efficiency and reduce the overall demand on the upper limb (Rankin et al., 2010). Clinical significance of the application of fraction of effective

force was manifested by the development of training programs (de Groot et al., 2002; Kotajarvi et al., 2006), guides to modify wheelchair propulsion (Aissaoui et al., 2002; Guo et al., 2006), and comparison of propulsion techniques (Boninger et al., 2002; Goosey-Tolfrey et al., 2006).

To expand upon this work, Rankin et al. (2010) used the modified SIMM model to investigate whether there was a relationship between fraction effective force and upper limb demand during the push phase of propulsion. Specifically, they used forward dynamics to quantify individual muscle stress, work and handrim force contributions at different values of fraction of effective force. Kinematic, kinetic, and surface EMG data were collected from a manual wheelchair user with paraplegia. Three optimizations were performed using a global optimization algorithm in their study. These forward dynamic simulations included: a simulation of the push phase and a maximization and minimization of fraction of effective force over the push phase while minimizing differences between the experimental joint kinematics and tangential handrim force. In the first simulation, the global optimization used an optimal tracking objective function to identify muscle excitation patterns that minimized the difference between simulated and experimental push phase data. Three consecutive push strokes were simulated for each optimization and minimum, maximum, and average fraction of effective force values were determined. Muscle stress was calculated as a percentage of maximum isometric force generated by each muscle at every time step. The simulations involving the minimizing and maximizing of fraction of effective force resulted in greater mean muscle stresses (23% and 112%) and total muscle work (28% and 71%) compared to the nominal fraction of effective force simulation (Rankin et al., 2010). The authors also observed

that the maximum fraction of effective force simulation shifted muscle use from the muscles crossing the elbow to those crossing the shoulder (e.g., rotator cuff muscles), which placed a greater demand on the shoulder muscles during propulsion (Rankin et al., 2010).

Rankin et al. (2011) also used the same model to investigate individual contribution of shoulder muscles to wheelchair propulsion. Specifically, they used forward dynamics to quantify how muscles deliver, absorb and/or transfer mechanical power during propulsion. The purpose of the study was to identify individual muscle contributions to mechanical energetics of wheelchair propulsion, as a means of understanding how the individual shoulder muscles work together to meet the mechanical demands of wheelchair propulsion. The clinical relevance of this study is based on the role muscle energetics play in the design of training techniques that help reduce upper limb demand during propulsion and improve rehabilitation outcomes. Kinematic, kinetic, and surface EMG data were collected from twelve manual wheelchair users as they propelled their wheelchair on a motor-driven treadmill at a self-selected overground speed for 30 seconds. The data were group-averaged to provide a comprehensive understanding of individual shoulder muscle contribution to wheelchair propulsion. Using a global optimization algorithm, they were able to identify muscle excitation patterns that minimized the difference between simulated and group-averaged propulsion data using an optimal tracking objective function. Muscle contributions to wheelchair propulsion were analyzed for the push phase and recovery phase of propulsion. The simulations determined that the shoulder flexors contributed the most to push phase and that the shoulder extensors contributed the most to recovery phase. The authors also

observed significant shoulder muscle activity during the transition from push to recovery, which presented as increased co-contraction and upper limb demand. Therefore, they suggested that strengthening the shoulder flexors and adopting propulsion techniques that improve transition mechanics may reduce upper limb demand and improve rehabilitation outcomes.

Although the work of Morrow et al. (2010) and Rankin et al. (2010; 2011) advanced wheelchair propulsion biomechanics, the musculature of their models are limited. The Stanford VA Model does not include the following deep shoulder muscles: upper and middle trapezius, serratus anterior, and rhomboids major. Investigations of muscle activity during wheelchair propulsion utilizing fine-wire EMG have indicated that the middle trapezius and serratus anterior are active during wheelchair propulsion (Mulroy et al., 2004). Therefore, it is imperative that these muscles are included in computer graphics-based models of wheelchair propulsion. Not only will the inclusion of these muscles provide a more complete visual representation of upper limb musculature, but a more complete analysis of upper limb muscle contribution to manual wheelchair propulsion in SCI will be obtained.

1.6 Research Direction

This dissertation aims to expand on the computational modeling work of Morrow et al. (2010) and Rankin et al. (2010; 2011) by constructing a freely accessible, computer graphics-based, patient-specific, musculoskeletal model of the shoulder complex that is capable of generating dynamic simulations of wheelchair propulsion (Wheelchair Propulsion Model). A major limitation to the models used by Morrow et al. (2010) and Rankin et al. (2010; 2011) is that they did not account for all of the muscles of the

shoulder complex. The fine-wire EMG studies of Mulroy et al. (1996; 2004) reveal that the serratus anterior, rhomboids major, and upper and middle trapezius have important roles in wheelchair propulsion. Therefore, these muscles will be included in the Wheelchair Propulsion Model.

The model will be constructed and evaluated by using OpenSim (Delp et al., 2007; Seth et al., 2011), a freely accessible modeling framework with patient-specific modeling capabilities for investigating dynamic simulations of movement. By using OpenSim to construct the model, it can be contributed to the OpenSim user community, thus making it freely accessible to other wheelchair biomechanics researchers. This will allow other researchers to access and modify the model to advance the field of wheelchair propulsion biomechanics. The advantage in constructing the model with OpenSim is that OpenSim provides a "common language" for clinicians and engineers, just as the ISB standards provided researchers with a standard coordinate system for the upper limb. This is how the framework allows for the construction, exchange, modification, and implementation of musculoskeletal model. Once contributed, the Wheelchair Propulsion Model can be accessed and modified by other researchers to better answer their research questions. This prevents wheelchair biomechanists from having to "reinvent the wheel" by constructing a new wheelchair propulsion model. The framework allows for patient-specificity by scaling the model to the height of the study participant while preserving the mass distribution of the participant (based on the participant's total weight).

The long-term goal is for the Wheelchair Propulsion Model to be used as a clinical tool. This dissertation is an initial step towards completing this goal. In order to evaluate the model's potential as a clinical tool, it must be evaluated with biomechanical

data obtained from a manual wheelchair user with SCI. Very few models have been evaluated with data from manual wheelchair users with tetraplegia (Rankin et al., 2011; van Drongelen et al., 2005a; 2005b; 2011). However, van Drongelen et al. (2005a; 2005b; 2011) did not use a patient-specific model nor did they publish the computed shoulder muscle forces for manual wheelchair users with tetraplegia (van Drongelen et al., 2005a). The review of experimental wheelchair propulsion biomechanics techniques revealed that the systematic collection, quantification, and comparison of kinematics, kinetics, and EMG provide an integrated approach to addressing shoulder motion during propulsion. Thus, this dissertation will expand on the traditional experimental biomechanical technique studies and the work of Dubowsky et al. (2009) by incorporating historical kinematic, kinetic, and fine-wire EMG data from a manual wheelchair user with tetraplegia in the model as a proof of concept study.

The work of Dubowsky et al. (2009) not only highlights the importance of kinematics, kinetics, and EMG in wheelchair propulsion studies, but also the significance of these data in understanding shoulder muscle forces. Their work highlights the importance of determining *in vivo* shoulder muscle forces by stating that differences in shoulder muscle forces increase shoulder joint forces, which may result in shoulder pain and pathology in manual wheelchair users. The focus of the proof of concept study is to provide insight on shoulder complex muscle contribution in manual wheelchair users with tetraplegia, which has not been addressed in the literature. Since this population has not been studied in the literature, it is most important to first understand shoulder complex muscle contribution to propulsion in this population. The next step, which will be addressed in future work, will be to use the model to determine shoulder joint contact

forces during propulsion. Thus, an investigation of the shoulder joint contact forces in this population, coupled with an investigation of the influence the shoulder muscle forces have on the shoulder joint contact forces, will provide the foundation of an investigation of minimizing shoulder joint forces in this population. Ultimately, this may lead to prescriptive interventions that could potentially address shoulder pain and pathology in manual wheelchair users with SCI.

In order to generate dynamic simulations of wheelchair propulsion, previous models estimated body segment mass and moment of inertia from studies on cadavers (Clauser et al., 1969; Dempster, 1955; Veeger et al., 1991). These cadaver studies were designed to determine anthropometrics for able-bodied populations. However, there are known changes in body composition that occur after a SCI, including muscle atrophy, loss of lean tissue mass and gain in body fat (Gater & Clasey, 2006; Gorgey et al., 2007; 2012; Jones et al., 1998; Spungen et al., 1995; 2000; 2003). Given these changes in body composition, this dissertation also explores the appropriateness of using the cadaver-based measures in a patient-specific model for manual wheelchair users with SCI. Specifically, the cadaver-based mass proportions for the right arm and trunk are compared with dual energy x-ray absorptiometry-based mass proportions for the right arm and trunk for non ambulatory manual wheelchair users with paraplegia and tetraplegia. Since patient-specificity is achieved by accounting for the patient's height and mass distribution, accurate masses for individuals with SCI need to be investigated. No previous studies have investigated SCI-specific anthropometrics based on dual energy x-ray absorptiometry. Moreover, the masses are also important for the inverse dynamics calculations. Therefore, an error in the masses used to generate the patient-specific

model will only be propagated throughout the rest of the computations generated by the model.

OpenSim simulations that will be used with the model include inverse kinematics and inverse dynamics. In order to determine muscle forces, either an inverse dynamics-based approach or a forwards dynamics-based approach is required. In addition to selecting an optimization approach, an objective (cost) function is also required. The muscle forces are determined by using Newton's equations of motion. However, there are more muscles than equations, so the problem is over-determined. Thus, the redundancy introduced in solving the muscular load sharing problem is addressed by minimizing an objective function. OpenSim provides three methods for determining the contribution of individual muscle forces to movement: static optimization, dynamic optimization and computed muscle control. Each approach as well as its advantages and disadvantages will be discussed in greater detail below.

Static optimization is an inverse dynamics-based approach and has been widely used with computer graphics-based models for gait studies. Recently, the optimization approach has been used with computer graphics-based models of wheelchair propulsion to determine *in vivo* shoulder joint contact forces and shoulder muscle forces (Dubowskly et al., 2008; Lin et al., 2004; Morrow et al., 2010; Sullivan et al., 2005; Sullivan et al., 2007; van Drongelen et al., 2005a; van Drongelen et al., 2005b). The main reason for the prevalence of static optimization studies in manual wheelchair propulsion may be that optimization approach is computationally efficient (Anderson & Pandy, 2001; de Zee et al., 2007; Erdemir et al., 2007; Lin et al., 2004; van Drongelen et al., 2005a). Computational expense is traditionally measured in terms of the computational

processing time needed to solve the optimization problem. Another reason for the prevalence of static optimization in these studies may be due to availability of joint kinematics data (Erdemir et al., 2007) and forces at the hand determined pushrim kinetic data following an analysis of manual wheelchair propulsion. With this approach, an objective function is used to address the redundancy introduced by solving the muscular load sharing problem. However, there are several disadvantages to the approach. One disadvantage is that the inverse dynamics-based technique is highly dependent on the accurate collection and processing of experimental kinematics (Davy & Audu, 1987; Patriarco et al., 1981). Another disadvantage is that the time-independent nature of the approach makes it relatively difficult to incorporate muscle physiology properly (Anderson & Pandy, 2001). Another disadvantage is that its time-independence of the objective function required by the approach may not permit the objectives of the motor task to be properly characterized (Hardt, 1978; Pandy et al., 1995). A final disadvantage of static optimization is that analyses based on inverse dynamics may not be appropriate for explaining muscle coordination principles (Kautz et al., 2000; Zajac, 1993). Nonetheless, static optimization is a popular approach and its small computational expense typically enables researchers to perform sensitivity analyses with their studies (Erdemir et al., 2007).

Dynamic optimization is a forward dynamics-based approach and is not subject to the criticisms of static optimization; therefore, it has the potential to offer a more powerful understanding of movement (Anderson & Pandy, 2001). Instead of solving the inverse dynamics problem, this approach involves inputting an initial set of muscle activations into a forward dynamics computer graphics-based musculoskeletal model.

The solution to the problem is compared against experimental data and the process is iterated by updating the muscle activations that best match the experimental kinematics (Erdemir et al., 2007). However, it is computationally expensive because it requires multiple numerical integrations to achieve optimal joint kinematics (Anderson & Pandy, 2001; Erdemir et al., 2007). This presents a major disadvantage for the approach's adoption in clinical settings, as quick results are typically encouraged (Erdemir et al., 2007; Fregly et al., 2012). Determining a set of muscle excitations that produce a coordinated movement is a challenging task (Delp et al., 2007). The literature reports the computational expense of generating coordinated muscle-actuated simulations of movement to range from days to weeks to months (Anderson & Pandy, 2001; Higginson et al., 2006; Neptune et al., 2001). This issue becomes more of a challenge when this approach is used with a model that contains many muscles and allows for complex excitation patterns (Thelen et al., 2003). As a result, researchers simplified their models by reducing the number of muscles in the model (Davy & Audu, 1987; Yamaguchi & Zajac, 1990) or simplified the muscle control signals (Neptune & Hull, 1998). However, these simplifications may still require thousands of integrations to solve dynamic optimization problems (Thelen et al., 2003).

In a study analyzing gait patterns, Anderson and Pandy (2001) determined that the results of static optimization and dynamic optimization are practically equivalent, suggesting that static optimization and dynamic optimization are similar optimization methods. The authors recommended the use of the static optimization technique for descriptive studies of determining joint contact and muscle forces when measured kinematics are available. They recommended the use of the dynamic optimization

technique when accurate experimental data are not available, activation dynamics plays an important role, an appropriate time-independent performance criterion (performance-based objective function, i.e., maximum height jumping) is not available, and the ability to predict a novel movement is desired (Anderson & Pandy, 2001).

To address the computational cost resulting from dynamic optimizations with simplified computer graphics-based models, Thelen et al. (2003) developed an efficient technique termed computed muscle control (CMC). This technique uses static optimization along with feed-forward and feedback controls to track desired kinematics (Reinbolt et al., 2011; Thelen et al., 2003). Therefore, CMC is not a dynamic optimization method (Thelen et al., 2003). What is unique about CMC is that it incorporates activation and contraction dynamics within the optimization problem formulation. Since CMC solutions are driven by excitations, the technique allows for changes in excitation to be introduced as a means of assessing how movement might change as a consequence to changes in motor control (Thelen & Anderson, 2006). In their simulation study implementing this technique, Thelen et al. (2003) were able to determine muscle excitations that reproduced measured pedaling dynamics in ten minutes. The reduction in computational time needed to determine the muscle excitations was over two orders of magnitude faster than conventional dynamic optimization techniques (Delp et al., 2007; Thelen et al., 2003). The speed of CMC makes it practical to generate patient-specific simulations of a wide variety of movements, so it has been incorporated in OpenSim's software (Delp et al., 2007; Delp et al., 2010). An initial limitation to the CMC technique is that the muscle forces needed to generate a desired set of accelerations can be computed at any point in time, but there are

delays between the muscle excitations and the generation of muscle forces (Thelen et al., 2003). This is more of a concern when using CMC to track rapid movements where the actuator delays have larger effects; so a method for accounting for actuator dynamics into the estimation of controls may be necessary (Lewis et al., 1993). To address these delays in muscle force production, Thelen and Anderson (2006) developed a modified CMC tracking algorithm. Using a residual (experimental and modeling errors) elimination algorithm in conjunction with the modified CMC algorithm, they were able to generate accurate patient-specific forward simulations of normal gait (one half of a gait cycle) using approximately 30 minutes of computer processing time. Another limitation is that CMC is not a dynamic optimization method, so only objective functions that can be evaluated at an instant in time can be used (Thelen et al., 2003). Another limitation to the CMC technique is that it is dependent on kinematic data and the results of the forward dynamic simulation are dependent on the quality of the kinematic data (Thelen et al., 2003).

Up to this point, computational expense has been discussed as the computational processing (wall clock) time spent to solve the optimization problem. While some researchers do report the wall clock time spent solving the optimization problem with the CMC approach, most do not report other aspects of computational expense: the individual researcher's time required to produce a reasonable simulation and quantitative measures of unreasonability (Reinbolt et al., 2011). Reinbolt et al. (2011) define a reasonable simulation as one that closely tracks experimental kinematics and obeys Newton's equations of motion relating ground reactions and body segment interactions. They define measures of unreasonability as kinematic tracking errors and residual

forces/torques needed to balance Newton's equations of motion (Reinbolt et al., 2011). OpenSim users who use CMC, like Reinbolt and colleagues (2011), admit that it takes them an excessive amount time to generate a reasonable simulation. Moreover, Reinbolt and colleagues (2011) state that depending upon one's reasonability tolerance, it may be take 1-3 days or up to a few months to generate one reasonable simulation. The authors determined that the OpenSim users were spending too much time selecting an unnecessary number of input parameters for CMC to generate a simulation that minimizes measures of unreasonability. To address this concern, the authors presented an optimization method to improve CMC. Using a nested (two-level) optimization approach with sidestepping data collected from a male amateur football player, the authors were able to obtain optimal input parameters for CMC that generated a simulation that closely tracked experimental data with limited residual forces and torques. When reporting the total computational expense to generate each simulation with their approach, the authors noted that the OpenSim user spent three research days on the problem and that the optimization problem was solved after 11.8 hours of wall clock time, which was about a 50% decrease in time. The authors suggest that improving CMC via optimization allows researchers to generate a forward dynamic simulation within a modest amount of time and without the need to choose extra input parameters. However, this nested optimization approach with CMC also requires collaboration from clinicians and engineers. A hidden cost in this approach is the time spent meeting to discuss the model and expected outcomes.

After reviewing the literature concerning the OpenSim optimization approaches that can be implemented to determine muscle forces as well as their advantages and

disadvantages, it is clear that the decision to select an inverse dynamics-based approach or a forward dynamics-based approach depends upon the availability of experimental data or the clinical/research question to be answered (Anderson & Pandy, 2001; Erdemir et al., 2007). Since the Wheelchair Propulsion Model will be evaluated as a potential clinical tool, it is imperative that the model be easy to use and the simulations do not require much computational time to generate results (Erdemir et al., 2007; Fregly et al., 2012). Due to the availability of measured kinematics and the computational efficiency (both in terms of the wall clock time needed to generate dynamic simulations and research days needed to investigate an optimal objective function) of the approach, the contribution of individual shoulder muscle forces to manual wheelchair propulsion will be determined by using static optimization.

The selection of an appropriate objective function for the optimization analysis is critical. The objective function most frequently selected for investigations of muscular loading in the upper limb is the sum of muscle forces squared (Buchanan & Shreeve, 1996; Happee, 1994; Nieminen et al., 1995; van der Helm, 1994). However, the work of van der Helm (1994) suggests that the minimization of muscle forces squared results in an overuse of favorably located muscles. The Wheelchair Propulsion Model is being constructed to determine the muscle contribution of shoulder complex muscles to wheelchair propulsion. Shoulder muscle imbalances and weakness are more pronounced in individuals with tetraplegia (Curtis et al., 1999; Powers et al., 1994). Therefore, this objective function was not optimal for this study because it might not determine an accurate contribution of muscle forces due to a bias towards favorably located muscles.

A review of the wheelchair propulsion optimization literature revealed that there was not a common objective function used for wheelchair propulsion simulations.

For example, van Drongelen et al. (2005a) used a minimum stress objective function to investigate glenohumeral joint contact forces and muscle forces during wheelchair related activities of daily living in individuals with paraplegia and tetraplegia and able-bodied individuals. However, their model was not patient-specific. Simulations of level wheelchair propulsion, reaching, and weight-relief lifting were generated. However, they never published their estimated muscle forces for the participants with tetraplegia. Moreover, they did not collect experimental EMG, but compared their glenohumeral joint contact forces with the findings from Veeger et al.'s (2002) shoulder loading during low intensity simulation study. They also interpreted their muscle force results based on Mulroy et al.'s (1996) fine-wire EMG study. Since the muscle forces were not published for the individuals with tetraplegia, it could not be determined whether this objective function was appropriate for the optimization study presented in this dissertation.

Dubowsky et al. (2008) constructed and validated their wheelchair propulsion model with the AnyBody Modeling System, which implements a min/max objective function to solve the redundancy of muscle recruitment problem. The AnyBody optimizer has demonstrated comparable results to the well-known polynomial and soft-saturation criterion types (Rasmussen et al., 2001). Their findings from the implementation of minimization of muscle effort as an objective function was supported by the findings of Nickels et al. (2003), suggesting that the criterion minimization of muscle effort gives reasonable correlation with experimental results (Dubowsky et al.,

2008). However, they quantitatively validated their model using a MAE analysis (discussed in detail in Chapter 4). In this analysis, they compared the estimated muscle forces for the right and left anterior deltoid, posterior deltoid, pectoralis major, trapezius, triceps, and biceps with the experimental surface EMG collected from two manual wheelchair users with paraplegia and an able-bodied individual. This dissertation intends to investigate fine-wire experimental EMG from thirteen shoulder complex muscles on the right side of the body. Moreover, Dubowsky et al.'s (2008) mean MAE values for all three participants for the right and left triceps demonstrated poor correlations. While the effect of the inclusion of additional muscles investigated in this study to their model with this objective function remains unknown, it is not encouraging to know that objective function implemented in Dubowsky et al.'s (2008) study determined triceps muscle forces that had a poor MAE with respect to the experimental EMG data collected. Although the mean MAE values across each individual participant were good, the MAEs were poor for the left bicep, left posterior deltoid, right pectoralis major, and left trapezius in one participant with paraplegia (in addition to the right and left triceps). The MAEs were poor for the right biceps for the other participant with paraplegia (in addition to the right and left triceps). Since this objective function resulted in poor MAE values for individuals with paraplegia and an able-bodied individual, it was assumed that this objective function may not be adequate for this study involving experimental data collected from a manual wheelchair user with tetraplegia.

For model validation, Morrow et al. (2010) selected three optimal criteria for the determination of the cost function used in the static optimization technique: (i) linear minimization of α, muscle activation (Kaufman et al., 1991); (ii) minimax formulation of

minimizing the maximum muscle stress (An et al., 1984); (iii) nonlinear minimization of the sum of muscle stress cubed (Lin et al., 2004). They also validated their model using MAE analyses. Although the MAE analyses for each optimization criterion investigated demonstrated good correlations for the seven muscles validated, they suggested that the linear approach be used based on the statistically equivalent results and computation time required. However, Morrow's model did not include all of the shoulder complex muscles and was investigated with data collected from a heterogeneous population of manual wheelchair users, none of which had tetraplegia. Also, the authors' MAE analysis was based on seven muscles: anterior deltoid, middle deltoid, posterior deltoid, pectoralis major, latissimus dorsi, triceps, and biceps. This study intended to investigate thirteen muscles of the shoulder complex. While Morrow et al. (2010) demonstrated that the three optimization criteria investigated were reasonable and appropriate choices for further application of their musculoskeletal and optimization model, it is not known whether those objective functions would be reasonable and appropriate for the Wheelchair Propulsion Model and propulsion study presented in this dissertation.

Given the complexity introduced by accounting for the shoulder complex muscles and the need to account for muscle contribution in an individual with tetraplegia as well as fine-wire EMG data collected from thirteen shoulder complex muscles, the objective function selected for this study was the minimization of the square of muscle activation, summed across all muscles (Anderson & Pandy, 2001; Crowninshield & Brand, 1981; Kaufman et al., 1991). This objective function was selected in accordance with van der Helm (1994), who suggested that the minimization of muscle stress squared allows for the distribution of muscle forces based on muscle cross-sectional area and is

computationally efficient. Since additional muscles will be included in the model, it is important to capture each muscle's contribution to wheelchair propulsion. Therefore, an objective function that allows for the distribution of muscle forces based on muscle cross-sectional area is desirable. It has been previously discussed how the static optimization approach is more computationally efficient than the dynamic optimization approach, in terms of the wall clock time needed to generate the simulation. Moreover, by thoroughly reviewing the literature and understanding the limitations of each objective function as a method to select an objective function, the investigator may reduce the time required to produce a reasonable simulation. This should also be a factor of computational efficiency since time more time was spent towards research days on the problem as opposed to the wall clock time required to run and analyze all of the simulations based on all of the objective functions implemented in previous studies.

After selecting an objective function for the static optimization approach and computing the shoulder complex muscle forces during propulsion, the computed muscle forces must be evaluated. Quantitative evaluations of the muscle forces will be performed, by means of cross correlation analyses and MAE calculations (de Zee et al., 2007; Dubowsky et al., 2008; Morrow et al., 2010). It is the belief of this research that the Wheelchair Propulsion Model is capable of determining the contribution of individual shoulder muscles to manual wheelchair propulsion. This model may potentially lead to the development of a clinical tool that optimizes manual wheelchair propulsion.

CHAPTER 2

CONSTRUCTION OF THE WHEELCHAIR PROPULSION MODEL

2.1 Introduction

One goal of this dissertation is to construct a patient-specific, computer graphics-based musculoskeletal model of the trunk and upper limb that is capable of generating dynamic simulations of wheelchair propulsion. To evaluate the potential of the model as a clinical tool, kinematic and kinetic data from an individual with tetraplegia will be implemented. Static optimization will be used to estimate the individual contribution of the shoulder muscles to wheelchair propulsion.

The model was constructed and evaluated with OpenSim, an open-source modeling framework that allows for the generation and analysis of dynamic profiles of movement (Delp et al., 2007; Seth et al., 2011). This framework has an end-user application with a graphical user interface (GUI) and a standardized set of file formats for defining and sharing neuromusculoskeletal models and related data (Seth et al., 2011). OpenSim contains a set of simulation tools that can be used to extract meaningful information from generated simulations and contains specialized tools for patient-specific modeling (Delp et al., 2007; Seth et al., 2011). OpenSim also includes a library of reusable musculoskeletal models (https://simtk.org/home/nmblmodels/ accessed on March 9, 2010) in these formats that have been constructed and published by various researchers, including the SIMM (Upper Extremity Model (Stanford VA Model) (Holzbaur et al., 2005) and the Head and Neck Model (Vasavada et al., 1998). SIMM models can be imported and analyzed in OpenSim (Delp et al., 2007).

2.2 Construction of Wheelchair Propulsion Model based on Stanford VA Model

Recently, Morrow et al. (2010) and Rankin et al. (2010; 2011) used the SIMM Upper Extremity Model (Holzbaur et al., 2005) to investigate dynamic simulations of wheelchair propulsion and wheelchair activities. However, their models did not include the following deep shoulder muscles: upper and middle trapezius, serratus anterior, and rhomboids major. Fine-wire EMG investigations by Mulroy et al. (1996; 2004) found that these muscles are active during wheelchair propulsion. Therefore, these muscles should be included in musculoskeletal models for wheelchair propulsion.

Recognizing the limitations of the shoulder musculature in the Stanford VA Model and given the open-source nature of the OpenSim, the muscles of interest could be added to the Stanford VA Model by adding them from other published library models or be created manually and added to the model (Figure 2.1).

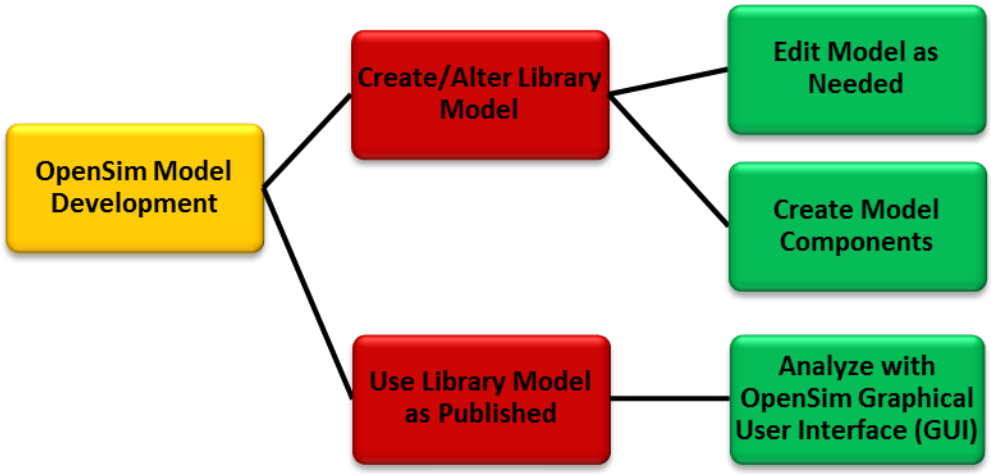

Figure 2.1 Outline of model development options in OpenSim, which includes a library of reusable musculoskeletal models. Users have the option to analyze these models with OpenSim tools to extract meaningful data and gain insight on movement. If the reusable models do not include features of interest (muscles, body segments, joints, degrees of freedom, etc), they can be added from other existing published models or manually added. Alternatively, a model may have muscles or body segments that are not necessary for a particular investigation. In these instances, the model components may be removed from the model.

The Head and Neck Model (Vasavada et al., 1998), a 3D model with 26 muscle compartments and three degrees of freedom (DOF), contains the upper and middle trapezius muscles. These muscles were added to the Stanford VA Model. However, the upper trapezius originated in the skull and inserted on the spine and the middle trapezius originated on the C7 spinous process and inserted on the scapula (Figure 2.2). The Stanford VA Model (Figure 2.2) does not have a skull, jaw, or spine, so these bones (bodies) were added to the model as well. Both the Stanford VA Model (Holzbaur et al., 2005) and the Head and Neck Model (Vasavada et al., 1998) are kinematic, so the Wheelchair Propulsion Model that resulted from adding these muscles and bodies of interest was kinematic as well. As a kinematic model, the Wheelchair Propulsion Model could only be used to track motion. Therefore, the force generating properties (segment mass and moment of inertia) needed for dynamic simulations were missing from the model. The goal of this dissertation includes constructing a model capable of estimating shoulder muscle forces, so a dynamic model was necessary. Therefore, the kinematic Wheelchair Propulsion Model was inappropriate.

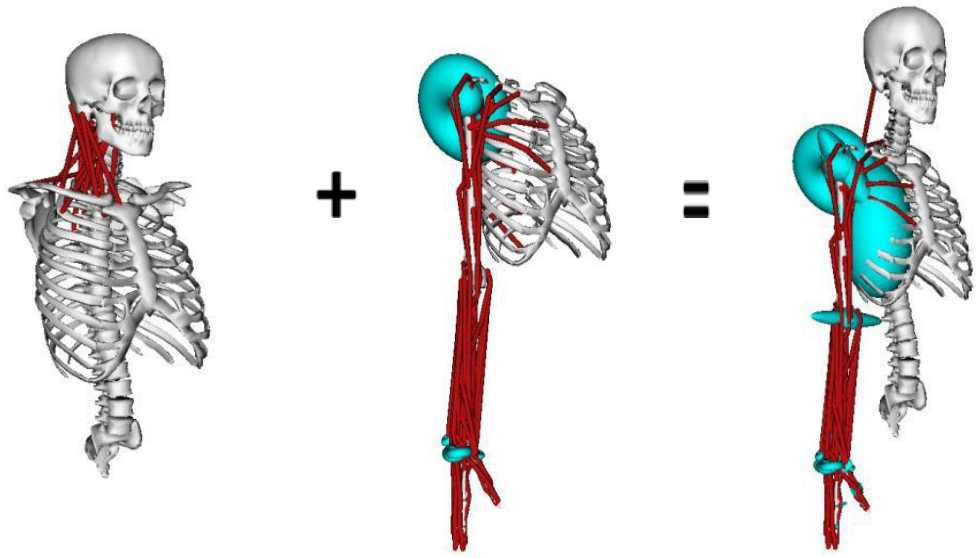

Figure 2.2 Construction of Wheelchair Propulsion Model based on Stanford VA Model. The skull, jaw, spine, and upper and middle trapezius muscles were taken from the Head and Neck Model (Vasavada et al., 1998) (left) and added to the Stanford VA Model (Holzbaur et al., 2005) (center), resulting in the kinematic Wheelchair Propulsion Model (right). The kinematic Wheelchair Propulsion Model has six DOF and 52 muscle compartments.

To create a dynamic version of the Wheelchair Propulsion Model, the segment masses and moment of inertia had to be added to the model. However, the Stanford VA Model contained "phantom bodies" (Holzbaur et al., 2005; Xu et al., 2012). Phantom bodies appear in the model file to help the model achieve a specific purpose, but they are invisible when the model is visualized. In the case of the Stanford VA Model, phantom bodies were included to match the kinematics of the shoulder. In the model, the motion of the shoulder is described by the collective motion of the shoulder girdle (clavicle, scapula, and humerus) and the motion of the clavicle and scapula is constrained to depend on the motion of the humerus (Holzbaur et al., 2005). In order to define motion at the shoulder girdle, phantom bodies were included. In addition to providing the segment masses and moments of inertia for the body segments, the segment mass and

moment of inertia would have to be specified for the phantom bodies. However, phantom bodies do not exist anatomically, so there are no cadaver studies from which to obtain these values. Very small values for mass and moment of inertia could have been assigned to the phantom bodies, but including these extra bodies in the model would have greatly increased the computational time needed to solve the optimization problem that determines individual muscle forces (J. Reinbolt, personal communication, December 16, 2010). The long-term goal is for the Wheelchair Propulsion Model to be used as a clinical tool. It is important that the model is easy to use and does not require much computational time to generate dynamic simulations of wheelchair propulsion (Fregly et al., 2012). Therefore, it was not feasible to create a dynamic version of the Wheelchair Propulsion Model by using the Stanford VA Model.

2.3 Construction of Wheelchair Propulsion Model Based on Arm 26 Model

The foundation of the dynamic Wheelchair Propulsion Model is the OpenSim Arm 26 Model (http://www.simtk.org accessed on December 9, 2010) (Figure 2.3). The Arm 26 Model is a 3D planar model that consists of the head, arm, chest, and spine and is actuated by the biceps, triceps and brachialis muscles. The rationale for this selection was that by adding complexity (DOF, segments with masses and moments of inertia and additional muscles) to a simple library model, a more accurate simulation of wheelchair propulsion would be generated (Odle et al., 2011). This eliminated the need for phantom bodies at the shoulder.

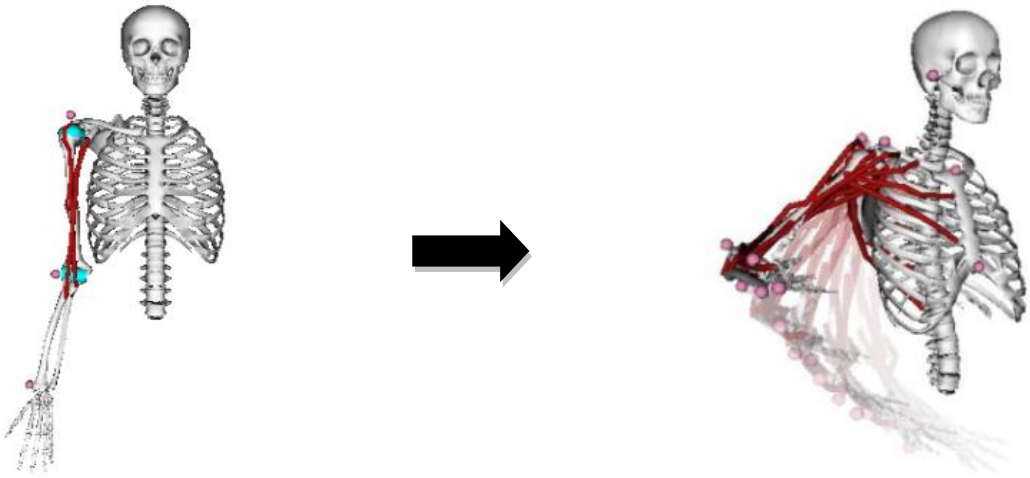

Figure 2.3 Construction of Wheelchair Propulsion Model based on Arm 26 Model: Left- Arm 26 example model; Right- dynamic Wheelchair Propulsion Model with seven degrees of freedom and 26 muscle-tendon actuators. The wrap objects have been excluded from view.

2.3.1 Upper Limb Kinematics and Dynamics

To account for the complexity of the upper limb, the shoulder was modeled as a ball and socket joint. Three DOF were added to the shoulder, one DOF was added to the elbow (forearm), and two DOF were added to the wrist (Figure 2.4).

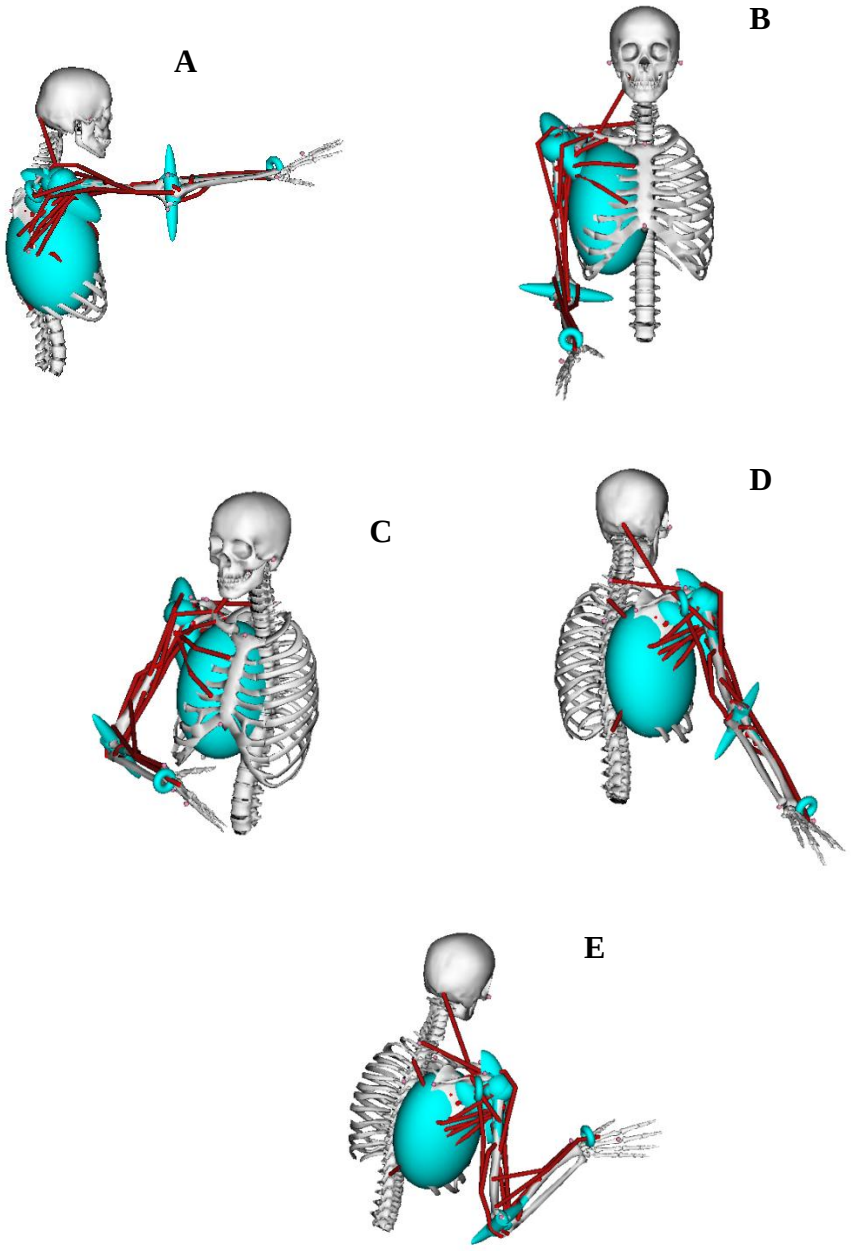

Figure 2.4 The Wheelchair Propulsion Model in different poses. The model is shown in (A) a lateral view with the arm in a 90° elevation plane (shoulder flexion). The model is shown in (B) an anterior view with the arm in a 0° plane of elevation (shoulder abduction). The model is shown in (C) an anteriomedial view with the arm in 75° of elevation angle. The model is shown is shown in (D) a posterior view with the elbow at full extension (130°). The model is shown in (E) a posteriolateral view with the wrist in ulnar deviation. The muscles of the trunk and upper limb are displayed in red. The turquoise objects on the model are the wrap objects. Wrap objects are used to constrain the muscle path and may have the shape of an ellipsoid, torus, cylinder or sphere (Delp et al., 2010).

The degrees of freedom at the shoulder are elevation plane, elevation angle, and internal-external rotation. The elevation plane DOF describes the orientation of the vertical plane in which the arm elevates relative to the frontal plane (Holzbaur et al., 2005). It ranges from 0° to 180°. The elevation angle represents the thoracohumeral angle and ranges from -90° to 130° in the model. Although this range allows for full range of motion in the model, it should be noted that the thoracohumeral angle of a manual wheelchair using patient with SCI will be a much smaller subset of this range. Shoulder rotation occurs about the long axis of the humerus and ranges from -90° (external rotation) to 90° (internal rotation). The overall motion of the shoulder joint is defined by the collective motion of the shoulder girdle and is described using spherical coordinates (Holzbaur et al., 2005). Movement of the shoulder girdle is determined by regression equations described by de Groot and Brand (2001), simplified to vary only with the elevation angle (Holzbaur et al., 2005). The order of rotations (Y,X',Y") for shoulder movement are consistent with the ISB recommendations (Holzbaur et al., 2005; Wu et al., 2005). Based on the ISB recommendations, shoulder flexion occurs in the 90° elevation plane and shoulder abduction occurs in the 0° elevation plane (Holzbaur et al., 2005; Wu et al., 2005).

The degrees of freedom at the elbow are flexion-extension and forearm rotation. Full extension is defined as 0° and flexion is defined as 130°. Forearm rotation is defined from -90° (supination) to 90° (prontation) (Holzbaur et al., 2005).

The degrees of freedom at the wrist are flexion-extension and ulnar-radial deviation. Wrist flexion is defined from -70° (extension) to 70° (flexion) and deviation is defined as -10° (radial) and 25° (ulnar) (Holzbaur et al., 2005).

The dynamic Wheelchair Propulsion Model and the Stanford VA Model have the same degrees of freedom at the shoulder, elbow, and wrist. Although the two models have the same degrees of freedom at the upper limb joints, the degrees of freedom for the shoulder in the Wheelchair Propulsion Model were achieved without the use of phantom bodies. Sample data were used to compare the shoulder joint kinematics of the two models and the shoulder joint kinematics of the dynamic Wheelchair Propulsion model are consistent with that of the Stanford VA model (Odle et al., 2011). This suggests that shoulder motion can be modeled without the use of phantom bodies. The phantom bodies posed difficulties in accounting for the dynamic properties needed to compute net joint moments and individual shoulder muscle forces. Thus, the Wheelchair Propulsion Model is a dynamic version of the Stanford VA Model.

Degrees of freedom were also added at the thorax (ground) to allow the model to translate and rotate about the X, Y, and Z axes. In OpenSim, the X-axis is defined as the anterior-posterior direction. The Y-axis is defined as the superior-inferior direction and the Z-axis is defined as the lateral-medial direction (Figure 2.5). Each body has a local coordinate system.

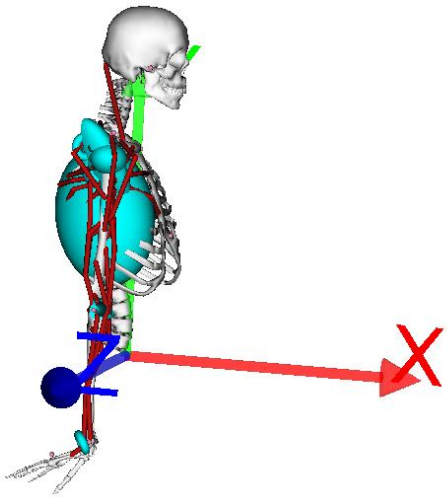

Figure 2.5 Global coordinate system of the model (based at ground). The positive X-axis is oriented anteriorly (red). The positive Y-axis is superiorly (green) and the positive Z-axis is oriented laterally (blue).

Body segment masses and moment based on cadaver studies (Dempster, 1955) were added originally added to the model. However, the model would later be used to generate a patient-specific model of an individual with tetraplegia. The literature has reported changes in body composition after a SCI. These changes include muscle atrophy, loss of lean tissue mass and gain in body fat (Gater & Clasey, 2006; Gorgey et al., 2007; 2012; Jones et al., 1998; Spungen et al., 1995; 2000; 2003). Considering these changes in body composition, an independent study was conducted to investigate the appropriateness of cadaver-based body segment mass estimates for SCI populations (Chapter 3).

2.3.2 Shoulder and Thoracohumeral Muscle Dynamics

The muscles that cross the shoulder, elbow, and wrist were added to the model (Table 2.1). Specifically, the upper and middle trapezius muscles were added to the

model from the Head and Neck model by using the OpenSim GUI. The serratus anterior and the rhomboids major were not included in any of the existing OpenSim library models, so they were added to the model via the OpenSim Muscle Editor GUI. The model will be used to determine muscle force, which is dependent upon the muscle path and its velocity (OpenSim Advanced User's Jamboree). Therefore, it was important to select the correct muscle path for the serratus anterior and rhomboids major.

Table 2.1 Muscle Modeling Parameters

Muscle	Peak Force (N)	Optimal Fiber Length (cm)	Tendon Slack Length (cm)
Shoulder			
Trapezius			
Upper	78	8.4	12.0
Middle	377	9.2	7.3
Serratus Anterior	677.3	17.5	0.3
Rhomboids Major	217.1	17.9	0.5
Deltoid			
Anterior	1142.6	9.8	9.3
Middle	1142.6	10.8	11.0
Posterior	259.9	13.7	3.8
Supraspinatus	487.8	6.8	4.0
Infraspinatus	1210.8	7.6	3.1
Subscapularis	1377.8	8.7	3.3
Teres minor	354.3	7.4	7.1
Teres major	425.4	16.2	2.0
Pectoralis major			
Clavicular	364.4	14.4	0.3
Sternal	515.4	13.8	8.9
Ribs	390.5	13.8	13.2
Latissimus dorsi			
Thoracic	389.1	25.4	12.0
Lumbar	389.1	23.3	17.7
Iliac	281.7	27.9	14.0
Coracobrachialis	242.5	9.3	9.7
Elbow			
Triceps			
Long	798.5	13.4	12
Lateral	624.3	11.4	9.8
Medial	624.3	11.4	9.1
Anconeus	350.0	2.7	1.8
Supinator	476.0	3.3	2.8
Biceps			
Long	624.3	11.6	27.2
Short	435.6	13.2	19.2
Brachialis	987.3	8.6	5.4
Brachioradialis	261.3	17.3	13.3

Note: Muscle modeling parameters obtained from Holzbaur et al., 2005 and Garner and Pandy, 2003.

In OpenSim, the muscle path is determined by a series of attachment points. There are four types of attachment points that can be implemented: fixed, via, moving muscle points and wrap points. Fixed points are a pair of adjacent points fixed to a body, connected by a straight line (muscle path). Via points are attached to a body, but are only included in the muscle path when a specified coordinate (joint angle) is in a specific range. For example, the quadriceps wraps over the distal femur when the knee flexes beyond a certain angle (Delp et al., 2010). Moving muscle points have X, Y, and/or Z offsets in a body's reference frame that are functions of coordinates. Wrap points have X, Y, and/or Z offsets that are calculated automatically by OpenSim in order to wrap a muscle over the surface of a wrap object (Delp et al., 2010). Wrapping objects are used to constrain the muscle path and may have the shape of an ellipsoid, torus, cylinder or sphere.

The serratus anterior and rhomboids major were modeled with fixed attachment points between their respective origin and insertion. To remain consistent with the Holzbaur et al. (2005) modeling approach (one path per muscle compartment to limit the amount of error generated by simplifying the muscle structure), each muscle was added to the model with one muscle path. Therefore, the serratus anterior was modeled with one muscle path and three attachment points (Figure 2.6) and the rhomboids major was modeled with one muscle path and two attachment points (Figure 2.6).

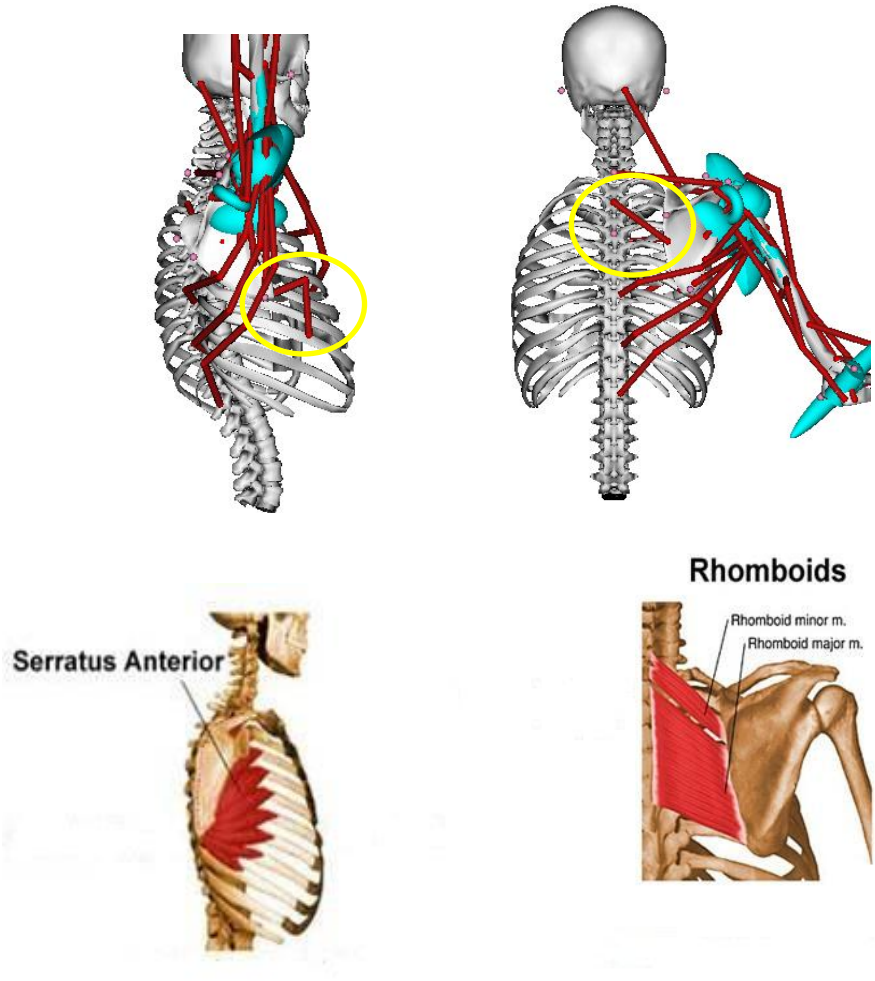

Figure 2.6 Design of the serratus anterior (above, left, circled) and the rhomboids major (above, right, circled) muscles. The serratus anterior originates at the scapula and inserts on the ribs, so it was modeled with three attachment points. In this figure, the red lines represent the muscles of the trunk and upper limb and the turquoise shapes are the wrap objects. The pink circles are the virtual markers placed on the model (to match the experimental marker set). Anatomical representations of the muscles are represented below. The anatomical representations were obtained from http://www.thansworld.com and accessed on March 26, 2013.

All muscles were defined with the Hill-type muscle model (Zajac, 1989). Parameters such as muscle length, tendon slack length, and peak force were obtained from the Stanford VA Model (Holzbaur et al., 2005) and Head and Neck Model (Vasavada et al., 1998) (Table 2.1). Published cadaver data for these parameters were not

available for the serratus anterior and the rhomboids major, so they were obtained from estimates generated by the Garner and Pandy (2003) upper limb model.

2.3.3 Summary

The dynamic Wheelchair Propulsion Model used in this dissertation is a 3D model with 13 DOF and is composed of 28 muscles and muscle compartments. The model is based on the Arm 26 Model, as the kinematic model generated from the Stanford VA Model was inappropriate for generating dynamic simulations of movement. The Wheelchair Propulsion Model is a dynamic version of the Stanford VA Model. The dynamic Wheelchair Propulsion Model was constructed by adding DOF to the shoulder, elbow, and wrist of the Arm 26 Model. Shoulder and thoracohumeral muscles were added to the model. Body segment masses and moments of inertia were obtained from cadaver studies by Dempster (1955). Muscle force generating properties were obtained from model by Garner and Pandy (2003), Holzbaur et al. (2005), and Vasavada et al. (1998).

CHAPTER 3

DUAL ENERGY X-RAY ABSORPTIOMETRY-BASED MASS MEASUREMENTS

3.1 Introduction

In addition to requiring the force generating properties for muscles, the dynamic model required the mass properties for the right arm and trunk. These body segment parameters (anthropometric parameters) are important for computing the net forces and moments (inverse dynamics). Since the individual muscle forces will be determined from the net forces, the accuracy of the results is dependent upon body segment joint and inertial parameters- joint position and orientation, mass, center of mass location, moment of inertia (Andrews & Mish, 1996; Durkin et al., 2002; Ganley & Powers 2004a; 2004b; Kingma et al., 1996; Pearsall & Reid, 1994; Pearsall et al., 1994; Rao et al., 2006; Reinbolt et al., 2007). These anthropometric values are obtained from estimates for segment mass, moment of inertia and radius of gyration properties, which were obtained from studies on male cadavers or small sample sizes (Chandler et al., 1975; Clauser et al., 1969; Dempster, 1955) and meant for use in able-bodied populations. Although these estimates were commonly used in the biomechanics community, there were concerns that they may not be suitable for all populations. Drillis and colleagues (1964) noted that the cadaver estimates did not reflect the age distribution of the normal population, differences in population body build, or the female population. There were also concerns regarding the differences between living and nonliving tissue (Durkin & Dowling, 2003; Martin et al., 1989; Pearsall & Reid, 1994; Reid, 1984).

To address these concerns, researchers estimated body segment parameters by utilizing experimental methods on living subjects (Drillis et al., 1964; Hatze, 1975; Peyton, 1986; Plagenhoef et al., 1982), predictive equations (Clauser et al., 1969; Drillis et al., 1964; Hanavan, 1964; Hatze, 1980; Jensen, 1993; Yeadon & Morlock, 1989) and medical imaging technology (Cheng et al., 2000; Huang, 1983; Martin et al., 1989; Pearsall et al., 1994; Zatsiorsky & Seluyanov, 1983). However, these models are limited to the methods on which they were generated as well as the sample populations studied (Cheng et al., 2000; Durkin & Dowling, 2003; Ganley & Powers, 2004a; 2005b). Some of the predictive equations (Hatze, 1980; Plangenhoef et al., 1982) were based on the assumption of uniform density distribution within the segments (Pearsall & Reid, 1994). The predictive equations based on regression methods or geometric modeling studies required few anthropometric measurements to estimate body segment parameters, so several assumptions were made in the generation of those equations (Durkin & Dowling, 2003). The medical imaging studies (based on magnetic resonance imaging, gamma ray scanning, or computerized tomography) allowed for accurate body segment parameter measurements, could be obtained *in vivo*, and served as a means for comparing populations and evaluating models. However, data collection was rather time consuming, expensive, and readily available facilities were limited; and the health risks from exposing subjects to radiation were a concern (Durkin et al., 2002; Durkin & Dowling, 2003; Ganley & Powers, 2004b; Lee et al., 2009; Pearsall & Reid, 1994).

Dual energy x-ray absoprtiometry (DXA) is an imaging technique that assesses bone density and body composition. It provides a regional distribution of bone, fat, and lean tissue mass (Jones et al., 1998; Mazess et al., 1990). Two x-ray beams of alternating

intensity are used to measure areal bone density and body composition is measured by comparing relative attenuation of the high and low energy in bone-free pixels (soft tissue), as seen in Figure 3.1 (Durkin et al., 2002; Gater & Clasey, 2006). This method is safe, quick, and cost effective (Jones et al., 1998; Kelly et al., 1998; Mazess et al., 1990).

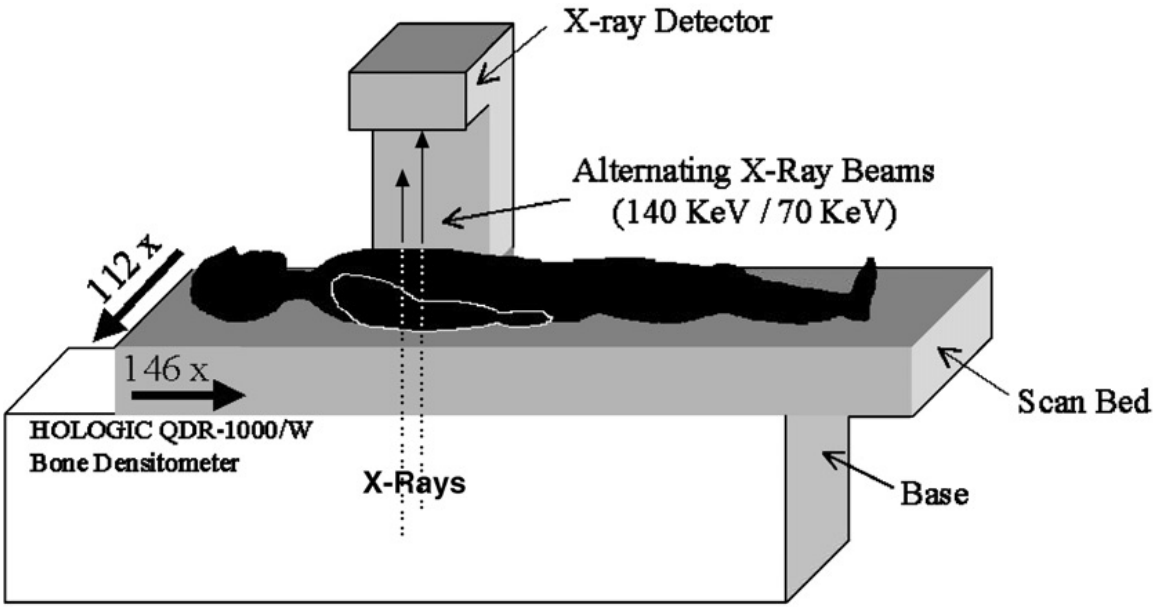

Figure 3.1 Schematic of a whole body scan using the Hologic QDR-1000/W densitometer. Scanning is conducted as the patient lies in a supine position on the table with pronated forearms and palms facing the table. In the event the patient is larger than the scanning surface, the patient may be asked to cross his or her arms across the chest or one arm may be scanned while the other hangs over the table, thus the value obtained for the scanned arm is used for both the right and left arms. Source: Durkin et al. (2002).

A unique feature of DXA is the ability to measure the mass of the entire body or a defined region of interest (ROI) (i.e., trunk, right arm, right leg) by an automated process provided in the software or user-defined settings (Arthurs & Andrews, 2009; Burkhart et al., 2009; Durkin et al., 2002), as shown in Figure 3.2. Recently, DXA has been investigated as a tool for the direct measurement of body segment parameters on humans (Arthurs & Andrews, 2009; Burkhart et al., 2009; Durkin et al., 2002; Ganley & Powers,

2004a; 2004b; Lee et al., 2009; Wicke et al., 2008). Durkin and colleagues (2002) demonstrated DXA as a valid method for obtaining patient-specific anthropometric parameters. They used DXA to measure length, mass, center of mass location, and moment of inertia of scanned objects. While several investigations were conducted to obtain body segment parameters for the lower limb to be used in conjunction with gait analyses (Ganley & Powers, 2004a; 2004b; Lee et al., 2009), there have been several investigations to obtain parameters for the upper limb and trunk (Arthurs & Andrews, 2009; Burkhart et al., 2009; Durkin & Dowling, 2003; Wicke et al., 2008). Ganley and Powers (2004a) utilized DXA to determine anthropometric parameters for children and even postulated that DXA may be an appropriate method for obtaining population-specific anthropometric parameters.

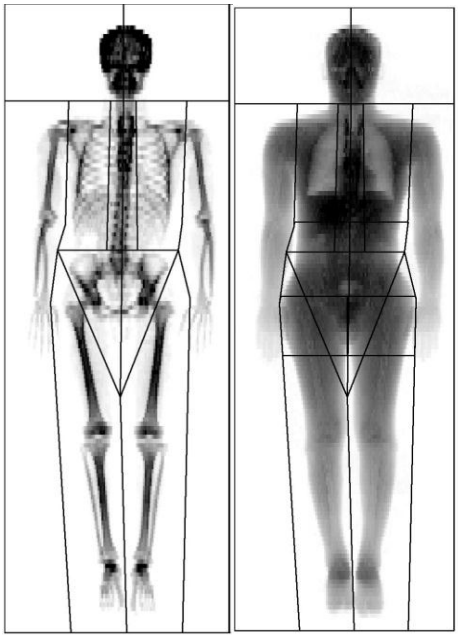

Figure 3.2 Sample total body DXA scans of a study participant. The scans show the hard (bone, left scan) and soft (fat and muscle, right scan) tissue masses of the ROIs selected for the body.

3.2 Motivation

To evaluate the potential of the Wheelchair Propulsion Model as a clinical tool, biomechanical data from an individual with tetraplegia, who had previously participated in a wheelchair propulsion study at the Kessler Foundation Research Center (West Orange, NJ) (Kessler), would be implemented in the model. The participant's data was maintained in a study database with 17 other study participants. Since the Wheelchair Propulsion Model is a novel model, a proof of concept study was performed with one participant. If the model demonstrated potential to serve as a clinical tool, data from the other participants would be implemented in the model. The Wheelchair Propulsion Model was designed to be patient-specific. OpenSim allows for patient-specificity by scaling the model to patient (Chapter 4). The mass values in the model would be used for inverse dynamics calculations as well (Chapter 4). Therefore, it is critical that the model's anthropometrics reflect the patient's mass distribution so that the motion, forces, and moments predicted by OpenSim are indicative of the patient performing manual wheelchair propulsion. However, there is a lack of knowledge regarding SCI-specific anthropometrics (Gater & Clasey, 2006).

Persons with SCI may experience changes in bone mineral composition over time (Biering-Sørensen et al., 1989; 1990; Bloomfield et al., 1996; Chantraine, 1978-1979; de Bruin et al., 2000; Eser et al., 2004; Jones et al., 1998; Spungen et al., 1995; Wilmet et al., 1995). As they age, they may also experience muscle atrophy, loss of lean tissue mass and gain in body fat (Gater & Clasey, 2006; Gorgey et al., 2007; 2012; Jones et al., 1998; Spungen et al., 1995; 2000; 2003). Clinicians and researchers have used DXA to assess these changes in body composition in persons with SCI (Bauman et al., 1999;

2010; Garland et al., 2008; Gater & Clasey, 2006; Jones et al., 1998; Spungen et al. 1995; 2003).

Considering the body composition changes that occur after SCI, the appropriateness of using the cadaver-based estimates was questioned. Previous wheelchair propulsion models used cadaver-based estimates for the body segment masses (Morrow et al., 2010; Rankin et al., 2011; van Drongelen et al., 2005a). The appropriateness of DXA-based measurements for SCI populations has not been investigated, so the following research question was posed: Is the DXA body segment technique more appropriate than the cadaver-based estimates for the SCI population?

In order to incorporate patient-specificity in the model, the inclusion of body segment masses from patient DXA scans was considered. However, DXA scans were not performed during the wheelchair propulsion study. On the other hand, Kessler maintained a database of DXA scans from non ambulatory study participants with tetraplegia and paraplegia and able-bodied controls. In the absence of having DXA scans for the study participants in the wheelchair propulsion database, the use of population-specific anthropometrics based on the participants in the DXA database was investigated. This is the equivalence of using population-specific anthropometrics when individual anthropometrics cannot be obtained (Ganley & Powers, 2004a; 2004b).

The purpose of this study was to obtain accurate mass values so that accurate simulation results can be generated with the patient-specific model. The relationship between accurate inverse dynamics results and the use of appropriate anthropometric parameters has been mentioned previously. Moreover, several OpenSim tools (Inverse Kinematics, Inverse Dynamics, and Static Optimization- Chapter 4) were implemented to

generate simulations of movement. In particular, the Inverse Dynamics Tool was used to generate the forces and moments of the upper limb during wheelchair propulsion. Body segment mass is an important variable in those equations. The Static Optimization Tool used the inverse dynamics results to determine the individual muscle forces in the model. If the incorrect body segment masses are included in the model, erroneous simulations will be generated and those errors will be propagated in the static optimization simulations.

The hypothesis of this study was that the cadaver-based estimates for the trunk and arm mass proportions would be less than the DXA-based mass proportions for participants with SCI. This hypothesis was based on the tendency of individuals with SCI to gain body fat over time. If there were differences between the measurements, the DXA-based measurements would be included in the model. If there were no differences between the measurements, then the cadaver-based estimates would be included in the model.

3.3 Methods

Kessler maintains a database of full-body DXA scans performed for various research studies. From this database, the full-body scans of 63 males (54 non ambulatory manual wheelchair users with SCI: 26 with tetraplegia and 28 with paraplegia; 9 able-body controls) were retrieved. These full-body scans were previously performed at Kessler using a General Electric (Fairfield, CT) Lunar Prodigy densitometer and analyzed with Encore 2008 version 12.02.023 software. All scans were recorded with participants lying in a supine position on the scanning table with their forearms pronated and palms facing the table (Figure 3.1). Participant demographics are listed in Table 3.1.

Table 3.1 Demographics of the Participants in the DXA Study

	Tetraplegia	Paraplegia	Controls
N	26	28	9
Age (years)	37.6 (± 10.7)	39.6 (± 12.3)	31.1 (±7.8)
Height (inches)	70.8 (± 2.9)	69.4 (± 3.0)	67.8 (± 3)
Weight (kilograms)	77.5 (± 16.7)	82.9 (± 18.2)	76. 2 (± 11.4)
Time Since Injury (years)	10.5 (± 8.6)	10.5 (± 11.0)	-

The total and lean masses of the right arm, trunk and total body were recorded from the scans of all participants. These body segments were selected because the right arm and trunk are the body segments included in the Wheelchair Propulsion Model. The ROIs were determined by using features in the accompanying Encore software. The boundaries for the regions of interest were consistent with the anatomical landmark boundaries defined in the cadaver work by Dempster and colleagues (Winter, 2005). Therefore, the total arm was defined as a segment that began at the glenohumeral joint and ended at the ulnar styloid. The trunk was defined as a segment with borders at the greater trochanter and the glenohumeral joint. The segment mass values were converted to proportion of total body mass and averaged across participants.

3.4 Statistical Analyses

3.4.1 SCI-Specific Body Segment Mass Study

To allow for statistical comparisons, the average and standard deviation of the DXA-based mass proportions were compared with the cadaver-based proportion estimates (Winter, 2005).

3.4.2 Comparisons between DXA Group and Wheelchair Propulsion Group

Two different study databases were used for the independent study and the proof of concept study (Table 3.2). Therefore, the participants with tetraplegia from each database had to be compared based on age and time since injury. This would determine whether the DXA-based population-specific anthropometrics could be implemented in the model. If there were differences between the DXA database group and the wheelchair propulsion database group, the results of the DXA analysis could not be applied to the model. This was significant because a statistical difference between the groups may suggest that the DXA-based measures were specific to a particular age group or group based on time since injury.

Table 3.2 Demographics of Participants in the Study Databases

	Database Study Group	
	DXA	Wheelchair Propulsion
N	26	18
Mean Age (years)	37.62	36.72
Standard Deviation (years)	10.65	11.93
Mean Time Since Injury (years)	10.48	11.92
Standard Deviation (years)	8.58	8.29

The hypothesis for this statistical test was that there was no difference between the two database groups. PASW Statistics 18 (SPSS Inc./IBM, Armonk, NY) was used to perform a one way analysis of variance (ANOVA, $\alpha = 0.05$) to determine whether there was a difference between the two groups' age and time since injury.

CHAPTER 4

OPENSIM SIMULATIONS

4.1 Motivation

The Wheelchair Propulsion Model was constructed to be a patient-specific model and capable of generating dynamic simulations of wheelchair propulsion. The model was constructed using OpenSim (Delp et al., 2007) so that it would available for reuse by other researchers. By contributing the model to the OpenSim Neuromusculoskeletal Model Library, researchers will be provided with free access to the model. This will encourage collaboration between researchers and promote the advancement of wheelchair propulsion biomechanics.

In order to determine the model's potential to serve as a clinical tool, it was critical to evaluate the model with biomechanical data (kinematics, kinetics, fine-wire EMG) from an individual with tetraplegia. Wheelchair propulsion data collected at Kessler from a study participant with tetraplegia (Yarossi et al., 2010) was used as input to the model. The significance of evaluating the model with data from a participant with tetraplegia is that few studies have been performed with this population (Rankin et al., 2011; van Drongelen et al., 2005a; 2011). Even though data were collected from 18 participants, the Wheelchair Propulsion Model is a novel model; so proof of concept was demonstrated with one participant. Once proof of concept has been established with one participant, future investigations will implement data from the other participants.

This dissertation is aimed at determining the potential of the model as a clinical tool, by determining the contribution to shoulder muscles forces to wheelchair propulsion. In order to serve as a clinical tool, an accurate and computationally

inexpensive technique is optimal. Patient-specific models will not be utilized in clinical settings until they are easy to use (Fregly et al., 2012). Therefore, the static optimization approach was selected, instead of the dynamic optimization approach, to estimate the in vivo muscle forces during wheelchair propulsion. Although static optimization has been widely utilized in gait studies, it has been demonstrated as a valid technique for estimating shoulder contact forces during wheelchair propulsion (Dubowsky et al., 2008; Morrow et al., 2010; van Drongelen et al., 2005a) and muscle forces during manual wheelchair propulsion (Lin et al., 2004; van Drongelen et al., 2005a).

4.2 Experimental Data

For the proof of concept study previously mentioned, the model was used to generate simulations of wheelchair propulsion with (historical) experimental data collected from a manual wheelchair user with tetraplegia. The participant was a 30 year old male with a C6 (complete) SCI. His height was 2 meters and he weighed 79.1 kilograms. At the time of testing, 14 years had passed since his SCI.

In a previous study (Yarossi et al., 2010) conducted at Kessler, biomechanical wheelchair propulsion data (kinematics, kinetics, fine-wire EMG) were collected and processed from the participant. Reflective markers were placed bilaterally on each wheel and the bony landmarks of the upper limbs, trunk and jaw. Marker placement (Figure 4.1) was in accordance with the ISB recommendations (Wu et al., 2005). Exceptions to these placements included a marker on the T3 spinous process (T3) instead of the T8 spinous process (T8) and a marker on the lateral-superior border of the acromion (ACJ) instead of the glenohumeral joint rotation center. Markers were also placed on the right (RTM) and left (LTM) tempero-mandibular joints and the head of the third metacarpal

joint (3MP). A passive marker motion capture system (M2 mcam cameras, Vicon Motion Systems, Oxford, UK) was used to collect three-dimensional kinematic data at 120 Hz. Post-processing of kinematic data entailed filtering with a fourth order Butterworth filter with a 7 Hz cutoff frequency.

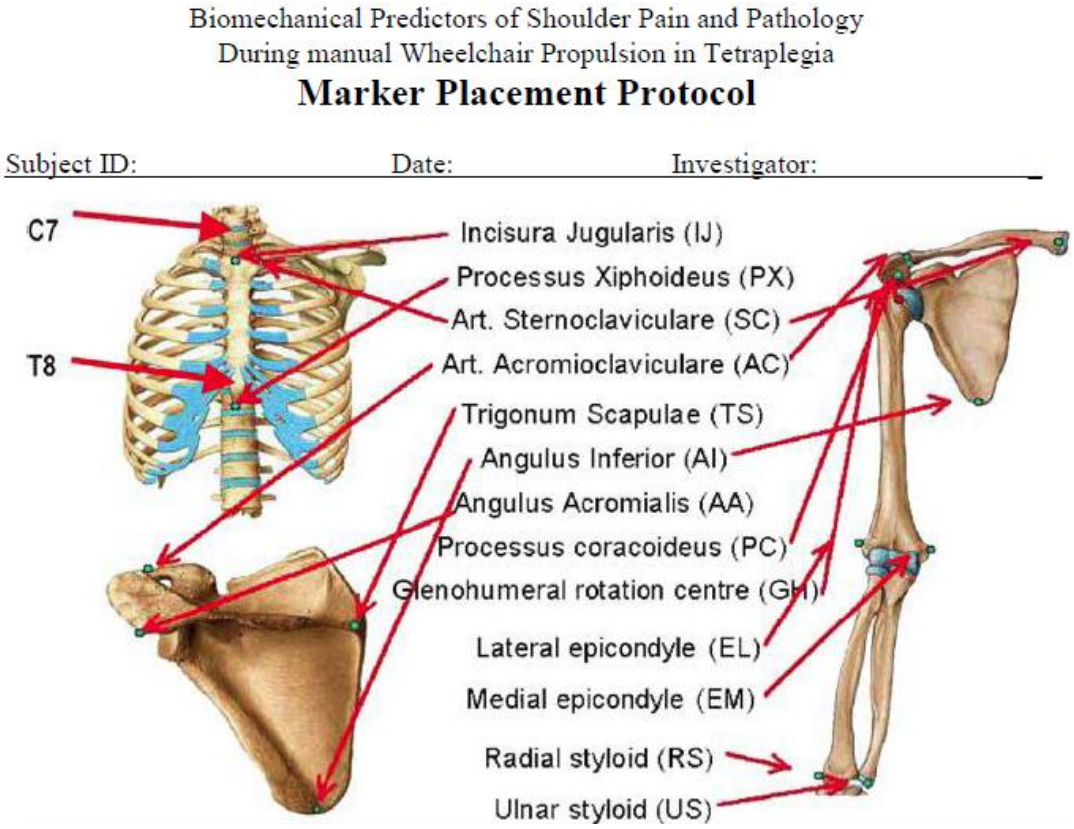

Figure 4.1 Marker placement protocol used to collect kinematic data. Data were processed for the right side only.

Smart^{WHEEL} devices (Three Rivers Holdings, LLC, Mesa, AZ), commercially available force and torque sensing pushrims, were placed on both sides of the participant's wheelchair. These devices recorded the force of the hands as they hit the pushrim. Kinetic data were collected at 240 Hz. Kinetic data collection was

synchronized with the kinematic data using an external trigger between the Smart^{WHEEL} computer and the Vicon workstation. The participant used his own wheelchair, which was secured to a dynamometer (Figure 4.2). The participant was instructed to propel his wheelchair on the dynamometer at 2 mph. Data collection trials lasted for 20 seconds and two to three trials were collected.

Figure 4.2 Experimental set up of the wheelchair propulsion study. Reflective markers were placed on the upper limb and trunk to track their position during the stroke cycle. Fine-wire electrodes were used to collect the muscle activity during the stroke cycle. Smart^{WHEELS} were placed bilaterally on the wheelchair to record the force exterted by the hand to push rim during propulsion The participant propelled his own wheelchair on a dynamometer that consisted of two independent steel tubular rollers (one for each wheel) using a four-belt tie-down system (Yarossi et al., 2010). Real-time speed feedback was presented on a monitor in front of the roller system.

Stainless steel nickel alloy insulated fine-wire electrodes (MA-300 EMG System, Motion Lab Systems, Inc., Baton Rouge, LA) were inserted into the following thirteen upper limb and trunk muscles: middle trapezius, upper trapezius, sternal pectoralis,

rhomboid major, anterior, middle, and posterior deltoids, supraspinatus, infraspinatus, subscapularis, serratus anterior, biceps, and triceps (Figure 1.1). One pole of thirteen pre-amplified electrodes was attached to the fine wires. The second pole was attached to Ag/AgCl surface electrodes placed over the surface of the muscle. The exception to this was the subscapularis because a second intramuscular needle electrode was attached. Data were collected at 2520 Hz with analog input to the Vicon workstation. Signals were low-pass filtered at 1250 Hz by the EMG collection unit (Motion Lab Systems, Inc., Baton Rouge, LA) and analog input to the Vicon workstation. EMG data post-processing entailed filtering to create a low end at 150 Hz and a high end at 500 Hz. Data were full wave rectified and root mean square average with 100ms window was applied to create a linear envelope of the signal. The linear envelope was normalized to the mean amplitude of the greatest one-second of muscle activity during a maximum voluntary contraction. Active EMG was defined as having an amplitude of greater than 5% of the maximum voluntary contraction for more than 5% of the stroke cycle. Although manual muscle test results were not available for the participant, he had triceps function.

4.3 Experimental Data Conversion

Although the experimental data collection trial lasted for 20 seconds, post-processed data from five consecutive right-sided push strokes were selected for analysis with the model. Each stroke cycle was defined as the push phase followed by the recovery phase. In the literature, rhe push phase is defined as the period when the hand is contact with the pushrim and applying force to the pushrim to maintain or increase wheelchair velocity, while the recovery phase is the period in between consecutive push phases when the arms are retracted in preparation for another push (Kwarciak et al., 2009; Sanderson &

Sommer, 1985). For data processing purposes, the push phase began at the point when the moment about the axle exceeded two standard deviations above the resting amplitude. The recovery phase was defined as the period in between consecutive push phases, and began at the point at which the moment fell below the threshold set at two standard deviations above baseline. All kinematic, kinetic, and EMG data were normalized to 100% of the stroke cycle.

In order to import the data in OpenSim, the experimental marker and force data needed to have specific files formats. Experimental marker data can only be imported as a track row column file (.trc) and the force data can only be imported as motion file (.mot). The experimental marker data were saved as a MATLAB (The Mathworks, Natick, MA) workspace file (.mat). The force data were saved as .mat files as well. Experimental EMG data cannot serve as model inputs, but are used to compare the estimated muscle forces. Additional detail on the EMG comparisons with the estimated muscle forces is discussed in Section 4.6.

The first approach to convert the experimental data was to use the gait extraction toolbox available on the OpenSim website (Dorn, 2008). This toolbox contains a series of programs (functions) written in MATLAB that allow users to convert their experimental data to the required OpenSim file formats. Even though the toolbox was designed to convert gait data, the functions were written so that users could to modify them to better fit their experimental data. Although wheelchair propulsion and gait are both cyclic and repetitive, their patterns of movement and methods of data collection, especially force are very different. Therefore, modifying the functions to the wheelchair

propulsion study presented several challenges, particularly due to the method in which the experimental kinetic data were obtained (Figure 4.3).

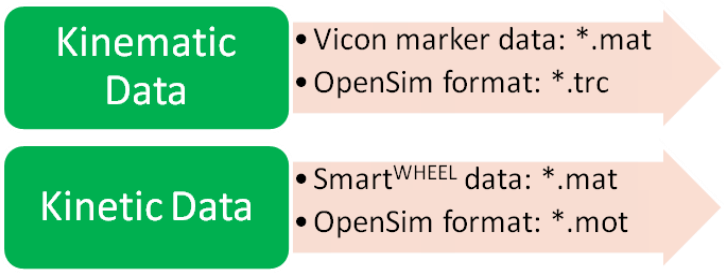

Figure 4.3 Comparison of experimental and required OpenSim file formats. The force data were collected with the Smart^{WHEEL} and saved with the MATLAB workspace (.mat) file extension. The gait extraction toolbox functions assume that all of the experimental data (kinematic, kinetic, and EMG) are saved as *.c3d files. Since the force data were not compatible with the toolbox, this approach for data conversion was not feasible.

As an alternative to using the gait extraction toolbox, MATLAB (version R2012a) functions, inspired by Tim Dorn's functions, were written to convert the experimental data to the appropriate OpenSim formats (Appendix A). When the model is added to the OpenSim model library, the data conversion functions will be included with the model so that researchers in the wheelchair biomechanics community will have access to them as well. Since the force data conversion functions were meant for gait applications, the contribution of a force data conversion function for wheelchair propulsion data is an important contribution to wheelchair biomechanists in the OpenSim user community.

4.4 Overview of OpenSim Simulations

Once the dynamic model was complete, virtual markers were placed on the model, reflecting the experimental marker placement. This was accomplished with the Marker Editor GUI in OpenSim. After marker placement was complete, simulations were

generated using the following OpenSim Tools (Figure 4.4): Scale, Inverse Kinematics, Inverse Dynamics, and Static Optimization. The generation of the patient-specific model and kinematic data tracking were dependent upon proper marker placement. If the marker placement was incorrect, errors would be propagated throughout the rest of the simulations (Chapter 3).

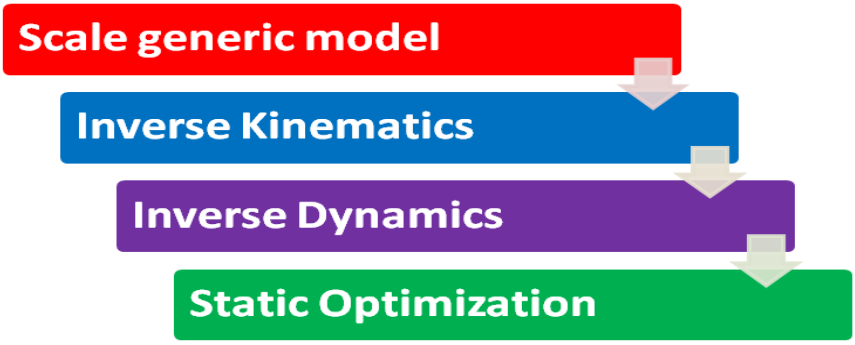

Figure 4.4 Overview of the OpenSim Tools used to generate dynamic simulations of wheelchair propulsion. To evaluate the model's potential as a clinical tool, a proof of concept study was conducted to estimate shoulder muscle forces during wheelchair propulsion using the Static Optimization Tool. In order to use the Static Optimization Tool, the model had to be scaled to the study participant and inverse kinematics and dynamics had to be computed.

4.4.1 Scale Tool

As constructed, the model was generic because it did not reflect the anthropometrics of a patient. Once the model reflects the anthropometrics of a patient, the model is a patient-specific model. Patient-specificity is achieved with the Scale Tool, which alters the anthropometry of the generic model so that it matches the patient's height and weight as closely as possible. Scaling is performed based on a combination of measured distances between X-Y-Z marker locations and manually-specified scale factors (Delp et al., 2010).

A more detailed description of the X-Y-Z marker location specifications will be discussed in Section 4.5.1.

4.4.2 Inverse Kinematics Tool

The Inverse Kinematics (IK) Tool computes the joint angles (generalized coordinates) for the model based on the experimental position data (Figure 4.5). The IK Tool matches the virtual markers on the scaled model with the experimental markers, as closely as possible, for each time frame of data.

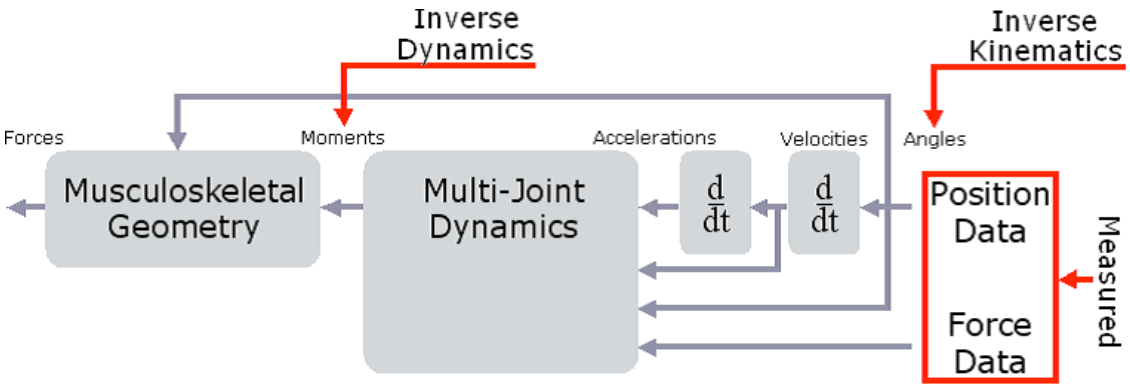

Figure 4.5 Overview of inverse kinematics and inverse dynamics computations in OpenSim. The Inverse Kinematics Tool computes joint angles based on experimental position data. The Inverse Dynamics Tool uses the experimental force data, computed velocities and accelerations (derived from experimental position data), and musculoskeletal geometry to compute moments. Source: *OpenSim Tutorial #3: Scaling, Inverse Kinematics, and Inverse Dynamics* by Hamner et al., accessed from http://www.simtk.org on March 9, 2010.

The IK Tool accomplishes this by solving a weighted least squares problem, whose solution is aimed to minimize both marker and coordinate errors, to determine the best match (Delp et al., 2010). The weights represent how close the match between the two marker sets should be made. For example, larger weightings penalize errors for that marker or coordinate more heavily and thus should match the experimental value more

closely (Delp et al., 2010). The weighted least squares problem solved by the IK Tool was:

$$\min_{q}\left[\sum_{i\in markers} w_i \left\| x_i^{\exp} - x_i(q) \right\|^2 + \sum_{j\in unprescribed\ coords} \omega_j \left(q_j^{\exp} - q_j\right)^2\right]$$

where q is the vector of generalized coordinates being solved for x_i^{exp} is the experimental position of marker i, $x_i(q)$ is the position of the corresponding marker on the model (which depends on the coordinate values), q_j^{exp} is the experimental value for coordinate j (Delp et al., 2010).

4.4.3 Inverse Dynamics Tool

In classical mechanics, the mass-dependent relationship between force and acceleration is expressed with equations of motion. In OpenSim, the equations of motion (Equation 4.1) are expressed with the inverse dynamics (ID) Tool.

$$\underbrace{M(q)\ddot{q} + C(q,\dot{q}) + G(q)}_{knowns} = \underbrace{\tau}_{unkowns} \qquad 4.1$$

where N is the number of degrees of freedom; $q, \dot{q}, \ddot{q} \in R^N$ are the vectors of generalized positions, velocities, and accelerations, respectively; $M(q) \in R^{NxN}$ is the system mass matrix; $C(q,\dot{q}) \in R^N$ is the vector of Coriolis and centrifugal forces;

$G(q) \in R^N$ is the vector of gravitational forces; and $\tau \in R^N$ is the vector of generalized forces (Delp et al., 2010).

4.4.4 Static Optimization Tool

The Static Optimization Tool further resolves the net joint moments generated by the ID Tool into individual muscle forces at each time frame of data. The Static Optimization Tool uses the known motion of the model to solve for the equations of motion for the unknown generalized forces based on the following muscle activation-to-force conditions (Equation 4.2, derived from Zajac, 1989):

$$\underbrace{\sum_{m=1}^{nm}\left[a_m f(F_m^0, l_m, v_m)\right] r_{m,j} = \tau_j}_{\textit{constrained by force–length–velocity properties}} \qquad 4.2$$

while minimizing the objective function (Equation 4.3):

$$J = \sum_{m=1}^{nm} (a_m)^p \qquad 4.3$$

where nm is the number of muscles in the model; a_m is the activation level of muscle m at a discrete time step; F_m^0 is its maximum isometric force; l_m is its length; v_m is its shortening velocity; $f(F_m^0, l_m, v_m)$ is its force-length-velocity surface; $r_{m,j}$ is its

moment arm about the j^{th} joint axis; τ_j is the generalized force acting about the j^{th} joint axis; and p is a user defined constant which represents the power to which the activation level is raised (Delp et al., 2010; Zajac, 1989). The value of p is user defined because it reflects the objective function selected. For this study, the objective function selected was the minimization of muscle activation squared, so p had a value of two (further discussed in Section 4.5.4).

The equations of motion (Equation 4.1) are underdetermined in terms of muscle forces because the number of unknown muscle forces exceeds the number of available equations. By minimizing the objective (cost) function (Equation 4.3), the redundancy introduced from the muscular load sharing problem is addressed (de Zee et al., 2007; Erdemir et al., 2007).

4.5 Procedures for OpenSim Simulations

4.5.1 Scale Tool

The inputs to the Scale Tool were experimental marker locations (recorded with the Vicon motion capture system) while the participant was in a seated stationary pose. The dimensions of each segment in the model were scaled so that the distances between the virtual markers matched the distances between the experimental markers. The model mass properties (mass and inertia tensor) were scaled as well as the dimensions of the body segments. Each body segment was defined by a minimum of three user-defined marker pairs (Table 4.1). Three pairs are needed to define the X-Y-Z dimensions of each body segment in the model. Thus, the Scale Tool generated a patient-specific model

based on the height, width, and length of the marker pairs defined for the ribs, humerus, scapula, hand, clavicle, radius, and ulna. Most of the body segments were defined with more than three marker pairs to improve scaling accuracy. Also, the mass of the body segments in the model were adjusted so that the total body mass was equivalent to the mass of the participant. Since the cadaver-based mean proportions for the right arm and trunk were within one standard deviation of the mean DXA-based mass proportions (Chapters 3 and 5), the cadaver-based mass proportions (Winter, 2005) were included in the model. Thus, the Scale Tool distributed the weight of each body segment as a proportion of the participant's total body weight. In summary, the Scale Tool generated a patient-specific model based on the height and weight of the participant. Mass distribution was preserved during scaling.

Table 4. 1 Segment Body Measurement Sets Selected to Scale the Model

Measurements	**Marker Pairs**
Ribs	AC-SN, T3-XP, C7-SN, C7-T3,SN-XP, T3-SN, CP-SN, C7-XP
Humerus	AC-EL, AC-EM, EM-US, EL-RS, EM-RS, EL-US
Scapula	AA-AI, AI-TS, TS-AA, AC-CP, AC-TS, AC-AA, AC-AI, CP-AI, CP-TS
Hand	3MP-US, RS-US, 3MP-RS
Clavicle	ACJ-AC, SN-ACJ, CP-ACJ
Ulna	US-EM, US-RS, US-3MP, US-EL
Radius	RS-EL, RS-US, RS-EM, RS-3MP

Legend: AC= Acromion, SN= Sternal Notch, T3= T3 spinous process , XP = Xiphoid Process, C7= C7 spinous process, CP= Coracoid Process, EL= Lateral Epicondyle, EM= Medial epicondyle, US = Ulnar Styloid, RS= Radial Styloid, AA= Angulis Acromialis, AI= Angulus Inferior, TS= Trigonum Scapulae, ACJ= Acromioclavicular Joint, 3MP= 3rd Metacarpal joint. Anatomical locations of markers are in Figure 4.1.

4.5.2 Inverse Kinematics Tool

The 2mph propulsion trial was separated into five consecutive stroke cycles (Yarossi et al., 2010) and each individual stroke cycle was analyzed with the IK Tool. The weighted least squares problem was solved with a weight of one.

While the IK Tool was running in OpenSim, the marker error root mean square (RMS) and max marker error were reported for each time frame of data in the OpenSim Messages window. The literature for gait applications has reported errors in estimations of kinematics when the RMS exceeds 1 cm (Cereatti et al., 2006; Chiari et al., 2005). Thus, the maximum allowance of error due to soft tissue artifact was 1 cm. Each frame of data was inspected to ensure that the marker RMS did not exceed 1 cm. If the marker RMS was unacceptable, options for decreasing the RMS error included, lowering the weight for the marker in the Scale Tool and/or IK Tool or moving the marker on the model via the Scale Tool and performing the IK simulation again. Across all five stroke cycles, none of the markers had a RMS greater than 1 cm. Therefore, no adjustments were made to the virtual markers on the scaled model.

The IK tool presents the kinematic curves as a function of time, but wheelchair propulsion data is presented as a function of the propulsion cycle. The stroke cycle is defined as having two phases: push and recovery. The push phase is defined as the period when the hand is contact with the pushrim and applying force to the pushrim to maintain or increase wheelchair velocity, while the recovery phase is the period in between consecutive push phases when the arms are retracted in preparation for another push (Kwarciak et al., 2009; Sanderson and Sommer, 1985). MATLAB code was written to present the results according to 100% stroke cycle and distinguish the push phase from the recovery phase of the propulsion cycle (Appendix B.1).

4.5.3 Inverse Dynamics Tool

The ID Tool used Equation (4.1) to solve for the net moments at each joint (e.g., generalized forces) in the model. The motion of the model is defined by the generalized

positions, velocities, and accelerations, so all of the terms on the left hand side of the equation are known (Delp et al., 2010). The ID Tool used the known motion of the model (motion file output by the IK tool) to solve for the unknown generalized forces. Higher frequency noise (i.e., skin movement artifacts) is amplified by numerical differentiation, so the computed kinematic profiles were filtered with a low-pass filter with a cutoff frequency of 6 Hertz (Yarossi et al., 2010) in OpenSim. MATLAB code was written to present the results according to 100% stroke cycle and distinguish the push phase from the recovery phase of the propulsion cycle (Appendix B.2).

4.5.4 Static Optimization Tool

The inputs to the Static Optimization Tool were the model, the motion file generated by the IK Tool, and the motion file containing the forces to be applied to the model. The muscle force generated was constrained to its force-length-velocity properties so that muscle physiology could be incorporated. However, the force-length-velocity properties used were determined for able-bodied populations, as force-length-velocity curves for SCI populations were not available.

As discussed in detail in Chapter 1, the objective function selected for this study was the minimization of muscle activation squared. The objective function was selected after performing a thorough review of the literature. As mentioned in Chapter 1, there is not a common objective function that is used with wheelchair propulsion simulation studies. This objective function was selected in accordance with van der Helm (1994), who suggested that the minimization of muscle stress squared allows for the distribution of muscle forces based on muscle cross-sectional area and is computationally efficient. The Wheelchair Propulsion Model contains the muscles of the shoulder complex, so it is

important to capture each muscle's contribution to wheelchair propulsion. Therefore, an objective function that allows for the distribution of muscle forces based on muscle cross-sectional area is desirable. Given the objective function selected for this study, the value for user defined constant p in Equation 4.3 was 2. Muscle activation is approximately equal to muscle stress multiplied by a proportionality constant, provided a muscle operates on the flat portion of its force-length curve at small contraction velocities (Equation 4.4):

$$a_m = \frac{F_m}{f(F_m^0, l_m, v_m)} \approx k\frac{F_m}{PCSA} \; when \; l_m \approx l_m^0 \; and \; v_m \approx 0.0 \qquad 4.4$$

where PCSA is the physiological cross-sectional area, F_m/PCSA is muscle stress, k is a constant, and l_m^0 is the optimal muscle-fiber length (Anderson & Pandy, 2001; Zajac, 1989). The values of these muscle properties were obtained from the Stanford VA Model (Holzbaur et al., 2005), Head and Neck Model (Vasavada et al., 1998), and Garner and Pandy's (2003) upper limb computational model. The values from the Stanford VA Model and the Vasavada model were obtained from cadaver studies of muscle properties. Since no cadaver data were available for the serratus anterior and rhomboid major, the muscle properties were obtained from the Garner and Pandy model, which was a computational model that estimated the muscle properties of the upper limb.

In order for the solution to converge (solution for minimization of objective function), the static optimization technique requires the muscles forces to balance the

external forces. Partial muscle paralysis due to tetraplegia was not accounted for in the model because it would entail decreasing the optimal force of the muscles, thus requiring more force in the remaining muscles to balance the external moment. As a result, the estimated muscle forces are most likely underestimated. In their optimization study of wheelchair related activities of daily living in manual wheelchair users with paraplegia and tetraplegia (compared with able-bodied controls), van Drongelen and colleagues (2005a) did not account for partial muscle paralysis in SCI for the same reason and anticipated that the differences in task performance would reflect the partial paralysis due to SCI. Extra actuators were also added (appended) to the coordinates in the model. Some of the muscles were not strong enough to achieve the propulsive movements in the amount of time it took the subject to propel during each stroke cycle. The appended actuators ensured that the model met the accelerations in the time required.

The Static Optimization Tool generated three outputs: controls (minimized by the Static Optimization Tool), muscle activations, and muscle forces. MATLAB code was written to present the results according to 100% stroke cycle and distinguish the push phase from the recovery phase of the propulsion cycle (Appendix B.3).

4.6 Statistical Analyses

While computer graphics-based models may be utilized to address clinical questions that cannot be answered with traditional experimental biomechanical techniques alone, the models must be validated. However, care has to be taken in the interpretation of results when investigating calculated muscle forces with experimentally collected EMG amplitudes (Dubowsky et al., 2008). Currently, there is no technique that allows for

direct measurement of muscle forces *in vivo* (Dubowsky et al., 2008; Erdemir et al., 2007; Nikooyan et al., 2010). As an alternative, a common method and accepted method for evaluating calculated muscle forces and model validation is to compare the muscle force or activation patterns with experimental EMG activity patterns (Crowninshield, 1978). In previous wheelchair propulsion optimization studies (Lin et al., 2004; van Drongelen et al., 2005a), researchers compared their results with EMG patterns from the literature. Dubowsky and colleagues (2008) and Morrow et al. (2010) compared their results with experimental EMG collected from the participants investigated, but surface EMG was collected in their studies. Therefore these researchers were limited to comparing the superficial muscles of the shoulder (anterior and posterior deltoids, upper trapezius, sternal portion of the pectoralis major, long head of the triceps, and biceps brachii). The current study is the first to compare estimated muscle force patterns with fine-wire EMG collected directly from the participant being studied. Temporal characteristics and the intensity of muscle firing during wheelchair propulsion can be compared with this indirect method of muscle force evaluation.

4.6.1 Cross Correlation Analyses

For a more quantitative approach (de Zee et al., 2007), cross correlations ($\alpha = 0.05$) of the muscle forces estimated by OpenSim and the experimental EMG were determined for each muscle for each stroke cycle. This allowed for a comparison of the amplitude of the estimated muscle force profile and the amplitude of the experimental EMG profile by determining the phasing between the two profiles. A MATLAB cross correlation code, modified from Forrest (2001), was used to calculate the cross correlation coefficients. The following terminology, modified from Portney and Watkins (2009), is used to reflect

the strength of associations observed between measures, |r|: 0.00 to 0.25, little to no relationship; 0.26 to 0.49, fair degree of relationship; 0.50 to 0.69 moderate to good relationship; > 0.70, good to excellent relationship.

4.6.2 Mean Absolute Error

Electromyography cannot verify the magnitude of the calculated muscle force (Crowninshield, 1978; Erdemir et al., 2007; Lin et al., 2004,). As a quantitative approach to evaluate the magnitude of the calculated force, the mean absolute error (MAE) between the experimental muscle activity and the estimated muscle activity was also calculated. The MAE has been used to validate a computational musculoskeletal model (de Zee et al., 2007) and has been used recently to validate musculoskeletal models that estimated shoulder joint contact forces during wheelchair propulsion (Dubowsky et al., 2008) and wheelchair activities (Morrow et al., 2010). Equation 4.5 expresses how the MAE is calculated:

$$MAE = \frac{1}{n}\sum_{i=1}^{n}\left|MA_i - EA_i\right| \qquad 4.5$$

where n is the number of frames within a propulsion cycle, MA_i is the measured EMG muscle activity as a percentage of maximum voluntary contraction on frame i, EA_i is the model estimated muscle activity as a percentage of maximum muscle force on frame i.

An average MAE of less than 0.10 represents an excellent quantitative correlation, while a value between 0.10 and 0.20 represents a good correlation, and a value greater than

0.20 represents a poor correlation (Dubowsky et al., 2008; Morrow et al., 2010). MATLAB code was written to compute the MAE for 100% stroke cycle for each stroke cycle (Appendix C).

CHAPTER 5

RESULTS

5.1 SCI-specific Segment Mass Analysis and Statistics

5.1.1 SCI-Specific Body Segment Mass Study

For all participants scanned using densitometry, the mean cadaver-based trunk lean mass proportion was within one standard deviation of the mean DXA-based trunk mass proportion (Table 5.1).

Table 5.1 DXA-based and Cadaver-based Body Segment Proportions

		Tetraplegia		**Paraplegia**		**Controls**	
		Arm	**Trunk**	**Arm**	**Trunk**	**Arm**	**Trunk**
DXA	Mean	0.057	0.501	0.072	0.509	0.060	0.480
	SD	±0.009	±0.032	±0.008	±0.035	±0.005	±0.032
Cadaver	Mean	0.050	0.497	0.050	0.497	0.050	0.497

Note: DXA-based body segment proportions are based on the ratio of lean mass of the segment to total body mass of the segment. Standard deviations of the cadaver body segment proportions were not available.

The cadaver-based arm mass proportions were different than the DXA-based mass proportions for the participants with paraplegia and the able-bodied controls. In contrast, the cadaver-based proportions were similar to those of the DXA-based mass proportions for the right arm and trunk for the participants with tetraplegia. Therefore, these cadaver-based estimates were included in the model.

5.1.2 Comparisons between DXA Group and Wheelchair Propulsion Group

The one-way multivariate ANOVA ($\alpha = 0.05$) demonstrated that there was no significant difference between the participants with tetraplegia from the DXA database and the participants with tetraplegia from the wheelchair propulsion database based on age ($p = 0.796$) or time since injury ($p = 0.582$). The results of the statistical test demonstrate that the DXA database group and the wheelchair propulsion database group are comparable for both age and time since injury. There was no difference in demographic variables between the DXA group and the wheelchair propulsion group. Lean tissue mass in the DXA group was not significantly different from the cadaver data. Therefore, it is valid to use these cadaver-based mass estimates as suitable body segment masses for patient-specificity and generation of dynamic simulations of wheelchair propulsion.

5.2 Scaling

Based on the defined measurements from the marker pairs (Chapter 4), scale factors (Table 5.2) were applied to scale the dimensions of the model to the participant. To generate a patient-specific model, the generic model's dimensions were scaled up.

Table 5.2 Scale Factors Applied to Scale Model Dimensions to Participant

Body Name	Measurement Used	Applied Scale Factor(s)
Ground	Unassigned	1.00
Ribs	Ribs	1.000073
Right Clavicle	Clavicle	1.00483
Right Scapula	Scapula	1.000192
Right Humerus	Humerus	1.000252
Right Ulna	Ulna	1.00259
Right Radius	Radius	1.000233
Right Hand	Hand	1.000257

5.3 Inverse Kinematics

The marker errors for all five consecutive stroke cycles met the required cutoff value of 1 cm. The outputs of the IK Tool were coordinates (measured in degrees) and marker positions (measured in meters). Shoulder kinematics were determined for elevation plane, elevation angle and rotation. Elbow kinematics were determined for elbow flexion and forearm rotation.

Shoulder elevation plane curves (Figure 5.1) were computed for all five stroke cycles. As shown in Figure 5.1, modeled kinematics during push phase were very consistent while there was greater variability during the recovery phase. The average peak shoulder elevation plane (across all five stroke cycles) was 38.5° (± 0.3°) during push phase and 37.2° (± 1.0°) during the recovery phase. During the recovery phase the hand is no longer constrained to the pushrim, so there is an increase in shoulder elevation plane variability.

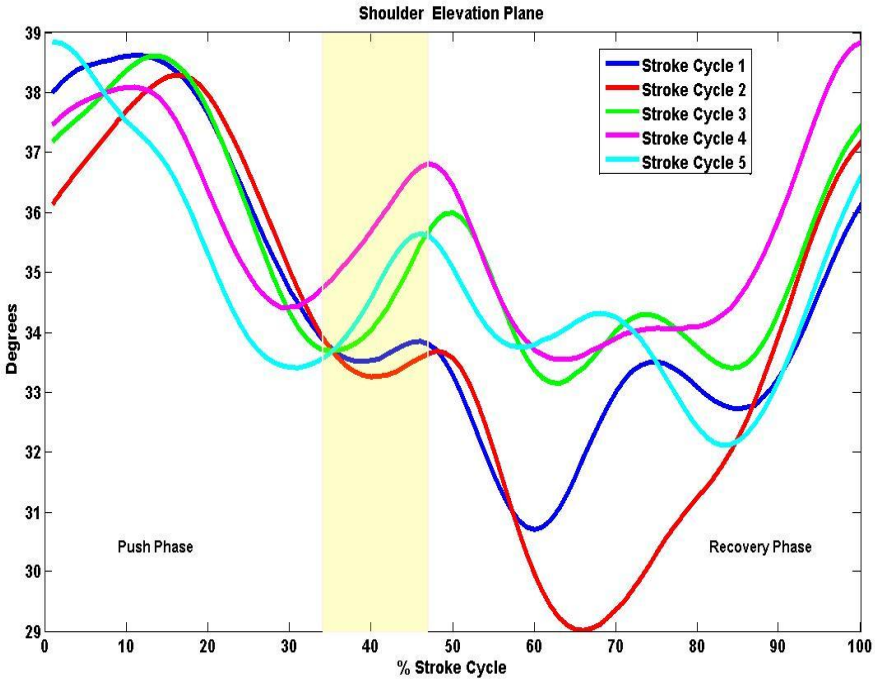

Figure 5.1 Shoulder elevation plane curves, per 100% stroke cycle, computed by the IK Tool for each stroke cycle. The elevation plane degree of freedom describes the orientation of the vertical plane in which the humerus elevates relative to the frontal plane (Holzbaur et al. 2005). The yellow bar indicates the transition from push phase to recovery phase across all five stroke cycles.

The elevation angle curves (Figure 5.2) for all stroke cycles were consistent with an average peak of 13.9° (± 10.1°) during push phase and 33° (± 3.4°) during recovery. The elevation angle curves also demonstrate the changes in the thoracohumeral angle during propulsion and recovery. The participant started propelling with his hand at the rear of the pushrim, a common starting position selected by persons with tetraplegia (Dallmeijer et al. 1998). At approximately 42% of the stroke cycle (during propulsion), the humerus is parallel to the vertical axis of the thorax and the thoracohumeral angle is increasing. At approximately 50% of the stroke cycle, the hand and humerus are repositioned to the rear of the pushrim and the thoracorhumeral angle decreased.

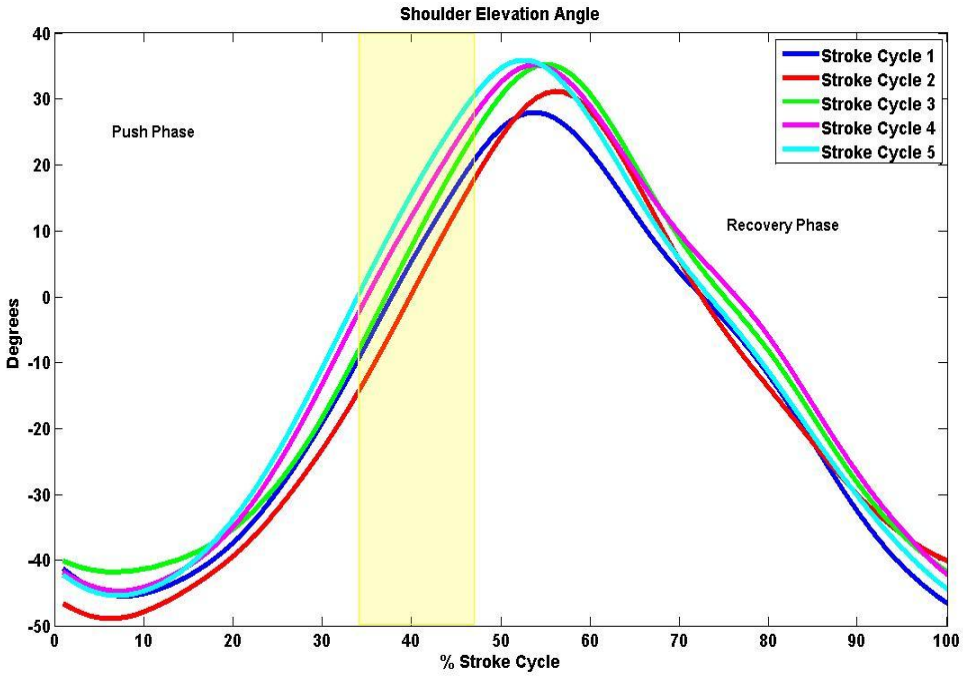

Figure 5.2 Shoulder elevation angle curves, per 100% stroke cycle, determined by the IK Tool for each stroke cycle. This figure demonstrates the changes in the thoracohumeral angle during propulsion. Neutral elevation angle (0°) for the shoulder is defined when the shaft of the humerus is parallel to the vertical (superior-inferior) axis of the thorax (Holzbaur et al. 2005). The yellow bar indicates the transition from push phase to recovery phase across all five stroke cycles.

The shoulder rotation curves (Figure 5.3) were highly consistent with an average peak of 56.6° (± 0.9°) during push phase and 56.7° (± 0.9°) during recovery. The shoulder rotation curves also describe how the shoulder joint rotated during propulsion. At the start of propulsion, the humerus, radius and hand are positioned at the rear of the pushrim and the shoulder was internally rotated. During propulsion the shoulder rotated externally. Peak external rotation occurred at approximately 52% of the stroke cycle (recovery phase). At the start of the following stroke cycle, the humerus, ulna, and hand were repositioned at the rear of the pushrim and the shoulder joint was internally rotated.

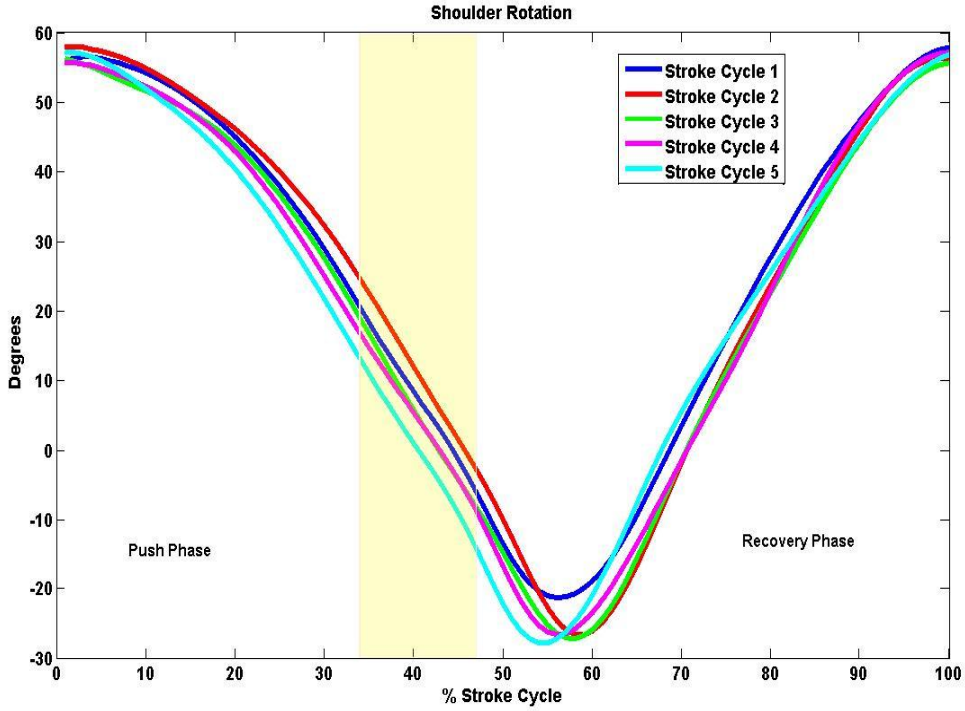

Figure 5.3 Shoulder rotation curves, per 100% stroke cycle, computed by the IK Tool for each stroke cycle. Positive values indicate internal rotation and negative values indicate external rotation. Neutral (0°) axial rotation is defined by the orientation of the humerus when the shoulder is at neutral elevation angle, the elbow is flexed 90°, and the forearm lies in the sagittal plane (Holzbaur et al. 2005). The yellow bar indicates the transition from push phase to recovery phase across all five stroke cycles.

The maximum and minimum values for each degree of freedom at the shoulder were determined for each stroke cycle and are listed in Table 5.3. Elevation angle maxima were most similar during Stroke Cycles 3, 4 and 5. The maxima were most similar for the shoulder elevation plane and rotation over all five stroke cycles. The minima for shoulder rotation were the most similar for Stroke Cycles 2-5.

Table 5.3 Maxima and Minima of Generated Shoulder Kinematics

	Elevation Plane		**Elevation Angle**		**Rotation**	
	Min (°)	Max (°)	Min (°)	Max (°)	Min (°)	Max (°)
Stroke Cycle 1	30.7	38.6	-46.5	27.8	-21.2	57.8
Stroke Cycle 2	29.0	38.3	-48.8	31.1	-26.5	57.8
Stroke Cycle 3	33.1	38.6	-41.7	35.1	-27.1	56.1
Stroke Cycle 4	33.5	38.8	-44.6	35.1	-26.5	57.1
Stroke Cycle 5	32.1	38.8	-45.3	35.7	-27.7	57.1

The IK Tool was also used to determine the elbow flexion and forearm rotation profiles during propulsion (Figure 5.4 and 5.5, respectively). The five elbow flexion curves (Figure 5.4) were highly consistent with an average peak of 85.7° (± 0.3°) during push phase and 67.9° (± 6.8°) during recovery. Elbow flexion is defined from 0° (full extension) to 130° (flexion) (Holzbaur et al. 2005). These curves illustrate an increase in elbow flexion during the first 25% of the stroke cycle (propulsion) followed by an increase in elbow extension at 25-50% of the stroke cycle. During recovery phase, elbow extension and flexion occurred from 50-65% and 65-85% of the stroke cycle, respectively. Maximum (85°) and minimum (45°) elbow flexion occurred at 25% and 85% of the stroke cycle, respectively. The data show that the participant's elbow was flexed for most of the push phase and about half of the recovery phase. The elbow was extended for about half of the recovery phase.

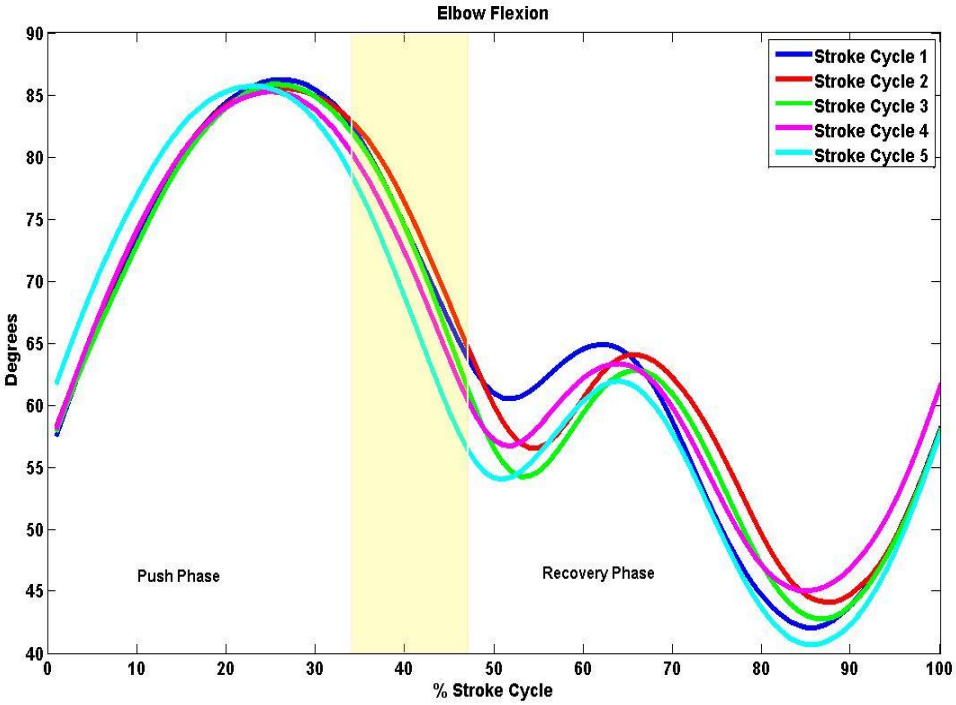

Figure 5.4 Elbow flexion curves, per 100% stroke cycle, computed by the IK Tool for each stroke cycle. Elbow flexion is defined from 0° (full extension) to 130° (flexion) (Holzbaur et al. 2005). The yellow bar indicates the transition from push phase to recovery phase across all five stroke cycles.

Forearm rotation is defined from -90° (supination) to 90° (prontation) (Holzbaur et al. 2005). The forearm rotation curves (Figure 5.5) demonstrate that the elbow was supinated during the push phase. The transition from supination to pronation occurred just at or after hand release and double-looping over the propulsive path. Peak elbow pronation occurred at approximately 80% of the stroke cycle. At initial position of the propulsive phase, the elbow position was less pronated and very close to neutral position. Forearm rotation had an average peak of 85.7° (± 2.3°) during push phase and 28.8° (± 4.5°) during recovery, across all five stroke cycles.

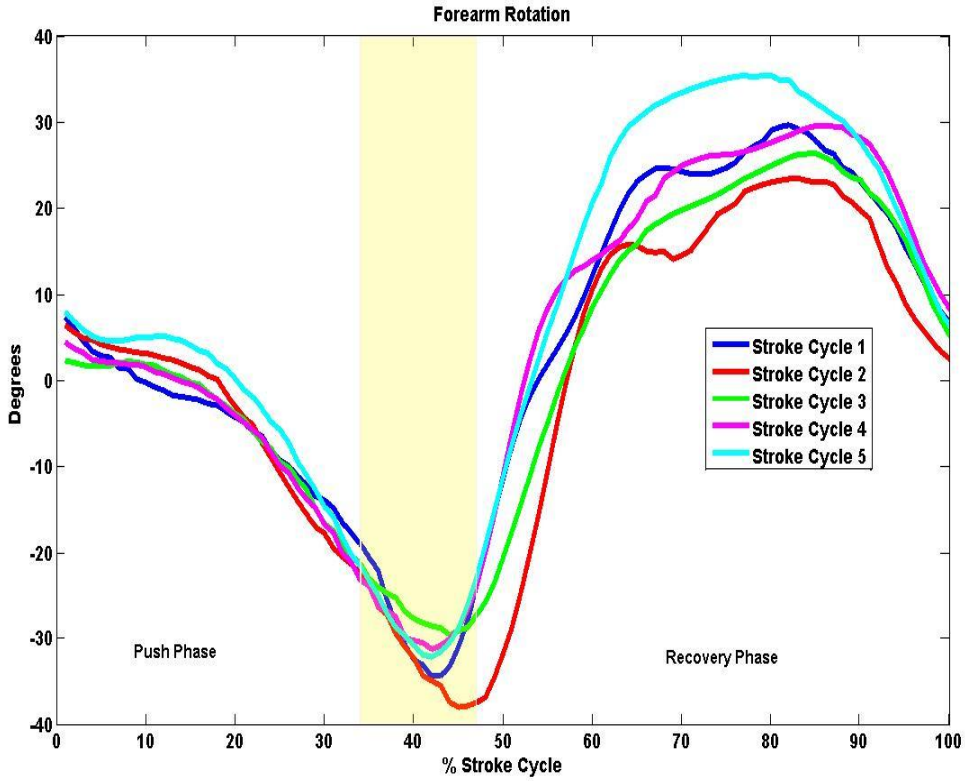

Figure 5.5 Forearm rotation (pronation-supination) curves, per 100% stroke cycle, computed by the IK Tool for each stroke cycle. Forearm rotation is defined from 90° (pronation) to -90° (supination) (Holzbaur et al. 2005). The yellow bar indicates the transition from push phase to recovery phase across all five stroke cycles.

The maxima and minima of the degrees of freedom at the elbow were also determined and are listed in Table 5.4. The elbow flexion maxima were most consistent over all five stroke cycles. The maxima and minima of forearm rotation were the least consistent across the stroke cycles.

Table 5.4 Maxima and Minima of Generated Elbow and Forearm Kinematics

	Elbow Flexion		**Forearm Rotation**	
	Min (°)	Max (°)	Min (°)	Max (°)
Stroke Cycle 1	42.1	86.1	-34.3	29.6
Stroke Cycle 2	44.2	85.5	-37.9	23.4
Stroke Cycle 3	42.8	85.8	-29.5	26.3
Stroke Cycle 4	45.1	85.2	-31.2	29.5
Stroke Cycle 5	40.8	85.6	-32.1	35.3

5.4 Inverse Dynamics

The ID Tool computed the moments at the shoulder for all five stroke cycles. Of the three shoulder degrees of freedom, the average peak moment about the shoulder elevation plane (Figure 5.6) was the greatest during the push phase (18.5 Nm ± 1.0 Nm) and the recovery phase (16 Nm ± 1.7 Nm). Peak shoulder elevation plane moment occurred during the push phase.

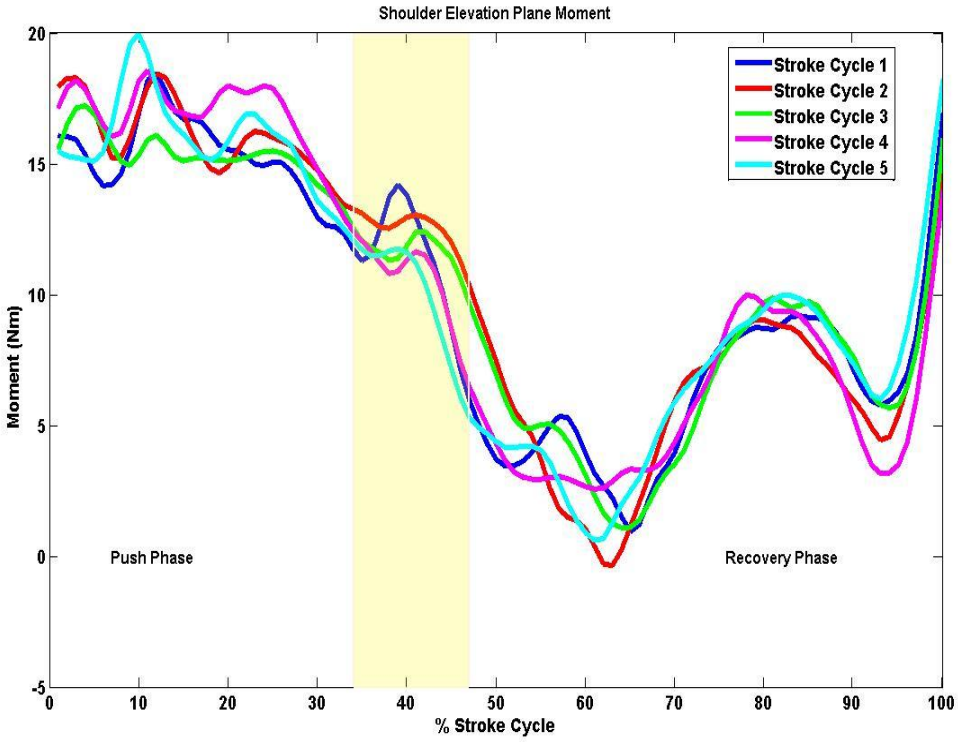

Figure 5.6 Shoulder elevation plane moment curves, per 100% stroke cycle, computed by ID Tool for each stroke cycle. The moment peaked at the beginning of the push phase. The yellow bar indicates the transition from push phase to recovery phase across all five stroke cycles.

The average peak moment responsible for shoulder elevation angle (Figure 5.7) was greater during the recovery phase (1.4 Nm ± 0.7 Nm) than the push phase (-4.6 Nm ± 0.9 Nm). Peak shoulder elevation angle moment occurred during the recovery phase.

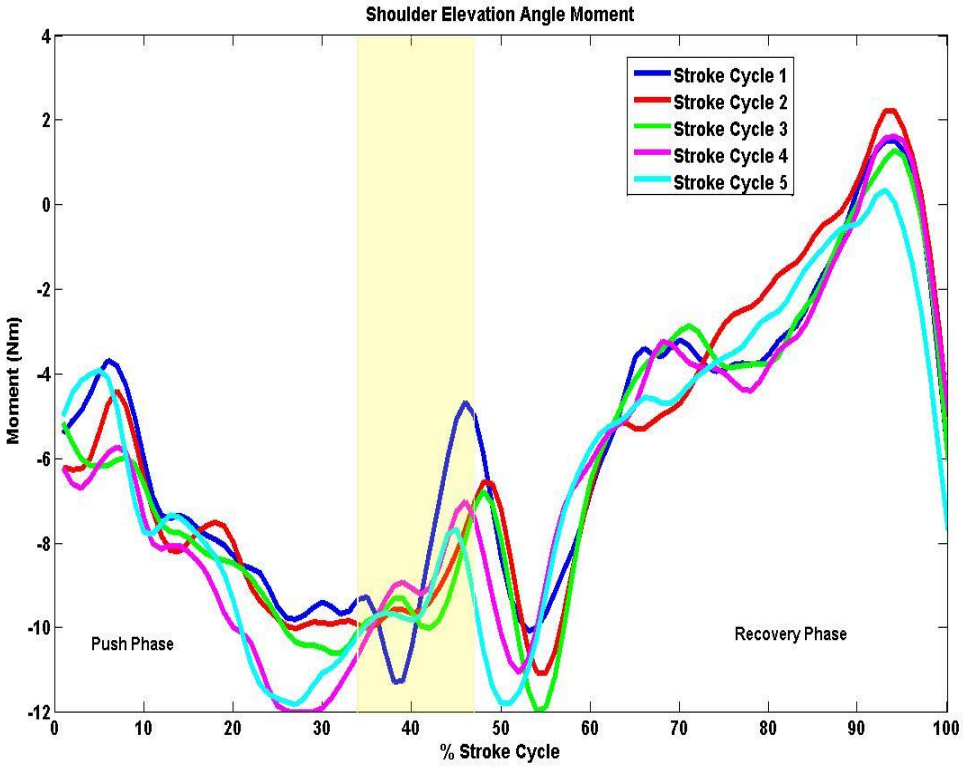

Figure 5.7 Shoulder elevation angle moment curves, per 100% stroke cycle, computed by ID Tool for each stroke cycle. The moment peaked at the end of the recovery phase for all stroke cycles. The yellow bar indicates the transition from push phase to recovery phase across all five stroke cycles.

The average peak moment responsible for shoulder rotation (Figure 5.8) was also greater during the recovery phase (-2.9 Nm ± 0.4 Nm) than the push phase (-0.27 Nm ± 0.3 Nm). Peak shoulder rotation moment occurred during the recovery phase.

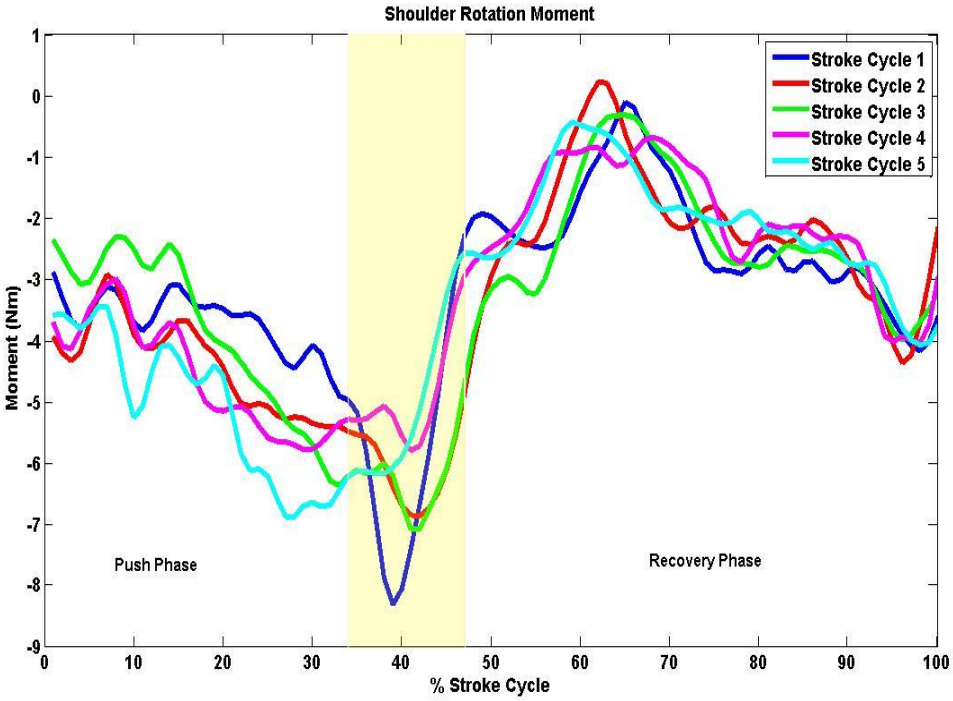

Figure 5.8 Shoulder rotation moment curves, per 100% stroke cycle, computed by the ID Tool for each stroke cycle. The moment peaked around the middle of the recovery phase for all stroke cycles. The yellow bar indicates the transition from push phase to recovery phase across all five stroke cycles.

Shoulder moment maxima and minima were determined for all three DOF at the shoulder (Table 5.5). The elevation angle minima and the elevation plane maxima were the most consistent over all five stroke cycles. The elevation plane minima were the least consistent over all five stroke cycles.

Table 5.5 Maxima and Minima of Generated Shoulder Moments

	Elevation Plane		Elevation Angle		Rotation	
	Min (Nm)	Max (Nm)	Min (Nm)	Max (Nm)	Min (Nm)	Max (Nm)
Stroke Cycle 1	1.0	18.4	-11.3	1.5	-8.3	-0.1
Stroke Cycle 2	-0.3	18.4	-11.1	2.2	-6.9	0.2
Stroke Cycle 3	1.1	17.2	-12.0	1.3	-7.1	-0.3
Stroke Cycle 4	2.6	18.5	-12.0	1.6	-5.8	-0.9
Stroke Cycle 5	0.6	19.9	-11.8	0.3	-6.9	-0.4

5.5 Static Optimization

The Static Optimization Tool determined the muscle forces generated during wheelchair propulsion. The maximum muscle forces generated during the push phase of propulsion are displayed in Figure 5.9. The muscles that generated the greatest average force over all five stroke cycles during the push phase were the serratus anterior (406.6 ± 42.5 N) and middle deltoid (310.1 ± 60.6 N). The posterior deltoid (124.7 ± 14.7 N), infraspinatus (78.6 ± 6.2 N), biceps (32.3 ± 18.5 N), middle trapezius (31.7 ± 60.6 N), subscapularis (19.2 ± 0.2 N), and supraspinatus (15.1 ± 7.0 N) also contributed to push phase of propulsion. The pectoralis major (6.2 ± 0.2 N), upper trapezius (3.0 ± 0.05 N), anterior deltoid (2.1 ± 0.8 N), triceps (1.6 ± 2.8 N), and rhomboids major (1.3 ± 0.0004 N), and contributed little to no force to the push phase of wheelchair propulsion.

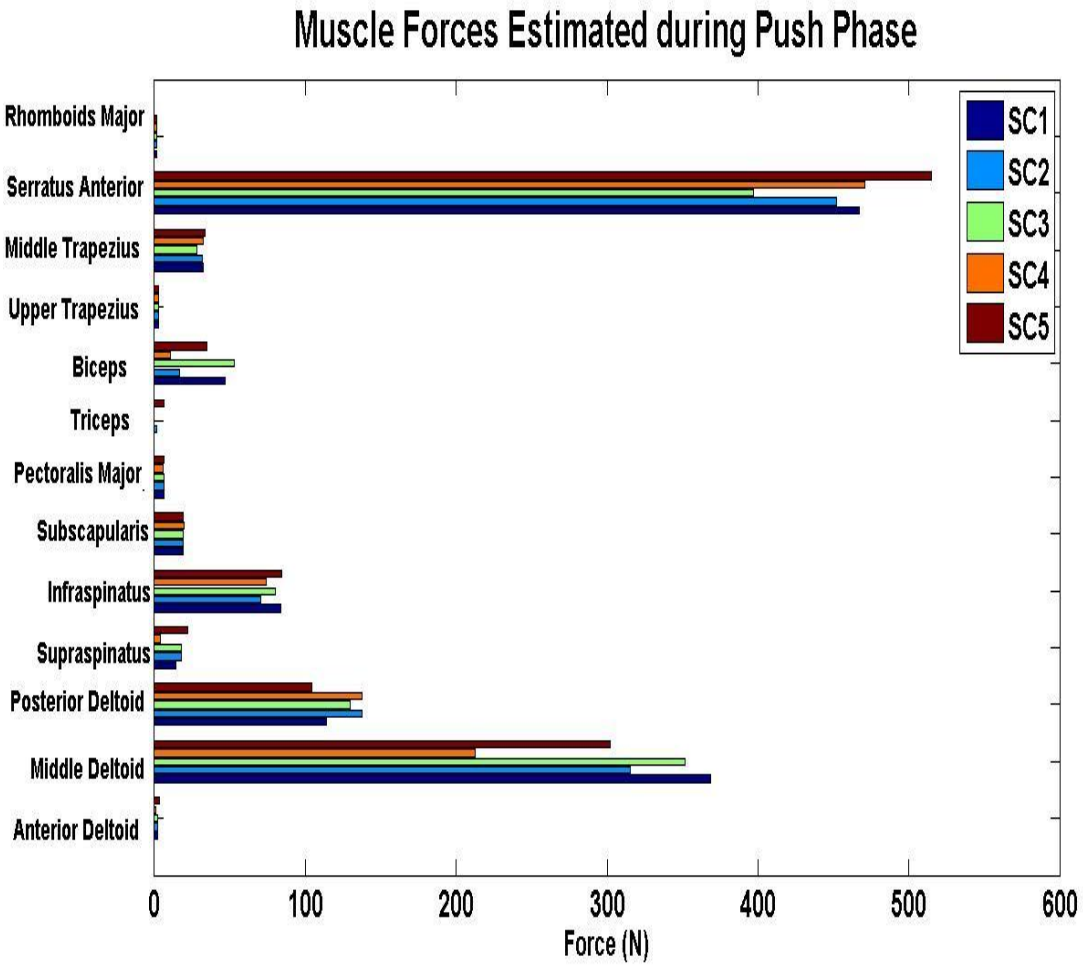

Figure 5.9 Estimated shoulder complex muscle forces during push phase of propulsion for all five stroke cycles. The muscles selected were the muscles for which experimental EMG was recorded.

The maximum muscle forces generated during the recovery phase of propulsion are displayed in Figure 5.10. The muscles that generated the greatest average force during the recovery phase (across all five stroke cycles) were the middle deltoid (244.8 ± 66.1 N), serratus anterior (199.6 ± 18.1 N), posterior deltoid (155.6 ± 13.3 N), and infraspinatus (129.8 ± 15.0 N). The supraspinatus (37 ± 7.4 N), triceps (27.8 ± 2.6 N), subscapularis (23.0 ± 3.7 N), and middle trapezius (14.1 ± 1.5 N) also contributed to the recovery phase of propulsion. The pectoralis major (6.4 ± 0.03 N), anterior deltoid (3.9 ±

0.6 N), rhomboids major (2.1 ± 0.7 N), upper trapezius (1.4 ± 0.1 N), and biceps (0.9 ± 0.1 N) generated little to no force during the recovery phase.

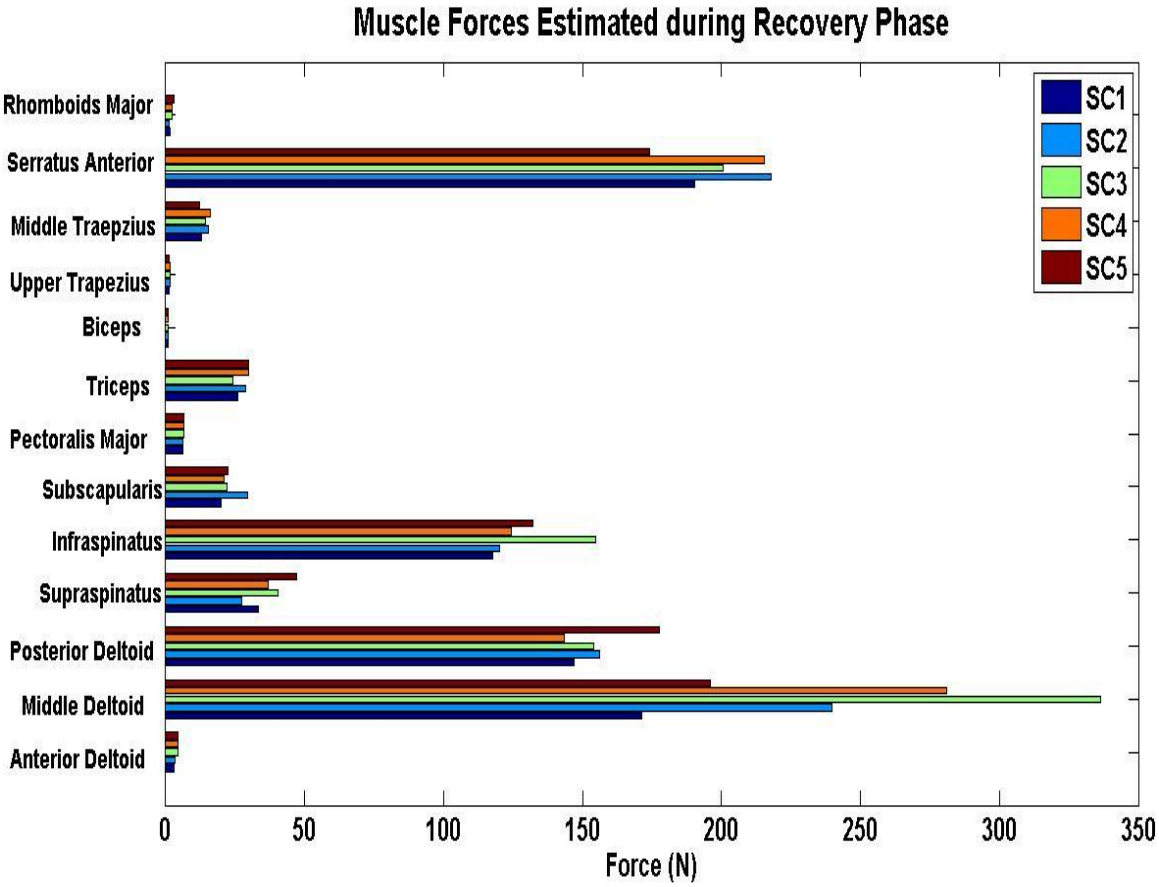

Figure 5.10 Estimated shoulder complex muscle forces during recovery phase of propulsion for all five stroke cycles. The muscles selected were the muscles for which experimental EMG was recorded.

5.6 Static Optimization Statistical Analyses

5.6.1 Cross Correlation Analyses

Cross correlation analyses were performed based on 100% stroke cycle, push phase, and recovery phase. The estimated muscle force profiles were compared with the

experimental EMG profile. After reviewing the raw EMG data, it was noted that there was an electrode placement issue for the pectoralis major, upper trapezius, and middle trapezius. Therefore, these three muscles were excluded from the cross correlation analyses because sufficient EMG could not be collected during testing.

5.6.1.1 Cross Correlation Analyses for 100% Stroke Cycle. The cross correlation coefficients for 100% stroke cycle were determined for all ten muscles investigated, per stroke cycle (Table 5.6). During Stroke Cycle 1, the muscle EMG and muscle force patterns with good to excellent relationships were the anterior and posterior (0.74 - 0.75) deltoids. The middle deltoid, supraspinatus, infraspinatus, triceps, biceps, and serratus anterior had moderate to good relationships (0.54 – 0.67). The subscapularis and rhomboids major had fair relationships (0.48). Negative correlations were observed for the middle deltoid and the subscapularis (-0.62 and -0.48, respectively).

Table 5.6 Cross Correlation Coefficients per 100% Stroke Cycle

Muscle	Stroke Cycle 1	Stroke Cycle 2	Stroke Cycle 3	Stroke Cycle 4	Stroke Cycle 5
Anterior Deltoid	0.74	0.69	0.73	0.80	0.72
Middle Deltoid	-0.62	-0.75	-0.63	-0.59	-0.73
Posterior Deltoid	0.75	0.68	0.65	0.68	0.68
Supraspinatus	0.56	-0.46	-0.40	-0.35	0.40
Infraspinatus	0.57	0.56	0.66	0.65	0.47
Subscapularis	-0.48	-0.52	0.67	-0.61	-0.57
Triceps	0.54	0.59	0.55	-0.45	-0.50
Biceps	0.67	0.50	0.76	0.81	0.72
Serratus Anterior	0.67	0.60	0.60	0.61	0.59
Rhomboids Major	0.48	-0.37	0.32	0.33	0.37

Legend: Green highlighting represents good to excellent relationship, yellow highlighting represents moderate to good relationship, and red highlighting represents fair relationship.

During Stroke Cycle 2, the middle deltoid had a good to excellent relationship. The anterior and posterior deltoids, infraspinatus, subscapularis, triceps, biceps, and serratus anterior had moderate to good relationships (0.50 – 0.69). The supraspinatus and rhomboids major had fair relationships (0.37 – 0.46). Negative correlations were observed for the middle deltoid (-0.75), supraspinatus (-0.46), subscapularis (-0.52), and rhomboids major (-0.37).

During Stroke Cycle 3, the anterior deltoid and biceps had good to excellent relationships (0.73 – 0.76). The middle and posterior deltoids, infraspinatus,

subscapularis, triceps, and serratus anterior had moderate to good relationships (0.55 - 0.67). The supraspinatus and rhomboids major had fair relationships (0.32 - 0.40). Negative correlations were observed for the middle deltoid and supraspinatus (-0.63 and -0. 35, respectively).

During Stroke Cycle 4, the anterior deltoid and biceps had good to excellent relationships (0.80 – 0.81). The middle and posterior deltoids, infraspinatus, subscapularis, and serratus anterior had moderate to good relationships (0.59 – 0.68). The supraspinatus, triceps, and rhomboids major had fair relationships (0.33 – 0.45). Negative correlations were observed for the middle deltoid (-0.59), supraspinatus (-0.35), subscapularis (-0.61), and triceps (-0.45).

During Stroke Cycle 5, the anterior and middle deltoids and the biceps had good to excellent relationships (0.72 – 0.73). The posterior deltoid, subscapularis, triceps, and serratus anterior had moderate to good relationships (0.50 – 0.72). The supraspinatus, infraspinatus, and rhomboids major had fair relationships (0.37 – 0.47). Negative correlations were observed for the middle deltoid (-0.73), subscapularis (-0.57), and triceps (-0.50).

In summary, the anterior deltoid had a good to excellent relationship over all five stroke cycles (0.69 – 0.80), while the rhomboids major had a fair relationship (0.32 – 0.48). The serratus anterior consistently maintained a moderate to good relationship (0.59 – 0.67) over all five stroke cycles. Positive correlations were consistently observed for the anterior and posterior deltoids, infraspinatus, biceps, and serratus anterior over all five stroke cycles. A negative correlation was consistently observed for the middle deltoid (-0.59 - -0.75) over all five stroke cycles. Based on the absolute value of the cross

correlation coefficients, the investigated muscles were divided into two groups: responders and non-responders (Figure 5.11).

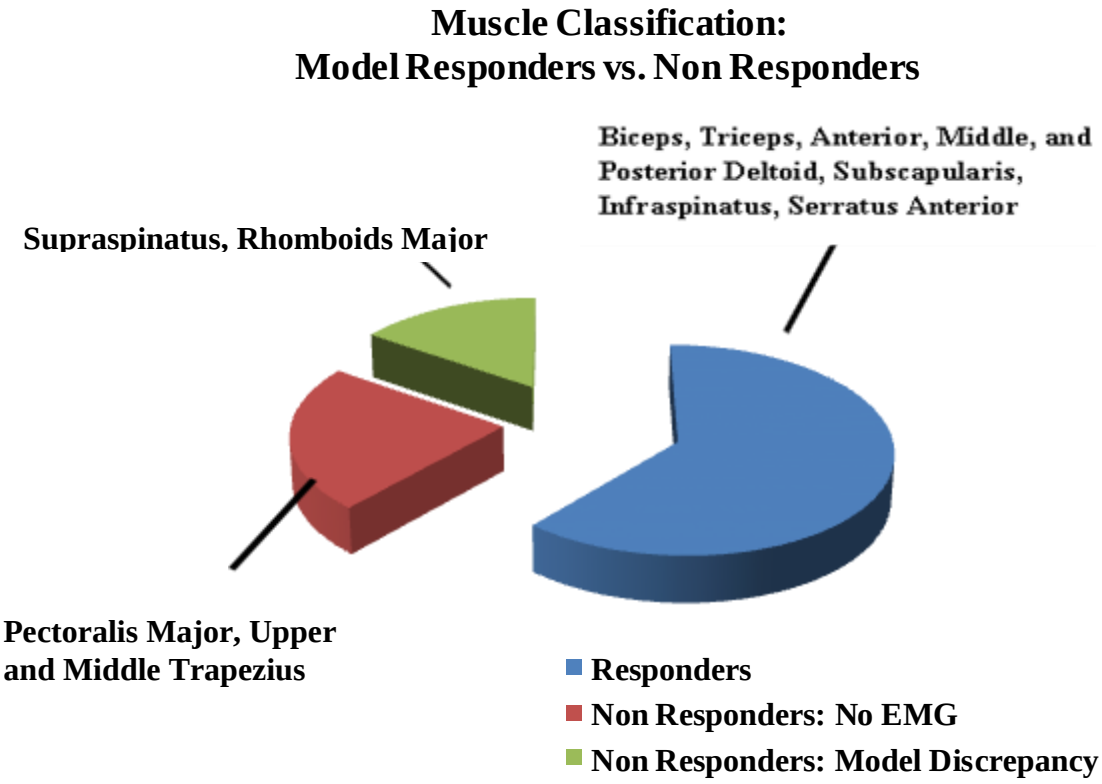

Figure 5.11 Muscle classification based on the cross correlation analyses of the estimated muscle force and the experimental EMG per 100% stroke cycle. The investigated muscles were identified as either model responders or non-responders. Muscles with consistent good to excellent relationships or moderate to good relationships over all five stroke cycles were defined as model responders. Model non responders were defined as muscles with consistent fair relationships over all five stroke cycles. A subgroup of muscles could not be included in the analyses because sufficient EMG could not be collected during testing and were also classified as model non responders.

5.6.1.2 Cross Correlation Analyses for the Push Phase of Propulsion. The cross correlation coefficients were also determined for the push phase of propulsion for all five stroke cycles (Table 5.7). During the push phase of Stroke Cycle 1, only the middle

deltoid had a good to excellent relationship (0.71). The anterior and posterior deltoids, supraspinatus, subscapularis, biceps, and rhomboids major had moderate to good relationships (0.50 – 0.68). The infraspinatus and rhomboids major had fair relationships (0.36 – 0.38). All of the correlations were positive. The Static Optimization Tool estimated that the triceps generated no force during push phase, so its cross correlation coefficient could not be determined.

Table 5.7 Push Phase Cross Correlation Coefficients

Muscle	Stroke Cycle 1: Push	Stroke Cycle 2: Push	Stroke Cycle 3: Push	Stroke Cycle 4: Push	Stroke Cycle 5: Push
Anterior Deltoid	**0.68**	**0.70**	**0.81**	**0.74**	**0.61**
Middle Deltoid	**0.71**	**0.63**	**0.53**	**0.59**	**0.54**
Posterior Deltoid	**0.60**	**0.55**	**0.50**	**0.60**	**0.72**
Supraspinatus	**0.58**	**0.46**	**0.52**	**0.35**	**0.57**
Infraspinatus	**0.38**	**-0.39**	**0.43**	**0.61**	**-0.58**
Subscapularis	**0.51**	**-0.58**	**0.55**	**0.52**	**0.50**
Triceps	*	**0.31**	*	*	**0.37**
Biceps	**0.50**	**0.59**	**0.58**	**0.66**	**0.57**
Serratus Anterior	**0.51**	**0.44**	**0.56**	**-0.42**	**-0.47**
Rhomboids Major	**0.36**	**0.50**	**-0.28**	**0.46**	**0.41**

Legend: Green highlighting represents good to excellent relationship, yellow highlighting represents moderate to good relationship, and red highlighting represents fair relationship. The Static Optimization Tool estimated no force for the triceps during the push phase of Strokes 1, 3, and 4, so the cross correlation could not be performed and is indicated with an asterisk.

During the push phase of Stroke Cycle 2, only the anterior deltoid had a good to excellent relationship (0.70). The middle and posterior deltoids, subscapularis, biceps,

and rhomboids major had moderate to good relationships (0.50- 0.63). The supraspinatus, infraspinatus, triceps, and serratus anterior had fair relationships (0.31 – 0.46). Negative correlations were observed for the infraspinatus (-0.39) and subscapularis (-0.58).

During the push phase of Stroke Cycle 3, the anterior deltoid was the only muscle with a good to excellent relationship (0.81). The middle and posterior deltoids, supraspinatus, subscapularis, biceps and serratus anterior had moderate to good relationships (0.50 – 0.58). The infraspinatus and rhomboids major had fair relationships (0.28 – 0.48). The rhomboids major was the only muscle with a negative correlation (-0.28). The Static Optimization Tool estimated that the triceps generated no force during the push phase, so its cross correlation coefficient could not be determined.

During the push phase of Stroke Cycle 4, the anterior deltoid was the only muscle with a good to excellent relationship (0.74). The middle and posterior deltoids, infraspinatus, subscapularis, and biceps had moderate to good relationships (0.52 – 0.66). The supraspinatus, serratus anterior, and rhomboids major had fair relationships (0.35 – 0.46). The only muscle with a negative correlation was the serratus anterior (-0.42). The Static Optimization Tool estimated that the triceps generated no force during the push phase, so its cross correlation coefficient could not be determined.

During the push phase of Stroke Cycle 5, the posterior deltoid was the only muscled with a good to excellent relationship (0.72). The anterior and middle deltoids, supraspinatus, infraspinatus, subscapularis, and biceps had moderate to good relationships (0.50 – 0.61). The triceps, serratus anterior, and rhomboids major had fair relationships (0.37 – 0.47). Negative correlations were observed for the infraspinatus (-0.58) and serratus anterior (-0.47).

In summary, positive correlations were observed for the anterior, middle and posterior deltoids, supraspinatus and biceps during the push phase of all five stroke cycles. Moderate to good relationships were observed for the subscapularis (0.50 – 0.58) and biceps (0.50 -0.66) across the push phase of all five stroke cycles. Only one muscle had a good to excellent correlation during the push phase of each stroke cycle. Stroke Cycles 1 and 3 each had the least number of muscles with fair relationships (two), while Stroke Cycle 2 had the most (four).

5.6.1.3 Cross Correlation Analyses for the Recovery Phase of Propulsion. The cross correlation coefficients were also determined for the recovery phase of propulsion for all five stroke cycles (Table 5.8).

Table 5.8 Recovery Phase Cross Correlation Coefficients

Muscle	Stroke Cycle 1: Recovery	Stroke Cycle 2: Recovery	Stroke Cycle 3: Recovery	Stroke Cycle 4: Recovery	Stroke Cycle 5: Recovery
Anterior Deltoid	**0.35**	**0.39**	**-0.42**	**0.57**	**0.31**
Middle Deltoid	**0.47**	**0.40**	**-0.44**	**-0.37**	**-0.43**
Posterior Deltoid	**-0.51**	**-0.36**	**-0.59**	**0.49**	**-0.68**
Supraspinatus	**0.61**	**-0.52**	**-0.44**	**-0.53**	**-0.58**
Infraspinatus	**0.78**	**0.87**	**0.81**	**0.66**	**0.83**
Subscapularis	**0.59**	**0.72**	**-0.65**	**-0.68**	**-0.60**
Triceps	**0.72**	**0.60**	**0.49**	**-0.40**	**0.50**
Biceps	**0.89**	**0.85**	**0.91**	**0.86**	**0.88**
Serratus Anterior	**0.43**	**-0.48**	**-0.56**	**-0.41**	**-0.41**
Rhomboids Major	**-0.42**	**-0.57**	**0.43**	**0.38**	**0.56**

Legend: Green highlighting represents good to excellent relationship, yellow highlighting represents moderate to good relationship, and red highlighting represents fair relationship.

During the recovery phase of Stroke Cycle 1, the infraspinatus, triceps, and biceps had good to excellent relationships (0.72 – 0.89). The posterior deltoid, supraspinatus and subscapularis had moderate to good relationships (0.51 – 61). The anterior and middle deltoids, serratus anterior, and rhomboids major had fair relationships (0.35 – 0.47). Negative correlations were observed for the posterior deltoid (-0.51) and rhomboids major (-0.42).

During the recovery phase of Stroke Cycle 2, the infraspinatus, subscapularis, and biceps had good to excellent relationships (0.72 – 0.87). The supraspinatus, triceps and rhomboids major had moderate to good relationships (0.52 – 0.60). The anterior, middle

and posterior deltoids and the serratus anterior had fair relationships (0.36 – 0.48). Negative correlations were observed for the posterior deltoid (-0.36), supraspinatus (-0.52), and serratus anterior (-0.48).

During the recovery phase of Stroke Cycle 3, the infraspinatus and biceps had good to excellent relationships (0.81 – 0.91). The posterior deltoid, subscapularis, and serratus anterior had moderate to good relationships (0.56 – 0.65). The anterior and middle deltoids, supraspinatus, triceps, and rhomboids major had fair relationships (0.42 – 0.49). Negative relationships were observed for the anterior (-0.42), middle (-0.44) and posterior (-0.59) deltoids, supraspinatus (-0.44), subscapularis (-0.65), and serratus anterior (-0.56).

During the recovery phase of Stroke Cycle 4, the biceps was the only muscle with a good to excellent relationship (0.86). The anterior deltoid, supraspinatus, infraspinatus and subscapularis had moderate to good relationships (0.53 – 0.68). The middle and posterior deltoids, triceps, serratus anterior and rhomboids major had fair relationships (0.37 – 0.49). Negative correlations were observed for the middle deltoid (-0.37), supraspinatus (-0.53), subscapularis (-0.68), triceps (-0.40), and serratus anterior (-0.41).

During the recovery phase of Stroke Cycle 5, the infraspinatus and biceps had good to excellent relationships (0.83 – 0.88). The posterior deltoid, supraspinatus, subscapularis, triceps and rhomboids major had moderate to good relationships (0.50 - 0.68). The anterior and middle deltoids and serratus anterior had fair relationships (0.31 – 0.43). Negative correlations were observed for the middle (-0.43) and posterior (-0.68) deltoids, supraspinatus (-0.58), subscapularis (-0.60) and serratus anterior (-0.41).

In summary, stroke Cycles 1 and 2 each had the greatest number of muscles with strong good to excellent relationships (3). Stroke Cycle 5 had the least number of muscles with fair relationships (3). Positive correlations were observed for only the infraspinatus and the biceps during the recovery phase of all five stroke cycles. Comparing the cross correlation coefficients of the push phase with those of the recovery phase, less negative correlation coefficients were observed during the push phase. Across all five stroke cycles, there were six negative correlation coefficients observed during the push phase and 22 negative correlation coefficients observed during the recovery phase.

5.6.2 Mean Absolute Error

The MAE was calculated for each muscle during each stroke cycle (Table 5.9). On average, the muscles that demonstrated excellent correlation (0.05 - 0.07) are: supraspinatus, infraspinatus, subscapularis, biceps, and serratus anterior. On average, the muscles that demonstrated good correlation (0.11) are: middle and posterior deltoid. The muscles that demonstrated poor correlation (0.23 – 0.34) are: anterior deltoid, triceps, and rhomboids major. Even though the anterior deltoid had a poor average correlation (0.23), it had a good correlation for Stroke Cycles 3, 4, and 5 (0.19 – 0.20). The muscles with the worst average correlation are the triceps (0.33) and the rhomboids major (0.34), which consistently had a poor correlation over each stroke cycle. The muscle with the best average correlation is the serratus anterior (0.05). On average, all five stroke cycles demonstrated good correlation (0.14).

Table 5.9 Mean Absolute Error (MAE) per Stroke Cycle

Muscle	Stroke Cycle 1	Stroke Cycle 2	Stroke Cycle 3	Stroke Cycle 4	Stroke Cycle 5	Average
Anterior Deltoid	**0.29**	**0.27**	**0.20**	**0.20**	**0.19**	**0.23**
Middle Deltoid	**0.11**	**0.11**	**0.11**	**0.12**	**0.12**	**0.11**
Posterior Deltoid	**0.11**	**0.10**	**0.10**	**0.11**	**0.12**	**0.11**
Supraspinatus	**0.07**	**0.06**	**0.06**	**0.06**	**0.07**	**0.06**
Infraspinatus	**0.07**	**0.06**	**0.06**	**0.07**	**0.07**	**0.07**
Subscapularis	**0.05**	**0.06**	**0.06**	**0.06**	**0.07**	**0.06**
Tricep	**0.32**	**0.33**	**0.32**	**0.32**	**0.34**	**0.33**
Bicep	**0.05**	**0.07**	**0.04**	**0.09**	**0.04**	**0.06**
Serratus Anterior	**0.05**	**0.05**	**0.06**	**0.05**	**0.04**	**0.05**
Rhomboids Major	**0.26**	**0.28**	**0.42**	**0.37**	**0.39**	**0.34**
Average	**0.14**	**0.14**	**0.14**	**0.14**	**0.15**	**0.14**

Legend: Green highlighting represents excellent correlation, yellow highlighting represents good correlation, and red highlighting represents poor correlation.

CHAPTER 6

DISCUSSION AND CONCLUSIONS

6.1 Dual Energy X-ray Absorptiometry-Based Mass Measurements

There were two goals for this dissertation. The first goal was to construct a patient-specific, computer graphics-based model for wheelchair propulsion simulations. Individuals with tetraplegia were the population of interest. A patient-specific model requires anthropometric data for scaling and the determination of kinetics. The anthropometric data must adequately reflect the anthropometry of the patient in order to accurately address any clinical determination. However, most of the previous wheelchair propulsion models (Dubowsky et al., 2008; Lin et al., 2004; Morrow et al., 2010; Rankin et al., 2010; 2011; van der Helm, 1994; van Drongelen et al., 2005a; 2005b; 2011) were constructed with anthropometrics determined from cadaver-based measures, which were obtained from elderly individuals (Clauser et al., 1969; Demptser, 1955; Hanavan, 1964) but meant for use in able-bodied populations. These models were primarily used with data from patients with paraplegia, so it may have been acceptable for them to include cadaver-based estimates to determine the arm and trunk segment masses. In the literature, it is not known whether the cadaver-based body segment mass estimates are suitable for the SCI population, especially for individuals with tetraplegia. Dual energy x-ray absorptiometry has been established as a viable method for obtaining patient-specific anthropometrics. Therefore, a study was conducted to determine and compare DXA-based masses of the trunk and arm with cadaver-based mass estimates for individuals with tetraplegia and paraplegia and able-bodied adults. The findings revealed that the cadaver-based masses were not different from the DXA-based masses for individuals

with tetraplegia. As a result, the cadaver-based mass proportions were included in the model.

The DXA mass distributions for the arm and trunk for all three groups studied are consistent with those published in the literature (Spungen et al., 2003). They found that the arm lean mass in individuals with tetraplegia was significantly less than those with paraplegia and the able-body controls. Since individuals with tetraplegia have partial muscle innervation of their upper limb muscles and experience muscle atrophy, it is plausible that the DXA-based mass proportion is similar to the cadaver-based estimate. The cadaver estimates were based on elderly populations (Chandler, 1975; Clauser et al., 1969; Dempster, 1955), who most likely encountered muscle atrophy due to aging. Moreover, in a DXA study on body composition of monozygotic twins, Spungen and colleagues (2000) concluded that individuals with paralysis from SCI experience an accelerated form of muscle wasting that is similar to the atrophy seen in elderly individuals (60-89 years old). Individuals with paraplegia may not have partial muscle innervation of the upper limb and may have more arm lean mass than those with tetraplegia, so it is reasonable that the DXA-based measures were greater than the cadaver-based estimate for the arm. Non ambulatory manual wheelchair users with paraplegia rely on their upper limbs due to lower limb paralysis or muscle impairment, so they most likely use their upper limbs more than able-bodied controls and would have a greater arm lean mass.

There was little difference between the groups for trunk mass, as the cadaver-based proportion was similar to the DXA-based mass proportions. These data seem plausible for individuals with tetraplegia and paraplegia, but questionable for able-

bodied controls. Individuals with tetraplegia have increased neurological impairment, decreased muscle activation, decreased trunk strength and reduced trunk stability compared to both paraplegia and able-bodied controls (Curtis et al., 1994a; 1999b; Kulig et al., 2001; Mulroy et al., 1996; Powers et al., 1994; Reyes et al., 1995**)**. In addition, depending on the neurological level of injury and trunk muscle weakness, the majority of manual wheelchair users with paraplegia also have poor trunk control (Yang et al., 2006).

However, it is questionable that the control group DXA mass proportion for the trunk was not different than the cadaver-based proportion. The small cohort of able-bodied controls with neurologically intact trunk musculature was relatively young and healthy. A limitation of DXA is that the technology cannot distinguish clearly between soft tissue and bone in the thorax because the arrangement of the ribs and spine prevents the x-ray beam from finding much bone-free soft tissue mass. As a result, estimates of thoracic composition tend to be imprecise (Roubenoff et al., 1993). Gater and Clasey (2006) also cited a similar limitation of DXA. Therefore, this limitation may explain the similarity between the DXA-based trunk mass measures and the cadaver-based mass estimates for all three groups, especially for the control group. Given the recent advances in DXA technology (Hull et al., 2009; Krueger et al., 2006; Soriano et al., 2004), further investigation is needed with a larger study population.

6.2 Static Optimization Simulations

A long term goal is to use the Wheelchair Propulsion Model as a clinical tool. As an initial evaluation of the model, a goal of this dissertation was to determine the forces of the shoulder complex muscles and identify their individual contribution to manual wheelchair propulsion in an individual with tetraplegia. The estimated forces were

verified by calculating the cross correlation coefficient of the estimated muscle force profile with the experimental EMG profile and the MAE between the estimated muscle activation profile and the experimental EMG profile.

6.2.1 Cross Correlation for Overall Stroke Cycle

The cross correlation time series analyses of 100% stroke cycle revealed that the biceps, triceps, subscapularis, infraspinatus, serratus anterior, anterior, middle and posterior deltoids had force profiles that had moderate to excellent relationships with their experimental EMG profiles. However, the rhomboids major and supraspinatus had force profiles that correlated only fair with experimental EMG profiles. These poor results for the rhomboids major and supraspinatus were potentially not due to the computational derivation of kinematics since the kinematics results were consistent with Rankin et al. (2011); so these errors are less likely propagated from the IK solutions.

The rhomboids major is an axioscapular muscle that is responsible for scapular retraction (Dyson-Hudson & Kirshblum, 2004). For the rhomboids major, the fair correlation with the experimental EMG may potentially be due to the simplified shoulder motion in the model. The motion of the clavicle and scapula are dependent upon movement of the humerus (Holzbaur et al., 2005). The current model design provides only limited scapula motion and prohibits scapular retraction, where the scapula cannot move in isolation (Holzbaur et al., 2005). It is possible that this model limitation affected the force generated by the rhomboids major.

The supraspinatus is a scapulohumeral muscle responsible for shoulder abduction (Dyson-Hudson & Kirshblum, 2004). It is possible that the poor correlation for the supraspinatus force and experimental EMG is due to the moment arm selected for the

muscle. The Wheelchair Propulsion Model features the same moment arms featured in the Stanford VA Model (Holzbaur et al., 2005). The motions of the scapula and clavicle vary only with humeral elevation, so the moment arms of the muscles that cross from the torso to the humerus are affected (Holzbaur et al., 2005). Importantly, scapula motion is determined by the motion the humerus, so both the scapula and clavicle are not modeled for independent motion (Holzbaur et al., 2005). No moment arm data for a shoulder with a moving scapula was available when Holzbaur et al. (2005) constructed the model, so it was difficult for them to quantify the degree of this effect. Since the motion of the scapula and clavicle is determined by the motion of the humerus, independent scapula or clavicle motion, as collected experimentally with EMG, was not measured using the model.

While there is a limitation to model as reflected in the correlations associated with the supraspinatus, the other scapulohumeral muscles, such as the deltoids and the rotator cuff muscles (infraspinatus and subscapularis), demonstrated moderate to good relationships. The deltoid muscles do not cross the trunk and humerus in the same manner as the rotator cuff muscles. The length of the muscle (and the moment arm) and the muscle force (OpenSim Advanced User's Jamboree) for the deltoid would be more reflective of a stronger relationship between force and EMG. Future research should be directed toward examining the differences in rotator cuff muscles.

6.2.2 Cross Correlations Push Phase versus Recovery Phase

The stroke cycle is defined as having two phases: push and recovery. The push phase is defined as the period when the hand is contact with the pushrim and applying force to the pushrim to maintain or increase wheelchair velocity, while the recovery phase is the

period in between consecutive push phases when the arms are retracted in preparation for another push (Kwarciak et al., 2009; Sanderson & Sommer, 1985). In their investigations of the biomechanics of their upper limb model, Holzbaur and colleagues (2005) observed joint coupling effects, noting that the biomechanics of a given joint in the upper limb were dependent upon the posture of the adjacent joints. When the hand is released from the pushrim in the recovery phase, wheelchair propulsion can be assessed from an open chain perspective. As the upper limb joints now have the ability to have different postures, joint coupling may be observed. As joint coupling occurs, the moment arms of the muscles that cross those joints change, affecting the force output (OpenSim Advanced User's Jamboree).

Cross correlation coefficients for the experimental EMG and force profiles were greater during the push phase, compared to recovery. Therefore, potentially, the model characterizes the push phase more effectively than recovery phase. However, it is interesting to note that during recovery the infraspinatus muscle forces correlated strongly to EMG activation. This would reflect the simplified motion of the model to vary only with the thoracohumeral (shoulder elevation) angle, as described by Holzbaur et al. (2005). The frequent observances of more poor correlations during the recovery phase than the push phase may be best explained by joint coupling effects in the upper limb (Holzbaur et al., 2005). These findings suggest that the Wheelchair Propulsion Model, to date, is most effective for simulating the push phase of propulsion rather than recovery.

6.2.3 Determination of MAE

While the evaluation of temporal characteristics and the intensity of muscle firing during overall and push and recovery phase of propulsion were useful, these time series analyses did not verify the magnitude of calculated muscle force (Crowninshield, 1978; Erdemir et al., 2007; Lin et al., 2004). The MAE was calculated to address the error in the muscle activation magnitude determined by the model and thus indirectly validate the model determination of muscle force (de Zee et al., 2007; Dubowsky et al., 2008; Morrow et al., 2010). An assumption in determining the MAE is that there is a linear relationship between EMG amplitude and muscle force, although there is no clear relationship between the two (Hof, 1999). However, previous researchers have used the MAE successfully to validate computational models (de Zee et al., 2007), particularly computational models that utilized static optimization to determine contact forces at the shoulder during wheelchair propulsion (Dubowsky et al., 2008; Morrow et al., 2010).

Good correlations for MAE and force magnitude were observed for seven of the ten of the muscles for each stroke cycle, while the remaining three muscles had poor correlations. These results of the MAE calculations were highly consistent across all stroke cycles and the mean MAEs across all stroke cycles concur with previous studies (Dubowsky et al., 2008; Morrow et al., 2010). Of the ten muscles investigated, the rhomboids major and triceps muscles consistently had poor correlations for each stroke cycle. This is indicative of no relationship between the muscle activation determined by the model and the experimental EMG.

The MAE calculated for the rhomboids major may be due to the limited scapula motion, defined by the model prohibiting scapular retraction. The scapula could not

move in isolation, as mentioned previously (Holzbaur et al., 2005). When comparing the muscle activation profile with the experimental EMG profile, no similarities between the two exist (Figure 6.1); further confirming that the model did not capture scapular retraction. In summary, the simplified scapula motion may have affected the results for both sets of correlations involving the rhomboids, the time series analyses and the MAEs.

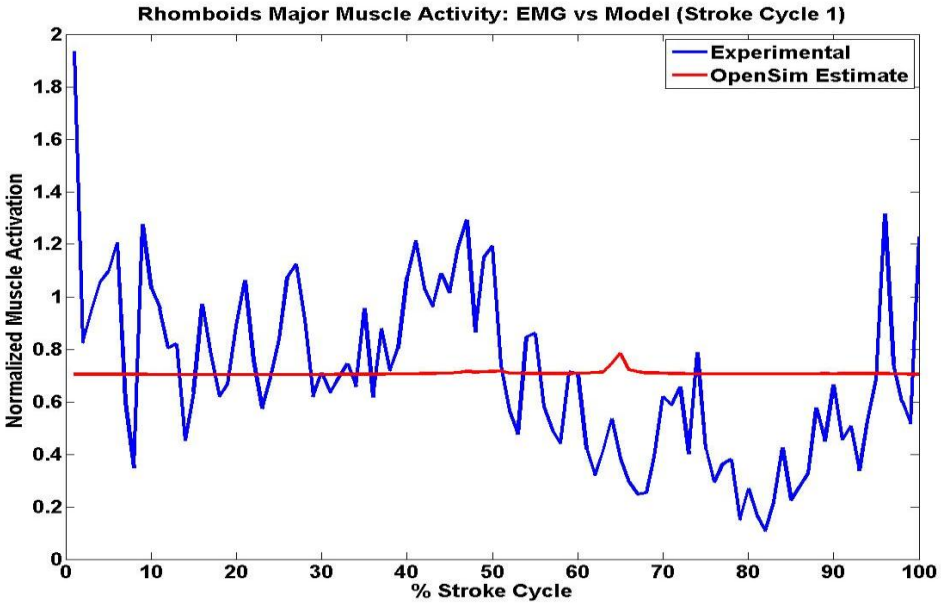

Figure 6.1 The experimental EMG profile (blue) and the calculated activation profile (red) of the rhomboids major for 100% stroke cycle (Stroke Cycle 1).

The triceps had a high MAE, indicative of a poor correlation for all stroke cycles. The triceps is an elbow extensor muscle and based on the kinematic profiles generated (Figure 5.4), the partcipant extended his elbow primarily in the recovery phase of the stroke cycle. Since the elbow was in a flexed position for much of the push phase in the model, the force generated by this muscle during the push phase was expected to be low. This was further confirmed by the low force output observed during the push phase for the triceps (Figure 5.9), as opposed to the greater force output observed during the

recovery phase (Figure 5.10). Dubowsky et al. (2008) also observed poor MAE values for the triceps muscle in a participant with paraplegia. They observed that the duration of experimental triceps activity was much longer than that which was calculated computationally. Since their participant was tested for full upper limb function, Dubowsky et al. (2008) suggested that the lack of parity between computational and experimental results may be due to the participant using his triceps in a compensatory manner as a result of limited trunk control. They inferred that future work with fine-wire EMG investigating other prominent muscles in wheelchair propulsion, such as the muscles of the rotator cuff, may shed light onto contraction/co-contraction results (Dubowsky et al., 2008). Fine-wire EMG was utilized with the current study. Based on the experimental EMG profile of the participant in this study, the triceps was most active between 20%-70% of the stroke cycle (Figure 6.2). However, the computational results suggest that the muscle force was generated between 45% and 98% of the stroke cycle (Figure 6.2). The rotator cuff muscles investigated (infraspinatus, supraspinatus, subscapularis) all had excellent MAE values (Table 5.9), so it is less likely that the lack of parity between computational and experimental results is due to compensatory use of the triceps. Moreover, Morrow et al. (2010) did not report MAE poor values for the triceps. For model validation, they selected three optimal criteria for the determination of the cost function used in the static optimization technique: (i) linear minimization of α, muscle activation (Kaufman et al., 1991); (ii) minimax formulation of minimizing the maximum muscle stress (An et al., 1984); (iii) nonlinear minimization of the sum of muscle stress cubed (Lin et al., 2004). Morrow et al. (2010) reported an excellent average MAE value for the triceps for each criterion. The objective function selected in this

current study was minimization of muscle activation squared (van der Helm, 1994). The objective function selected by Dubowsky et al. (2008) was minimization of muscle effort. This suggests that the poor MAE values reported may be due to the optimization criterion selected. At the very least, future work should investigate different optimization criteria for the selection of an optimal cost function for the static optimization technique. Furthermore, the muscles should be validated with MAE in conjunction with fine-wire EMG.

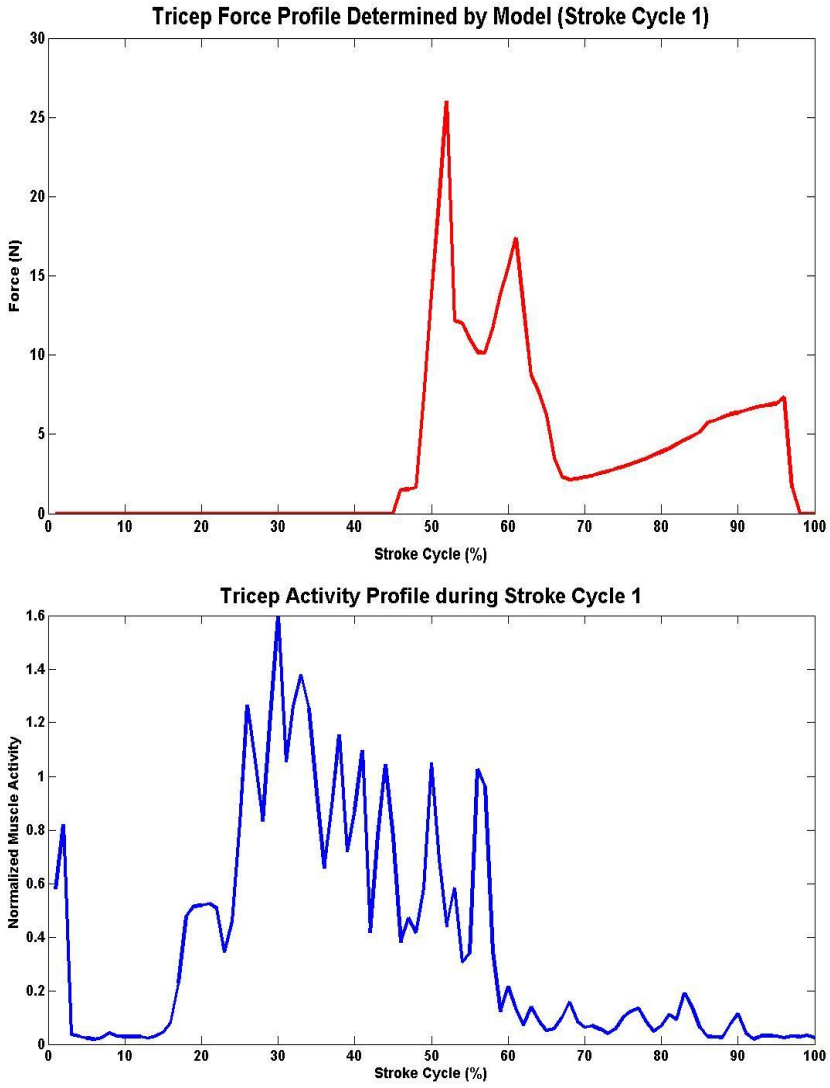

Figure 6.2 Triceps force profile computed for 100% stroke cycle (top) and experimental triceps EMG profile during 100% stroke cycle (bottom). The computed force profile demonstrates triceps activity for about 45% - 98% of the stroke cycle. However, the experimental EMG profile demonstrates triceps activity for 20% -70% of the stroke cycle.

6.3 Limitations

There are a number of limitations to the study. A significant limitation of this study is the sample size. The model evaluation was designed as a proof of concept study, so only one participant was investigated. It is important to note that the findings presented from the patient-specific model are indicative of the participant studied and may not necessarily be

indicative of all manual wheelchair users with tetraplegia. However, other computer graphics-based models have been evaluated and validated successfully with one study participant (de Zee et al., 2007; Rankin et al., 2010; Reinbolt et al., 2005; Wilkenfeld et al., 2006).

Another limitation is that the determination of DXA-based segment masses contained a small able-bodied sample size, as compared to the tetraplegia and paraplegia groups. However, despite the small sample size, the results were still similar to other studies (Spungen et al., 2003). Also, the center of mass location and moment of inertia segment values are important in determining inverse dynamics. Since there was no difference between the DXA-based and the cadaver-based mass proportions for the individuals with tetraplegia, it was assumed that the cadaver-based proportions for center of mass location and moment of inertia could be included in the model for patients with tetraplegia. Other models have used cadaver-based proportions for wheelchair propulsion simulations of individuals with SCI (Dubowsky et al., 2008; Morrow et al., 2010; Rankin et al., 2010; 2011; van Drongelen et al., 2005a).

The Wheelchair Propulsion Model is based on the OpenSim Arm 26 Model, but its upper limb kinematics are consistent with the Stanford VA Model developed by Holzbaur and colleagues (2005). Therefore, the limitations to shoulder movement previously discussed for the Stanford VA Model are also limitations in the Wheelchair Propulsion Model. Specifically, the motion of the scapula and clavicle were constrained to depend on the motion of the humerus, so the motion of the shoulder girdle is very simplified. The motions of the scapula and humerus vary only humeral elevation. The

limited scapula motion may have affected the muscle force estimates for the muscles responsible for scapular motion, such as the rhomboids major.

The muscle parameters in the model for optimal force, muscle length and tendon slack length were all obtained from cadaver studies. The parameters included for the serratus anterior and the rhomboids major were obtained from estimated data from the Garner and Pandy (2003) upper limb model. There were no values for these muscles in the literature and Garner and Pandy (2003) noted that their model overestimated muscle parameters for the upper limb muscles. It is possible that the parameters for the serratus anterior included in the model are overestimated. This may explain why the serratus anterior generated the greatest max forces than all of the muscles investigated during the push phase.

A limitation of the static optimization technique is that it is performed per frame (quasi-static), even though the motions analyzed are dynamic (Morrow et al., 2010). Also, extra actuators were appended to the coordinates in the model so that the joints could achieve the computed acceleration for each time point. Static optimization attempts to solve the redundancy problem for actuators and muscles by using the accelerations computed from the ID solution as a constraint (de Zee et al., 2007; Erdemir et al., 2007). When the muscles in a model are weak, coordinate actuators can be appended to joints in the model. The amount of actuation needed at a given joint can be determined and the muscles can be strengthened accordingly. Partial muscle paralysis due to SCI was not considered in the model, so the optimal forces on the muscles were not increased or decreased (van Drongelen et al., 2005a). As a result, it is possible that the actuators may have contributed more than muscles, affecting the results of the static

optimization simulations. In their wheelchair propulsion simulation study, van Drongelen and colleagues (2005a) hypothesized that the muscle forces generated by individuals with tetraplegia would be greater than individuals with paraplegia and able-bodied individuals. They did not account for partial muscle paralysis in their simulations and assumed that it would manifest itself in the differences in task performance among the three participant groups investigated. Therefore, the need to append coordinate actuators at the joints may be evidence of the partial muscle paralysis manifesting itself in the model. The optimal forces of the muscles in the model used in this study were obtained from published cadaver studies (Dempster, 1955), with the exception of the serratus anterior and the rhomboids major (obtained from the Garner and Pandy (2003) upper limb model). Given the accelerations generated by the ID tool, the static optimization simulations would not converge unless actuators were appended to the model. Therefore, the optimal forces (based on cadaver-based estimates for segment mass and moment of inertia and meant for use with able-bodied populations) may not have been adequate for the participant with tetraplegia investigated. The appended coordinate actuators may have compensated for partial muscle paralysis due to tetraplegia, by providing the additional (reserve) force required at a given joint so the muscles could be strengthened accordingly. To address these concerns, future work should investigate a force-tension-length curves that are more reflective of individuals with SCI.

Lastly, evaluation of the model with experimental EMG was greatly affected by the sensitivity of EMG timing of activation. The experimental data were originally collected to investigate the biomechanical predictors shoulder pain in manual wheelchair users with tetraplegia (Yarossi et al., 2010). Thus far, EMG analyses from the original

work have determined the level of muscle activation (amplitude and phasing) relative to the kinematics during the push cycle (Yarossi et al., 2010). Since these data were not collected with the intention of being incorporated in a patient-specific model, the precision of EMG onset and offset times received very little attention. Therefore, it is possible that this lack of precision or sensitivity could have affected the correlation analyses. Future work should include the development of EMG algorithms that more clearly identify the onset and offset times, followed by the recalculation of the correlations. As previously mentioned, a significant limitation to the current work is that all of the analyses, results and discussion are based on one individual. Therefore, future work should examine the larger cohort of individuals with tetraplegia who participated in the original study. Potentially, the larger group would allow for the calculation of all the muscle forces by using experimental EMG data that was not adequately recorded in the present case study.

6.4 Summary

The two goals of this project were to: (i) construct a dynamic, patient-specific model of the upper limb and trunk of a individual with tetraplegia and (ii) use the model to determine the individual contributions of the shoulder complex muscles to wheelchair propulsion.

The Wheelchair Propulsion Model was constructed and evaluated using OpenSim. The model contains shoulder and trunk muscles that have been commonly investigated in wheelchair propulsion biomechanics studies, in addition to the upper and middle trapezius, serratus anterior, and rhomboids major (not featured in previous models). SCI-specific trunk and arm segment mass ratios were investigated using DXA to ensure that

dynamic properties reflecting SCI were included in the model. The DXA analysis was significant to both the construction of the model as well as the simulations performed because appropriate segment mass values are critical for obtaining accurate simulation results. There was no difference between the cadaver-based and DXA-based mass proportions for the right arm and trunk in individuals with tetraplegia, so the cadaver-based mass proportions were included in the model.

To determine the model's ability to compute shoulder complex muscle forces, biomechanical data collected from an individual with tetraplegia were implemented. The static optimization technique was selected to determine the contribution of individual muscle forces to wheelchair propulsion. Based on the simulations, the muscles that contributed to the push phase of wheelchair propulsion are: serratus anterior, middle and posterior deltoids, infraspinatus, biceps, middle trapezius, subscapularis and supraspinatus. The muscles that contributed to the recovery phase are: middle deltoid, serratus anterior, posterior deltoid, infraspinatus, supraspinatus, triceps, subscapularis, and middle trapezius.

Previous research studies have only utilized surface EMG (Dubowsky et al., 2008; Lin et al., 2004; Rankin et al., 2011). This is the first study to evaluate muscle forces with fine-wire EMG collected on the individual being investigated. The significance of collecting the fine-wire EMG is to record the activity of the deep shoulder complex musculature, as it may provide further insight to joint coupling (Holzbaur et al., 2005). Evaluation of the muscle forces was achieved by performing cross correlation analyses of the estimated muscle forces and the experimental fine-wire EMG as well as calculating the MAE of the estimated activation and the fine-wire EMG. The cross-

correlation analyses addressed the amplitude of the estimated forces with the EMG, while the MAE addressed the magnitude of the estimated activation with EMG. The cross correlation analyses per 100% stroke cycle demonstrated that a majority of the muscles investigated had a moderate to excellent relationship with the experimental EMG over all five stroke cycles. Cross correlation analyses were also performed for the push phase and the recovery phase. These findings suggest that the Wheelchair Propulsion Model is most effective for estimating muscle forces generated during the push phase of wheelchair propulsion. The overall MAE for each stroke cycle demonstrated a good correlation between the simulated muscle activations and the experimental muscle activity, furthering confirming the model's ability to estimate muscle forces during wheelchair propulsion.

As evidenced in this dissertation, constructing and validating a computer graphics-based neuromusculoskeletal model is not a simple task. This proof of concept study was initially designed as an evaluation of the model with all the experimental data collected from 18 participants in the Kessler wheelchair propulsion study. However, there were challenges in scaling and computing the inverse kinematics of 17 participants. These participants were excluded from this study because the IK tool reported RMS errors over 1 cm for some of the markers and after adjusting the virtual markers and re-scaling the generic model to the participant several times, acceptable RMS errors were still not obtained. To address this issue, marker weights would have to be assigned to the markers in the model. An investigation would have to be performed for each individual participant to determine the marker weights. To the knowledge of the investigator, the literature does not describe how to determine marker weights, so the investigation would

purely be based on trial and error. This would greatly increase the computational time needed to develop and evaluate the model, as research time would need to be spent investigating and evaluating appropriate marker weights for each participant. As an alternative, the proof of concept study with one participant was proposed.

The literature reveals that other computer graphics-based models have been evaluated with data from one participant (de Zee et al., 2007; Rankin et al., 2010; Reinbolt et al., 2005; Wilkenfeld et al., 2006). Since the Wheelchair Propulsion Model is a novel model, the one participant design of the proof of concept study allowed the investigator to spend more time teething out the computed muscle force data. This provided the investigator with a better understanding of the applications and limitations of the model as well as highlighting what needs to be addressed/improved in future versions of the model. Most importantly, it facilitated the future evaluation of the model with the data from the additional study participants. Also, the data evaluated with the model was historical data. The one participant proof of concept design also provided insight on how experimental data should be collected and processed for future evaluations with the model.

The construction and evaluation of the model described in this dissertation was computationally expensive, in terms of research time spent constructing the model and converting and evaluating the historical experimental data. Since this is a novel model, the upfront computational expense needed to construct and evaluate/validate the model was expected to be high. After modifying the model to address the previously mentioned limitations, the computational expense associated with the model is expected to decrease greatly. It is encouraging to know that the potential investigations that may contribute to

the field and potential clinical interventions that may be designed with the model over time will ultimately outweigh these upfront or "start-up" costs. An example of this is the Smart^{WHEEL}, the force and torque sensing pushrims used to collect kinetic data in the wheelchair propulsion study. This biomechanical tool was initially designed and created for research studies (Asato et al., 1993). However, seeing a clinical need for the tool, a clinical version of the Smart^{WHEEL} was developed (Cooper, 2009). Thus, the long term goal of constructing the model is to address the need for a clinical evaluation/predictive tool to investigate the relationship between wheelchair propulsion and shoulder pain and injury. This dissertation is the first step towards the clinical application of a wheelchair propulsion model. Moreover, the purpose of constructing the model using OpenSim is to contribute it to OpenSim's Neuromuscular Biomechanics Library. This will provide researchers in the wheelchair propulsion biomechanics community with free access to the model and, hopefully, will further advance the field of wheelchair propulsion biomechanics. The MATLAB functions written to convert experimental data to the appropriate OpenSim formats will be included with model. This will promote new knowledge and allow for greater collaboration amongst researchers and advance the field of wheelchair biomechanics.

6.5 Research Contributions

The Wheelchair Propulsion Model is a significant contribution to the wheelchair biomechanics community and the OpenSim user community. The model will be contributed to OpenSim's Neuromusculoskeletal Biomechanics Library so that researchers can freely access it. The Wheelchair Propulsion Model is a patient-specific

model that contains the superficial and deep musculature of the shoulder complex. This is significant because researchers who used the Stanford VA Model for wheelchair propulsion studies (Morrow et al., 2010; Rankin et al., 2010; 2011) were unable to completely investigate of the deep musculature of the shoulder complex. Also, the model contains a skull, neck, jaw, and spine. Previous studies did not include these body segments, so the shoulder complex muscles that cross these body segments (i.e., upper and middle trapezius, rhomboids major, serratus anterior) could not be modeled or investigated. Although these body segments were stationary in the model, it was important to include them in the model because they served as the attachment points for the shoulder complex muscles. Future versions of this model may explore the inclusion of motion at the trunk, neck, head, and spine. The Wheelchair Propulsion Model adds on to the work of Morrow (2010) and Rankin (2010, 2011) by constructing a model that contains the shoulder complex muscles. Although Dubowsky's (2008) model contained the shoulder complex muscles, the model was not freely available, so researchers had to create additional models for wheelchair propulsion investigations. Contributing the model to the OpenSim user community will provide wheelchair biomechanists with a common model that can be used or modified for other studies.

In addition to contributing the model to the OpesSim user community, the MATLAB codes used to convert the experimental data will be contributed. This is a significant contribution because the kinetic data conversion codes available on the OpenSim website were primarily written for gait studies using force plates. Wheelchair propulsion studies use instrumented pushrims to obtain kinetic data, so the conversion codes were not appropriate for wheelchair propulsion applications. In addition to being

provided with access to the model, researchers will be able to access these codes. This will enable them to incorporate their data in the model and advance the field of wheelchair propulsion biomechanics.

A majority of the estimated muscle force profiles had moderate to strong relationships with experimental fine-wire EMG profiles. The average MAE of the muscles investigated consistently demonstrated a good correlation across all stroke cycles. Previous studies were limited to surface EMG (Dubowsky et al., 2008; Rankin et al., 2011). The significance of utilizing fine-wire EMG was to enable the investigation of the deep shoulder complex musculature. No study has utilized fine-wire EMG collected on the participant investigated. As a potential clinical tool, this may be useful for clinicians who are interested in designing and evaluating interventions or personalized recommendations for patients.

This model was specifically constructed for the SCI population, particularly for individuals with tetraplegia. Models used to investigate wheelchair biomechanics in SCI included cadaver-based estimates for body segment mass parameters (Dubowsky et al., 2008; Morrow et al., 2010; Rankin et al., 2011; van Drongelen et al., 2005a). However, the appropriateness of these estimates for the SCI population was not known. A study investigating the use of DXA to determine body segment masses revealed that the cadaver-based mass proportions for the arm and trunk were similar to the DXA-based proportions for individuals with tetraplegia. However, the findings also reveal that the cadaver-based arm estimates are different than the DXA-based proportions for individuals with paraplegia. This is potentially a major contribution for SCI anthropometrics. This may also be an important contribution for patient-specific

modeling, as the goal is to match the model as closely to the patient as possible in order to make appropriate recommendations.

6.6 Future Work

This dissertation provided an initial investigation in determining muscle forces of the shoulder complex during wheelchair propulsion in an individual with SCI. Further investigations regarding sample size, increasing scapula motion, and detailed EMG processing can enhance the model so that more realistic simulations of wheelchair propulsion can be generated.

More DXA scans of individuals with tetraplegia and paraplegia, as well as able-bodied adults, are needed to conduct a large scale study of DXA-based body segment masses. The results of the independent study need to be verified with a larger study. A larger study may also provide insight on whether SCI-specific DXA-based center of mass locations and moments of inertia for the upper limb and trunk are necessary.

Proof of concept has been established with one participant from the wheelchair propulsion study database. The findings presented in this dissertation demonstrate the Wheelchair Propulsion Model's potential to serve as a clinical tool. Therefore, the model should be evaluated with data from additional participants from the wheelchair propulsion study database. This will provide further insight on whether there are trends among shoulder complex muscle force contribution to wheelchair propulsion or the findings from this dissertation are specific to the individual investigated. Also, the force-length-velocity curves used with the model were based on cadaver data meant for able-bodied populations. These investigations with data from additional participants will provide the foundation for an investigation of a force-length-velocity curve for SCI

populations. These investigations will also provide a foundation for investigating shoulder joint contact forces in manual wheelchair users with tetraplegia and their potential risk to shoulder injury, as demonstrated by the work of Dubowsky et al. (2008) and Morrow et al (2010). Muscle contributions to the subtasks of the push and recovery phase, as demonstrated by the work of Rankin et al. (2011), can be investigated for manual wheelchair users with tetraplegia.

The deep scapula muscles did not have good or excellent relationships with the experimental EMG in the correlation analyses because scapula motion was limited. Future investigations should address the restrictions to scapula motion. The shoulder in the Wheelchair Propulsion Model is based on thoracohumeral motion, so scapula motion is limited by the design of the model (Holzbaur et al., 2005). Future investigations may explore regression equations that may increase scapula motion in the model. Future investigations may also explore adjustments to muscle parameters that may be implemented within the model to compensate for the limited scapula motion.

Lastly, the importance of EMG processing has been highlighted. Future work should entail a method of accurately determining the onset of muscle activation, correcting the EMG signal based on phasing, and assessing the sensitivity of EMG processing prior to the evaluation of static optimization results. The significance EMG of processing was demonstrated in the cross correlation analyses. The cause for the observances of negative correlations is not known. It may be due to the EMG processing, the model design. Before the data from the other participants are evaluated with the model, the negative correlations determined from the cross correlation analyses of the

present study must be investigated further. This will entail a thorough review of the raw EMG data as well as going over the model.

APPENDIX A

MATLAB DATA CONVERSION CODES

These codes were used to convert the experimental kinematic and kinetic data into the accepted OpenSim formats.

A. 1 Kinematic Data Conversion Code

```
%MAT2TRC is a function that converts kinematic data saved in a .MAT file to a .TRC
%file for use in OpenSim. Function inspired by Tim Dorn (University of Melbourne,
%November 2008) to convert data in .C3D format to .TRC format.
%Written by Brooke Odle on August 6, 2012

function mat2trc(subjectid, trialtype)

if nargin ~= 2
    Error('Adequate inputs not entered!');
end

if trialtype(1)=='S'
    trialsetting = 'SS';
    datafile = ['Y:\All Studies\tetraplegia wheelchair
            propulsion\Subject
            Folders\',subjectid,'\','Preprocess\',
            trialsetting,'\', 'PreKinematics.mat'];
    load (datafile);
    %Trochs only captured in setpo, not propulsive condition trials
    %(mkr positions are not the same for static vs. dynamic trials-
    %should come from file with 96 cols)
    SN= [kin(:,1).*(-1) kin(:,3) kin(:,2)];
    XP= [kin(:,4).*(-1) kin(:,6) kin(:,5)];
    C7= [kin(:,7).*(-1) kin(:,9) kin(:,8)];
    T3= [kin(:,10).*(-1) kin(:,12) kin(:,11)];
    LTM= [kin(:,13).*(-1) kin(:,15) kin(:,14)];
    RTM= [kin(:,37).*(-1) kin(:,39) kin(:,38)];
    RAC= [kin(:,40).*(-1) kin(:,42) kin(:,41)];
    RLE= [kin(:,43).*(-1) kin(:,45) kin(:,44)];
    RUL= [kin(:,46).*(-1) kin(:,48) kin(:,47)];
    RRA= [kin(:,49).*(-1) kin(:,51) kin(:,50)];
    RME= [kin(:,82).*(-1) kin(:,84) kin(:,83)];
    RACJ= [kin(:,79).*(-1) kin(:,81) kin(:,80)];
    RTS= [kin(:,85).*(-1) kin(:,87) kin(:,86)];
    RAA= [kin(:,88).*(-1) kin(:,90) kin(:,89)];
```

```
    RAI= [kin(:,91).*(-1) kin(:,93) kin(:,92)];
    RCP= [kin(:,94).*(-1) kin(:,96) kin(:,95)];
    RThreeMP= [kin(:,52).*(-1) kin(:,54) kin(:,53)];

elseif trialtype(1)=='2'
    trialsetting= '2mph';
    datafile = ['Y:\All Studies\tetraplegia wheelchair
            propulsion\Subject
            Folders\',subjectid,'\','Preprocess\',
            trialsetting,'\', 'PreKinematics.mat'];
    load (datafile);
    %Trochs only captured in setpo, not propulsive condition trials
    %(mkr positions are not the same for static vs. dynamic trials-
    %should come from file with 96 cols)
    SN= [kin(:,1).*(-1) kin(:,3) kin(:,2)];
    XP= [kin(:,4).*(-1) kin(:,6) kin(:,5)];
    C7= [kin(:,7).*(-1) kin(:,9) kin(:,8)];
    T3= [kin(:,10).*(-1) kin(:,12) kin(:,11)];
    LTM= [kin(:,13).*(-1) kin(:,15) kin(:,14)];
    RTM= [kin(:,37).*(-1) kin(:,39) kin(:,38)];
    RAC= [kin(:,40).*(-1) kin(:,42) kin(:,41)];
    RLE= [kin(:,43).*(-1) kin(:,45) kin(:,44)];
    RUL= [kin(:,46).*(-1) kin(:,48) kin(:,47)];
    RRA= [kin(:,49).*(-1) kin(:,51) kin(:,50)];
    RME= [kin(:,82).*(-1) kin(:,84) kin(:,83)];
    RACJ= [kin(:,79).*(-1) kin(:,81) kin(:,80)];
    RTS= [kin(:,85).*(-1) kin(:,87) kin(:,86)];
    RAA= [kin(:,88).*(-1) kin(:,90) kin(:,89)];
    RAI= [kin(:,91).*(-1) kin(:,93) kin(:,92)];
    RCP= [kin(:,94).*(-1) kin(:,96) kin(:,95)];
    RThreeMP= [kin(:,52).*(-1) kin(:,54) kin(:,53)];

elseif trialtype(1)=='4'
   trialsetting= '4mph';
   datafile = ['Y:\All Studies\tetraplegia wheelchair
            propulsion\Subject
            Folders\',subjectid,'\','Preprocess\',
            trialsetting,'\', 'PreKinematics.mat'];
   load (datafile);

  %Trochs only captured in setpo, not propulsive condition trials (mkr
  %positions are not the same for static vs. dynamic trials- should
  %come from file with 96 cols)
   SN= [kin(:,1).*(-1) kin(:,3) kin(:,2)];
   XP= [kin(:,4).*(-1) kin(:,6) kin(:,5)];
   C7= [kin(:,7).*(-1) kin(:,9) kin(:,8)];
```

```
    T3= [kin(:,10).*(-1) kin(:,12) kin(:,11)];
    LTM= [kin(:,13).*(-1) kin(:,15) kin(:,14)];
    RTM= [kin(:,37).*(-1) kin(:,39) kin(:,38)];
    RAC= [kin(:,40).*(-1) kin(:,42) kin(:,41)];
    RLE= [kin(:,43).*(-1) kin(:,45) kin(:,44)];
    RUL= [kin(:,46).*(-1) kin(:,48) kin(:,47)];
    RRA= [kin(:,49).*(-1) kin(:,51) kin(:,50)];
    RME= [kin(:,82).*(-1) kin(:,84) kin(:,83)];
    RACJ= [kin(:,79).*(-1) kin(:,81) kin(:,80)];
    RTS= [kin(:,85).*(-1) kin(:,87) kin(:,86)];
    RAA= [kin(:,88).*(-1) kin(:,90) kin(:,89)];
    RAI= [kin(:,91).*(-1) kin(:,93) kin(:,92)];
    RCP= [kin(:,94).*(-1) kin(:,96) kin(:,95)];
    RThreeMP= [kin(:,52).*(-1) kin(:,54) kin(:,53)];

elseif trialtype(1)=='P'
   trialsetting = 'static';
   datafile = ['Y:\All Studies\Brooke PhD files\Converted subject data
            files\Raw_static\',subjectid,'\', 'SETPO.mat'];

   %The following 6 lines of code were taken from Andy Kwarciak's
   %tetra data analysis mfiles codes (PreprocessTetra.m)
    kin1=load(datafile);
    kin=kin1.temp;
   [kinrows,kincolumns]=size(kin);
   [b,a]=butter(2,7/60);   %defines 4th order Butterworth filter with
                     %7Hz cutoff frequency
      for i=1:kincolumns
         filteredkin(:,i)=filtfilt(b,a,kin(:,i));
      end
   kin=(filteredkin);

   %Define marker positions, adjust to Pitt GCS by making X negative &
   %swapping Y and Z

   %Trochs only captured in setpo, not propulsive condition trials
   %(mkr positions are not the same for static vs. dynamic trials-
   %should come from file with 102 cols)
   SN= [kin(:,1).*(-1) kin(:,3) kin(:,2)];
   XP= [kin(:,4).*(-1) kin(:,6) kin(:,5)];
   C7= [kin(:,7).*(-1) kin(:,9) kin(:,8)];
   T3= [kin(:,10).*(-1) kin(:,12) kin(:,11)];
   LTM= [kin(:,13).*(-1) kin(:,15) kin(:,14)];
   RTM= [kin(:,37).*(-1) kin(:,39) kin(:,38)];
   RAC= [kin(:,40).*(-1) kin(:,42) kin(:,41)];
   RLE= [kin(:,43).*(-1) kin(:,45) kin(:,44)];
```

```
    RUL= [kin(:,46).*(-1) kin(:,48) kin(:,47)];
    RRA= [kin(:,49).*(-1) kin(:,51) kin(:,50)];
    RME=[kin(:,88).*(-1) kin(:,90) kin(:,89)];
    RACJ= [kin(:,85).*(-1) kin(:,87) kin(:,86)];
    RTS= [kin(:,91).*(-1) kin(:,93) kin(:,92)];
    RAA=[kin(:,94).*(-1) kin(:,96) kin(:,95)];
    RAI= [kin(:,97).*(-1) kin(:,99) kin(:,98)];
    RCP= [kin(:,100).*(-1) kin(:,102) kin(:,101)];
    RThreeMP= [kin(:,52).*(-1) kin(:,54) kin(:,53)];

else
    Error ('Incorrect trial condition entered!');
end

data_reform= [SN XP C7 T3 LTM RTM RAC RLE RUL RRA RThreeMP RME RACJ
RTS RAA RAI RCP];

%Marker names are the same names used in the OpenSim Arm 726 Shoulder
%Model
data.marker_names= {'sternal_notch', 'XP', 'C7', 'T3', 'TM_L',
                    'TM_R','r_acromion', 'r_humerus_epicondyle',
                    'r_ulnar_styloid', 'r_radius_styloid', '3MP', 'EM',
                    'ACJ', 'TS', 'AA', 'AI', 'CP'};

PathFileType = 4;
name= sprintf('%s%s.trc', subjectid,trialsetting);
datatype = '(X/Z/Y)';
DataRate = 120;
CameraRate = 120;
NumFrames = length(kin);
NumMarkers = length(data.marker_names);
Units = 'mm';
OrigDataRate = DataRate;
OrigDataStartFrame = kin(1);
OrigNumFrames = NumFrames;
tim= length(kin)/DataRate;
t=linspace(0,tim,length(kin))';
frame=1:length(kin);
markerpos = [t, data_reform];

% TRC File Header
fid=fopen(name, 'w');

if fid < 0
    fprintf('\nERROR: %s could not be opened for writing...\n\n',
                name);
```

```
    return
end

fprintf(fid, 'PathFileType\t%d\t%s\t%s\t\n', PathFileType, datatype,
        name);
fprintf(fid,
       'DataRate\tCameraRate\tNumFrames\tNumMarkers\tUnits\
        tOrigDataRate\tOrigDataStartFrame\tOrigNumFrames\n');
fprintf(fid, '%d\t%d\t%d\t%d\t%s\t%d\t%d\t%d\n', ...
       DataRate, CameraRate, NumFrames, NumMarkers, Units,
       OrigDataRate, OrigDataStartFrame, OrigNumFrames);
fprintf(fid, 'Frame#\tTime\t');

% TRC File Body
for i = 1:NumMarkers
    fprintf(fid, '%s\t\t\t', data.marker_names{i});
end

fprintf(fid, '\n\t\t');

for i = 1:NumMarkers
    fprintf(fid, 'X%d\tZ%d\tY%d\t', i, i, i);
end

fprintf(fid, '\n\n');

% marker position values
for i = 1:NumFrames
    fprintf(fid, '%d\t', frame(i));
    fprintf(fid, '%.5f\t', markerpos(i,:));
    fprintf(fid, '\n');
end

fclose(fid);

fprintf('Saved (tab delimited) marker positions to: %s\n', name);
```

A. 2 Kinetic Data Conversion Codes

A.2.1 Kinetic Data Conversion Code #1

```
%MAT_CONV is a function that converts kinetic data saved in a .MAT file to a .MOT
%file for use in OpenSim. Specifically, it sets up the data matrix with the variables
%needed (Forces, Moments, Hub marker x-y-z locations) and calls MAT2MOT.M,
```

```
%which converts the data matrix to .MOT format. Function inspired by Tim Dorn
%(University of Melbourne, November 2008) to convert data in .C3D format to .MOT
%format.
%Written by Brooke Odle on August 6, 2012

function mat_conv(subjectid, trialtype)

if nargin ~= 2
    Error('Adequate inputs not entered!');
end

if trialtype(1)=='S'
    trialsetting = 'SS';
elseif trialtype(1)=='2'
    trialsetting= '2mph';
elseif trialtype(1)=='4'
   trialsetting= '4mph';
else
   Error ('Incorrect propulsion condition entered!');
end

datafile1 = ['Y:\All Studies\tetraplegia wheelchair propulsion\Subject
          Folders\',subjectid,'\','Preprocess\',trialsetting,'\',
          'PreKinematics.mat'];
load (datafile1);

datafile2= ['Y:\All Studies\tetraplegia wheelchair propulsion\Subject
          Folders\',subjectid,'\','Preprocess\',trialsetting,'\',
          'PreKinetics.mat'];
load(datafile2);

DRate= 120;
tim= length(FxSW)/DRate;
t=linspace(0,tim,length(FxSW))';

RHUB= kin(:, [55, 57, 56]);
%Ensure that the number of samples in RHUB equal the number of forces %and
moments collected with the SW. The discrepancy in the number of %data points by
Vicon vs. SW may be due to Vicon and SW not being %synched together to run
simultaneously or that subjects started with %hand off rim and moved hand from back of
rim to front, so it would %take some time before the hand exerted a force on the rim.
if length(RHUB)~= length(FxSW)
   d=length(RHUB)-length(FxSW);
   if d >0
      RHUB = kin ((d+1:end), [kin(:,55).*(-1), kin(:,57),
       kin(:,56)]);
```

```
    else
        disp('ERROR')
    end
end

datamatrix=[t,FxSW,FySW,FzSW,RHUB,MxSW,MySW,MzSW];

%OpenSim will only read .MOT files with specific headers in a specific order: Time,
%ground_force_vx, ground_force_vy, ground_force_vz, ground_force_px,
%ground_force_py, ground_force_pz, ground_torque_x, ground_torque_y,
%ground_torque_z). For the tetra study, ground_force_vx/vy/vz refer to SW forces
%(FxSw, FySW, FzSW), the point about where the moment is calculated on the SW
%(assumed to be the hub, according to Koontz el al. 2005) refer to the x/y/z positions
%of the Right Hub (RHUB), and ground_torque_x/y/z refer to the moments collected
%by the SW (MxSW, MySW, MzSW)
colnames(1,1) = {'Time'};
colnames(1,2) = {'ground_force_vx'};
colnames(1,3) = {'ground_force_vy'};
colnames(1,4) = {'ground_force_vz'};
colnames(1,5) = {'ground_force_px'};
colnames(1,6) = {'ground_force_py'};
colnames(1,7) = {'ground_force_pz'};
colnames(1,8) = {'ground_torque_x'};
colnames(1,9) = {'ground_torque_y'};
colnames(1,10) = {'ground_torque_z'};

fname= sprintf('%s%s.mot', subjectid,trialsetting);

mat2mot(datamatrix,colnames,fname);
```

A.2.2 Kinetic Data Conversion Code #2

```
%MAT2MOT is a function that converts kinetic data saved in a .MAT file to a .MOT file
%for use in OpenSim. It is used in conjunction with MAT_CONV.M,which sets up the
%data matrix of kinetic variables to be written in .MOT format. Function inspired by
%Tim Dorn (University of Melbourne, November 2008) to convert data in .C3D format
%to .MOT format. Written by Brooke Odle on August 6, 2012 to convert data from
%.MAT to .MOT.

function mat2mot(datamatrix, colnames, filename)

[datarows,datacols] = size(datamatrix);
time=datamatrix(:,1);
range= [time(1), time(end)];
```

```
if length (colnames) ~= datacols
   error('Number of column names (%d) do not match the number of
        columns in the data (%d) \n', length(colnames), datacols);
end


%.MOT file header
fid = fopen(filename,'w');

if fid < 0
   fprintf('\n ERROR: %s could not be opened for writing ...\n\n',
         filename);
end

fprintf(fid, '%s\nnRows=%d\nnColumns=%d\n\n', filename, datarows,
      datacols);

fprintf(fid, 'name %s\ndatacolumns %d\ndatarows %d\nrange %f
      %f\nendheader\n\n', ...
      filename, datacols, datarows, range(1), range(2));

%.MOT file body
cols= [ ];

for i = 1:datacols,
   if i==1
      cols = [cols, colnames{1}];
   else
      cols = [cols, sprintf('\t%s', colnames{i})];
   end
end

cols = [cols, '\n'];

fprintf(fid, cols);

for i=1:datarows,
   fprintf(fid, '%20.10f\t', datamatrix(i,:));
   fprintf(fid, '\n');
end

fclose(fid)

fprintf('Saved motion file: %s\n', filename);
```

APPENDIX B

MATLAB CODES FOR ADDITIONAL ANALYSES OF RESULTS

These codes were used to post-process the inverse kinematics, inverse dynamics, and static optimization results computed by the Wheelchair Propulsion Model.

B.1 Inverse Kinematics Results Analysis Code

```
%IK_PLOT is a function that plots inverse kinematics results computed by OpenSim's
%Inverse Kinematics Tool. It plots the shoulder and elbow angles as a function of
%100% stroke cycle since OpenSim plots the results as a function of time. Lines are
%included to represent average transition from push to recovery. The max and min of
%each angle is also computed per stroke cycle.
%Written by Brooke Odle on March 23, 2013 and modified August 2013

kin_sho= input('Enter the kinematic profile you would like to evaluate: ', 's');

switch kin_sho
   case 'elev_angle'
       elev_angle_1=importdata('t1o4_IK_results_SC1.xlsx');
       new_elev_angle_1=resample1to100(elev_angle_1.data(:,8));
       elev_angle_2=importdata('t1o4_IK_results_SC2.xlsx');
       new_elev_angle_2=resample1to100(elev_angle_2.data(:,8));
       elev_angle_3=importdata('t1o4_IK_results_SC3_2.xlsx');
       new_elev_angle_3=resample1to100(elev_angle_3.data(:,8));
       elev_angle_4=importdata('t1o4_IK_results_SC4_2.xlsx');
       new_elev_angle_4=resample1to100(elev_angle_4.data(:,8));
       elev_angle_5=importdata('t1o4_IK_results_SC5.xlsx');
       new_elev_angle_5=resample1to100(elev_angle_5.data(:,8));

        %Reports max and min values for each stroke cycle
        eamx1= max(new_elev_angle_1)
        eamx2= max(new_elev_angle_2)
        eamx3= max(new_elev_angle_3)
        eamx4= max(new_elev_angle_4)
        eamx5= max(new_elev_angle_5)
        eamn1= min(new_elev_angle_1)
        eamn2= min(new_elev_angle_2)
        eamn3= min(new_elev_angle_3)
        eamn4= min(new_elev_angle_4)
        eamn5= min(new_elev_angle_5)

        %Reports peak (mean, stdev) for push phase
```

```
eapkp1=max(new_elev_angle_1(1:45,1));
eapkp2=max(new_elev_angle_2(1:47,1));
eapkp3=max(new_elev_angle_3(1:42,1));
eapkp4=max(new_elev_angle_4(1:34,1));
eapkp5=max(new_elev_angle_5(1:44,1));
ea_push=[eapkp1 eapkp2 eapkp3 eapkp4 eapkp5];
ea_push_avg= mean(ea_push);
ea_push_std= std(ea_push);


%Reports peak (mean, stdev) for recovery phase
eapkr1=max(new_elev_angle_1(46:100,1));
eapkr2=max(new_elev_angle_2(48:100,1));
eapkr3=max(new_elev_angle_3(43:100,1));
eapkr4=max(new_elev_angle_4(35:100,1));
eapkr5=max(new_elev_angle_5(45:100,1));
ea_rec=[eapkr1 eapkr2 eapkr3 eapkr4 eapkr5];
ea_rec_avg= mean(ea_rec);
ea_rec_std= std(ea_rec);

    %Plots profile of movement for each stroke cycle
    plot(new_elev_angle_1)
    hold on
    plot(new_elev_angle_2,'r')
    plot(new_elev_angle_3,'g')
    plot(new_elev_angle_4,'m')
    plot(new_elev_angle_5,'c')
    plot ([34 34], ylim, 'k') %Transition from push to rec
    plot ([47 47], ylim, 'k') %Transition from push to rec
    title ('Shoulder Elevation Angle')
    xlabel('% Stroke Cycle')
    ylabel('Degrees')
        legend('Stroke Cycle 1','Stroke Cycle 2','Stroke Cycle
            3','Stroke Cycle 4','Stroke Cycle 5')

case 'elev_plane'
    elev_plane_1=importdata('t1o4_IK_results_SC1.xlsx');
    new_elev_plane_1=resample1to100(elev_plane_1.data(:,9));
    elev_plane_2=importdata('t1o4_IK_results_SC2.xlsx');
    new_elev_plane_2=resample1to100(elev_plane_2.data(:,9));
    elev_plane_3=importdata('t1o4_IK_results_SC3_2.xlsx');
    new_elev_plane_3=resample1to100(elev_plane_3.data(:,9));
    elev_plane_4=importdata('t1o4_IK_results_SC4_2.xlsx');
    new_elev_plane_4=resample1to100(elev_plane_4.data(:,9));
    elev_plane_5=importdata('t1o4_IK_results_SC5.xlsx');
    new_elev_plane_5=resample1to100(elev_plane_5.data(:,9));
```

```
%Reports max and min values for each stroke cycle
epmx1= max(new_elev_plane_1)
epmx2= max(new_elev_plane_2)
epmx3= max(new_elev_plane_3)
epmx4= max(new_elev_plane_4)
epmx5= max(new_elev_plane_5)
epmn1= min(new_elev_plane_1)
epmn2= min(new_elev_plane_2)
epmn3= min(new_elev_plane_3)
epmn4= min(new_elev_plane_4)
epmn5= min(new_elev_plane_5)

 %Reports peak (mean, stdev) for push phase
 eppkp1=max(new_elev_plane_1(1:45,1));
 eppkp2=max(new_elev_plane_2(1:47,1));
 eppkp3=max(new_elev_plane_3(1:42,1));
 eppkp4=max(new_elev_plane_4(1:34,1));
 eppkp5=max(new_elev_plane_5(1:44,1));

 ep_push=[eppkp1 eppkp2 eppkp3 eppkp4 eppkp5];
 ep_push_avg= mean(ep_push);
 ep_push_std= std(ep_push);

 %Reports peak (mean, stdev) for recovery phase
 eppkr1=max(new_elev_plane_1(46:100,1));
 eppkr2=max(new_elev_plane_2(48:100,1));
 eppkr3=max(new_elev_plane_3(43:100,1));
 eppkr4=max(new_elev_plane_4(35:100,1));
 eppkr5=max(new_elev_plane_5(45:100,1));
 ep_rec=[eppkr1 eppkr2 eppkr3 eppkr4 eppkr5];
 ep_rec_avg= mean(ep_rec);
 ep_rec_std= std(ep_rec);

    %Plots profile of movement for each stroke cycle
    plot(new_elev_plane_1)
    hold on
    plot(new_elev_plane_2,'r')
    plot(new_elev_plane_3,'g')
    plot(new_elev_plane_4,'m')
    plot(new_elev_plane_5,'c')
    plot ([34 34], ylim, 'k') %Transition from push to rec
    plot ([47 47], ylim, 'k') %Transition from push to rec
    title ('Shoulder  Elevation Plane')
    xlabel('% Stroke Cycle')
    ylabel('Degrees ')
```

```
        legend('Stroke Cycle 1','Stroke Cycle 2','Stroke Cycle
            3','Stroke Cycle 4','Stroke Cycle 5')


case 'rotation'
        rot_1=importdata('t1o4_IK_results_SC1.xlsx');
        new_rot_1=resample1to100(rot_1.data(:,10));
        rot_2=importdata('t1o4_IK_results_SC2.xlsx');
        new_rot_2=resample1to100(rot_2.data(:,10));
        rot_3=importdata('t1o4_IK_results_SC3_2.xlsx');
        new_rot_3=resample1to100(rot_3.data(:,10));
        rot_4=importdata('t1o4_IK_results_SC4_2.xlsx');
        new_rot_4=resample1to100(rot_4.data(:,10));
        rot_5=importdata('t1o4_IK_results_SC5.xlsx');
        new_rot_5=resample1to100(rot_5.data(:,10));

         %Reports max and min values for each stroke cycle
         rotmx1= max(new_rot_1)
         rotmx2= max(new_rot_2)
         rotmx3= max(new_rot_3)
         rotmx4= max(new_rot_4)
         rotmx5= max(new_rot_5)
         rotmn1= min(new_rot_1)
         rotmn2= min(new_rot_2)
         rotmn3= min(new_rot_3)
         rotmn4= min(new_rot_4)
         rotmn5= min(new_rot_5)

         %Reports peak (mean, stdev) for push phase
         rotpkp1=max(new_rot_1(1:45,1));
         rotpkp2=max(new_rot_2(1:47,1));
         rotpkp3=max(new_rot_3(1:42,1));
         rotpkp4=max(new_rot_4(1:34,1));
         rotpkp5=max(new_rot_5(1:44,1));
         rot_push=[rotpkp1 rotpkp2 rotpkp3 rotpkp4 rotpkp5];
         rot_push_avg= mean(rot_push);
         rot_push_std= std(rot_push);

         %Reports peak (mean, stdev) for recovery phase
         rotpkr1=max(new_rot_1(46:100,1));
         rotpkr2=max(new_rot_2(48:100,1));
         rotpkr3=max(new_rot_3(43:100,1));
         rotpkr4=max(new_rot_4(35:100,1));
         rotpkr5=max(new_rot_5(45:100,1));
         rot_rec=[rotpkr1 rotpkr2 rotpkr3 rotpkr4 rotpkr5];
         rot_rec_avg= mean(rot_rec);
```

```
rot_rec_std= std(rot_rec);

    %Plots profile of movement for each stroke cycle
    plot(new_rot_1)
    hold on
    plot(new_rot_2,'r')
    plot(new_rot_3,'g')
    plot(new_rot_4,'m')
    plot(new_rot_5,'c')
    plot ([34 34], ylim, 'k') %Transition from push to rec
    plot ([47 47], ylim, 'k') %Transition from push to rec
    title ('Shoulder Rotation')
    xlabel('% Stroke Cycle')
    ylabel('Degrees ')
    legend('Stroke Cycle 1','Stroke Cycle 2','Stroke Cycle
        3','Stroke Cycle 4','Stroke Cycle 5')

case 'elbow flex'
    eflex_1=importdata('t1o4_IK_results_SC1.xlsx');
    new_eflex_1=resample1to100(eflex_1.data(:,11));
    eflex_2=importdata('t1o4_IK_results_SC2.xlsx');
    new_eflex_2=resample1to100(eflex_2.data(:,11));
    eflex_3=importdata('t1o4_IK_results_SC3_2.xlsx');
    new_eflex_3=resample1to100(eflex_3.data(:,11));
    eflex_4=importdata('t1o4_IK_results_SC4_2.xlsx');
    new_eflex_4=resample1to100(eflex_4.data(:,11));
    eflex_5=importdata('t1o4_IK_results_SC5.xlsx');
    new_eflex_5=resample1to100(eflex_5.data(:,11));

    %Reports max and min values for each stroke cycle
    efmx1= max(new_eflex_1)
    efmx2= max(new_eflex_2)
    efmx3= max(new_eflex_3)
    efmx4= max(new_eflex_4)
    efmx5= max(new_eflex_5)
    efmn1= min(new_eflex_1)
    efmn2= min(new_eflex_2)
    efmn3= min(new_eflex_3)
    efmn4= min(new_eflex_4)
    efmn5= min(new_eflex_5)

    %Reports peak (mean, stdev) for push phase
    eflexpkp1=max(new_eflex_1(1:45,1));
    eflexpkp2=max(new_eflex_2(1:47,1));
    eflexpkp3=max(new_eflex_3(1:42,1));
    eflexpkp4=max(new_eflex_4(1:34,1));
```

```
        eflexpkp5=max(new_eflex_5(1:44,1));
        eflex_push=[eflexpkp1 eflexpkp2 eflexpkp3 eflexpkp4
                eflexpkp5];
        eflex_push_avg= mean(eflex_push);
        eflex_push_std= std(eflex_push);

        %Reports peak (mean, stdev) for recovery phase
        eflexpkr1=max(new_eflex_1(46:100,1));
        eflexpkr2=max(new_eflex_2(48:100,1));
        eflexpkr3=max(new_eflex_3(43:100,1));
        eflexpkr4=max(new_eflex_4(35:100,1));
        eflexpkr5=max(new_eflex_5(45:100,1));
        eflex_rec=[eflexpkr1 eflexpkr2 eflexpkr3 eflexpkr4
                eflexpkr5];
        eflex_rec_avg= mean(eflex_rec);
        eflex_rec_std= std(eflex_rec);

            %Plots profile of movement for each stroke cycle
            plot(new_eflex_1)
            hold on
            plot(new_eflex_2,'r')
            plot(new_eflex_3,'g')
            plot(new_eflex_4,'m')
            plot(new_eflex_5,'c')
            plot ([34 34], ylim, 'k') %Transition from push to rec
            plot ([47 47], ylim, 'k') %Transition from push to rec
            title ('Elbow Flexion')
            xlabel('% Stroke Cycle')
            ylabel('Degrees ')
            legend('Stroke Cycle 1','Stroke Cycle 2','Stroke Cycle
                3','Stroke Cycle 4','Stroke Cycle 5')

case 'forearm rot'
    forerot_1=importdata('t1o4_IK_results_SC1.xlsx');
     new_forerot_1=resample1to100(forerot_1.data(:,12));
     forerot_2=importdata('t1o4_IK_results_SC2.xlsx');
     new_forerot_2=resample1to100(forerot_2.data(:,12));
     forerot_3=importdata('t1o4_IK_results_SC3_2.xlsx');
     new_forerot_3=resample1to100(forerot_3.data(:,12));
     forerot_4=importdata('t1o4_IK_results_SC4_2.xlsx');
     new_forerot_4=resample1to100(forerot_4.data(:,12));
     forerot_5=importdata('t1o4_IK_results_SC5.xlsx');
     new_forerot_5=resample1to100(forerot_5.data(:,12));

      %Reports max and min values for each stroke cycle
      eprmx1= max(new_epron_1)
```

```
eprmx2= max(new_epron_2)
eprmx3= max(new_epron_3)
eprmx4= max(new_epron_4)
eprmx5= max(new_epron_5)

eprmn1= min(new_epron_1)
eprmn2= min(new_epron_2)
eprmn3= min(new_epron_3)
eprmn4= min(new_epron_4)
eprmn5= min(new_epron_5)

%Reports peak (mean, stdev) for push phase
forerotpkp1=max(new_forerot_1(1:45,1));
forerotpkp2=max(new_forerot_2(1:47,1));
forerotpkp3=max(new_forerot_3(1:42,1));
forerotpkp4=max(new_forerot_4(1:34,1));
forerotpkp5=max(new_forerot_5(1:44,1));
forerot_push=[forerotpkp1 forerotpkp2 forerotpkp3
        forerotpkp4 forerotpkp5];
forerot_push_avg= mean(forerot_push);
forerot_push_std= std(forerot_push);

%Reports peak (mean, stdev) for recovery phase
forerotpkr1=max(new_forerot_1(46:100,1));
forerotpkr2=max(new_forerot_2(48:100,1));
forerotpkr3=max(new_forerot_3(43:100,1));
forerotpkr4=max(new_forerot_4(35:100,1));
forerotpkr5=max(new_forerot_5(45:100,1));
forerot_rec=[forerotpkr1 forerotpkr2 forerotpkr3 forerotpkr4
        forerotpkr5];
forerot_rec_avg= mean(forerot_rec);
forerot_rec_std= std(forerot_rec);

    %Plots profile of movement for each stroke cycle
    plot(new_forerot_1)
    hold on
    plot(new_forerot_2,'r')
    plot(new_forerot_3,'g')
    plot(new_forerot_4,'m')
    plot(new_forerot_5,'c')
    plot ([34 34], ylim, 'k') %Transition from push to rec
    plot ([47 47], ylim, 'k') %Transition from push to rec
    title ('Forearm Rotation')
    xlabel('% Stroke Cycle')
    ylabel('Degrees')
    legend('Stroke Cycle 1','Stroke Cycle 2','Stroke Cycle
```

```
                3','Stroke Cycle 4','Stroke Cycle 5')
otherwise
    display('Selection not understood. Try again!')
end
```

B.2 Inverse Dynamics Results Analysis Code

```
%ID_PLOT is a function that plots inverse dynamics results computed by OpenSim's
%Inverse Dynamics Tool. It plots the shoulder moments as a function of 100% stroke
%cycle since OpenSim plots the results as a function of time. A line is included to
%represent average transition from push to recovery. The %max and min of each
%moment is also computed per stroke cycle.
%Written by Brooke Odle on April 2, 2013 and modified August 2013

force_sho= input('Enter the force you would like to evaluate: ', 's');

switch force_sho
    case 'elev_angle'
    elev_angle_1=importdata('t1o4_IDresults_SC1_InverseDynamics.sto');
    new_elev_angle_1=resample1to100(elev_angle_1.data(:,8));
    elev_angle_2=importdata('t1o4_scaled_IDresults_SC2_InverseDynamics.
                sto');
    new_elev_angle_2=resample1to100(elev_angle_2.data(:,8));
    elev_angle_3=importdata('t1o4_scaled_IDresults_SC3_InverseDynamics.
                sto');
    new_elev_angle_3=resample1to100(elev_angle_3.data(:,8));
    elev_angle_4=importdata('t1o4_scaled_IDresults_SC4_InverseDynamics.
                sto');
    new_elev_angle_4=resample1to100(elev_angle_4.data(:,8));
    elev_angle_5=importdata('t1o4_scaled_IDresults_SC5_InverseDynamics.
                sto');
   new_elev_angle_5=resample1to100(elev_angle_5.data(:,8));

  %Reports max and min values for each stroke cycle
     eamx1= max(new_elev_angle_1)
     eamx2= max(new_elev_angle_2)
     eamx3= max(new_elev_angle_3)
     eamx4= max(new_elev_angle_4)
     eamx5= max(new_elev_angle_5)
     eamn1= min(new_elev_angle_1)
     eamn2= min(new_elev_angle_2)
     eamn3= min(new_elev_angle_3)
     eamn4= min(new_elev_angle_4)
     eamn5= min(new_elev_angle_5)
```

```
%Reports peak (mean, stdev) for push phase
        eapkp1=max(new_elev_angle_1(1:45,1));
        eapkp2=max(new_elev_angle_2(1:47,1));
        eapkp3=max(new_elev_angle_3(1:42,1));
        eapkp4=max(new_elev_angle_4(1:34,1));
        eapkp5=max(new_elev_angle_5(1:44,1));
        ea_push=[eapkp1 eapkp2 eapkp3 eapkp4 eapkp5];
        ea_push_avg= mean(ea_push);
        ea_push_std= std(ea_push);

        %Reports peak (mean, stdev) for recovery phase
        eapkr1=max(new_elev_angle_1(46:100,1));
        eapkr2=max(new_elev_angle_2(48:100,1));
        eapkr3=max(new_elev_angle_3(43:100,1));
        eapkr4=max(new_elev_angle_4(35:100,1));
        eapkr5=max(new_elev_angle_5(45:100,1));
        ea_rec=[eapkr1 eapkr2 eapkr3 eapkr4 eapkr5];
        ea_rec_avg= mean(ea_rec);
        ea_rec_std= std(ea_rec);

            %Plots profile of movement for each stroke cycle
            plot(new_elev_angle_1)
            hold on
            plot(new_elev_angle_2,'r')
            plot(new_elev_angle_3,'g')
            plot(new_elev_angle_4,'m')
            plot(new_elev_angle_5,'c')
            plot ([34 34], ylim, 'k') %Transition from push to rec
            plot ([47 47], ylim, 'k') %Transition from push to rec
            title ('Shoulder Elevation Angle Moment')
            xlabel('% Stroke Cycle')
            ylabel('Moment (Nm) ')
            legend('Stroke Cycle 1','Stroke Cycle 2','Stroke Cycle
                3','Stroke Cycle 4','Stroke Cycle 5')

 case 'elev_plane'
   elev_plane_1=importdata('t1o4_IDresults_SC1_InverseDynamics.sto');
   new_elev_plane_1=resample1to100(elev_plane_1.data(:,9));
   elev_plane_2=importdata('t1o4_scaled_IDresults_SC2_InverseDynamic
                        s.sto');
   new_elev_plane_2=resample1to100(elev_plane_2.data(:,9));
   elev_plane_3=importdata('t1o4_scaled_IDresults_SC3_InverseDynamic
                    s.sto');
    new_elev_plane_3=resample1to100(elev_plane_3.data(:,9));
    elev_plane_4=importdata('t1o4_scaled_IDresults_SC4_InverseDynamic
                                    s.sto');
```

```
new_elev_plane_4=resample1to100(elev_plane_4.data(:,9));
elev_plane_5=importdata('t1o4_scaled_IDresults_SC5_InverseDynamic
                        s.sto');
new_elev_plane_5=resample1to100(elev_plane_5.data(:,9));

   %Reports max and min values for each stroke cycle
   epmx1= max(new_elev_plane_1)
   epmx2= max(new_elev_plane_2)
   epmx3= max(new_elev_plane_3)
   epmx4= max(new_elev_plane_4)
   epmx5= max(new_elev_plane_5)
   epmn1= min(new_elev_plane_1)
   epmn2= min(new_elev_plane_2)
   epmn3= min(new_elev_plane_3)
   epmn4= min(new_elev_plane_4)
   epmn5= min(new_elev_plane_5)

    %Reports peak (mean, stdev) for push phase
    eppkp1=max(new_elev_plane_1(1:45,1));
    eppkp2=max(new_elev_plane_2(1:47,1));
    eppkp3=max(new_elev_plane_3(1:42,1));
    eppkp4=max(new_elev_plane_4(1:34,1));
    eppkp5=max(new_elev_plane_5(1:44,1));

    ep_push=[eppkp1 eppkp2 eppkp3 eppkp4 eppkp5];
    ep_push_avg= mean(ep_push);
    ep_push_std= std(ep_push);

    %Reports peak (mean, stdev) for recovery phase
    eppkr1=max(new_elev_plane_1(46:100,1));
    eppkr2=max(new_elev_plane_2(48:100,1));
    eppkr3=max(new_elev_plane_3(43:100,1));
    eppkr4=max(new_elev_plane_4(35:100,1));
    eppkr5=max(new_elev_plane_5(45:100,1));
    ep_rec=[eppkr1 eppkr2 eppkr3 eppkr4 eppkr5];
    ep_rec_avg= mean(ep_rec);
    ep_rec_std= std(ep_rec);

        %Plots profile of movement for each stroke cycle
        plot(new_elev_plane_1)
        hold on
        plot(new_elev_plane_2,'r')
        plot(new_elev_plane_3,'g')
        plot(new_elev_plane_4,'m')
        plot(new_elev_plane_5,'c')
        plot ([34 34], ylim, 'k') %Transition from push to rec
```

```
        plot ([47 47], ylim, 'k') %Transition from push to rec
        title ('Shoulder Elevation Plane Moment')
        xlabel('% Stroke Cycle')
        ylabel('Moment (Nm) ')
        legend('Stroke Cycle 1','Stroke Cycle 2','Stroke Cycle
            3','Stroke Cycle 4','Stroke Cycle 5')

case 'rotation'
  rot_1=importdata('t1o4_IDresults_SC1_InverseDynamics.sto');
  new_rot_1=resample1to100(rot_1.data(:,10));
  rot_2=importdata('t1o4_scaled_IDresults_SC2_InverseDynamics.sto');
  new_rot_2=resample1to100(rot_2.data(:,10));
  rot_3=importdata('t1o4_scaled_IDresults_SC3_InverseDynamics.sto');
  new_rot_3=resample1to100(rot_3.data(:,10));
  rot_4=importdata('t1o4_scaled_IDresults_SC4_InverseDynamics.sto');
  new_rot_4=resample1to100(rot_4.data(:,10));
  rot_5=importdata('t1o4_scaled_IDresults_SC5_InverseDynamics.sto');
  new_rot_5=resample1to100(rot_5.data(:,10));

     %Reports max and min values for each stroke cycle
     rotmx1= max(new_rot_1)
     rotmx2= max(new_rot_2)
     rotmx3= max(new_rot_3)
     rotmx4= max(new_rot_4)
     rotmx5= max(new_rot_5)
     rotmn1= min(new_rot_1)
     rotmn2= min(new_rot_2)
     rotmn3= min(new_rot_3)
     rotmn4= min(new_rot_4)
     rotmn5= min(new_rot_5)

      %Reports peak (mean, stdev) for push phase
      rotpkp1=max(new_rot_1(1:45,1));
      rotpkp2=max(new_rot_2(1:47,1));
      rotpkp3=max(new_rot_3(1:42,1));
      rotpkp4=max(new_rot_4(1:34,1));
      rotpkp5=max(new_rot_5(1:44,1));
      rot_push=[rotpkp1 rotpkp2 rotpkp3 rotpkp4 rotpkp5];
      rot_push_avg= mean(rot_push);
      rot_push_std= std(rot_push);

      %Reports peak (mean, stdev) for recovery phase
      rotpkr1=max(new_rot_1(46:100,1));
      rotpkr2=max(new_rot_2(48:100,1));
      rotpkr3=max(new_rot_3(43:100,1));
      rotpkr4=max(new_rot_4(35:100,1));
```

```
        rotpkr5=max(new_rot_5(45:100,1));
        rot_rec=[rotpkr1 rotpkr2 rotpkr3 rotpkr4 rotpkr5];
        rot_rec_avg= mean(rot_rec);
        rot_rec_std= std(rot_rec);

            %Plots profile of movement for each stroke cycle
            plot(new_rot_1)
            hold on
            plot(new_rot_2,'r')
            plot(new_rot_3,'g')
            plot(new_rot_4,'m')
            plot(new_rot_5,'c')
            plot ([34 34], ylim, 'k') %Transition from push to rec
            plot ([47 47], ylim, 'k') %Transition from push to rec
            title ('Shoulder Rotation Moment')
            xlabel('% Stroke Cycle')
            ylabel('Moment (Nm) ')
            legend('Stroke Cycle 1','Stroke Cycle 2','Stroke Cycle
                3','Stroke Cycle 4','Stroke Cycle 5')
 otherwise
     display('Selection not understood. Try again!')
end
```

B.3 Static Optimization Results Analysis Code

```
%MUSCLE_FORCES_PLOT is a function that plots the muscle forces of interest,
%estimated by OpenSim's Static Optimization Tool, as a function of peak force
%generated during push phase and peak force generated during recovery phase. The
%estimated muscle forces are presented as horizontal bar plots.
%Written by Brooke Odle on April 2, 2013

%Imports .sto files of muscle forces estimated by OpenSim's Static
%OptimizationTool
os_mf_SC1=importdata('t1o4_scaled_StaticOptimization_force_updmuscles_S
            C1.sto');
os_mf_SC2=importdata('t1o4_scaled_StaticOptimization_force_updmuscles_S
            C2.sto');
os_mf_SC3=importdata('t1o4_scaled_StaticOptimization_force_updmuscles_S
            C3.sto');
os_mf_SC4=importdata('t1o4_scaled_StaticOptimization_force_updmuscles_S
            C4.sto');
os_mf_SC5=importdata('t1o4_scaled_StaticOptimization_force_updmuscles_S
            C5.sto');
```

```
%Reshapes all muscle forces to 100% SC for all 13 muscles being
%compared with EMG

 %Anterior Deltoid
 new_os_ad_SC1=resample1to100(os_mf_SC1.data(:,2));
 new_os_ad_SC2=resample1to100(os_mf_SC2.data(:,2));
 new_os_ad_SC3=resample1to100(os_mf_SC3.data(:,2));
 new_os_ad_SC4=resample1to100(os_mf_SC4.data(:,2));
 new_os_ad_SC5=resample1to100(os_mf_SC5.data(:,2));

 %Middle Deltoid
 new_os_md_SC1=resample1to100(os_mf_SC1.data(:,3));
 new_os_md_SC2=resample1to100(os_mf_SC2.data(:,3));
 new_os_md_SC3=resample1to100(os_mf_SC3.data(:,3));
 new_os_md_SC4=resample1to100(os_mf_SC4.data(:,3));
 new_os_md_SC5=resample1to100(os_mf_SC5.data(:,3));

 %Posterior Deltoid
 new_os_pd_SC1=resample1to100(os_mf_SC1.data(:,4));
 new_os_pd_SC2=resample1to100(os_mf_SC2.data(:,4));
 new_os_pd_SC3=resample1to100(os_mf_SC3.data(:,4));
 new_os_pd_SC4=resample1to100(os_mf_SC4.data(:,4));
 new_os_pd_SC5=resample1to100(os_mf_SC5.data(:,4));

 %Supraspinatus
 new_os_sup_SC1=resample1to100(os_mf_SC1.data(:,5));
 new_os_sup_SC2=resample1to100(os_mf_SC2.data(:,5));
 new_os_sup_SC3=resample1to100(os_mf_SC3.data(:,5));
 new_os_sup_SC4=resample1to100(os_mf_SC4.data(:,5));
 new_os_sup_SC5=resample1to100(os_mf_SC5.data(:,5));

 %Infraspinatus
 new_os_inf_SC1=resample1to100(os_mf_SC1.data(:,6));
 new_os_inf_SC2=resample1to100(os_mf_SC2.data(:,6));
 new_os_inf_SC3=resample1to100(os_mf_SC3.data(:,6));
 new_os_inf_SC4=resample1to100(os_mf_SC4.data(:,6));
 new_os_inf_SC5=resample1to100(os_mf_SC5.data(:,6));

 %Subscapularis
 new_os_sub_SC1=resample1to100(os_mf_SC1.data(:,7));
 new_os_sub_SC2=resample1to100(os_mf_SC2.data(:,7));
 new_os_sub_SC3=resample1to100(os_mf_SC3.data(:,7));
 new_os_sub_SC4=resample1to100(os_mf_SC4.data(:,7));
 new_os_sub_SC5=resample1to100(os_mf_SC5.data(:,7));
```

```
%Pectoralis Major
new_os_pec_SC1=resample1to100(os_mf_SC1.data(:,10));
new_os_pec_SC2=resample1to100(os_mf_SC2.data(:,10));
new_os_pec_SC3=resample1to100(os_mf_SC3.data(:,10));
new_os_pec_SC4=resample1to100(os_mf_SC4.data(:,10));
new_os_pec_SC5=resample1to100(os_mf_SC5.data(:,10));


%Triceps
new_os_tri_SC1=resample1to100(os_mf_SC1.data(:,17));
new_os_tri_SC2=resample1to100(os_mf_SC2.data(:,17));
new_os_tri_SC3=resample1to100(os_mf_SC3.data(:,17));
new_os_tri_SC4=resample1to100(os_mf_SC4.data(:,17));
new_os_tri_SC5=resample1to100(os_mf_SC5.data(:,17));

%Biceps
new_os_bi_SC1=resample1to100(os_mf_SC1.data(:,22));
new_os_bi_SC2=resample1to100(os_mf_SC2.data(:,22));
new_os_bi_SC3=resample1to100(os_mf_SC3.data(:,22));
new_os_bi_SC4=resample1to100(os_mf_SC4.data(:,22));
new_os_bi_SC5=resample1to100(os_mf_SC5.data(:,22));

%Upper Trapezius
new_os_up_trap_SC1=resample1to100(os_mf_SC1.data(:,28));
new_os_up_trap_SC2=resample1to100(os_mf_SC2.data(:,28));
new_os_up_trap_SC3=resample1to100(os_mf_SC3.data(:,28));
new_os_up_trap_SC4=resample1to100(os_mf_SC4.data(:,28));
new_os_up_trap_SC5=resample1to100(os_mf_SC5.data(:,28));

%Middle Trapezius
new_os_mid_trap_SC1=resample1to100(os_mf_SC1.data(:,29));
new_os_mid_trap_SC2=resample1to100(os_mf_SC2.data(:,29));
new_os_mid_trap_SC3=resample1to100(os_mf_SC3.data(:,29));
new_os_mid_trap_SC4=resample1to100(os_mf_SC4.data(:,29));
new_os_mid_trap_SC5=resample1to100(os_mf_SC5.data(:,29));

%Serratus Anterior
new_os_serr_ant_SC1=resample1to100(os_mf_SC1.data(:,30));
new_os_serr_ant_SC2=resample1to100(os_mf_SC2.data(:,30));
new_os_serr_ant_SC3=resample1to100(os_mf_SC3.data(:,30));
new_os_serr_ant_SC4=resample1to100(os_mf_SC4.data(:,30));
new_os_serr_ant_SC5=resample1to100(os_mf_SC5.data(:,30));

%Rhomboid Major
new_os_rhom_SC1=resample1to100(os_mf_SC1.data(:,31));
new_os_rhom_SC2=resample1to100(os_mf_SC2.data(:,31));
```

```
new_os_rhom_SC3=resample1to100(os_mf_SC3.data(:,31));
new_os_rhom_SC4=resample1to100(os_mf_SC4.data(:,31));
new_os_rhom_SC5=resample1to100(os_mf_SC5.data(:,31));

    %Finds max force of each muscle for each stroke cycle during
    %push phase:
    %Stroke Cycle 1 (Push phase = 45%)
    ad_push_SC1=new_os_ad_SC1(1:45,1);
    md_push_SC1=new_os_md_SC1(1:45,1);
    pd_push_SC1=new_os_pd_SC1(1:45,1);
    sup_push_SC1=new_os_sup_SC1(1:45,1);
    inf_push_SC1=new_os_inf_SC1(1:45,1);
    sub_push_SC1=new_os_sub_SC1(1:45,1);
    pec_push_SC1=new_os_pec_SC1(1:45,1);
    tri_push_SC1=new_os_tri_SC1(1:45,1);
    bi_push_SC1=new_os_bi_SC1(1:45,1);
    uptrap_push_SC1=new_os_up_trap_SC1(1:45,1);
    midtrap_push_SC1=new_os_mid_trap_SC1(1:45,1);
    serrant_push_SC1=new_os_serr_ant_SC1(1:45,1);
    rhommaj_push_SC1=new_os_rhom_SC1(1:45,1);
    ad_max_1=max(ad_push_SC1);
    md_max_1=max(md_push_SC1);
    pd_max_1=max(pd_push_SC1);
    sup_max_1=max(sup_push_SC1);
    inf_max_1=max(inf_push_SC1);
    sub_max_1=max(sub_push_SC1);
    pec_max_1=max(pec_push_SC1);
    tri_max_1=max(tri_push_SC1);
    bi_max_1=max(bi_push_SC1);
    uptrap_max_1=max(uptrap_push_SC1);
    midtrap_max_1=max(midtrap_push_SC1);
    serrant_max_1=max(serrant_push_SC1);
    rhommaj_max_1=max(rhommaj_push_SC1);

    %Stroke Cycle 2 (Push phase = 47%)
    ad_push_SC2=new_os_ad_SC2(1:47,1);
    md_push_SC2=new_os_md_SC2(1:47,1);
    pd_push_SC2=new_os_pd_SC2(1:47,1);
    sup_push_SC2=new_os_sup_SC2(1:47,1);
    inf_push_SC2=new_os_inf_SC2(1:47,1);
    sub_push_SC2=new_os_sub_SC2(1:47,1);
    pec_push_SC2=new_os_pec_SC2(1:47,1);
    tri_push_SC2=new_os_tri_SC2(1:47,1);
    bi_push_SC2=new_os_bi_SC2(1:47,1);
    uptrap_push_SC2=new_os_up_trap_SC2(1:47,1);
    midtrap_push_SC2=new_os_mid_trap_SC2(1:47,1);
```

```
serrant_push_SC2=new_os_serr_ant_SC2(1:47,1);
rhommaj_push_SC2=new_os_rhom_SC2(1:47,1);
ad_max_2=max(ad_push_SC2);
md_max_2=max(md_push_SC2);
pd_max_2=max(pd_push_SC2);
sup_max_2=max(sup_push_SC2);
inf_max_2=max(inf_push_SC2);
sub_max_2=max(sub_push_SC2);
pec_max_2=max(pec_push_SC2);
tri_max_2=max(tri_push_SC2);
bi_max_2=max(bi_push_SC2);
uptrap_max_2=max(uptrap_push_SC2);
midtrap_max_2=max(midtrap_push_SC2);
serrant_max_2=max(serrant_push_SC2);
rhommaj_max_2=max(rhommaj_push_SC2);

%Stroke Cycle 3 (Push phase = 42%)
ad_push_SC3=new_os_ad_SC3(1:42,1);
md_push_SC3=new_os_md_SC3(1:42,1);
pd_push_SC3=new_os_pd_SC3(1:42,1);
sup_push_SC3=new_os_sup_SC3(1:42,1);
inf_push_SC3=new_os_inf_SC3(1:42,1);
sub_push_SC3=new_os_sub_SC3(1:42,1);
pec_push_SC3=new_os_pec_SC3(1:42,1);
tri_push_SC3=new_os_tri_SC3(1:42,1);
bi_push_SC3=new_os_bi_SC3(1:42,1);
uptrap_push_SC3=new_os_up_trap_SC2(1:42,1);
midtrap_push_SC3=new_os_mid_trap_SC3(1:42,1);
serrant_push_SC3=new_os_serr_ant_SC3(1:42,1);
rhommaj_push_SC3=new_os_rhom_SC3(1:42,1);
ad_max_3=max(ad_push_SC3);
md_max_3=max(md_push_SC3);
pd_max_3=max(pd_push_SC3);
sup_max_3=max(sup_push_SC3);
inf_max_3=max(inf_push_SC3);
sub_max_3=max(sub_push_SC3);
pec_max_3=max(pec_push_SC3);
tri_max_3=max(tri_push_SC3);
bi_max_3=max(bi_push_SC3);
uptrap_max_3=max(uptrap_push_SC3);
midtrap_max_3=max(midtrap_push_SC3);
serrant_max_3=max(serrant_push_SC3);
rhommaj_max_3=max(rhommaj_push_SC3);
```

```
%Stroke Cycle 4 (Push phase = 34%)
ad_push_SC4=new_os_ad_SC4(1:34,1);
md_push_SC4=new_os_md_SC4(1:34,1);
pd_push_SC4=new_os_pd_SC4(1:34,1);
sup_push_SC4=new_os_sup_SC4(1:34,1);
inf_push_SC4=new_os_inf_SC4(1:34,1);
sub_push_SC4=new_os_sub_SC4(1:34,1);
pec_push_SC4=new_os_pec_SC4(1:34,1);
tri_push_SC4=new_os_tri_SC4(1:34,1);
bi_push_SC4=new_os_bi_SC4(1:34,1);
uptrap_push_SC4=new_os_up_trap_SC4(1:34,1);
midtrap_push_SC4=new_os_mid_trap_SC4(1:34,1);
serrant_push_SC4=new_os_serr_ant_SC4(1:34,1);
rhommaj_push_SC4=new_os_rhom_SC4(1:34,1);
ad_max_4=max(ad_push_SC4);
md_max_4=max(md_push_SC4);
pd_max_4=max(pd_push_SC4);
sup_max_4=max(sup_push_SC4);
inf_max_4=max(inf_push_SC4);
sub_max_4=max(sub_push_SC4);
pec_max_4=max(pec_push_SC4);
tri_max_4=max(tri_push_SC4);
bi_max_4=max(bi_push_SC4);
uptrap_max_4=max(uptrap_push_SC4);
midtrap_max_4=max(midtrap_push_SC4);
serrant_max_4=max(serrant_push_SC4);
rhommaj_max_4=max(rhommaj_push_SC4);

%Stroke Cycle 5 (Push phase = 44%)
ad_push_SC5=new_os_ad_SC5(1:44,1);
md_push_SC5=new_os_md_SC5(1:44,1);
pd_push_SC5=new_os_pd_SC5(1:44,1);
sup_push_SC5=new_os_sup_SC5(1:44,1);
inf_push_SC5=new_os_inf_SC5(1:44,1);
sub_push_SC5=new_os_sub_SC5(1:44,1);
pec_push_SC5=new_os_pec_SC5(1:44,1);
tri_push_SC5=new_os_tri_SC5(1:44,1);
bi_push_SC5=new_os_bi_SC5(1:44,1);
uptrap_push_SC5=new_os_up_trap_SC5(1:44,1);
midtrap_push_SC5=new_os_mid_trap_SC5(1:44,1);
serrant_push_SC5=new_os_serr_ant_SC5(1:44,1);
rhommaj_push_SC5=new_os_rhom_SC5(1:44,1);
ad_max_5=max(ad_push_SC5);
md_max_5=max(md_push_SC5);
pd_max_5=max(pd_push_SC5);
sup_max_5=max(sup_push_SC5);
```

```
inf_max_5=max(inf_push_SC5);
sub_max_5=max(sub_push_SC5);
pec_max_5=max(pec_push_SC5);
tri_max_5=max(tri_push_SC5);
bi_max_5=max(bi_push_SC5);
uptrap_max_5=max(uptrap_push_SC5);
midtrap_max_5=max(midtrap_push_SC5);
serrant_max_5=max(serrant_push_SC5);
rhommaj_max_5=max(rhommaj_push_SC5);

%Places max forces into one matrix per stroke cycle:
SC_1_max=[ad_max_1 md_max_1 pd_max_1 sup_max_1 inf_max_1
      sub_max_1 pec_max_1, tri_max_1 bi_max_1 uptrap_max_1
      midtrap_max_1 serrant_max_1 rhommaj_max_1];
SC_2_max=[ad_max_2 md_max_2 pd_max_2 sup_max_2 inf_max_2
      sub_max_2 pec_max_2, tri_max_2 bi_max_2 uptrap_max_2
      midtrap_max_2 serrant_max_2 rhommaj_max_2];
SC_3_max=[ad_max_3 md_max_3 pd_max_3 sup_max_3 inf_max_3
      sub_max_3 pec_max_3, tri_max_3 bi_max_3 uptrap_max_3
      midtrap_max_3 serrant_max_3 rhommaj_max_3];
SC_4_max=[ad_max_4 md_max_4 pd_max_4 sup_max_4 inf_max_4
      sub_max_4 pec_max_4, tri_max_4 bi_max_4 uptrap_max_4
      midtrap_max_4 serrant_max_4 rhommaj_max_4];
SC_5_max=[ad_max_5 md_max_5 pd_max_5 sup_max_5 inf_max_5
      sub_max_5 pec_max_5, tri_max_5 bi_max_5 uptrap_max_5
      midtrap_max_5 serrant_max_5 rhommaj_max_5];

%Groups muscle forces by muscle for all 5 SC and computes mean
%and standard deviation for each muscle across all 5 SC
ad=[ad_max_1; ad_max_2; ad_max_3; ad_max_4; ad_max_5];
ad_push_avg=mean (ad);
ad_push_std=std(ad);
md=[md_max_1; md_max_2; md_max_3; md_max_4; md_max_5];
md_push_avg=mean(md);
md_push_std=std(md);
pd=[pd_max_1; pd_max_2; pd_max_3; pd_max_4; pd_max_5];
pd_push_avg=mean(pd);
pd_push_std=std(pd);
sup=[sup_max_1; sup_max_2; sup_max_3; sup_max_4; sup_max_5];
sup_push_avg=mean(sup);
sup_push_std=std(sup);
inf=[inf_max_1; inf_max_2; inf_max_3; inf_max_4; inf_max_5];
inf_push_avg=mean(inf);
inf_push_std=std(inf);
sub=[sub_max_1; sub_max_2; sub_max_3; sub_max_4; sub_max_5];
sub_push_avg=mean(sub);
```

```
sub_push_std=std(sub);
pec=[pec_max_1; pec_max_2; pec_max_3; pec_max_4; pec_max_5];
pec_push_avg=mean(pec);
pec_push_std=std(pec);
tri=[tri_max_1; tri_max_2; tri_max_3; tri_max_4; tri_max_5];
tri_push_avg=mean(tri);
tri_push_std=std(tri);
bi=[bi_max_1; bi_max_2; bi_max_3; bi_max_4; bi_max_5];
bi_push_avg=mean(bi);
bi_push_std=std(bi);
uptrap=[uptrap_max_1; uptrap_max_2; uptrap_max_3; uptrap_max_4;
      uptrap_max_5];
uptrap_push_avg=mean(uptrap);
uptrap_push_std=std(uptrap);
midtrap=[midtrap_max_1; midtrap_max_2; midtrap_max_3;
       midtrap_max_4; midtrap_max_5];
midtrap_push_avg=mean(midtrap);
midtrap_push_std=std(midtrap);
serrant=[serrant_max_1; serrant_max_2; serrant_max_3;
       serrant_max_4; serrant_max_5];
serrant_push_avg=mean(serrant);
serrant_push_std=std(serrant);
rhommaj=[rhommaj_max_1; rhommaj_max_2; rhommaj_max_3;
       rhommaj_max_4; rhommaj_max_5];
rhommaj_push_avg=mean(rhommaj);
rhommaj_push_std=std(rhommaj);

%Creates one big matrix for all 13 muscles
muscles = [ad md pd sup inf sub pec tri bi uptrap midtrap
         serrant rhommaj];
            %Plots max forces for all 13 muscles for each Stroke Cycle %(Push)
    barh(muscles')
    title ('Muscle Forces Estimated during Push Phase')
    xlabel('Force (N)')
    legend('SC1', 'SC2', 'SC3', 'SC4', 'SC5')

%Finds max force of each muscle for each stroke cycle during
%recovery phase:
 %Stroke Cycle 1 (Recovery phase = 46-100%)
 ad_rec_SC1=new_os_ad_SC1(46:100,1);
 md_rec_SC1=new_os_md_SC1(46:100,1);
 pd_rec_SC1=new_os_pd_SC1(46:100,1);
 sup_rec_SC1=new_os_sup_SC1(46:100,1);
 inf_rec_SC1=new_os_inf_SC1(46:100,1);
 sub_rec_SC1=new_os_sub_SC1(46:100,1);
 pec_rec_SC1=new_os_pec_SC1(46:100,1);
```

```
tri_rec_SC1=new_os_tri_SC1(46:100,1);
bi_rec_SC1=new_os_bi_SC1(46:100,1);
uptrap_rec_SC1=new_os_up_trap_SC1(46:100,1);
midtrap_rec_SC1=new_os_mid_trap_SC1(46:100,1);
serrant_rec_SC1=new_os_serr_ant_SC1(46:100,1);
rhommaj_rec_SC1=new_os_rhom_SC1(46:100,1);
ad_rmax_1=max(ad_rec_SC1);
md_rmax_1=max(md_rec_SC1);
pd_rmax_1=max(pd_rec_SC1);
sup_rmax_1=max(sup_rec_SC1);
inf_rmax_1=max(inf_rec_SC1);
sub_rmax_1=max(sub_rec_SC1);
pec_rmax_1=max(pec_rec_SC1);
tri_rmax_1=max(tri_rec_SC1);
bi_rmax_1=max(bi_rec_SC1);
uptrap_rmax_1=max(uptrap_rec_SC1);
midtrap_rmax_1=max(midtrap_rec_SC1);
serrant_rmax_1=max(serrant_rec_SC1);
rhommaj_rmax_1=max(rhommaj_rec_SC1);

%Stroke Cycle 2 (Recovery phase = 48-100%)
ad_rec_SC2=new_os_ad_SC2(48:100,1);
md_rec_SC2=new_os_md_SC2(48:100,1);
pd_rec_SC2=new_os_pd_SC2(48:100,1);
sup_rec_SC2=new_os_sup_SC2(48:100,1);
inf_rec_SC2=new_os_inf_SC2(48:100,1);
sub_rec_SC2=new_os_sub_SC2(48:100,1);
pec_rec_SC2=new_os_pec_SC2(48:100,1);
tri_rec_SC2=new_os_tri_SC2(48:100,1);
bi_rec_SC2=new_os_bi_SC2(48:100,1);
uptrap_rec_SC2=new_os_up_trap_SC2(48:100,1);
midtrap_rec_SC2=new_os_mid_trap_SC2(48:100,1);
serrant_rec_SC2=new_os_serr_ant_SC2(48:100,1);
rhommaj_rec_SC2=new_os_rhom_SC2(48:100,1);
ad_rmax_2=max(ad_rec_SC2);
md_rmax_2=max(md_rec_SC2);
pd_rmax_2=max(pd_rec_SC2);
sup_rmax_2=max(sup_rec_SC2);
inf_rmax_2=max(inf_rec_SC2);
sub_rmax_2=max(sub_rec_SC2);
pec_rmax_2=max(pec_rec_SC2);
tri_rmax_2=max(tri_rec_SC2);
bi_rmax_2=max(bi_rec_SC2);
uptrap_rmax_2=max(uptrap_rec_SC2);
midtrap_rmax_2=max(midtrap_rec_SC2);
serrant_rmax_2=max(serrant_rec_SC2);
```

```
rhommaj_rmax_2=max(rhommaj_rec_SC2);

%Stroke Cycle 3 (Recovery phase = 43-100%)
ad_rec_SC3=new_os_ad_SC3(43:100,1);
md_rec_SC3=new_os_md_SC3(43:100,1);
pd_rec_SC3=new_os_pd_SC3(43:100,1);
sup_rec_SC3=new_os_sup_SC3(43:100,1);
inf_rec_SC3=new_os_inf_SC3(43:100,1);
sub_rec_SC3=new_os_sub_SC3(43:100,1);
pec_rec_SC3=new_os_pec_SC3(43:100,1);
tri_rec_SC3=new_os_tri_SC3(43:100,1);
bi_rec_SC3=new_os_bi_SC3(43:100,1);
uptrap_rec_SC3=new_os_up_trap_SC2(43:100,1);
midtrap_rec_SC3=new_os_mid_trap_SC3(43:100,1);
serrant_rec_SC3=new_os_serr_ant_SC3(43:100,1);
rhommaj_rec_SC3=new_os_rhom_SC3(43:100,1);
ad_rmax_3=max(ad_rec_SC3);
md_rmax_3=max(md_rec_SC3);
pd_rmax_3=max(pd_rec_SC3);
sup_rmax_3=max(sup_rec_SC3);
inf_rmax_3=max(inf_rec_SC3);
sub_rmax_3=max(sub_rec_SC3);
pec_rmax_3=max(pec_rec_SC3);
tri_rmax_3=max(tri_rec_SC3);
bi_rmax_3=max(bi_rec_SC3);
uptrap_rmax_3=max(uptrap_rec_SC3);
midtrap_rmax_3=max(midtrap_rec_SC3);
serrant_rmax_3=max(serrant_rec_SC3);
rhommaj_rmax_3=max(rhommaj_rec_SC3);

%Stroke Cycle 4 (Recovery phase = 35-100%)
ad_rec_SC4=new_os_ad_SC4(35:100,1);
md_rec_SC4=new_os_md_SC4(35:100,1);
pd_rec_SC4=new_os_pd_SC4(35:100,1);
sup_rec_SC4=new_os_sup_SC4(35:100,1);
inf_rec_SC4=new_os_inf_SC4(35:100,1);
sub_rec_SC4=new_os_sub_SC4(35:100,1);
pec_rec_SC4=new_os_pec_SC4(35:100,1);
tri_rec_SC4=new_os_tri_SC4(35:100,1);
bi_rec_SC4=new_os_bi_SC4(35:100,1);
uptrap_rec_SC4=new_os_up_trap_SC4(35:100,1);
midtrap_rec_SC4=new_os_mid_trap_SC4(35:100,1);
serrant_rec_SC4=new_os_serr_ant_SC4(35:100,1);
rhommaj_rec_SC4=new_os_rhom_SC4(35:100,1);
ad_rmax_4=max(ad_rec_SC4);
md_rmax_4=max(md_rec_SC4);
```

```
pd_rmax_4=max(pd_rec_SC4);
sup_rmax_4=max(sup_rec_SC4);
inf_rmax_4=max(inf_rec_SC4);
sub_rmax_4=max(sub_rec_SC4);
pec_rmax_4=max(pec_rec_SC4);
tri_rmax_4=max(tri_rec_SC4);
bi_rmax_4=max(bi_rec_SC4);
uptrap_rmax_4=max(uptrap_rec_SC4);
midtrap_rmax_4=max(midtrap_rec_SC4);
serrant_rmax_4=max(serrant_rec_SC4);
rhommaj_rmax_4=max(rhommaj_rec_SC4);

%Stroke Cycle 5 (Recovery  phase = 45-100%)
ad_rec_SC5=new_os_ad_SC5(45:100,1);
md_rec_SC5=new_os_md_SC5(45:100,1);
pd_rec_SC5=new_os_pd_SC5(45:100,1);
sup_rec_SC5=new_os_sup_SC5(45:100,1);
inf_rec_SC5=new_os_inf_SC5(45:100,1);
sub_rec_SC5=new_os_sub_SC5(45:100,1);
pec_rec_SC5=new_os_pec_SC5(45:100,1);
tri_rec_SC5=new_os_tri_SC5(45:100,1);
bi_rec_SC5=new_os_bi_SC5(45:100,1);
uptrap_rec_SC5=new_os_up_trap_SC5(45:100,1);
midtrap_rec_SC5=new_os_mid_trap_SC5(45:100,1);
serrant_rec_SC5=new_os_serr_ant_SC5(45:100,1);
rhommaj_rec_SC5=new_os_rhom_SC5(45:100,1);
ad_rmax_5=max(ad_rec_SC5);
md_rmax_5=max(md_rec_SC5);
pd_rmax_5=max(pd_rec_SC5);
sup_rmax_5=max(sup_rec_SC5);
inf_rmax_5=max(inf_rec_SC5);
sub_rmax_5=max(sub_rec_SC5);
pec_rmax_5=max(pec_rec_SC5);
tri_rmax_5=max(tri_rec_SC5);
bi_rmax_5=max(bi_rec_SC5);
uptrap_rmax_5=max(uptrap_rec_SC5);
midtrap_rmax_5=max(midtrap_rec_SC5);
serrant_rmax_5=max(serrant_rec_SC5);
rhommaj_rmax_5=max(rhommaj_rec_SC5);

%Places max forces into one matrix per stroke cycle:
SC_1_rmax=[ad_rmax_1 md_rmax_1 pd_rmax_1 sup_rmax_1 inf_rmax_1
        sub_rmax_1 pec_rmax_1, tri_rmax_1 bi_rmax_1
        uptrap_rmax_1 midtrap_rmax_1 serrant_rmax_1
        rhommaj_rmax_1];
SC_2_rmax=[ad_rmax_2 md_rmax_2 pd_rmax_2 sup_rmax_2 inf_rmax_2
```

```
        sub_rmax_2 pec_rmax_2, tri_rmax_2 bi_rmax_2
        uptrap_rmax_2 midtrap_rmax_2 serrant_rmax_2
        rhommaj_rmax_2];
SC_3_rmax=[ad_rmax_3 md_rmax_3 pd_rmax_3 sup_rmax_3 inf_rmax_3
                    sub_rmax_3 pec_rmax_3, tri_rmax_3 bi_rmax_3
        uptrap_rmax_3 midtrap_rmax_3 serrant_rmax_3
        rhommaj_rmax_3];
SC_4_rmax=[ad_rmax_4 md_rmax_4 pd_rmax_4 sup_rmax_4 inf_rmax_4

                    sub_rmax_4 pec_rmax_4, tri_rmax_4 bi_rmax_4
                    uptrap_rmax_4 midtrap_rmax_4 serrant_rmax_4
                    rhommaj_rmax_4];
SC_5_rmax=[ad_rmax_5 md_rmax_5 pd_rmax_5 sup_rmax_5 inf_rmax_5
        sub_rmax_5 pec_rmax_5, tri_rmax_5 bi_rmax_5
        uptrap_rmax_5 midtrap_rmax_5 serrant_rmax_5
        rhommaj_rmax_5];

%Groups muscle forces by muscle for all 5 SC and computes mean
%and standard deviation for each muscle across all 5 SC
ad_rec=[ad_rmax_1; ad_rmax_2; ad_rmax_3; ad_rmax_4; ad_rmax_5];
ad_rec_avg=mean(ad_rec);
ad_rec_std=std(ad_rec);
md_rec=[md_rmax_1; md_rmax_2; md_rmax_3; md_rmax_4; md_rmax_5];
md_rec_avg=mean(md_rec);
md_rec_std=std(md_rec);
pd_rec=[pd_rmax_1; pd_rmax_2; pd_rmax_3; pd_rmax_4; pd_rmax_5];
pd_rec_avg=mean(pd_rec);
pd_rec_std=std(pd_rec);
sup_rec=[sup_rmax_1; sup_rmax_2; sup_rmax_3; sup_rmax_4;
      sup_rmax_5];
sup_rec_avg=mean(sup_rec);
sup_rec_std=std(sup_rec);
inf_rec=[inf_rmax_1; inf_rmax_2; inf_rmax_3; inf_rmax_4;
      inf_rmax_5];
inf_rec_avg=mean(inf_rec);
inf_rec_std=std(inf_rec);
sub_rec=[sub_rmax_1; sub_rmax_2; sub_rmax_3; sub_rmax_4;
      sub_rmax_5];
sub_rec_avg=mean(sub_rec);
sub_rec_std=std(sub_rec);
pec_rec=[pec_rmax_1; pec_rmax_2; pec_rmax_3; pec_rmax_4;
      pec_rmax_5];
pec_rec_avg=mean(pec_rec);
pec_rec_std=std(pec_rec);
tri_rec=[tri_rmax_1; tri_rmax_2; tri_rmax_3; tri_rmax_4;
      tri_rmax_5];
```

```
tri_rec_avg=mean(tri_rec);
tri_rec_std=std(tri_rec);
bi_rec=[bi_rmax_1; bi_rmax_2; bi_rmax_3; bi_rmax_4; bi_rmax_5];
bi_rec_avg=mean(bi_rec);
bi_rec_std=std(bi_rec);
uptrap_rec=[uptrap_rmax_1; uptrap_rmax_2; uptrap_rmax_3;
          uptrap_rmax_4; uptrap_rmax_5];
uptrap_rec_avg=mean(uptrap_rec);
uptrap_rec_std=std(uptrap_rec);
midtrap_rec=[midtrap_rmax_1; midtrap_rmax_2; midtrap_rmax_3;
          midtrap_rmax_4; midtrap_rmax_5];
midtrap_rec_avg=mean(midtrap_rec);
midtrap_rec_std=std(midtrap_rec);
serrant_rec=[serrant_rmax_1; serrant_rmax_2; serrant_rmax_3;
          serrant_rmax_4; serrant_rmax_5];
serrant_rec_avg=mean(serrant_rec);
serrant_rec_std=std(serrant_rec);
rhommaj_rec=[rhommaj_rmax_1; rhommaj_rmax_2; rhommaj_rmax_3;
          rhommaj_rmax_4; rhommaj_rmax_5];
rhommaj_rec_avg=mean(rhommaj_rec);
rhommaj_rec_std=std(rhommaj_rec);

%Creates one big matrix for all 13 muscles
muscles_rec = [ad_rec md_rec pd_rec sup_rec inf_rec sub_rec
            pec_rec tri_rec bi_rec uptrap_rec midtrap_rec
            serrant_rec rhommaj_rec];

    %Plots max forces for all 13 muscles for each Stroke Cycle
    %(Recovery)
    figure;
    barh(muscles_rec')
    title ('Muscle Forces Estimated during Recovery Phase')
    xlabel('Force (N)')
    legend('SC1', 'SC2', 'SC3', 'SC4', 'SC5')
```

APPENDIX C

MATLAB MEAN ABSOLUTE ERROR CODE

This code was used to compute the mean absolute error between the muscle activations estimated by the Wheelchair Propulsion Model and the experimental EMG profiles.

```
%MAE_COMP is a function that imports and reshapes muscle forces and activations
%computed by OpenSim's Static optimization Tool (per stroke  cycle. The
%experimental EMG (% MVC) is also loaded. The Mean Absolute Error (MAE) for each
%muscle of interest is computed and stored in a matrix, containing the muscle MAE
%values for all five consecutive stroke cycles. Lastly, a .mat file containing experimental
%EMG, estimated force & normalized activation is saved for each muscle (entire trial,
%push phase, & recovery phase) per stroke cycle.
%Written by Brooke Odle on April 4, 2013

%Imports .sto files of muscle forces estimated by OpenSim's Static
%OptimizationTool
os_mf_SC1=importdata('t1o4_scaled_StaticOptimization_force_updmuscles_S
            C1.sto');
os_mf_SC2=importdata('t1o4_scaled_StaticOptimization_force_updmuscles_S
            C2.sto');
os_mf_SC3=importdata('t1o4_scaled_StaticOptimization_force_updmuscles_S
            C3.sto');
os_mf_SC4=importdata('t1o4_scaled_StaticOptimization_force_updmuscles_S
            C4.sto');
os_mf_SC5=importdata('t1o4_scaled_StaticOptimization_force_updmuscles_S
            C5.sto');

    %Reshapes all muscle forces to 100% SC for all 13 muscles being
    %compared with EMG
    %Anterior Deltoid
    new_os_ad_SC1=resample1to100(os_mf_SC1.data(:,2));
    new_os_ad_SC2=resample1to100(os_mf_SC2.data(:,2));
    new_os_ad_SC3=resample1to100(os_mf_SC3.data(:,2));
    new_os_ad_SC4=resample1to100(os_mf_SC4.data(:,2));
    new_os_ad_SC5=resample1to100(os_mf_SC5.data(:,2));

    %Middle Deltoid
    new_os_md_SC1=resample1to100(os_mf_SC1.data(:,3));
    new_os_md_SC2=resample1to100(os_mf_SC2.data(:,3));
    new_os_md_SC3=resample1to100(os_mf_SC3.data(:,3));
    new_os_md_SC4=resample1to100(os_mf_SC4.data(:,3));
    new_os_md_SC5=resample1to100(os_mf_SC5.data(:,3));
```

```
%Posterior Deltoid
new_os_pd_SC1=resample1to100(os_mf_SC1.data(:,4));
new_os_pd_SC2=resample1to100(os_mf_SC2.data(:,4));
new_os_pd_SC3=resample1to100(os_mf_SC3.data(:,4));
new_os_pd_SC4=resample1to100(os_mf_SC4.data(:,4));
new_os_pd_SC5=resample1to100(os_mf_SC5.data(:,4));

%Supraspinatus
new_os_sup_SC1=resample1to100(os_mf_SC1.data(:,5));
new_os_sup_SC2=resample1to100(os_mf_SC2.data(:,5));
new_os_sup_SC3=resample1to100(os_mf_SC3.data(:,5));
new_os_sup_SC4=resample1to100(os_mf_SC4.data(:,5));
new_os_sup_SC5=resample1to100(os_mf_SC5.data(:,5));

%Infraspinatus
new_os_inf_SC1=resample1to100(os_mf_SC1.data(:,6));
new_os_inf_SC2=resample1to100(os_mf_SC2.data(:,6));
new_os_inf_SC3=resample1to100(os_mf_SC3.data(:,6));
new_os_inf_SC4=resample1to100(os_mf_SC4.data(:,6));
new_os_inf_SC5=resample1to100(os_mf_SC5.data(:,6));

%Subscapularis
new_os_sub_SC1=resample1to100(os_mf_SC1.data(:,7));
new_os_sub_SC2=resample1to100(os_mf_SC2.data(:,7));
new_os_sub_SC3=resample1to100(os_mf_SC3.data(:,7));
new_os_sub_SC4=resample1to100(os_mf_SC4.data(:,7));
new_os_sub_SC5=resample1to100(os_mf_SC5.data(:,7));

%Pectoralis Major
new_os_pec_SC1=resample1to100(os_mf_SC1.data(:,10));
new_os_pec_SC2=resample1to100(os_mf_SC2.data(:,10));
new_os_pec_SC3=resample1to100(os_mf_SC3.data(:,10));
new_os_pec_SC4=resample1to100(os_mf_SC4.data(:,10));
new_os_pec_SC5=resample1to100(os_mf_SC5.data(:,10));

%Triceps
new_os_tri_SC1=resample1to100(os_mf_SC1.data(:,17));
new_os_tri_SC2=resample1to100(os_mf_SC2.data(:,17));
new_os_tri_SC3=resample1to100(os_mf_SC3.data(:,17));
new_os_tri_SC4=resample1to100(os_mf_SC4.data(:,17));
new_os_tri_SC5=resample1to100(os_mf_SC5.data(:,17));

%Biceps
new_os_bi_SC1=resample1to100(os_mf_SC1.data(:,22));
new_os_bi_SC2=resample1to100(os_mf_SC2.data(:,22));
```

```
new_os_bi_SC3=resample1to100(os_mf_SC3.data(:,22));
new_os_bi_SC4=resample1to100(os_mf_SC4.data(:,22));
new_os_bi_SC5=resample1to100(os_mf_SC5.data(:,22));

%Upper Trapezius
new_os_up_trap_SC1=resample1to100(os_mf_SC1.data(:,28));
new_os_up_trap_SC2=resample1to100(os_mf_SC2.data(:,28));
new_os_up_trap_SC3=resample1to100(os_mf_SC3.data(:,28));
new_os_up_trap_SC4=resample1to100(os_mf_SC4.data(:,28));
new_os_up_trap_SC5=resample1to100(os_mf_SC5.data(:,28));

%Middle Trapezius
new_os_mid_trap_SC1=resample1to100(os_mf_SC1.data(:,29));
new_os_mid_trap_SC2=resample1to100(os_mf_SC2.data(:,29));
new_os_mid_trap_SC3=resample1to100(os_mf_SC3.data(:,29));
new_os_mid_trap_SC4=resample1to100(os_mf_SC4.data(:,29));
new_os_mid_trap_SC5=resample1to100(os_mf_SC5.data(:,29));

%Serratus Anterior
new_os_serr_ant_SC1=resample1to100(os_mf_SC1.data(:,30));
new_os_serr_ant_SC2=resample1to100(os_mf_SC2.data(:,30));
new_os_serr_ant_SC3=resample1to100(os_mf_SC3.data(:,30));
new_os_serr_ant_SC4=resample1to100(os_mf_SC4.data(:,30));
new_os_serr_ant_SC5=resample1to100(os_mf_SC5.data(:,30));

%Rhomboid Major
new_os_rhom_SC1=resample1to100(os_mf_SC1.data(:,31));
new_os_rhom_SC2=resample1to100(os_mf_SC2.data(:,31));
new_os_rhom_SC3=resample1to100(os_mf_SC3.data(:,31));
new_os_rhom_SC4=resample1to100(os_mf_SC4.data(:,31));
new_os_rhom_SC5=resample1to100(os_mf_SC5.data(:,31));

%Finds max force of each muscle for each stroke cycle
%Stroke Cycle 1
ad_max_1=max(new_os_ad_SC1);
md_max_1=max(new_os_md_SC1);
pd_max_1=max(new_os_pd_SC1);
sup_max_1=max(new_os_sup_SC1);
inf_max_1=max(new_os_inf_SC1);
sub_max_1=max(new_os_sub_SC1);
pec_max_1=max(new_os_pec_SC1);
tri_max_1=max(new_os_tri_SC1);
bi_max_1=max(new_os_bi_SC1);
uptrap_max_1=max(new_os_up_trap_SC1);
midtrap_max_1=max(new_os_mid_trap_SC1);
serrant_max_1=max(new_os_serr_ant_SC1);
```

```
rhommaj_max_1=max(new_os_rhom_SC1);


%Stroke Cycle 2
ad_max_2=max(new_os_ad_SC2);
md_max_2=max(new_os_md_SC2);
pd_max_2=max(new_os_pd_SC2);
sup_max_2=max(new_os_sup_SC2);
inf_max_2=max(new_os_inf_SC2);
sub_max_2=max(new_os_sub_SC2);
pec_max_2=max(new_os_pec_SC2);
tri_max_2=max(new_os_tri_SC2);
bi_max_2=max(new_os_bi_SC2);
uptrap_max_2=max(new_os_up_trap_SC2);
midtrap_max_2=max(new_os_mid_trap_SC2);
serrant_max_2=max(new_os_serr_ant_SC2);
rhommaj_max_2=max(new_os_rhom_SC2);

%Stroke Cycle 3
ad_max_3=max(new_os_ad_SC3);
md_max_3=max(new_os_md_SC3);
pd_max_3=max(new_os_pd_SC3);
sup_max_3=max(new_os_sup_SC3);
inf_max_3=max(new_os_inf_SC3);
sub_max_3=max(new_os_sub_SC3);
pec_max_3=max(new_os_pec_SC3);
tri_max_3=max(new_os_tri_SC3);
bi_max_3=max(new_os_bi_SC3);
uptrap_max_3=max(new_os_up_trap_SC3);
midtrap_max_3=max(new_os_mid_trap_SC3);
serrant_max_3=max(new_os_serr_ant_SC3);
rhommaj_max_3=max(new_os_rhom_SC3);

%Stroke Cycle 4
ad_max_4=max(new_os_ad_SC4);
md_max_4=max(new_os_md_SC4);
pd_max_4=max(new_os_pd_SC4);
sup_max_4=max(new_os_sup_SC4);
inf_max_4=max(new_os_inf_SC4);
sub_max_4=max(new_os_sub_SC4);
pec_max_4=max(new_os_pec_SC4);
tri_max_4=max(new_os_tri_SC4);
bi_max_4=max(new_os_bi_SC4);
uptrap_max_4=max(new_os_up_trap_SC4);
midtrap_max_4=max(new_os_mid_trap_SC4);
```

```
serrant_max_4=max(new_os_serr_ant_SC4);
rhommaj_max_4=max(new_os_rhom_SC4);


%Stroke Cycle 5
ad_max_5=max(new_os_ad_SC5);
md_max_5=max(new_os_md_SC5);
pd_max_5=max(new_os_pd_SC5);
sup_max_5=max(new_os_sup_SC5);
inf_max_5=max(new_os_inf_SC5);
sub_max_5=max(new_os_sub_SC5);
pec_max_5=max(new_os_pec_SC5);
tri_max_5=max(new_os_tri_SC5);
bi_max_5=max(new_os_bi_SC5);
uptrap_max_5=max(new_os_up_trap_SC5);
midtrap_max_5=max(new_os_mid_trap_SC5);
serrant_max_5=max(new_os_serr_ant_SC5);
rhommaj_max_5=max(new_os_rhom_SC5);

%Imports estimated activation files computed by Static Optimization:
os_ma_SC1=importdata('t1o4_scaled_StaticOptimization_activation_updmusc
            les_SC1.sto');
os_ma_SC2=importdata('t1o4_scaled_StaticOptimization_activation_updmusc
            les_SC2.sto');
os_ma_SC3=importdata('t1o4_scaled_StaticOptimization_activation_updmusc
            les_SC3.sto');
os_ma_SC4=importdata('t1o4_scaled_StaticOptimization_activation_updmusc
            les_SC4.sto');
os_ma_SC5=importdata('t1o4_scaled_StaticOptimization_activation_updmusc
            les_SC5.sto');

%Reshapes all muscle activations to 100% SC for all 13 muscles being compared with
EMG
    %Anterior Deltoid
    ma_os_ad_SC1=resample1to100(os_ma_SC1.data(:,2));
    ma_os_ad_SC2=resample1to100(os_ma_SC2.data(:,2));
    ma_os_ad_SC3=resample1to100(os_ma_SC3.data(:,2));
    ma_os_ad_SC4=resample1to100(os_ma_SC4.data(:,2));
    ma_os_ad_SC5=resample1to100(os_ma_SC5.data(:,2));

    %Middle Deltoid
    ma_os_md_SC1=resample1to100(os_ma_SC1.data(:,3));
    ma_os_md_SC2=resample1to100(os_ma_SC2.data(:,3));
    ma_os_md_SC3=resample1to100(os_ma_SC3.data(:,3));
    ma_os_md_SC4=resample1to100(os_ma_SC4.data(:,3));
    ma_os_md_SC5=resample1to100(os_ma_SC5.data(:,3));
```

```
%Posterior Deltoid
ma_os_pd_SC1=resample1to100(os_ma_SC1.data(:,4));
ma_os_pd_SC2=resample1to100(os_ma_SC2.data(:,4));
ma_os_pd_SC3=resample1to100(os_ma_SC3.data(:,4));
ma_os_pd_SC4=resample1to100(os_ma_SC4.data(:,4));
ma_os_pd_SC5=resample1to100(os_ma_SC5.data(:,4));

%Supraspinatus
ma_os_sup_SC1=resample1to100(os_ma_SC1.data(:,5));
ma_os_sup_SC2=resample1to100(os_ma_SC2.data(:,5));
ma_os_sup_SC3=resample1to100(os_ma_SC3.data(:,5));
ma_os_sup_SC4=resample1to100(os_ma_SC4.data(:,5));
ma_os_sup_SC5=resample1to100(os_ma_SC5.data(:,5));

%Infraspinatus
ma_os_inf_SC1=resample1to100(os_ma_SC1.data(:,6));
ma_os_inf_SC2=resample1to100(os_ma_SC2.data(:,6));
ma_os_inf_SC3=resample1to100(os_ma_SC3.data(:,6));
ma_os_inf_SC4=resample1to100(os_ma_SC4.data(:,6));
ma_os_inf_SC5=resample1to100(os_ma_SC5.data(:,6));

%Subscapularis
ma_os_sub_SC1=resample1to100(os_ma_SC1.data(:,7));
ma_os_sub_SC2=resample1to100(os_ma_SC2.data(:,7));
ma_os_sub_SC3=resample1to100(os_ma_SC3.data(:,7));
ma_os_sub_SC4=resample1to100(os_ma_SC4.data(:,7));
ma_os_sub_SC5=resample1to100(os_ma_SC5.data(:,7));

%Pectoralis Major
ma_os_pec_SC1=resample1to100(os_ma_SC1.data(:,10));
ma_os_pec_SC2=resample1to100(os_ma_SC2.data(:,10));
ma_os_pec_SC3=resample1to100(os_ma_SC3.data(:,10));
ma_os_pec_SC4=resample1to100(os_ma_SC4.data(:,10));
ma_os_pec_SC5=resample1to100(os_ma_SC5.data(:,10));

%Triceps
ma_os_tri_SC1=resample1to100(os_ma_SC1.data(:,17));
ma_os_tri_SC2=resample1to100(os_ma_SC2.data(:,17));
ma_os_tri_SC3=resample1to100(os_ma_SC3.data(:,17));
ma_os_tri_SC4=resample1to100(os_ma_SC4.data(:,17));
ma_os_tri_SC5=resample1to100(os_ma_SC5.data(:,17));

%Biceps
ma_os_bi_SC1=resample1to100(os_ma_SC1.data(:,22));
ma_os_bi_SC2=resample1to100(os_ma_SC2.data(:,22));
```

```
ma_os_bi_SC3=resample1to100(os_ma_SC3.data(:,22));
ma_os_bi_SC4=resample1to100(os_ma_SC4.data(:,22));
ma_os_bi_SC5=resample1to100(os_ma_SC5.data(:,22));

%Upper Trapezius
ma_os_up_trap_SC1=resample1to100(os_ma_SC1.data(:,28));
ma_os_up_trap_SC2=resample1to100(os_ma_SC2.data(:,28));
ma_os_up_trap_SC3=resample1to100(os_ma_SC3.data(:,28));
ma_os_up_trap_SC4=resample1to100(os_ma_SC4.data(:,28));
ma_os_up_trap_SC5=resample1to100(os_ma_SC5.data(:,28));

%Middle Trapezius
ma_os_mid_trap_SC1=resample1to100(os_ma_SC1.data(:,29));
ma_os_mid_trap_SC2=resample1to100(os_ma_SC2.data(:,29));
ma_os_mid_trap_SC3=resample1to100(os_ma_SC3.data(:,29));
ma_os_mid_trap_SC4=resample1to100(os_ma_SC4.data(:,29));
ma_os_mid_trap_SC5=resample1to100(os_ma_SC5.data(:,29));

%Serratus Anterior
ma_os_serr_ant_SC1=resample1to100(os_ma_SC1.data(:,30));
ma_os_serr_ant_SC2=resample1to100(os_ma_SC2.data(:,30));
ma_os_serr_ant_SC3=resample1to100(os_ma_SC3.data(:,30));
ma_os_serr_ant_SC4=resample1to100(os_ma_SC4.data(:,30));
ma_os_serr_ant_SC5=resample1to100(os_ma_SC5.data(:,30));

%Rhomboid Major
ma_os_rhom_SC1=resample1to100(os_ma_SC1.data(:,31));
ma_os_rhom_SC2=resample1to100(os_ma_SC2.data(:,31));
ma_os_rhom_SC3=resample1to100(os_ma_SC3.data(:,31));
ma_os_rhom_SC4=resample1to100(os_ma_SC4.data(:,31));
ma_os_rhom_SC5=resample1to100(os_ma_SC5.data(:,31));

%Expresses estimated activation as %max force per stroke cycle
%(Normalized estimated activation)
%Stroke Cycle 1
new_ad1=(100*ma_os_ad_SC1)/ad_max_1;
new_md1=(100*ma_os_md_SC1)/md_max_1;
new_pd1=(100*ma_os_pd_SC1)/pd_max_1;
new_sup1=(100*ma_os_sup_SC1)/sup_max_1;
new_inf1=(100*ma_os_inf_SC1)/inf_max_1;
new_sub1=(100*ma_os_sub_SC1)/sub_max_1;
new_pec1=(100*ma_os_pec_SC1)/pec_max_1;
new_tri1=(100*ma_os_tri_SC1)/tri_max_1;
new_bi1=(100*ma_os_bi_SC1)/bi_max_1;
new_uptrap1=(100*ma_os_up_trap_SC1)/uptrap_max_1;
new_midtrap1=(100*ma_os_mid_trap_SC1)/midtrap_max_1;
```

```
new_serrant1=(100*ma_os_serr_ant_SC1)/serrant_max_1;
new_rhommaj1=(100*ma_os_rhom_SC1)/rhommaj_max_1;


%Stroke Cyle 2
new_ad2=(100*ma_os_ad_SC2)/ad_max_2;
new_md2=(100*ma_os_md_SC2)/md_max_2;
new_pd2=(100*ma_os_pd_SC2)/pd_max_2;
new_sup2=(100*ma_os_sup_SC2)/sup_max_2;
new_inf2=(100*ma_os_inf_SC2)/inf_max_2;
new_sub2=(100*ma_os_sub_SC2)/sub_max_2;
new_pec2=(100*ma_os_pec_SC2)/pec_max_2;
new_tri2=(100*ma_os_tri_SC2)/tri_max_2;
new_bi2=(100*ma_os_bi_SC2)/bi_max_2;
new_uptrap2=(100*ma_os_up_trap_SC2)/uptrap_max_2;
new_midtrap2=(100*ma_os_mid_trap_SC2)/midtrap_max_2;
new_serrant2=(100*ma_os_serr_ant_SC2)/serrant_max_2;
new_rhommaj2=(100*ma_os_rhom_SC2)/rhommaj_max_2;

%Stroke Cycle 3
new_ad3=(100*ma_os_ad_SC3)/ad_max_3;
new_md3=(100*ma_os_md_SC3)/md_max_3;
new_pd3=(100*ma_os_pd_SC3)/pd_max_3;
new_sup3=(100*ma_os_sup_SC3)/sup_max_3;
new_inf3=(100*ma_os_inf_SC3)/inf_max_3;
new_sub3=(100*ma_os_sub_SC3)/sub_max_3;
new_pec3=(100*ma_os_pec_SC3)/pec_max_3;
new_tri3=(100*ma_os_tri_SC3)/tri_max_3;
new_bi3=(100*ma_os_bi_SC3)/bi_max_3;
new_uptrap3=(100*ma_os_up_trap_SC3)/uptrap_max_3;
new_midtrap3=(100*ma_os_mid_trap_SC3)/midtrap_max_3;
new_serrant3=(100*ma_os_serr_ant_SC3)/serrant_max_3;
new_rhommaj3=(100*ma_os_rhom_SC3)/rhommaj_max_3;

%Stroke Cycle 4
new_ad4=(100*ma_os_ad_SC4)/ad_max_4;
new_md4=(100*ma_os_md_SC4)/md_max_4;
new_pd4=(100*ma_os_pd_SC4)/pd_max_4;
new_sup4=(100*ma_os_sup_SC4)/sup_max_4;
new_inf4=(100*ma_os_inf_SC4)/inf_max_4;
new_sub4=(100*ma_os_sub_SC4)/sub_max_4;
new_pec4=(100*ma_os_pec_SC4)/pec_max_4;
new_tri4=(100*ma_os_tri_SC4)/tri_max_4;
new_bi4=(100*ma_os_bi_SC4)/bi_max_4;
new_uptrap4=(100*ma_os_up_trap_SC4)/uptrap_max_4;
new_midtrap4=(100*ma_os_mid_trap_SC4)/midtrap_max_4;
```

```
new_serrant4=(100*ma_os_serr_ant_SC4)/serrant_max_4;
new_rhommaj4=(100*ma_os_rhom_SC4)/rhommaj_max_4;


%Stroke Cycle 5
new_ad5=(100*ma_os_ad_SC5)/ad_max_5;
new_md5=(100*ma_os_md_SC5)/md_max_5;
new_pd5=(100*ma_os_pd_SC5)/pd_max_5;
new_sup5=(100*ma_os_sup_SC5)/sup_max_5;
new_inf5=(100*ma_os_inf_SC5)/inf_max_5;
new_sub5=(100*ma_os_sub_SC5)/sub_max_5;
new_pec5=(100*ma_os_pec_SC5)/pec_max_5;
new_tri5=(100*ma_os_tri_SC5)/tri_max_5;
new_bi5=(100*ma_os_bi_SC5)/bi_max_5;
new_uptrap5=(100*ma_os_up_trap_SC5)/uptrap_max_5;
new_midtrap5=(100*ma_os_mid_trap_SC5)/midtrap_max_5;
new_serrant5=(100*ma_os_serr_ant_SC5)/serrant_max_5;
new_rhommaj5=(100*ma_os_rhom_SC5)/rhommaj_max_5;

%Loads and reshapes experimental EMG to 100% SC
   %Anterior Deltoid
load('ant_delt_exp.mat');
new_exp_ad_SC1=resample1to100(ant_delt_SC1_exp');
new_exp_ad_SC2=resample1to100(ant_delt_SC2_exp');
new_exp_ad_SC3=resample1to100(ant_delt_SC3_exp');
new_exp_ad_SC4=resample1to100(ant_delt_SC4_exp');
new_exp_ad_SC5=resample1to100(ant_delt_SC5_exp');

   %Middle Deltoid
load ('mid_delt_exp.mat');
new_exp_md_SC1=resample1to100(mid_delt_SC1_exp');
new_exp_md_SC2=resample1to100(mid_delt_SC2_exp');
new_exp_md_SC3=resample1to100(mid_delt_SC3_exp');
new_exp_md_SC4=resample1to100(mid_delt_SC4_exp');
new_exp_md_SC5=resample1to100(mid_delt_SC5_exp');

   %Posterior Deltoid
load('post_delt_exp.mat');
new_exp_pd_SC1=resample1to100(post_delt_SC1_exp');
new_exp_pd_SC2=resample1to100(post_delt_SC2_exp');
new_exp_pd_SC3=resample1to100(post_delt_SC3_exp');
new_exp_pd_SC4=resample1to100(post_delt_SC4_exp');
new_exp_pd_SC5=resample1to100(post_delt_SC5_exp');

   %Supraspinatus
load('supraspin_exp.mat');
```

```
new_exp_sup_SC1=resample1to100(supraspin_SC1_exp');
new_exp_sup_SC2=resample1to100(supraspin_SC2_exp');
new_exp_sup_SC3=resample1to100(supraspin_SC3_exp');
new_exp_sup_SC4=resample1to100(supraspin_SC4_exp');
new_exp_sup_SC5=resample1to100(supraspin_SC5_exp');

    %Infraspinatus
load('infra_exp.mat');
new_exp_inf_SC1=resample1to100(infra_SC1_exp');
new_exp_inf_SC2=resample1to100(infra_SC2_exp');
new_exp_inf_SC3=resample1to100(infra_SC3_exp');
new_exp_inf_SC4=resample1to100(infra_SC4_exp');
new_exp_inf_SC5=resample1to100(infra_SC5_exp');

    %Subscapularis
load('subscap_exp.mat');
new_exp_sub_SC1=resample1to100(subscap_SC1_exp');
new_exp_sub_SC2=resample1to100(subscap_SC2_exp');
new_exp_sub_SC3=resample1to100(subscap_SC3_exp');
new_exp_sub_SC4=resample1to100(subscap_SC4_exp');
new_exp_sub_SC5=resample1to100(subscap_SC5_exp');

    %Pec Major
load('hum_pec_exp.mat');
new_exp_pec_SC1=resample1to100(hum_pec_SC1_exp');
new_exp_pec_SC2=resample1to100(hum_pec_SC2_exp');
new_exp_pec_SC3=resample1to100(hum_pec_SC3_exp');
new_exp_pec_SC4=resample1to100(hum_pec_SC4_exp');
new_exp_pec_SC5=resample1to100(hum_pec_SC5_exp');

    %Triceps
load('tricep_exp.mat');
new_exp_tri_SC1=resample1to100(tricep_SC1_exp');
new_exp_tri_SC2=resample1to100(tricep_SC2_exp');
new_exp_tri_SC3=resample1to100(tricep_SC3_exp');
new_exp_tri_SC4=resample1to100(tricep_SC4_exp');
new_exp_tri_SC5=resample1to100(tricep_SC5_exp');

    %Biceps
load('bicep_exp.mat');
new_exp_bi_SC1=resample1to100(bicep_SC1_exp');
new_exp_bi_SC2=resample1to100(bicep_SC2_exp');
new_exp_bi_SC3=resample1to100(bicep_SC3_exp');
new_exp_bi_SC4=resample1to100(bicep_SC4_exp');
new_exp_bi_SC5=resample1to100(bicep_SC5_exp');
```

```
    %Upper Trap
load('up_trap_exp.mat');
new_exp_up_trap_SC1=resample1to100(up_trap_SC1_exp');
new_exp_up_trap_SC2=resample1to100(up_trap_SC2_exp');
new_exp_up_trap_SC3=resample1to100(up_trap_SC3_exp');
new_exp_up_trap_SC4=resample1to100(up_trap_SC4_exp');
new_exp_up_trap_SC5=resample1to100(up_trap_SC5_exp');

    %Mid Trap
load('mid_trap_exp.mat');
new_exp_mid_trap_SC1=resample1to100(mid_trap_SC1_exp');
new_exp_mid_trap_SC2=resample1to100(mid_trap_SC2_exp');
new_exp_mid_trap_SC3=resample1to100(mid_trap_SC3_exp');
new_exp_mid_trap_SC4=resample1to100(mid_trap_SC4_exp');
new_exp_mid_trap_SC5=resample1to100(mid_trap_SC5_exp');

    %Serratus
load('serr_ant_exp.mat');
new_exp_serr_ant_SC1=resample1to100(serr_ant_SC1_exp');
new_exp_serr_ant_SC2=resample1to100(serr_ant_SC2_exp');
new_exp_serr_ant_SC3=resample1to100(serr_ant_SC3_exp');
new_exp_serr_ant_SC4=resample1to100(serr_ant_SC4_exp');
new_exp_serr_ant_SC5=resample1to100(serr_ant_SC5_exp');

    %Rhomboid
load('rhom_exp.mat');
new_exp_rhom_SC1=resample1to100(rhom_SC1_exp');
new_exp_rhom_SC2=resample1to100(rhom_SC2_exp');
new_exp_rhom_SC3=resample1to100(rhom_SC3_exp');
new_exp_rhom_SC4=resample1to100(rhom_SC4_exp');
new_exp_rhom_SC5=resample1to100(rhom_SC5_exp');

%Computes Mean Absolute Error for each muscle for each stroke cycle
    %Stroke Cycle 1
ad_mae_SC1=mean(abs(new_exp_ad_SC1-new_ad1));
md_mae_SC1=mean(abs(new_exp_md_SC1-new_md1));
pd_mae_SC1=mean(abs(new_exp_pd_SC1-new_pd1));
sup_mae_SC1=mean(abs(new_exp_sup_SC1-new_sup1));
inf_mae_SC1=mean(abs(new_exp_inf_SC1-new_inf1));
sub_mae_SC1=mean(abs(new_exp_sub_SC1-new_sub1));
pec_mae_SC1=mean(abs(new_exp_pec_SC1-new_pec1));
tri_mae_SC1=mean(abs(new_exp_tri_SC1-new_tri1));
bi_mae_SC1=mean(abs(new_exp_bi_SC1-new_bi1));
uptrap_mae_SC1=mean(abs(new_exp_up_trap_SC1-new_uptrap1));
midtrap_mae_SC1=mean(abs(new_exp_mid_trap_SC1-new_midtrap1));
serrant_mae_SC1=mean(abs(new_exp_serr_ant_SC1-new_serrant1));
```

```
rhommaj_mae_SC1=mean(abs(new_exp_rhom_SC1-new_rhommaj1));


%Stroke Cycle 2
ad_mae_SC2=mean(abs(new_exp_ad_SC2-new_ad2));
md_mae_SC2=mean(abs(new_exp_md_SC2-new_md2));
pd_mae_SC2=mean(abs(new_exp_pd_SC2-new_pd2));
sup_mae_SC2=mean(abs(new_exp_sup_SC2-new_sup2));
inf_mae_SC2=mean(abs(new_exp_inf_SC2-new_inf2));
sub_mae_SC2=mean(abs(new_exp_sub_SC2-new_sub2));
pec_mae_SC2=mean(abs(new_exp_pec_SC2-new_pec2));
tri_mae_SC2=mean(abs(new_exp_tri_SC2-new_tri2));
bi_mae_SC2=mean(abs(new_exp_bi_SC2-new_bi2));
uptrap_mae_SC2=mean(abs(new_exp_up_trap_SC2-new_uptrap2));
midtrap_mae_SC2=mean(abs(new_exp_mid_trap_SC2-new_midtrap2));
serrant_mae_SC2=mean(abs(new_exp_serr_ant_SC2-new_serrant2));
rhommaj_mae_SC2=mean(abs(new_exp_rhom_SC2-new_rhommaj2));

%Stroke Cycle 3
ad_mae_SC3=mean(abs(new_exp_ad_SC3-new_ad3));
md_mae_SC3=mean(abs(new_exp_md_SC3-new_md3));
pd_mae_SC3=mean(abs(new_exp_pd_SC3-new_pd3));
sup_mae_SC3=mean(abs(new_exp_sup_SC3-new_sup3));
inf_mae_SC3=mean(abs(new_exp_inf_SC3-new_inf3));
sub_mae_SC3=mean(abs(new_exp_sub_SC3-new_sub3));
pec_mae_SC3=mean(abs(new_exp_pec_SC3-new_pec3));
tri_mae_SC3=mean(abs(new_exp_tri_SC3-new_tri3));
bi_mae_SC3=mean(abs(new_exp_bi_SC3-new_bi3));
uptrap_mae_SC3=mean(abs(new_exp_up_trap_SC3-new_uptrap3));
midtrap_mae_SC3=mean(abs(new_exp_mid_trap_SC3-new_midtrap3));
serrant_mae_SC3=mean(abs(new_exp_serr_ant_SC3-new_serrant3));
rhommaj_mae_SC3=mean(abs(new_exp_rhom_SC3-new_rhommaj3));

%Stroke Cycle 4
ad_mae_SC4=mean(abs(new_exp_ad_SC4-new_ad4));
md_mae_SC4=mean(abs(new_exp_md_SC4-new_md4));
pd_mae_SC4=mean(abs(new_exp_pd_SC4-new_pd4));
sup_mae_SC4=mean(abs(new_exp_sup_SC4-new_sup4));
inf_mae_SC4=mean(abs(new_exp_inf_SC4-new_inf4));
sub_mae_SC4=mean(abs(new_exp_sub_SC4-new_sub4));
pec_mae_SC4=mean(abs(new_exp_pec_SC4-new_pec4));
tri_mae_SC4=mean(abs(new_exp_tri_SC4-new_tri4));
bi_mae_SC4=mean(abs(new_exp_bi_SC4-new_bi4));
uptrap_mae_SC4=mean(abs(new_exp_up_trap_SC4-new_uptrap4));
midtrap_mae_SC4=mean(abs(new_exp_mid_trap_SC4-new_midtrap4));
```

```
serrant_mae_SC4=mean(abs(new_exp_serr_ant_SC4-new_serrant4));
rhommaj_mae_SC4=mean(abs(new_exp_rhom_SC4-new_rhommaj4));


%Stroke Cycle 5
ad_mae_SC5=mean(abs(new_exp_ad_SC5-new_ad5));
md_mae_SC5=mean(abs(new_exp_md_SC5-new_md5));
pd_mae_SC5=mean(abs(new_exp_pd_SC5-new_pd5));
sup_mae_SC5=mean(abs(new_exp_sup_SC5-new_sup5));
inf_mae_SC5=mean(abs(new_exp_inf_SC5-new_inf5));
sub_mae_SC5=mean(abs(new_exp_sub_SC5-new_sub5));
pec_mae_SC5=mean(abs(new_exp_pec_SC5-new_pec5));
tri_mae_SC5=mean(abs(new_exp_tri_SC5-new_tri5));
bi_mae_SC5=mean(abs(new_exp_bi_SC5-new_bi5));
uptrap_mae_SC5=mean(abs(new_exp_up_trap_SC5-new_uptrap5));
midtrap_mae_SC5=mean(abs(new_exp_mid_trap_SC5-new_midtrap5));
serrant_mae_SC5=mean(abs(new_exp_serr_ant_SC5-new_serrant5));
rhommaj_mae_SC5=mean(abs(new_exp_rhom_SC5-new_rhommaj5));

%Puts all MAE values per muscle into a matrix so that all 5 SC
%values can be viewed at once for a muscle
ad_mae=    [ad_mae_SC1      ad_mae_SC2      ad_mae_SC3
          ad_mae_SC4      ad_mae_SC5];
md_mae=    [md_mae_SC1      md_mae_SC2      md_mae_SC3
          md_mae_SC4      md_mae_SC5];
pd_mae=    [pd_mae_SC1      pd_mae_SC2      pd_mae_SC3
          pd_mae_SC4      pd_mae_SC5];
sup_mae=   [sup_mae_SC1     sup_mae_SC2     sup_mae_SC3
          sup_mae_SC4     sup_mae_SC5];
inf_mae=   [inf_mae_SC1     inf_mae_SC2     inf_mae_SC3
          inf_mae_SC4     inf_mae_SC5];
sub_mae=   [sub_mae_SC1     sub_mae_SC2     sub_mae_SC3
          sub_mae_SC4     sub_mae_SC5];
pec_mae=   [pec_mae_SC1     pec_mae_SC2     pec_mae_SC3
          pec_mae_SC4     pec_mae_SC5];
tri_mae=   [tri_mae_SC1     tri_mae_SC2     tri_mae_SC3
          tri_mae_SC4     tri_mae_SC5];
bi_mae=    [bi_mae_SC1      bi_mae_SC2      bi_mae_SC3
          bi_mae_SC4      bi_mae_SC5];
uptrap_mae= [uptrap_mae_SC1   uptrap_mae_SC2   uptrap_mae_SC3
          uptrap_mae_SC4   uptrap_mae_SC5];
midtrap_mae=[midtrap_mae_SC1  midtrap_mae_SC2  midtrap_mae_SC3
          midtrap_mae_SC4  midtrap_mae_SC5];
serrant_mae=[serrant_mae_SC1  serrant_mae_SC2  serrant_mae_SC3
          serrant_mae_SC4  serrant_mae_SC5];
rhom_mae=   [rhommaj_mae_SC1  rhommaj_mae_SC2  rhommaj_mae_SC3
```

```
            rhommaj_mae_SC4  rhommaj_mae_SC5];

%Saves .mat file of experimental EMG, estimated force & normalized activation for each
muscle (entire trial, push phase, & recovery phase)
%Anterior Deltoid
   %Stroke Cycle 1
      %Entire Propulsive Cycle
      ad_SC1=[new_exp_ad_SC1 new_os_ad_SC1 new_ad1];
      save adSC1data ad_SC1
      %Push phase
      ad_SC1_push=[new_exp_ad_SC1(1:45,1) new_os_ad_SC1(1:45,1)
               new_ad1(1:45,1)];
      save adSC1pushdata ad_SC1_push
      %Recovery phase
      ad_SC1_rec=[new_exp_ad_SC1(46:100,1) new_os_ad_SC1(46:100,1)
              new_ad1(46:100,1)];
      save adSC1recdata ad_SC1_rec
   %Stroke Cycle 2
      %Entire Propulsive Cycle
      ad_SC2=[new_exp_ad_SC2 new_os_ad_SC2 new_ad2];
      save adSC2data ad_SC2
      %Push phase
      ad_SC2_push=[new_exp_ad_SC2(1:47,1) new_os_ad_SC2(1:47,1)
               new_ad2(1:47,1)];
      save adSC2pushdata ad_SC2_push
      %Recovery phase
      ad_SC2_rec=[new_exp_ad_SC2(48:100,1) new_os_ad_SC2(48:100,1)
              new_ad2(48:100,1)];
      save adSC2recdata ad_SC2_rec
   %Stroke Cycle 3
      %Entire Propulsive Cycle
      ad_SC3=[new_exp_ad_SC3 new_os_ad_SC3 new_ad3];
      save adSC3data ad_SC3
      %Push phase
      ad_SC3_push=[new_exp_ad_SC3(1:42,1) new_os_ad_SC3(1:42,1)
               new_ad3(1:42,1)];
      save adSC3pushdata ad_SC3_push
      %Recovery phase
      ad_SC3_rec=[new_exp_ad_SC3(43:100,1) new_os_ad_SC3(43:100,1)
              new_ad3(43:100,1)];
      save adSC3recdata ad_SC3_rec
   %Stroke Cycle 4
      %Entire Propulsive Cycle
      ad_SC4=[new_exp_ad_SC4 new_os_ad_SC4 new_ad4];
      save adSC4data ad_SC4
      %Push phase
```

```
    ad_SC4_push=[new_exp_ad_SC4(1:34,1) new_os_ad_SC4(1:34,1)
            new_ad4(1:34,1)];
    save adSC4pushdata ad_SC4_push
    %Recovery phase
    ad_SC4_rec=[new_exp_ad_SC4(35:100,1) new_os_ad_SC4(35:100,1)
          new_ad4(35:100,1)];
    save adSC4recdata ad_SC4_rec
  %Stroke Cycle 5
    %Entire Propulsive Cycle
    ad_SC5=[new_exp_ad_SC5 new_os_ad_SC5 new_ad5];
    save adSC5data ad_SC5
    %Push phase
    ad_SC5_push=[new_exp_ad_SC5(1:44,1) new_os_ad_SC5(1:44,1)
            new_ad5(1:44,1)];
    save adSC5pushdata ad_SC5_push
    %Recovery phase
    ad_SC5_rec=[new_exp_ad_SC5(45:100,1) new_os_ad_SC5(45:100,1)
          new_ad5(45:100,1)];
    save adSC5recdata ad_SC5_rec

%Middle Deltoid
  %Stroke Cycle 1
    %Entire Propulsive Cycle
    md_SC1=[new_exp_md_SC1 new_os_md_SC1 new_md1];
    save mdSC1data md_SC1
    %Push phase
    md_SC1_push=[new_exp_md_SC1(1:45,1) new_os_md_SC1(1:45,1)
            new_md1(1:45,1)];
    save mdSC1pushdata md_SC1_push
    %Recovery phase
    md_SC1_rec=[new_exp_md_SC1(46:100,1) new_os_md_SC1(46:100,1)
          new_md1(46:100,1)];
    save mdSC1recdata md_SC1_rec
  %Stroke Cycle 2
    %Entire Propulsive Cycle
    md_SC2=[new_exp_md_SC2 new_os_md_SC2 new_md2];
    save mdSC2data md_SC2
    %Push phase
    md_SC2_push=[new_exp_md_SC2(1:47,1) new_os_md_SC2(1:47,1)
            new_md2(1:47,1)];
    save mdSC2pushdata md_SC2_push
    %Recovery phase
    md_SC2_rec=[new_exp_md_SC2(48:100,1) new_os_md_SC2(48:100,1)
          new_md2(48:100,1)];
    save mdSC2recdata md_SC2_rec
  %Stroke Cycle 3
```

```
    %Entire Propulsive Cycle
    md_SC3=[new_exp_md_SC3 new_os_md_SC3 new_md3];
    save mdSC3data md_SC3

    %Push phase
    md_SC3_push=[new_exp_md_SC3(1:42,1) new_os_md_SC3(1:42,1)
            new_md3(1:42,1)];
    save mdSC3pushdata md_SC3_push
    %Recovery phase
    md_SC3_rec=[new_exp_md_SC3(43:100,1) new_os_md_SC3(43:100,1)
           new_md3(43:100,1)];
    save mdSC3recdata md_SC3_rec
  %Stroke Cycle 4
    %Entire Propulsive Cycle
    md_SC4=[new_exp_md_SC4 new_os_md_SC4 new_md4];
    save mdSC4data md_SC4
    %Push phase
    md_SC4_push=[new_exp_md_SC4(1:34,1) new_os_md_SC4(1:34,1)
            new_md4(1:34,1)];
    save mdSC4pushdata md_SC4_push
    %Recovery phase
    md_SC4_rec=[new_exp_md_SC4(35:100,1) new_os_md_SC4(35:100,1)
           new_md4(35:100,1)];
    save mdSC4recdata md_SC4_rec
  %Stroke Cycle 5
    %Entire Propulsive Cycle
    md_SC5=[new_exp_md_SC5 new_os_md_SC5 new_md5];
    save mdSC5data md_SC5
    %Push phase
    md_SC5_push=[new_exp_md_SC5(1:44,1) new_os_md_SC5(1:44,1)
            new_md5(1:44,1)];
    save mdSC5pushdata md_SC5_push
    %Recovery phase
    md_SC5_rec=[new_exp_md_SC5(45:100,1) new_os_md_SC5(45:100,1)
           new_md5(45:100,1)];
    save mdSC5recdata md_SC5_rec

%Posterior Deltoid
  %Stroke Cycle 1
    %Entire Propulsive Cycle
    pd_SC1=[new_exp_pd_SC1 new_os_pd_SC1 new_pd1];
    save pdSC1data pd_SC1
    %Push phase
    pd_SC1_push=[new_exp_pd_SC1(1:45,1) new_os_pd_SC1(1:45,1)
            new_pd1(1:45,1)];
    save pdSC1pushdata pd_SC1_push
```

```
    %Recovery phase
    pd_SC1_rec=[new_exp_pd_SC1(46:100,1) new_os_pd_SC1(46:100,1)
            new_pd1(46:100,1)];
    save pdSC1recdata pd_SC1_rec
%Stroke Cycle 2
    %Entire Propulsive Cycle
    pd_SC2=[new_exp_pd_SC2 new_os_pd_SC2 new_pd2];
    save pdSC2data pd_SC2
    %Push phase
    pd_SC2_push=[new_exp_pd_SC2(1:47,1) new_os_pd_SC2(1:47,1)
             new_pd2(1:47,1)];
    save pdSC2pushdata pd_SC2_push
    %Recovery phase
    pd_SC2_rec=[new_exp_pd_SC2(48:100,1) new_os_pd_SC2(48:100,1)
            new_pd2(48:100,1)];
    save pdSC2recdata pd_SC2_rec
%Stroke Cycle 3
    %Entire Propulsive Cycle
    pd_SC3=[new_exp_pd_SC3 new_os_pd_SC3 new_pd3];
    save pdSC3data pd_SC3
    %Push phase
    pd_SC3_push=[new_exp_pd_SC3(1:42,1) new_os_pd_SC3(1:42,1)
             new_pd3(1:42,1)];
    save pdSC3pushdata pd_SC3_push
    %Recovery phase
    pd_SC3_rec=[new_exp_pd_SC3(43:100,1) new_os_pd_SC3(43:100,1)
            new_pd3(43:100,1)];
    save pdSC3recdata pd_SC3_rec
%Stroke Cycle 4
    %Entire Propulsive Cycle
    pd_SC4=[new_exp_pd_SC4 new_os_pd_SC4 new_pd4];
    save pdSC4data pd_SC4
    %Push phase
    pd_SC4_push=[new_exp_pd_SC4(1:34,1) new_os_pd_SC4(1:34,1)
             new_pd4(1:34,1)];
    save pdSC4pushdata pd_SC4_push
    %Recovery phase
    pd_SC4_rec=[new_exp_pd_SC4(35:100,1) new_os_pd_SC4(35:100,1)
            new_pd4(35:100,1)];
    save pdSC4recdata pd_SC4_rec
%Stroke Cycle 5
    %Entire Propulsive Cycle
    pd_SC5=[new_exp_pd_SC5 new_os_pd_SC5 new_pd5];
    save pdSC5data pd_SC5
    %Push phase
    pd_SC5_push=[new_exp_pd_SC5(1:44,1) new_os_pd_SC5(1:44,1)
```

```
            new_pd5(1:44,1)];
        save pdSC5pushdata pd_SC5_push
        %Recovery phase
        pd_SC5_rec=[new_exp_pd_SC5(45:100,1) new_os_pd_SC5(45:100,1)
            new_pd5(45:100,1)];
        save pdSC5recdata pd_SC5_rec

%Supraspinatus
    %Stroke Cycle 1
        %Entire Propulsive Cycle
        sup_SC1=[new_exp_sup_SC1 new_os_sup_SC1 new_sup1];
        save supSC1data sup_SC1
        %Push phase
        sup_SC1_push=[new_exp_sup_SC1(1:45,1) new_os_sup_SC1(1:45,1)
            new_sup1(1:45,1)];
        save supSC1pushdata sup_SC1_push
        %Recovery phase
        sup_SC1_rec=[new_exp_sup_SC1(46:100,1) new_os_sup_SC1(46:100,1)
            new_sup1(46:100,1)];
        save supSC1recdata sup_SC1_rec
    %Stroke Cycle 2
        %Entire Propulsive Cycle
        sup_SC2=[new_exp_sup_SC2 new_os_sup_SC2 new_sup2];
        save supSC2data sup_SC2
        %Push phase
        sup_SC2_push=[new_exp_sup_SC2(1:47,1) new_os_sup_SC2(1:47,1)
            new_sup2(1:47,1)];
        save supSC2pushdata sup_SC2_push
        %Recovery phase
        sup_SC2_rec=[new_exp_sup_SC2(48:100,1) new_os_sup_SC2(48:100,1)
            new_sup2(48:100,1)];
        save supSC2recdata sup_SC2_rec
    %Stroke Cycle 3
        %Entire Propulsive Cycle
        sup_SC3=[new_exp_sup_SC3 new_os_sup_SC3 new_sup3];
        save supSC3data sup_SC3
        %Push phase
        sup_SC3_push=[new_exp_sup_SC3(1:42,1) new_os_sup_SC3(1:42,1)
            new_sup3(1:42,1)];
        save supSC3pushdata sup_SC3_push
        %Recovery phase
        sup_SC3_rec=[new_exp_sup_SC3(43:100,1) new_os_sup_SC3(43:100,1)
            new_sup3(43:100,1)];
        save supSC3recdata sup_SC3_rec
    %Stroke Cycle 4
        %Entire Propulsive Cycle
```

```
    sup_SC4=[new_exp_sup_SC4 new_os_sup_SC4 new_sup4];
    save supSC4data sup_SC4
    %Push phase
    sup_SC4_push=[new_exp_sup_SC4(1:34,1) new_os_sup_SC4(1:34,1)
            new_sup4(1:34,1)];
    save supSC4pushdata sup_SC4_push
    %Recovery phase
    sup_SC4_rec=[new_exp_sup_SC4(35:100,1) new_os_sup_SC4(35:100,1)
           new_sup4(35:100,1)];
    save supSC4recdata sup_SC4_rec
  %Stroke Cycle 5
    %Entire Propulsive Cycle
    sup_SC5=[new_exp_sup_SC5 new_os_sup_SC5 new_sup5];
    save supSC5data sup_SC5
    %Push phase
    sup_SC5_push=[new_exp_sup_SC5(1:44,1) new_os_sup_SC5(1:44,1)
            new_sup5(1:44,1)];
    save supSC5pushdata sup_SC5_push
    %Recovery phase
    sup_SC5_rec=[new_exp_sup_SC5(45:100,1) new_os_sup_SC5(45:100,1)
           new_sup5(45:100,1)];
    save supSC5recdata sup_SC5_rec


%Infraspinatus
  %Stroke Cycle 1
    %Entire Propulsive Cycle
    inf_SC1=[new_exp_inf_SC1 new_os_inf_SC1 new_inf1];
    save infSC1data inf_SC1
    %Push phase
    inf_SC1_push=[new_exp_inf_SC1(1:45,1) new_os_inf_SC1(1:45,1)
            new_inf1(1:45,1)];
    save infSC1pushdata inf_SC1_push
    %Recovery phase
    inf_SC1_rec=[new_exp_inf_SC1(46:100,1) new_os_inf_SC1(46:100,1)
           new_inf1(46:100,1)];
    save infSC1recdata inf_SC1_rec
  %Stroke Cycle 2
    %Entire Propulsive Cycle
    inf_SC2=[new_exp_inf_SC2 new_os_inf_SC2 new_inf2];
    save infSC2data inf_SC2
    %Push phase
    inf_SC2_push=[new_exp_inf_SC2(1:47,1) new_os_inf_SC2(1:47,1)
            new_inf2(1:47,1)];
    save infSC2pushdata inf_SC2_push
    %Recovery phase
```

```
    inf_SC2_rec=[new_exp_inf_SC2(48:100,1) new_os_inf_SC2(48:100,1)
            new_inf2(48:100,1)];
    save infSC2recdata inf_SC2_rec

  %Stroke Cycle 3
    %Entire Propulsive Cycle
    inf_SC3=[new_exp_inf_SC3 new_os_inf_SC3 new_inf3];
    save infSC3data inf_SC3
    %Push phase
    inf_SC3_push=[new_exp_inf_SC3(1:42,1) new_os_inf_SC3(1:42,1)
            new_inf3(1:42,1)];
    save infSC3pushdata inf_SC3_push
    %Recovery phase
    inf_SC3_rec=[new_exp_inf_SC3(43:100,1) new_os_inf_SC3(43:100,1)
            new_inf3(43:100,1)];
    save infSC3recdata inf_SC3_rec
  %Stroke Cycle 4
    %Entire Propulsive Cycle
    inf_SC4=[new_exp_inf_SC4 new_os_inf_SC4 new_inf4];
    save infSC4data inf_SC4
    %Push phase
    inf_SC4_push=[new_exp_inf_SC4(1:34,1) new_os_inf_SC4(1:34,1)
            new_inf4(1:34,1)];
    save infSC4pushdata inf_SC4_push
    %Recovery phase
    inf_SC4_rec=[new_exp_inf_SC4(35:100,1) new_os_inf_SC4(35:100,1)
            new_inf4(35:100,1)];
    save infSC4recdata inf_SC4_rec
  %Stroke Cycle 5
    %Entire Propulsive Cycle
    inf_SC5=[new_exp_inf_SC5 new_os_inf_SC5 new_inf5];
    save infSC5data inf_SC5
    %Push phase
    inf_SC5_push=[new_exp_inf_SC5(1:44,1) new_os_inf_SC5(1:44,1)
            new_inf5(1:44,1)];
    save infSC5pushdata inf_SC5_push
    %Recovery phase
    inf_SC5_rec=[new_exp_inf_SC5(45:100,1) new_os_inf_SC5(45:100,1)
            new_inf5(45:100,1)];
    save infSC5recdata inf_SC5_rec

%Subscapularis
  %Stroke Cycle 1
    %Entire Propulsive Cycle
    sub_SC1=[new_exp_sub_SC1 new_os_sub_SC1 new_sub1];
    save subSC1data sub_SC1
```

```
    %Push phase
    sub_SC1_push=[new_exp_sub_SC1(1:45,1) new_os_sub_SC1(1:45,1)
                  new_sub1(1:45,1)];
    save subSC1pushdata sub_SC1_push
    %Recovery phase
    sub_SC1_rec=[new_exp_sub_SC1(46:100,1) new_os_sub_SC1(46:100,1)
                 new_sub1(46:100,1)];
    save subSC1recdata sub_SC1_rec
%Stroke Cycle 2
    %Entire Propulsive Cycle
    sub_SC2=[new_exp_sub_SC2 new_os_sub_SC2 new_sub2];
    save subSC2data sub_SC2
    %Push phase
    sub_SC2_push=[new_exp_sub_SC2(1:47,1) new_os_sub_SC2(1:47,1)
                  new_sub2(1:47,1)];
    save subSC2pushdata sub_SC2_push
    %Recovery phase
    sub_SC2_rec=[new_exp_sub_SC2(48:100,1) new_os_sub_SC2(48:100,1)
                 new_sub2(48:100,1)];
    save subSC2recdata sub_SC2_rec
%Stroke Cycle 3
    %Entire Propulsive Cycle
    sub_SC3=[new_exp_sub_SC3 new_os_sub_SC3 new_sub3];
    save subSC3data sub_SC3
    %Push phase
    sub_SC3_push=[new_exp_sub_SC3(1:42,1) new_os_sub_SC3(1:42,1)
                  new_sub3(1:42,1)];
    save subSC3pushdata sub_SC3_push
    %Recovery phase
    sub_SC3_rec=[new_exp_sub_SC3(43:100,1) new_os_sub_SC3(43:100,1)
                 new_sub3(43:100,1)];
    save subSC3recdata sub_SC3_rec
%Stroke Cycle 4
    %Entire Propulsive Cycle
    sub_SC4=[new_exp_sub_SC4 new_os_sub_SC4 new_sub4];
    save subSC4data sub_SC4
    %Push phase
    sub_SC4_push=[new_exp_sub_SC4(1:34,1) new_os_sub_SC4(1:34,1)
                  new_sub4(1:34,1)];
    save subSC4pushdata sub_SC4_push
    %Recovery phase
    sub_SC4_rec=[new_exp_sub_SC4(35:100,1) new_os_sub_SC4(35:100,1)
                 new_sub4(35:100,1)];
    save subSC4recdata sub_SC4_rec
%Stroke Cycle 5
    %Entire Propulsive Cycle
```

```
        sub_SC5=[new_exp_sub_SC5 new_os_sub_SC5 new_sub5];
        save subSC5data sub_SC5
        %Push phase
        sub_SC5_push=[new_exp_sub_SC5(1:44,1) new_os_sub_SC5(1:44,1)
                  new_sub5(1:44,1)];
        save subSC5pushdata sub_SC5_push
        %Recovery phase
        sub_SC5_rec=[new_exp_sub_SC5(45:100,1) new_os_sub_SC5(45:100,1)
                 new_sub5(45:100,1)];
        save subSC5recdata sub_SC5_rec

%Triceps
    %Stroke Cycle 1
        %Entire Propulsive Cycle
        tri_SC1=[new_exp_tri_SC1 new_os_tri_SC1 new_tri1];
        save triSC1data tri_SC1
        %Push phase
        tri_SC1_push=[new_exp_tri_SC1(1:45,1) new_os_tri_SC1(1:45,1)
                  new_tri1(1:45,1)];
        save triSC1pushdata tri_SC1_push
        %Recovery phase
        tri_SC1_rec=[new_exp_tri_SC1(46:100,1) new_os_tri_SC1(46:100,1)
                 new_tri1(46:100,1)];
        save triSC1recdata tri_SC1_rec
    %Stroke Cycle 2
        %Entire Propulsive Cycle
        tri_SC2=[new_exp_tri_SC2 new_os_tri_SC2 new_tri2];
        save triSC2data tri_SC2
        %Push phase
        tri_SC2_push=[new_exp_tri_SC2(1:47,1) new_os_tri_SC2(1:47,1)
                  new_tri2(1:47,1)];
        save triSC2pushdata tri_SC2_push
        %Recovery phase
        tri_SC2_rec=[new_exp_tri_SC2(48:100,1) new_os_tri_SC2(48:100,1)
                 new_tri2(48:100,1)];
        save triSC2recdata tri_SC2_rec
    %Stroke Cycle 3
        %Entire Propulsive Cycle
        tri_SC3=[new_exp_tri_SC3 new_os_tri_SC3 new_tri3];
        save triSC3data tri_SC3
        %Push phase
        tri_SC3_push=[new_exp_tri_SC3(1:42,1) new_os_tri_SC3(1:42,1)
                  new_tri3(1:42,1)];
        save triSC3pushdata tri_SC3_push
        %Recovery phase
        tri_SC3_rec=[new_exp_tri_SC3(43:100,1) new_os_tri_SC3(43:100,1)
```

```
            new_tri3(43:100,1)];
    save triSC3recdata tri_SC3_rec


  %Stroke Cycle 4
    %Entire Propulsive Cycle
    tri_SC4=[new_exp_tri_SC4 new_os_tri_SC4 new_tri4];
    save triSC4data tri_SC4
    %Push phase
    tri_SC4_push=[new_exp_tri_SC4(1:34,1) new_os_tri_SC4(1:34,1)
             new_tri4(1:34,1)];
    save triSC4pushdata tri_SC4_push
     %Recovery phase
    tri_SC4_rec=[new_exp_tri_SC4(35:100,1) new_os_tri_SC4(35:100,1)
            new_tri4(35:100,1)];
    save triSC4recdata tri_SC4_rec
  %Stroke Cycle 5
    %Entire Propulsive Cycle
    tri_SC5=[new_exp_tri_SC5 new_os_tri_SC5 new_tri5];
    save triSC5data tri_SC5
    %Push phase
    tri_SC5_push=[new_exp_tri_SC5(1:44,1) new_os_tri_SC5(1:44,1)
             new_tri5(1:44,1)];
    save triSC5pushdata tri_SC5_push
    %Recovery phase
    tri_SC5_rec=[new_exp_tri_SC5(45:100,1) new_os_tri_SC5(45:100,1)
            new_tri5(45:100,1)];
    save triSC5recdata tri_SC5_rec

%Biceps
   %Stroke Cycle 1
    %Entire Propulsive Cycle
    bi_SC1=[new_exp_bi_SC1 new_os_bi_SC1 new_bi1];
    save biSC1data bi_SC1
    %Push phase
    bi_SC1_push=[new_exp_bi_SC1(1:45,1) new_os_bi_SC1(1:45,1)
            new_bi1(1:45,1)];
    save biSC1pushdata bi_SC1_push
    %Recovery phase
    bi_SC1_rec=[new_exp_bi_SC1(46:100,1) new_os_bi_SC1(46:100,1)
           new_bi1(46:100,1)];
    save biSC1recdata bi_SC1_rec
   %Stroke Cycle 2
    %Entire Propulsive Cycle
    bi_SC2=[new_exp_tri_SC2 new_os_bi_SC2 new_bi2];
    save biSC2data bi_SC2
```

```
    %Push phase
    bi_SC2_push=[new_exp_bi_SC2(1:47,1) new_os_bi_SC2(1:47,1)
            new_bi2(1:47,1)];
    save biSC2pushdata bi_SC2_push
    %Recovery phase
    bi_SC2_rec=[new_exp_bi_SC2(48:100,1) new_os_bi_SC2(48:100,1)
           new_bi2(48:100,1)];
    save biSC2recdata bi_SC2_rec
  %Stroke Cycle 3
    %Entire Propulsive Cycle
    bi_SC3=[new_exp_bi_SC3 new_os_bi_SC3 new_bi3];
    save biSC3data bi_SC3
    %Push phase
    bi_SC3_push=[new_exp_bi_SC3(1:42,1) new_os_bi_SC3(1:42,1)
            new_bi3(1:42,1)];
    save biSC3pushdata bi_SC3_push
    %Recovery phase
    bi_SC3_rec=[new_exp_bi_SC3(43:100,1) new_os_bi_SC3(43:100,1)
           new_bi3(43:100,1)];
    save biSC3recdata bi_SC3_rec
 %Stroke Cycle 4
    %Entire Propulsive Cycle
    bi_SC4=[new_exp_bi_SC4 new_os_bi_SC4 new_bi4];
    save biSC4data bi_SC4
    %Push phase
    bi_SC4_push=[new_exp_bi_SC4(1:34,1) new_os_bi_SC4(1:34,1)
            new_bi4(1:34,1)];
    save biSC4pushdata bi_SC4_push
    %Recovery phase
    bi_SC4_rec=[new_exp_bi_SC4(35:100,1) new_os_bi_SC4(35:100,1)
           new_bi4(35:100,1)];
    save biSC4recdata bi_SC4_rec
 %Stroke Cycle 5
    %Entire Propulsive Cycle
    bi_SC5=[new_exp_bi_SC5 new_os_bi_SC5 new_bi5];
    save biSC5data bi_SC5
    %Push phase
    bi_SC5_push=[new_exp_bi_SC5(1:44,1) new_os_bi_SC5(1:44,1)
            new_bi5(1:44,1)];
    save biSC5pushdata bi_SC5_push
    %Recovery phase
    bi_SC5_rec=[new_exp_bi_SC5(45:100,1) new_os_bi_SC5(45:100,1)
           new_bi5(45:100,1)];
    save biSC5recdata bi_SC5_rec

%Serratus Anterior
```

```
%Stroke Cycle 1
   %Entire Propulsive Cycle
   sa_SC1=[new_exp_serr_ant_SC1 new_os_serr_ant_SC1 new_serrant1];
   save saSC1data sa_SC1
   %Push phase
   sa_SC1_push=[new_exp_serr_ant_SC1(1:45,1)
            new_os_serr_ant_SC1(1:45,1)
            new_serrant1(1:45,1)];
   save saSC1pushdata sa_SC1_push
   %Recovery phase
   sa_SC1_rec=[new_exp_serr_ant_SC1(46:100,1)
           new_os_serr_ant_SC1(46:100,1)
           new_serrant1(46:100,1)];
   save saSC1recdata sa_SC1_rec
%Stroke Cycle 2
   %Entire Propulsive Cycle
   sa_SC2=[new_exp_serr_ant_SC2 new_os_serr_ant_SC2 new_serrant2];
   save saSC2data sa_SC2
   %Push phase
   sa_SC2_push=[new_exp_serr_ant_SC2(1:47,1)
            new_os_serr_ant_SC2(1:47,1)
            new_serrant2(1:47,1)];
   save saSC2pushdata sa_SC2_push
   %Recovery phase
   sa_SC2_rec=[new_exp_serr_ant_SC2(48:100,1)
           new_os_serr_ant_SC2(48:100,1)
           new_serrant2(48:100,1)];
   save saSC2recdata sa_SC2_rec
%Stroke Cycle 3
   %Entire Propulsive Cycle
   sa_SC3=[new_exp_serr_ant_SC3 new_os_serr_ant_SC3 new_serrant3];
   save saSC3data sa_SC3
   %Push phase
   sa_SC3_push=[new_exp_serr_ant_SC3(1:42,1)
            new_os_serr_ant_SC3(1:42,1)
            new_serrant3(1:42,1)];
   save saSC3pushdata sa_SC3_push
   %Recovery phase
   sa_SC3_rec=[new_exp_serr_ant_SC3(43:100,1)
           new_os_serr_ant_SC3(43:100,1)
           new_serrant3(43:100,1)];
   save saSC3recdata sa_SC3_rec
%Stroke Cycle 4
   %Entire Propulsive Cycle
   sa_SC4=[new_exp_serr_ant_SC4 new_os_serr_ant_SC4 new_serrant4];
   save saSC4data sa_SC4
```

```
    %Push phase
    sa_SC4_push=[new_exp_serr_ant_SC4(1:34,1)
                 new_os_serr_ant_SC4(1:34,1)
                 new_serrant4(1:34,1)];
    save saSC4pushdata sa_SC4_push
    %Recovery phase
    sa_SC4_rec=[new_exp_serr_ant_SC4(35:100,1)
                new_os_serr_ant_SC4(35:100,1)
                new_serrant4(35:100,1)];
    save saSC4recdata sa_SC4_rec
  %Stroke Cycle 5
    %Entire Propulsive Cycle
    sa_SC5=[new_exp_serr_ant_SC5 new_os_serr_ant_SC5 new_serrant5];
    save saSC5data sa_SC5
    %Push phase
    sa_SC5_push=[new_exp_serr_ant_SC5(1:44,1)
                 new_os_serr_ant_SC5(1:44,1)
                 new_serrant5(1:44,1)];
    save saSC5pushdata sa_SC5_push
    %Recovery phase
    sa_SC5_rec=[new_exp_serr_ant_SC5(45:100,1)
                new_os_serr_ant_SC5(45:100,1)
                new_serrant5(45:100,1)];
    save saSC5recdata sa_SC5_rec

%Rhomboids Major
  %Stroke Cycle 1
    %Entire Propulsive Cycle
    rm_SC1=[new_exp_rhom_SC1 new_os_rhom_SC1 new_rhommaj1];
    save rmSC1data rm_SC1
    %Push phase
    rm_SC1_push=[new_exp_rhom_SC1(1:45,1) new_os_rhom_SC1(1:45,1)
                 new_rhommaj1(1:45,1)];
    save rmSC1pushdata rm_SC1_push
    %Recovery phase
    rm_SC1_rec=[new_exp_rhom_SC1(46:100,1)
                new_os_rhom_SC1(46:100,1)
                new_rhommaj1(46:100,1)];
    save rmSC1recdata rm_SC1_rec
  %Stroke Cycle 2
    %Entire Propulsive Cycle
    rm_SC2=[new_exp_rhom_SC2 new_os_rhom_SC2 new_rhommaj2];
    save rmSC2data rm_SC2
    %Push phase
    rm_SC2_push=[new_exp_rhom_SC2(1:47,1) new_os_rhom_SC2(1:47,1)
                 new_rhommaj2(1:47,1)];
```

```
    save rmSC2pushdata rm_SC2_push
    %Recovery phase
    rm_SC2_rec=[new_exp_rhom_SC2(48:100,1)
                new_os_rhom_SC2(48:100,1)
                new_rhommaj2(48:100,1)];
    save rmSC2recdata rm_SC2_rec
%Stroke Cycle 3
    %Entire Propulsive Cycle
    rm_SC3=[new_exp_rhom_SC3 new_os_rhom_SC3 new_rhommaj3];
    save rmSC3data rm_SC3
    %Push phase
    rm_SC3_push=[new_exp_rhom_SC3(1:42,1) new_os_rhom_SC3(1:42,1)
                 new_rhommaj3(1:42,1)];
    save rmSC3pushdata rm_SC3_push
    %Recovery phase
    rm_SC3_rec=[new_exp_rhom_SC3(43:100,1)
                new_os_rhom_SC3(43:100,1)
                new_rhommaj3(43:100,1)];
    save rmSC3recdata rm_SC3_rec
%Stroke Cycle 4
    %Entire Propulsive Cycle
    rm_SC4=[new_exp_rhom_SC4 new_os_rhom_SC4 new_rhommaj4];
    save rmSC4data rm_SC4
    %Push phase
    rm_SC4_push=[new_exp_rhom_SC4(1:34,1) new_os_rhom_SC4(1:34,1)
                 new_rhommaj4(1:34,1)];
    save rmSC4pushdata rm_SC4_push
    %Recovery phase
    rm_SC4_rec=[new_exp_rhom_SC4(35:100,1)
                new_os_rhom_SC4(35:100,1)
                new_rhommaj4(35:100,1)];
    save rmSC4recdata rm_SC4_rec
%Stroke Cycle 5
    %Entire Propulsive Cycle
    rm_SC5=[new_exp_rhom_SC5 new_os_rhom_SC5 new_rhommaj5];
    save rmSC5data rm_SC5
    %Push phase
    rm_SC5_push=[new_exp_rhom_SC5(1:44,1) new_os_rhom_SC5(1:44,1)
                 new_rhommaj5(1:44,1)];
    save rmSC5pushdata rm_SC5_push
    %Recovery phase
    rm_SC5_rec=[new_exp_rhom_SC5(45:100,1)
                new_os_rhom_SC5(45:100,1)
                new_rhommaj5(45:100,1)];
    save rmSC5recdata rm_SC5_rec
```

REFERENCES

Aissaoui, R., Arabi, H., Lacoste, M., Zalzal, V., & Dansereau, J. (2002). Biomechanics of manual wheelchair propulsion in elderly: System tilt and back recline angles. *American Journal of Physical Medicine and Rehabilitation*, 81, 94-100.

An, K. N., Kwak, B. W., Chao, E. Y., & Morrey, B. F. (1984). Determination of muscle and joint forces: A new technique to solve the indeterminate problem. *Journal of Biomechanical Engineering*, 106, 364-367.

Anderson, F. C. & Pandy, M. G. (2001). Static and dynamic optimization solutions for gait are practically equivalent. *Journal of Biomechanics*, 34, 153-161.

Andrews, J. G. & Mish, S. P. (1996). Methods for investigating the sensitivity of joint resultants to body segment parameter variations. *Journal of Biomechanics*, 29(5), 651-654.

Arthurs, K. L. & Andrews, D. M. (2009). Upper extremity soft and rigid tissue mass prediction using segment anthropometric measures and DXA. *Journal of Biomechanics*, 42, 389-394.

Asato, K. T., Cooper, R. A., Robertson, R. N., & Ster, J. F. (1993). Smart^{Wheels}: Development and testing of a system for measuring manual wheelchair propulsion dynamics. *IEEE Transactions on Biomedical Engineering*, 40(12), 1320-1324.

Bauman, W. A., Spungen, A. M., Wang, J., Pierson, R. N., & Schwartz, E. (1999). Continuous loss of bone during chronic immobilization: A monozygotic twin study. *Osteoporosis International*, 10, 123-127.

Bauman, W. A., Kirshblum, S., Cirnigliario, C., Forrest, G. F., & Spungen, A. M. (2010). Underestimation of bone loss of the spine with posterior-anterior dual-energy X-ray absorptiometry in patients with spinal cord injury. *The Journal of Spinal Cord Medicine*, 33(3), 214-220.

Bayley, J. C., Cochran, T. P., & Sledge, C. B. (1987). The weight-bearing shoulder. The impingement syndrome in paraplegics. *Journal of Bone Joint Surgery. American Volume*, 69, 676-678.

Biering-Sørensen, F., Bohr, H., & Schaadt, O. (1988). Bone mineral content of the lumbar spine and lower extremities years after spinal cord lesion. *Paraplegia*, 26, 293-301.

Biering-Sørensen, F., Bohr, H., & Schaadt, O. (1990). Longitudinal study of bone mineral content in the lumbar spine, the forearm, and the lower extremities after spinal cord injury. *European Journal of Clinical Investigation*, 20, 330-335.

Bloomfield, S. A., Mysiw, W. J., & Jackson, R. D. (1996). Bone mass and endocrine adaptations to training in spinal cord injured individuals. *Bone*, 19(1), 61-68.

Boninger, M. L., Cooper, R. A., Baldwin, M. A., Shimada, S. A., & Koontz, A. M. (1999). Wheelchair pushrim kinetics: body weight and median nerve function. *Archives of Physical Medicine and Rehabilitation*, 80, 910-915.

Boninger, M. L., Cooper, R. A., Robertson, R. N., & Shimada, S. D. (1997). Three-dimensional pushrim forces during two speeds of wheelchair propulsion. *American Journal of Physical Medicine and Rehabilitation*, 76, 420-426.

Boninger, M. L., Souza, A. L., Cooper, R. A., Fitzgerald, S. G., Koontz, A. M., & Fay, B. T. (2002). Propulsion patterns and pushrim biomechanics in manual wheelchair propulsion. *Archives of Physical Medicine and Rehabilitation*, 83, 718-723.

Buchanan, T. S. & Shreeve, D. A. (1996). An evaluation of optimization techniques for the prediction of muscle activation patterns during isometric tasks. *Journal of Biomechanical Engineering*, 118, 565-574.

Burkhart, T. A., Arthurs, K. L., & Andrews, D. M. (2009). Manual segmentation of DXA scan images in reliable upper and lower extremity soft and rigid tissue mass estimates. *Journal of Biomechanics*, 42, 1138-1142.

Burnham, R. S., Curtis, K. A., & Reid, D. C. (1995). Shoulder problems in the wheelchair athlete. In: Petrone, F. A. (editor). *Athletic Injuries of the Shoulder.* New York: McGraw-Hill, Inc., 375-381.

Cahill,A., Fredine, H., & Zilberman, L. (2008). Initial briefing: Prevalence of paralysis including spinal cord injuries in the United States. *Christopher and Dana Reeve Foundation Paralysis Resource Center*, April 21, 2009.

Cappozzo, A., Leo, T., & Pedotti, A. (1975). A general computing method for the analysis of human locomotion. *Journal of Biomechanics*, 8, 307-320.

Cappozzo, A., Figura, F., Leo, T., & Marchetti, M. (1978). Movements and mechanical energy changes of the upper part of the human body during walking. In *Biomechanics VI-A*, edited by E. Asmussen and K. Jørgensen, 272-279. University Park Press, Baltimore, MD.

Cereatti, A., Della Croce, U., & Cappozzo, A. (2006). Reconstruction of skeletal movement using skin markers: Comparative assessment of bone pose estimators. *Journal of NeuroEngineering and Rehabilitation*, 3(7), doi:10.1186/1743-0003-3-7.

Cerquiglini, S., Figura, F., & Marchetti, M. (1981). Biomechanics of wheelchair propulsion. *Biomechanics VIII A. Proceedings of the Seventh International Congress of Biomechanics, Warsaw, Poland*. University Park Press, Baltimore, MD.

Chandler, R. F., Clauser, C. E., McConville, J. T., Reynolds, H. M., & Young, J. W. (1975). Investigation of the inertial properties of the human body. AMRL Technical Report (TR-71-137), *Aerospace Medical Research Laboratories*, Wright-Patterson Air Force Base, OH.

Chantraine, A. (1978-1979). Actual concept of osteoporosis in paraplegia. *Paraplegia*, 16: 51-58.

Charlton, I. W. & Johnson, G. R. (2006). A model for the prediction of the forces at the glenohumeral joint. *Proceedings of the Institution of Mechanical Engineers, Part H*, 220(H8), 801-812.

Cheng, C. K., Chen, H. H., Chen, C. S., Lee, C. L., & Chen, C. Y. (2000). Segment inertial properties of Chinese adults determined from magnetic resonance imaging. *Clinical Biomechanics (Los Angeles, CA)*, 15(8), 559-566.

Chiari, L. Della Croce, U., Leardini, A., & Cappozzo, A. (2005). Human movement analysis using stereophotogrammetry Part 2: Instrumental errors. *Gait and Posture*, 21, 197-211.

Clauser, C. E., McConville, J. T., & Young, J. W. (1969). Weight, volume, and center of mass of segments of the human body. AMRL Technical Report (TR-69-70), *Aerospace Medical Research Laboratories*, Wright-Patterson Air Force Base, OH.

Collinger, J. L., Boninger, M. L., Koontz, A. M., Price, R., Sisto, S. A., Tolerico, M. L., & Cooper, R. A. (2008). Shoulder biomechanics during the push phase of wheelchair propulsion: A multisite study of persons with paraplegia. *Archives of Physical Medicine and Rehabilitation*, 89, 667-676.

Consortium for Spinal Cord Medicine. (2005). Preservation of upper limb function following spinal cord injury: A clinical practice guideline for health-care professionals. *J Spinal Cord Med*, 28, 433-470.

Cooper, R. A. (2009). SmartWheel: From concept to clinical practice. *Prosthetics and Orthotics International*, 33(3), 198-209.

Cooper, R. A., Boninger, M. L., Shimada, S. D., & Lawrence, B. M. (1999). Glenohumeral joint kinematics and kinetics for three coordinate system representations during wheelchair propulsion. *American Journal of Physical Medicine and Rehabilitation*, 78(5), 435- 446.

Correa, T. A., Baker, R., Graham, H. K., & Pandy, M. G. (2011). Accuracy of generic musculoskeletal models in predicting the functional roles of muscles in human gait. *Journal of Biomechanics*, 44, 2096-2105.

Crowninshield, R. D. (1978). Use of optimization techniques to predict muscle forces. *Journal of Biomechanical Engineering*, 100, 88-92.

Crowninshield, R. D. & Brand, R. A. (1981). A physiologically based criterion of muscle force prediction in locomotion. *Journal of Biomechanics*, 14, 793-801.

Curtis, K. A., Tyner, T. M., Zachary, L., Lentell, G., Brink, D., Didyk, T., … Pacillas, B. (1999). Effect of a standard exercise protocol on shoulder pain in long-term wheelchair users. *Spinal Cord*, 37, 421-429.

Curtis, K. A., Drysdale, G. A., Lanza, R. D., Kolber, M., Vitolo, R. S., & West, R. (1999). Shoulder pain in wheelchair users with tetraplegia and paraplegia. *Archives of Physical Medicine and Rehabilitation*, 80, 453- 457.

Dallmeijer, A. J., van der Woude, L. H., Veeger, H. J., & Hollander, A. P. (1998). Effectiveness of force application in manual wheelchair propulsion in persons with spinal cord injuries. *American Journal of Physical Medicine and Rehabilitation*, 77, 213-221.

Damsgaard, M., Rasmussen, J., Christensen, S.T., Surma, E., & de Zee, M. (2006). Analysis of musculoskeletal systems in the AnyBody Modeling System. *Simulation Modelling Practice and Theory*, 14, 1100-1111.

Davy, D. T. & Audu, M. L. (1987). A dynamic optimization technique for predicting muscle forces in the swing phase of gait. *Journal of Biomechanics*, 20, 187-201.

de Bruin, E. D., Dietz, V., Dambacher, M. A., & Stüssi, E. (2000). Longitudinal changes in bone in men with spinal cord injury. *Clinical Rehabilitation*, 14, 145-152.

de Groot, J. H., & Brand, R. (2001). A three-dimensional regression model of the shoulder rhythm. *Clinical Biomechanics*, 16, 735-743.

de Groot, S., Veeger, D. H., Hollander, A. P., & van der Woude, L. H. (2002). Wheelchair propulsion technique and mechanical efficiency after 3 weeks of practice. *Medicine and Science in Sports and Exercise*, 34, 756-766.

de Zee, M., Dalstra, M., Cattaneo, P. M., Rasmussen, J., Svensson, P., & Melsen, B. (2007). Validation of a musculo-skeletal model of the mandible and its application to the mandibular distraction osteogenesis. *Journal of Biomechanics*, 40, 1192-1201.

Delp, S. L., Anderson, F. C., Arnold, A .S., Loan, P., Habib, A., John, C. T., … Thelen, D. G. (2007). OpenSim: Open-source software to create and analyze dynamic simulations of movement. *IEEE Transactions on Biomedical Engineering*, 54(11), 1940-1949.

Delp, S. L., Anderson, F., Guendelman, E., Habib, A., Hamner, S., Holzbaur, K, … John, C. (2010). OpenSim User's Guide, Release 2.4.

Dempster, W. T. (1955). Space requirements of the seated operator. WADC. Technical Report (TR-55-159). Wright-Patterson Air Force Base, OH.

Desroches, G., Chèze, L., & Dumas, R. (2010). Expression of joint moment in the joint coordinate system. *Journal of Biomechanical Engineering*, 132(11), doi: 10.1115/1.4002537.

Dorn, T. W. (2008). Gait Extract Toolbox for Matlab, Version 1.71 (2008).

Drillis, R., Contini, R., & Bluestein, M. (1964). Body Segment Parameters. *Artificial Limbs*, 8(1), 44-66.

Dubowsky, S. R., Rasmussen, J., Sisto, S. A., & Langrana, N. A. (2008). Validation of a musculoskeletal model of wheelchair propulsion and its application to minimizing shoulder joint forces. *Journal of Biomechanics*, 41(14), 2981-2988.

Durkin, J. L., & Dowling, J. J. (2003). Analysis of body segment parameter differences between four human populations and the estimation errors of four popular mathematical models. *Journal of Biomechanical Engineering*, 125, 515-522.

Durkin, J. L., Dowling, J. J., & Andrews, D. M. (2002). The measurement of body segment inertial parameters using dual energy X-ray absorptiometry. *Journal of Biomechanics*, 25, 1575-1580.

Dyson-Hudson, T. A., & Kirshblum, S. C. (2004). Shoulder pain in chronic spinal cord injury, Part I: Epidemiology, etiology, and pathomechanics. *Journal of Spinal Cord Medicine*, 27, 4-17.

Erdemir, A., McLean, S., Herzog, W., & van der Bogert, A. J. (2007). Model-based estimation of muscle forces exerted during movements. *Clinical Biomechanics*, 22, 131-154.

Eser, P., Frotzler, A., Zehnder, Y., Wick, L., Knecht, H., Denoth, J, & Schiessl, H. (2004). Relationship between the duration of paralysis and bone structure: A pQCT study of spinal cord injured individuals. *Bone*, 34(5), 869-880.

Finley, M., Rasch, E., Keyser, R., & Rodgers, M. (2004). The biomechanics of wheelchair propulsion in individuals with and without upper-limb impairment. *Journal of Rehabilitation Research and Development*, 41, 395-402.

Forrest, G. F. (2001). *Role of intersegmental dynamics during locomotion: Implications for control of head stability*. (Doctoral dissertation). Retrieved from Temple University, Philadelphia, PA. (DISS E 2001 F677).

Fregly, B. J., Boninger, M. L., & Reinkensmeyer, D. J. (2012). Personalize neuromusculoskeletal modeling to improve treatment of mobility impairments: A perspective from European research sites. *Journal of Neuroengineering and Rehabilitation*, 9, 18.

Ganley, K. J., & Powers, C. M. (2004). Anthropometric parameters in children: A comparison of values obtained from dual energy x-ray absorptiometry and cadaver-based estimates. *Gait and Posture*, 19, 133-140.

Ganley, K. J., & Powers, C. M. (2004). Determination of lower extremity anthropometric parameters using dual energy X-ray absorptiometry: The influence on net joint moments during gait. *Clinical Biomechanics*, 19, 50-56.

Garland, D. E., Adkins, R. H., & Stewart, C. A. (2008). Five-year longitudinal bone evaluations in individuals with chronic complete spinal cord injury. *Journal of Spinal Cord Medicine*, 31, 543-550.

Garner, B. A. & Pandy, M. G. (2003). Estimation of musculotendon properties in the human upper limb. *Annals of Biomedical Engineering*, 31, 207-220.

Gater, D. R. & Clasey, J. L. (2006). Body composition assessment in spinal cord injury clinical trials. *Topics in Spinal Cord Injury Rehabilitation*, 11(3), 36-49.

Geisler, F. H., Dorsey, F. C., & Coleman, W. P. (1993). Past and current clinical studies with GM-1 ganglioside in acute spinal cord injury. *Annals of Emergency Medicine*, 22(6), 1041-1047.

Gellman, H., Sie, I., & Waters, R. L. (1988). Late complications of the weight-bearing upper extremity in the paraplegia patient. *Clinical Orthopaedics and Related Research*, 233, 132-135.

Goosey-Tolfrey, V. L., Lenton, J. P., Fowler, N., van der Woude, L., Nicholson, G., & Batterham, A. (2006). The influence of push frequency on force application during steady-state hand-rim wheelchair propulsion. *Medicine and Science in Sports and Exercise*, 38, S395-S396.

Gorgey, A. S., Dolbow, D R., & Gater, D. R. (2012). A model of predicition and cross-validation of fat-free mass in men with motor complete spinal cord injury. *Archives of Physical Medicine and Rehabilitation*, 93, 1240-1245.

Gorgey, A. S. & Dudley, G. A. (2007). Skeletal muscle atrophy and increased intramuscular fat after incomplete spinal cord injury. *Spinal Cord*, 45, 304-309.

Guo, L. Y., Su, F. C., & An, K. N. (2006). Effect of handrim diameter on manual wheelchair propulsion: Mechanical energy and power flow analysis. *Clinical Biomechanics*, 21, 107-115.

Hanavan, E. P. (1964). A mathematical model of the human body. AMRL Technical Report (TR-64-102), Aerospace Medical Research Laboratories, Wright-Patterson Air Force Base, OH.

Happee, R. (1994). Inverse dynamic optimization including muscular dynamics, a new simulation method applied to goal directed movements. *Journal of Biomechanics*, 27, 953-960.

Harburn, K. L. & Spaudling, S. J. (1986). Muscle activity in the spinal cord-injured during wheelchair ambulation. *American Journal of Occupational Therapy*, 40, 629-636.

Hardt, D. E. (1978). Determining muscle forces in the leg during human walking: An application and evaluation of optimization methods. *Journal of Biomechanical Engineering*, 100, 72-78.

Hatze, H. (1975). A new method for the simultaneous measurement of the moment of inertia, the damping coefficient and the location of the centre of mass of a body segment in situ. *European Journal of Applied Physiology*, 34, 217-226.

Hatze, H. (1980). A mathematical model for the computational determination of parameter values of anthropometric segments. *Journal of Biomechanics*, 13(10), 833-843.

Higginson, J., Zajac, F. E., Neptune, R. R., Kautz, S. A., & Delp, S. L. (2006). Muscle contributions to support during gait in an individual with post-stroke hemiparesis. *Journal of Biomechanics*, 39, 1769-1777.

Hobson, D. A. & Tooms, R. E. (1992). Seated lumbar/pelvic alignment. A comparison between spinal cord-injured and non-injured groups. *Spine*, 17, 293-298.

Hof, A. L. (1997). The relationship between electromyogram and muscle force. *Sportverletz Sportschaden*, 11(3), 79-86.

Högfors, C., Sigholm, G. & Herberts, P. (1987). Biomechanical model of the human shoulder-I. Elements. *Journal of Biomechanics*, 20(2), 157-166.

Högfors, C., Perterson, B., Sigholm, G., & Herberts, P. (1991). Biomechanical model of the human shoulder joint-II. The shoulder rhythm. *Journal of Biomechanics*, 24(8), 699-709.

Holzbaur, K. R., Murray, W. M., & Delp, S. L. (2005). A Model of the upper extremity for simulating musculoskeletal surgery and analyzing neuromuscular control. *Annals of Biomedical Engineering*, 33(6), 829-840.

Huang, H. K. (1983). Evaluation of cross-sectional geometry and mass density distributions of humans and laboratory animals using computerized tomography. *Journal of Biomechanics*, 16(10), 821-832.

Hull, H., He, Q., Thornton, J., Javed, F., Allen, L., Wang, J., … Gallagher, D. (2009). iDXA, Prodigy, and DPXL dual-energy x-ray absorptiometry whole body scans: A cross-calibration study. *Journal of Clinical Densitometry: Assessment of Skeletal Health*, 12(1), 95-102.

Jensen, R. K. (1993). Human morphology: Its role in the mechanics of movement. *Journal of Biomechanics*, 26(Suppl. 1), 81-94.

Jones, L. M., Goulding, A., & Gerrard, D. F. (1998). DEXA: A practical and accurate tool to demonstrate total and regional bone loss, lean tissue loss, and fat mass gain in paraplegia. *Spinal Cord*, 36, 637-640.

Karlsson, D. & Peterson, B. (1992). Towards a model for force predictions in the human shoulder. *Journal of Biomechanics*, 25(2), 189-199.

Kaufman, K. R, An, K. N., Litchy, W. J., & Chao, E. Y. S. (1991). Physiological prediction of muscle forces: II. Application to isokinetic exercise, *Neuroscience*, 40, 793-804.

Kautz, S. A., Neptune, R. R., & Zajac, F. E. (2000). General coordination principles elucidated by forward dynamics: Minimum fatigue does not explain muscle excitation in dynamic tasks. *Motor Control*, 4, 75-80.

Kelly, T. L., Berger, N., & Richardson, T. L. (1998). DXA body composition: Theory and practice. *Applied Radiation and Isotopes*, 49(5-6), 511-513.

Kingma, I., Toussaint, H. M., De Looze, M. P., & Van Dieen, J. H. (1996). Segment inertial parameter evaluation in two anthropometric models by application of a dynamic linked segment model. *Journal of Biomechanics*, 29(5), 693-704.

Kirshblum, S. C., Burns, S. P., Biering-Sørensen, F., Donovan, W., Graves, D. E., Jha, A., … Waring, W. (2011). International Standards for Neurological Classification of Spinal Cord Injury (revised 2011). *Journal of Spinal Cord Medicine*, 34(6), 535- 546.

Koontz, A. M., Cooper, R. A., Boninger, M. L., Souza, A. L., & Fay, B. T. (2002). Shoulder kinematics and kinetics during two speeds of wheelchair propulsion. *Journal of Rehabilitation Research and Development*, 39(6), 635-650.

Kotajarvi, B. R., Basford, J. R., An, K. N., Morrow, D. A., & Kaufman, K. R. (2006). The effect of visual biofeedback on the propulsion effectiveness of experienced wheelchair users. *Archives of Physical Medicine and Rehabilitation*, 87, 510-515.

Krueger, D., Checovich, M., Vallarta-Ast, N., Gemar, D., & Binkley, N. (2006). Comparison of total body paramters as measured using GE Healthcare Lunar Prodigy and Lunar iDXA densitometers. *Journal of Bone Mineral Research*, 21 (Suppl 1),SS25, ASBMR Annual Meeting, Philadelphia, PA.

Kulig, K., Rao, S. S., Mulroy, S. J., Newsam, C. J., Gronley, J. K., Bontrager, E. L., & Perry, J. (1998). Shoulder joint kinetics during the push phase of wheelchair propulsion. *Clinical Orthopaedics and Related Research*, 354, 132-143.

Kulig, K., Newsam, C. J., Mulroy, S. J., Rao, S., Gronley, J. K., Bontrager, E. L., & Perry, J. (2001). The effect of level of spinal cord injury on shoulder joint kinetics during manual wheelchair propulsion. *Clinical Biomechanics*, 16, 744-751.

Kwarciak, A. M., Sisto, S. A., Yarossi, M., Price, R., Komaroff, E., & Boninger, M. L. (2009). Redefining the manual wheelchair stroke cycle: Identification and impact of nonpropulsive pushrim contact. *Archives of Physical Medicine and Rehabiliation*, 90, 20-26.

Lee, M. K., Le, N. S., Fang, A. C., & Koh, M. T. H. (2009). Measurement of body segment parameters using dual energy X-ray absorptiometry and three-dimensional geometry: An application in gait analysis. *Journal of Biomechanics*, 42, 217-222.

Lewis, F. L., Abdallah, C. T., & Dawson, D. M. (1993). *Control of robot manipulators*. Macmillan Publishing Company, New York.

Lin, C. J., Lin, P. C., Su, F. C., & An, K. N. (2009). Biomechanics of wheelchair propulsion. *Journal of Mechanics in Medicine and Biology*, 9, 229-242.

Lin, H. T., Su, F. C., Wu, H. W., & An, K. N. (2004). Muscle force analysis in the shoulder mechanism during wheelchair propulsion. *Proceedings of the Institutions of Mechanical Engineers, Part H: Journal of Engineering in Medicine*, 218, 213-221.

Lloyd, D. G. & Besier, T. G. (2003). An EMG-driven musculoskeletal model to estimate muscle forces and knee joint moments in vivo. *Journal of Biomechanics*, 36(6), 765-776.

Martin, P.E., Mungiole, M., Marzke, M. W., & Longhill, J. M. (1989). The use of magnetic resonance imaging for measuring segment inertial properties. *Journal of Biomechanics*, 22(4), 367- 376.

Mazess, R. B., Barden, H. S., Bisek, J. P., & Hanson, J. (1990). Dual-energy X-ray absorptiometry for total-body and regional bone-mineral and soft-tissue composition. *American Journal of Clinical Nutrition*, 51, 1106-1112.

Mercer, J. L., Boninger, M. Koontz, A., Ren, D., Dyson-Hudson, T., & Cooper, R. A. (2006). Shoulder joint kinetics and pathology in manual wheelchair users. *Clinical Biomechanics*, 21, 781-789.

Minkel, J. L. (2000). Seating and mobility considerations for people with spinal cord injury. *Physical Therapy*, 80, 701-709.

Morrow, M. M. B., Hurd, W. J., Kaufman, K. R., & An, K. N. (2009). Upper-limb joint kinetics expression during wheelchair propulsion. *Journal of Rehabilitation Research & Development*, 46(7), 939-944.

Morrow, M. M. B., Kaufman, K. R., & An, K. N. (2010). Shoulder model validation and joint contact forces during wheelchair activities. *Journal of Biomechanics*, 43, 2487-2492.

Mulroy, S. J., Gronley, JK, Newsam, C. J., & Perry, J. (1996). Electromyographic activity of shoulder muscles during wheelchair propulsion by paraplegic persons. *Archives of Physical Medicine and Rehabilitation*, 77(2), 187-193.

Mulroy, S. J., Farrokhi, S., Newsam, C. J., & Perry, J. (2004). Effects of spinal cord injury level on the activity of shoulder muscles during wheelchair propulsion: An electromyographic study. *Archives of Physical Medicine and Rehabilitation*, 85, 925-934.

Mulroy, S. J., Newsam, C. J., Gutierrez, D. D., Requejo, P., Gronley, J. K., Haubert, L. L., & Perry, J. (2005). Effect of fore-aft seat position on shoulder demands during wheelchair propulsion: pat 1. A kinetic analysis. *Journal of Spinal Cord Medicine*, 28, 214-221.

National Spinal Cord Injury Statistical Center. (2013). Spinal Cord Injury Facts and Figures at a Glance. *Journal of Spinal Cord Medicine*, 36(3), 254-255.

Neptune, R. R. & Hull, M. L. (1998). Evaluation of performance criteria for simulation of submaximal steady-state cycling using a forward dynamic model. *Journal of Biomechanical Engineering*, 120, 334-341.

Neptune, R. R., Kautz, S. A., & Zajac, F. E. (2001). Contributions of the individual ankle plantar flexors to support, forward progression and swing initiation during walking. *Journal of Biomechanics*, 34, 1387-1398.

Newsam, C. J., Rao, S. S., Mulroy, S. J., Gronley, J. K., Bontrager, E. L., & Perry, J. (1999). Three dimensional upper extremity motion during manual wheelchair propulsion in men with different levels of SCI. *Gait & Posture*, 10(3), 223-232.

Nichols, P. J., Norman, P. A., & Ennis, J. R. (1979). Wheelchair user's shoulder? Shoulder pain in patients with spinal cord lesions. *Scandinavian Journal of Rehabilitation Medicine*, 11, 29-32.

Nickel, J. C., Iwasaki, L. R., Walker, R. D., McLachlan, K. R., & McCall, W. D. (2003). Human masticatory muscle forces during static biting. *Journal of Dental Research*, 82, 212-217.

Nieminen, H., Niemi, J., Takala, E. P., & Viikari-Juntura, E. (1995). Load-sharing patterns in the shoulder during isometric flexion tasks. *Journal of Biomechanics*, 28, 555-566.

Nikooyan, A. A., Veeger, H. E. J., Westerhoof, P., Graichen, F., Bergmann, G.,& van der Helm, F. C. T. (2010). Validation of the Delft shoulder and elbow model using in-vivo glenohumeral joint contact forces. *Journal of Biomechanics*, 43, 3007-3014.

Odle, B. M., Forrest, G. F., Reinbolt, J., & Dyson-Hudson, T. A. (2011). Development of an OpenSim shoulder model for manual wheelchair users with tetraplegia. *Proceedings of the ASME 2011 International Mechanical Engineering Congress & Exposition*, Denver, CO, November 11–17.

OpenSim Advanced User's Jamboree. (2009). Advanced User Workshop Manual. Stanford University, Stanford, CA, August 12-14, 2009.

Pandy, M. G. & Andriacchi, T. P. (2010). Muscle and joint function in human locomotion. *Annual Review of Biomedical Engineering*, 12, 401-433.

Pandy, M. G., Garner, B. A., & Anderson, F. C. (1995). Optimal control of non-ballistic muscular movements: A constraint-based performance criterion for rising from a chair. *Journal of Biomechanical Engineering*, 117, 1185-1198.

Patriarco, A. G., Mann, R. W., Simon, S. R., & Mansour, J. M. (1981). An evaluation of the approaches of optimization models in the prediction of muscle forces during human gait. *Journal of Biomechanics*, 14, 513-525.

Pearsall, D. J. & Reid, J. G. (1994). The study of human body segment parameters in biomechanics. *Sports Medicine*, 18(2), 126-140.

Pearsall, D. J., Reid, J. G., & Ross, R. (1994). Inertial properties of the human trunk of males determined from magnetic resonance imaging. *Annals of Biomedical Engineering*, 22, 692-706.

Pentland, W. E. & Twomey, L. T. (1991). The weight-bearing upper extremity in women with long term paraplegia. *Paraplegia*, 29(8), 521-530.

Pentland, W. E. & Twomey, L. T. (1994) Upper limb function in persons with long term paraplegia and implications for independence: Part I. *Paraplegia*, 32, 211-218.

Peyton, J. A. (1986). Determination of the moment of inertia of limb segments by a simple method. *Journal of Biomechanics*, 19(5), 405-410.

Plagenhoef, S., Evans, F. G., & Abdelnour, T. (1983). Anatomical data for analyzing human motion. *Research Quarterly for Exercise and Sport*, 54(2), 169-178.

Portney, L. G. & Watkins, M. P. (3rd edition). (2008). *Foundations of clinical research: Applications to practice*. Upper Saddle River, NJ, Pearson/Prentice Hall.

Powers, C. M., Newsam, C. J., Gronley, J. K, Fontaine, C. A., & Perry, J. (1994). Isometric shoulder torque in subjects with spinal cord injury. *Archives of Physical Medicine and Rehabilitation*, 75, 761-765.

Rankin, J. W., Kwarciak, A. M., Richter, W. M., & Neptune, R. R. (2010). The influence of altering push force effectiveness on upper extremity demand during wheelchair propulsion. *Journal of Biomechanics*, 43, 2771-2779.

Rankin, J. W., Richter, W. M., & Neptune, R. R. (2011). Individual muscle contributions to push and recovery subtasks during wheelchair propulsion. *Journal of Biomechanics*, 44, 1246-1252.

Rao, G., Amarantini, D., Berton, E. & Favier, D. (2006). Influence of body segments' parameters estimation models on inverse dynamics solutions during gait. *Journal of Biomechanics*, 39, 1531-1536.

Rasmussen, J., Damsgaard, M., & Voigt, M. (2001). Muscle recruitment by the min/max criterion- a comparative numerical study. *Journal of Biomechanics*, 34, 409-415.

Reid, J. G. (1984). Physical properties of the human trunk as determined by computed tomography. *Archives of Physical Medicine and Rehabilitation*, 65, 246-250.

Reinbolt, J. A., Schutte, J. F., Fregly, B. J., Koh, B. I., Haftka, R. T., George, A. D., & Mitchell, K. H. (2005). Determination of patient-specific multi-joint kinematic models through two-level optimization. *Journal of Biomechanics*, 38, 621-626.

Reinbolt, J. A., Haftka, R. T., Chmielewski, T. L., & Fregly, B. J. (2007). Are patient-specific joint and inertial parameters necessary for accurate inverse dynamics analyses of gait? *IEEE Transactions on Biomedical Engineering*, 54(5), 782-793.

Reinbolt, J. A., Seth, A., & Delp, S. L. (2011). Simulation of human movement: Applications using OpenSim. 2011 Symposium on Human Body Dynamics, *Procedia IUTAM*, 2, 186-198.

Reyes, M. L., Gronley, J. K., Newsam, C. J., Mulroy, S. J., & Perry, J. (1995). Electromyographic analysis of shoulder muscles of men with low-level paraplegia during a weight relief raise. *Archives of Physical Medicine and Rehabilitation*, 76, 433-439.

Roubenoff, R., Kehayias, J. J., Dawson-Hughes, B. & Heymsfield, S. B. (1993). Use of dual-energy x-ray absorptiometry in body-composition studies: not yet a "gold standard." *American Journal of Clinical Nutrition*, 58, 589-591.

Sanderson, D. J. & Sommer, H. J. (1985). Kinematic features of wheelchair propulsion. *Journal of Biomechanics*. 18, 423-429.

Scelza, W. M., & Dyson-Hudson, T. A. (2011). Neuromusculoskeletal complications of spinal cord injury. In S. Kirshblum & D. I. Campagnola (2nd ed.), *Spinal Cord Medicine* (pp. 282-308). Baltimore, MD: Lippincott Williams & Wilkins.

Seth, A., Sherman, M., Reinbolt, J. A., & Delp, S. L. (2011). OpenSim: A musculoskeletal modeling and simulation framework for in silico investigations and exchange. 2011 Symposium on Human Body Dynamics, *Procedia IUTAM*, 2, 212-232.

Sie, I. H., Waters, R. L., Adkins, R. H., & Gellman, H. (1992). Upper extremity pain the postrehabilitation spinal cord injured patient. *Archives of Physical Medicine and Rehabilitation*, 73, 44-48.

Soriano, J-M. P., Ioannidou, E., Wang, J., Thornton, J.C., Horlick, M. N., Gallagher, D., … Pierson Jr., R. N. (2004). Pencil-beam vs. fan-beam dual-energy x-ray absorptiometry comparisons across four systems. *Journal of Clinical Densitometry*, 7(3), 281-289.

Spungen, A. M., Bauman, W. A., Wang, J., & Pierson, R. N. (1995). Measurement of body fat in individuals with tetraplegia: A comparison of eight clinical methods. *Paraplegia*, 33, 402-408.

Spungen, A. M., Wang, J., Pierson, R. N., & Bauman, W. A. (2000). Soft tissue body composition differences in monozygotic twins discordant for spinal cord injury. *Journal of Applied Physiology*, 88, 1310-1315.

Spungen, A. M., Adkins, R. H., Stewart, C. A., Wang, J., Pierson, Jr., R. N., Waters, R. L., & Bauman, W. A. (2003). Factors influencing body composition in persons with spinal cord injury: A cross-sectional study. *Journal of Applied Physiology*, 95, 2398-2407.

Sullivan, S. R., Langrana, N. A., & Sisto, S. A. (2005). Multibody computational biomechanical model of the upper body. *Proceedings of the ASME 2005 International Design Engineering Technical Conference and Computers and Information in Engineering Conference*, Long Beach, CA, September 24-28.

Sullivan, S. R., Langrana, N. A., & Sisto, S. A. (2007). Shoulder mechanics Analytical modeling and validation. *Proceedings of the American Society of Biomechanics Annual Conference*, Palo Alto, CA, August 22-25.

Thelen, D. G., Anderson, F. C., & Delp, S. L. (2003). Generating dynamic simulations of movement using computed muscle control. *Journal of Biomechanics*, 36, 321-328.

Thelen, D. G. & Anderson, F. C. (2006). Using computed muscle control to generate forward dynamic simulations of human walking from experimental data. *Journal of Biomechanics*, 39, 1107-1115.

van der Helm, F.C.T. (1994). A finite element musculoskeletal model of the shoulder mechanism. *Journal of Biomechanics*, 27, 551-569.

van Drongelen, S., van der Woude, L. H., Janssen, T. W., Angenot, E. L., Chadwick, E. K., & Veeger, DJ. H. (2005). Glenohumeral contact forces and muscle forces evaluated in wheelchair-related activities of daily living in able-bodied subjects versus subjects with paraplegia and tetraplegia. *Archives of Physical Medicine and Rehabilitation*, 86, 1434-1440.

van Drongelen, S., van der Woude, L. H., Janssen, T. W., Angenot, E. L., Chadwick, E. K., & Veeger, DJ. H. (2005). Mechanical load on the upper extremity during wheelchair activities. *Archives of Physical Medicine and Rehabilitation*, 86, 1214-1220.

van Drongelen, S., van der Woude, L. H. V., & Veeger, H. E. J. (2011). Load on the shoulder complex during wheelchair propulsion and weight relief lifting. *Clinical Biomechanics*, 26, 452-457.

Vasavda, A. N., Li, S., & Delp, S. L. (1998). Influence of muscle morphometry and moment arms on the moment-generating capacity of human neck muscles. *Spine*, 24(4), 412-422.

Veeger, H. E. J., Yu, B., An, K. N., & Rozendal, R. H. (1997). Parameters for modeling the upper extremity. *Journal of Biomechanics*, 30(6), 647-652.

Veeger, H. E. J., Rozendaal, L. A., & van der Helm, F. C. T. (2002). Load on the shoulder in low intensity wheelchair propulsion. *Clinical Biomechanics*, 17, 211-218.

Wicke, J., Dumas, G. A., & Costigan, P. A. (2008). Trunk density profile estimates from dual X-ray absorptiometry. *Journal of biomechanics*, 41, 861-867.

Wilk, K. E, Arrigo, C. A., & Andrews, J. R. (1997). Current concepts: The stabilizing structures of the glenohumeral joint. *Journal of Orthopaedic and Sports Physical Therapy*, 25(6), 364-379.

Wilkenfeld, A., Audu, M. L., & Triolo, R. J. (2006). Feasibility of functional electrical stimulation for control of seated posture after spinal cord injury: A simulation study. *Journal of Rehabilitation Research and Development*, 43(2), 139-152.

Wilmet, E., Ismail, A. A., Heilporn, A., Welraeds, D., & Bergmann, P. (1995). Longitudinal study of the bone mineral content and of soft tissue composition after spinal cord section. *Paraplegia*, 33, 674-677.

Winter, D. A. (3rd edition). (2005). *Biomechanics and motor control of human movement*. Hoboken, NJ: John Wiley & Sons, Inc.

Wu, G., van der Helm, F. C. T., Veeger, H. E. J., Makhsous, M., Van Roy, P., Anglin, C., … Buchholz, B. (2005). ISB recommendation on definitions of joint coordinate systems of various joints for reporting of human joint motion- Part II: Shoulder, elbow, wrist, and hand. *Journal of Biomechanics*, 38, 981-992.

Xu, X., Lin J. H., & McGorry, R. (2012). Coordinate transformation between shoulder kinematic descriptions in the Holzbaur et al. model and ISB sequence. *Journal of Biomechanics*, 45, 2715-2718.

Yamaguchi, G. T. & Zajac, F. E. (1990). Restoring unassisted natural gait to paraplegics via functional neuromuscular stimulation: A computer simulation. *IEEE Transactions of Biomedical Engineering*, 37, 886-902.

Yang, Y. S., Koontz, A. M., Triolo, R. J., Mercer, J. L., & Boninger, M. L., (2006). Surface electromyography activity of trunk muscles during wheelchair propulsion. *Clinical Biomechanics*, 21, 1032-1041.

Yarossi, M., Dyson-Hudson, T. A., Forrest, G., Kwarciak, A., & Sisto, S. A. (2010). Shoulder kinematics and kinetics during wheelchair propulsion in persons with tetraplegia. *Proceedings of the American Society of Biomechanics*. Providence, RI, August 18-21.

Yeadon, M. R. & Morlock, M. (1989). The appropriate use of regression equations for the estimation of segmental inertia parameters. *Journal of Biomechanics*, 22(6/7), 683-689.

Zajac, F. E. (1989). Muscle and tendon: Properties, models, scaling, and application to biomechanics and motor control. *Critical Reviews in Biomedical Engineering*, 17(4), 359-411.

Zajac, F. E. (1993). Muscle coordination of movement: A perspective. *Journal of Biomechanics*, 26 (Suppl 1), 109-124.

Zatsiorsky, V. & Seluyanov, V. (1983). The mass and inertial characteristics of the main segments of the human body. In Biomechanics VIII-B, edited by Matsui and Kobayashi. *Human Kinetics*, Champagne, IL, 1152-1159.